Structures and Functions of the Post-Mortem Brain: An Experimental Evaluation of the Residual Properties of Fixed Neural Tissues

By

Nicolas Rouleau

A thesis submitted in partial fulfillment

of the requirements for the degree of

Doctor of Philosophy (PhD) in Biomolecular Sciences

Faculty of Graduate Studies

Laurentian University

Sudbury, Ontario

THESIS DEFENCE COMMITTEE/COMITÉ DE SOUTENANCE DE THÈSE
Laurentian Université/Université Laurentienne
Faculty of Graduate Studies/Faculté des études supérieures

Title of Thesis Titre de la thèse	Structures and Functions of the Post-Mortem Brain: An Experimental Evaluation of the Residual Properties of Fixed Neural Tissues
Name of Candidate Nom du candidat	Rouleau, Nicolas
Degree Diplôme	Doctor of Philosophy
Department/Program Département/Programme	Biomolecular Sciences
Date of Defence Date de la soutenance	August 18, 2017

APPROVED/APPROUVÉ

Thesis Examiners/Examinateurs de thèse:

Dr. Michael Persinger
(Supervisor/Directeur(trice) de thèse)

Dr. Robert Lafrenie
(Committee member/Membre du comité)

Dr. Abdelwahab Omri
(Committee member/Membre du comité)

Dr. Jiapei Dai
(External Examiner/Examinateur externe)

Dr. Frank Mallory
(Internal Examiner/Examinateur interne)

Approved for the Faculty of Graduate Studies
Approuvé pour la Faculté des études supérieures
Dr. David Lesbarrères
Monsieur David Lesbarrères
Dean, Faculty of Graduate Studies
Doyen, Faculté des études supérieures

ACCESSIBILITY CLAUSE AND PERMISSION TO USE

Abstract

Does brain function irreversibly cease after death? Billions of years of evolution and hundreds of thousands of years of human development have inculcated within us an intuition that death is a deep pit from which thoughts and behaviour cannot emerge. This dissertation serves to challenge the assumption of neurofunctional loss after death by employing modern technology to observe alternative mechanisms by which information can be processed by fixed, post-mortem neural tissues. The central aim of the thesis was to measure periodic, electric potential differences (μV) characteristic of the psychological definition of “response” within neuroanatomical loci while the fixed tissues were exposed to patterned current, complex electromagnetic fields, chemical probes, and other experimental conditions. The findings presented here show that fixed post-mortem tissues express regional, electrical anisotropies which can be modulated by various applications of electrochemical energy and that the areas surrounding the hippocampus are most responsive. We show that neuropathology secondary to repeated and protracted seizure activity can be detected in post-mortem rat brains with coupled depressions of low-frequency signal periodicities. Our findings demonstrate that injections of current into coronal sections of fixed human brain tissue are most potent when patterned to simulate neuronal spike-trains and the dominant frequency of the equivalent living tissue subsection. We also show that fixed, post-mortem brain tissues act as electromagnetic filters, expressing signals non-randomly and preferentially within the right cerebral hemisphere. Further findings indicate that receptor agonist-antagonist probes (e.g., glutamate and ketamine) as well as other chemical applications can induce regional electrical responses as well as habituation-type phenomena over repeated exposure.

These responses are paired and can be inversely related to photon emission from the tissue proper as inferred by photomultiplier tube measurements. The bases of the electrochemical responses are thought to be due to phenomena associated with pH and ionic gradients in general as inferred by our experiments with post-mortem rat brains. The aforementioned experimental results are then synthesized to produce a working hypothesis upon which further research can be based. We conclude that the brain's structure-function relationship is sufficient to elicit post-mortem responses characteristic of a composite material of otherwise unknown potential.

Keywords: post-mortem brain, brain death, hippocampus, electrophysiology, theta rhythm; neuroanatomy, materials sciences, ex vivo

Acknowledgements

Most notably, I would like to express infinite thanks to Dr. Michael A. Persinger, my supervisor and mentor. His brilliance, insights, and generosity are only matched by his willingness to combat intellectual dishonesty and moral cowardice wherever it is found. I am forever in debt to Dr. Persinger, who pushed me past mediocrity with an invaluable set of tools and gave me the time and space to explore. I am proud to have been part of his Neuroscience Research Group. Thanks are also owed to my committee members, Dr. Robert Lafrenie and Dr. Abdelwahab Omri, whose comments and suggestions were instrumental in completing the dissertation. I'd also like to thank the neuroscientist and philosopher Sam Harris for his work on free will. His insights on agency, consciousness, and artificial intelligence have been extraordinarily helpful. Sincere thanks are owed to my colleagues for challenging me. In particular, my early conversations with Brandon Michaud and Ryan C. Burke were extraordinarily useful. I extend my deepest gratitude to my collaborators and co-authors in the Neuroscience Research Group for their contributions. Whether aggressively challenging ideas or musing on Philosophy Fridays (usually with Lucas Tessaro), I found my time with all of you to be most enjoyable.

To my family, acknowledgements of your support are best expressed outside the written format. However, some particulars can't be omitted. Nirosha J. Murugan, my wife and confidant, thank you for everything you do – you are my continuing inspiration. In a vast and unforgiving Universe of profound symmetry I am lucky to have found you, my anti-particle, right under my nose. Don't ever stop being the bright and powerful person that you are. Thanks to my parents, Laura and Robert, who never doubted my capacities,

introduced me to argumentation, and fostered my early creativity. I won't let any of it go to waste. Thanks to my brothers, Michael and Marcus, for their patience, generosity, and continuing support. Family pays dividends unlike any other early life advantage and I couldn't be more thankful.

Those who promote open-access publishing and genuine scientific inquiry deserve acknowledgments for their efforts to improve upon the contemporary system which too often relies upon the undue authority of appointed editors, chairs, and committees. No thanks can be expressed to patrons and administrators of orthodoxy and those who value narratives over data – the results of your obstructions do not go unnoticed and won't be forgotten. Nothing is sacred. Debate about all things, uncensored and for the sake of itself, must be promoted above impulses to guard taboos or avoid hurt feelings if we have any intention to mature as a species. Conflicts of ideas and uncomfortable conversations are necessary in scientific pursuit. Those who retreat to echo chambers or spaces of intellectual safety make the relative weakness of their positions evident. Agreeableness is not virtuous – it is antithetical to the pursuit of truth which requires dissent, either by dialectic or by falsification of hypotheses. It is my hope that individuals in positions of power who disagree with this fundamental proposition kindly step aside so as to let the rest of us take aim at problems both fundamental and technical in search of solutions.

Table of Contents

List of Tables

List of Figures

Abbreviations

5-HTP	**5-hydroxytryptophan**
AMG	**Amygdala**
ANOVA	**Analysis of Variance**
BA	**Brodmann Area**
CA1	**Cornu Ammonis 1**
CMB	**Cosmic Microwave Background**
CSF	**Cerebrospinal Fluid**
DAC	**Digital-to-Analog Converter**
DNA	**Deoxyribonucleic Acid**
EFA	**Ethanol-Formalin Acetic Acid**
EPSP	**Excitatory Post-Synaptic Potential**
HG	**Heschl's Gyrus**
HFD	**Higuchi Fractal Dimensions**
IPSP	**Inhibitory Post-Synaptic Potential**
Kp	**Planetary Index**
KW	**Kruskal-Wallis**
LSD	**Lysergic Acid Diethylamide**
LTP	**Long Term Potentiation**
MFG	**Middle Frontal Gyrus**
MRI	**Magnetic Resonance Imaging**

NAD	**Nicotinamide Adenine Dinucleotide**
NADP	**Nicotinamide Adenine Dinucleotide Phosphate**
NMDA	**N-methyl-D-aspartate**
NOAA	**National Oceanic and Atmospheric Administration**
OCP	**Occipital Pole**
ORG	**Orbital Gyrus**
PAR, PHG	**Parahippocampal Gyrus**
pH	**Percent Hydrogen**
PMT	**Photomultiplier Tube**
sLORETA, LORETA	**Standardized Low-Resolution Electromagnetic Tomography**
SEM	**Standard Error of the Mean**
SPD, PD	**Spectral Power Density**
SPSS	**Statistical Package for Social Sciences**
SUP	**Superior Parietal Lobule**
QEEG, qEEG	**Quantitative Electroencephalography**

Symbols & Scientific Notations

µV, mV, V	**Volt**
J	**Joule**
Hz, kHz, GHz	**Hertz**
W	**Watts**
nm, µm, mm, cm, m	**Meters**
µm, ms, s	**Seconds**
nM, µm, mM, M	**Molar**
ng, µm, mg, g, kg	**Grams**
cc	**Cubic Centimeters**
pA, A	**Amperes**
H+	**Hydrogen Ion**
Ω, kΩ, R	**Ohm**
LC	**Inductor-Capacitor**
η	**Eta**
r	**Pearson r**
rho	**Spearman rho**
nT, µT, T	**Tesla**
B	**Field Strength**
N	**Newtons**
dH_2O	**Distilled Water**

X	**Chi**
Λ, λ	**Lambda**
$NaHCO_3$	**Sodium Bicarbonate**
NaCl	**Sodium Chloride**
KCl	**Potassium Chloride**
$CaCl_2$	**Calcium Chloride**
$MgCl_2$	**Magnesium Chloride**
K_2HPO_4	**Dipotassium Phosphate**
$-CH_2-$	**Methylene Bridge**
OH^-	**Hydroxide**
f	**Frequency**
F	**Farads**

Chapter 1

Introduction

Complexities of the Brain

Brains are structurally complex organs which process patterned information in the form of electrochemical impulses. They plan and execute motor sequences such as walking and talking just as they perceive environmental stimuli and contemplate their own existence. Brains are, in many ways, general purpose computing machines which re-wire themselves, optimizing outputs contingent upon a history of inputs. The brain's capacity to change its own structure allows it to store packets of information as long-term engrams which form the bases of memory (Bliss & Collingridge, 1993), though to describe the brain as a sophisticated hard drive or safety deposit box reserved for experiential artifacts of personal significance would be neglecting its most impressive feature – one which has eluded both definition and direct measurement. Its capacity to generate recursive and re-entrant electrical sates is thought to give rise to consciousness – a function unique to brains wherein matter is imbued with the capacity to experience (Lutz & Thompson, 2003). However, the means by which matter becomes conscious has been contested for centuries without significant advancements.

The concept of consciousness has eluded a comprehensive definition. To briefly summarize years of research and debate, we have learned several key features which I will list here. First, consciousness is intimately tied to awareness – the brain's capacity to register and direct attention to stimuli or sources of brain-relevant energy of origins both

internal and external (Stuss, Picton, & Alexander, 2001). Second, it is characterized by "qualia" (Churchland, 1985) – such as the redness of an apple – which are units of experience heretofore unquantified in any scientific sense with the exception of self-report, requiring language – a serious hurdle to overcome when attempting to study consciousness in non-verbal systems (e.g., other animals). Third, consciousness is thought to be generated by recurrent loops of electrical activity between the cerebral cortices and the thalamus (Llinas, Ribary, Contreras & Pedroarena, 1998), a diencephalic structure located at the rostral end of the brainstem which serves as a signal operator, sorting through many millions of bits of information every second. Fourth, ablation of certain brain structures seems to abolish consciousness in part or whole. These include the periaqueductal gray (Baily & Davis, 1942; Watt, 2000), reticular nuclei (Papez, 1956; Parvizi & Damasio, 2001), and the cerebral cortices proper (Shewmon, Holmes, & Byrne, 1999). Fifth, consciousness can be altered by psychotropic drugs and most potently by those which act upon serotonergic pathways (e.g., N,N-Dimethyltryptamine or DMT), as well as hypnotics (e.g., pentobarbital), and anesthetics (e.g., ketamine). Sixth, consciousness can be described as a spectrum (Tart, 1972) ranging from unconscious states (e.g., normal sleep, syncope, etc.), to conscious states (e.g., awake, alert, etc.), with variations in between (e.g., hypnopompic and hypnogogic states, etc.). Seventh, consciousness is very likely not experienced equally across species. The seminal paper "What is it like to be a bat?" illustrated that conscious experience is a "single point of view" which can be distantly unrelated to those of other humans or members of other species (Nagel, 1974). Eight, it is currently not possible to prove that any particular system is conscious – only that it responds reliably as would be expected in a conscious system.

There are undoubtedly other features of consciousness which are not reported here, however, listing these problems even incompletely is sufficient to demonstrate the difficulties one faces when grappling with this subject. That is, a scientific study of consciousness is replete with philosophical and practical problems which have impeded research to no end. And yet questions related to consciousness are central to the human experience. Perhaps most central is a question which continues to be a major source of anxiety to both individuals and to the human species as a whole: “Where do I go when I die?”. That is, when the brain “ceases to function”, does conscious experience persist or does it dissipate?

Brain Death: Is it the End?

It is suspected that consciousness is irreversibly ceased at death. Corpses, as it were, do not appear to think or do much of anything which would be analogous to the living human body. The salience of this latter point only increases as time elapses after death. That consciousness is abruptly and irreversibly removed from the brain at death is, however, not entirely accurate. Indeed, the brain continues to function conventionally for at least tens of minutes after death (Norton et al., 2016). The experiences of individuals who have incurred cardiovascular insults sufficient to be labeled “deceased” by clinicians are well-known in the neuroscientific community, ranging from the classic “light at the end of the tunnel” phenomenon (i.e., visual scotoma), to the classic out-of-body experience (Blanke, Landis, Spinelli & Seeck, 2004). These experiences are thought to be expressed as a consequence of regional, vascular insufficiency – a cerebral Swan Song potentiated by an oxygen-starved occipital cortex in the case of the visual scotoma (Facco & Agrillo, 2012). In any case, cardiovascular death does not necessitate irreversible

unconsciousness. Acknowledging cardiovascular death's impracticality as a marker for what most mean by the word "death" or an end from which we do not return, clinicians have instead moved toward a model of death which centers on loss of brain function (American Clinical Neurophysiology Society, 2006). Brain death, characterized by < 2 uV electric potentials for 30 minutes over the scalp as inferred by electroencephalography (EEG) with interelectrode impedances under 10,000 Ohms, but over 100 Ohms has been used as a biomarker predicting long-term non-responsiveness to neuropsychological tests which assess CNS function and preservation of consciousness (American Clinical Neurophysiology Society, 2006; Norton et al., 2016). Though it's true that brains can become apparently irreversibly unconscious, even on life-support systems, inference of death remains largely based upon the absence of motor responses. We casually assume that, if a brain cannot produce motor outputs such as moving limbs, blinking, vocalizing, or nodding, it is unconscious and that as time elapses, the likelihood that it is irreversibly unconscious becomes more certain.

If, however, consciousness is currently unquantifiable, modern postulations regarding the permanence of its absence, though practical, are made in ignorance. Though sizeable portions of the cerebral cortices are dedicated to motor output (e.g., the frontal eye fields, pre-central gyrus, etc.), the majority of the surface area is dedicated to sensory processing. Therefore reliance upon motor indicators, though practical, is invalid as an indicator of whether "brain function" has indeed ceased – not to mention consciousness. Disorders of full-body paralysis with preserved consciousness such as Locked-In Syndrome (LIS) are behaviourally identical to that of corpses – in both cases there is no sign of movement (with some exceptions of vertical eye movement in LIS).

Indeed, administrations of paralytics can immobilize the body while preserving consciousness. The use of motor signs cannot be relied upon when attempting to assess one's capacity to experience.

One major problem with the study of unconsciousness and death is that we are, in effect, studying the absence of something. To study absence requires peripheral interactions as measurement is based upon the transduction of energy. Indeed, all measurements are simply physical interactions which have been captured so as to be observed outside the narrow timeframe within which they were originally generated. To study a black hole (which emits no light) with the use of a telescope (which collects light), an astronomer might direct its measurement device to the event horizon surrounding the black hole to observe subtle Hawking radiation or observe "lensing" of stars caused by massive gravitational distortions of space-time (Bartelmann & Schneider, 2001). Likewise, the study of brain death has been largely confined to electrophysiological measurements of brain activity and experiences reported immediately before death – at the temporal periphery of unconsciousness. We currently assume that brains are functional when we can 1) measure changing electrophysiological and neurochemical correlates of brain activity, and 2) record meaningful motor responses. At present, the cessation of neurophysiology and motor output defines death. Therefore measurements of neurophysiology and motor output cannot be employed post-mortem, making a study of brain function after death categorically impossible. How can function be assessed in a system – a post-mortem brain – whose defining characteristic is an absence of function? It can't be. If the post-mortem brain is capable of any function, the assumption of "death" must be rejected at the outset of our investigation, even if artificially rejected for the

purposes of scientific exploration. Though consciousness will likely continue to remain outside of the realm of scientific inquiry, perhaps a sophisticated study of brains which are understood to be irreversibly unconscious can propel the field forward in unexpected ways. At present, there have been no serious studies of post-mortem brain function tied to quantifiable, objective referents despite substantial study surrounding its post-mortem structure. The present document serves as a historical first attempt to quantify functional capacities within fixed, post-mortem brains without prejudice regarding the character of said functions.

Fundamentals of Neuroanatomy

To understand an object's function, observe its structure. The human brain is composed of hundreds of billions cells organized into highly-ordered networks (Azevedo et al., 2009). Its volume is approximately 1,300 cc (Gibson, 1988) and is primarily composed of water (70 %), with protein, fats, carbohydrates, nucleic acids, and metals (30% combined). Indeed, variations in water content over cerebral space (i.e., gradients) can be observed using T2-weighted magnetic resonance imaging (Whittall et al., 1997). There are two categories within which brain cells can be classified: neurons and glia. Other cells within the brain include endothelial cells which constitute the complex intracerebral vasculature as well as other minor subtypes. The general organization of the brain is best delineated by subdividing the central neuraxis into regions of distinct embryological origin: the telencephalon, diencephalon, mesencephalon, metencephalon, myelencephalon, and spinal cord. These distinct regions, together constituting the central nervous system (CNS), are encased in bone (either the cranium or vertebral column). For our purposes, I will only discuss the telencephalon as it represents both the majority of

the cerebral mass and the prime region of interest associated with our questions regarding the potential functions of post-mortem brains. Peripheral, satellite systems of neural tissue outside of the cranium and vertebral column, the peripheral nervous system, will not be discussed here.

The human brain can be thought of as a series of concentric tissue-shells which are asymmetrically represented along the left-right axis of a midline which runs through the entire organ and through which fluid continually flows. The telencephalon or cerebrum, characterized by the most superficial and stereotypical structures of the brain – gyri and sulci which give the brain its distinct raveled aesthetic – can be further divided into major structural subcomponents. At the boundary between the brain and the external space, represented along the superficial-most millimeters of the gyri and sulci (1.5 mm – 4.5 mm), is the cerebral cortex (Carpenter & Sutin, 1983; Creutzfeldt, 1977). Generally, it consists of multiple layers or laminae which extend out proximally-to-distally from the center of the brain. Each layer is cytoarchitecturally distinct, made up of different cell bodies and appendages. For instance, the most superficial layer – the molecular layer – is largely composed of dendritic arbors emanating from deeper cells and interconnections between these (Carpenter & Sutin, 1983). By contrast, layers three (III) and five (IV) are characterized by large pyramid-shaped cell bodies and their basal dendrites. The human brain expresses three distinct cortical cytoarchitectures which differ as a function of number of layers and which are related to phylogenetic development.

The first and most typical structure, the neocortex, is composed of 6 layers. Distinguished from other cortical structures, it is expressed widely across the cerebral cortical manifold. The neocortex is composed of alternating laminae of more and less cell-

dense regions. The second cortical structure, the paleocortex, is composed of 4 to 5 layers. The third cortical structure, the archicortex, is composed of 3 layers (Carpenter & Sutin, 1983). These three cortical structures intersect at a point within the human brain: the entorhinal-hippocampal junction within the parahippocampal gyrus where memory formation and sensory integration are performed (Braak & Braak, 1992; Zola-Morgan, Squire, Amaral, & Suzuki, 1989). The allocortex (i.e., the archicortex and paleocortex) is thought to have evolved from the pallium (Rodriguez et al., 2002), a structure ubiquitous to vertebrates consisting of a layer of gray matter (i.e., conductive cell bodies) sandwiched between layers of white matter (i.e., non-conductive axonal sheathes). Incidentally, the reverse of this structural organization, two conductive plates separated by a non-conductive or dielectric medium, is a capacitor which can store charge. Nevertheless, the allocortex, in turn, gives rise to a deep telencephalic structure which could be central to hypothesized post-mortem brain functions: the hippocampus.

Deep within the cerebrum, embedded among diffuse bundles of axons which run to and from the cerebral cortices are clusters of cells known as the basal ganglia, the nuclei of the basal forebrain, and the hippocampi (Crosby, Humphrey & Lauer, 1962). For the purposes of brevity, I will only focus on the hippocampus. This structure, composed of two interlocking C-shaped discs, is a continuation of the allocortex (Amunts et al., 2005). The parahippocampal gyrus, a cortical structure which runs externally and superficially along the hippocampus, is unique in that it undergoes morphological changes at its anterior and medial extension, converting from a 6 layered neocortex to a 3 layered allocortex at the entorhinal extension (Blatt, Pandya & Rosene, 2003) – ultimately forming the hippocampus. The hippocampus proper is also unique in that its structure, like the

brain as a whole, can be described as a series of concentric, shelled boundary conditions though these are incomplete or unclosed at points along the hippocampal body. The hippocampus is the principle sub-organ of the brain associated with long-term memory formation (Bliss & Collingbridge, 1993). Complete, bilateral ablation results in dense anterograde amnesia (Zola-Morgan, Squire & Amaral, 1986) whereas electrical stimulation evokes stored memories as forced-thought (Gloor, Olivier, Quesney, Andermann & Horowitz, 1982).

The tissue-structure of the brain, though defined by its cellular constituents, is clearly organized in such a way that it might express material-like properties which are not contingent upon cellular integrity. That is, just as water within dying cells continue to provide a medium within which chemical reactions can readily occur, post-mortem brains might remain functionally consequential objects despite loss of individualized cell structure-function. Before considering the possibility of post-mortem brain function, I should describe in detail the conventional mechanisms which are thought to underlie the normal, everyday neurophysiology of the living brain.

Fundamentals of Neurophysiology

Neurobiologically, the brain performs its myriad functions by patterning electrochemical signals across highly-interconnected though quasi-independent networks. Neurons, post-mitotic somatic cells, maintain an extracellular-intracellular charge gradient by tightly regulating Na^+ (outward) and K^+ (inward) currents by way of active transport across the plasma membrane (Morth et al., 2007). This ATP-coupled sodium-potassium pump is responsible for the generation of the resting membrane

potential (-60 to -70 mV) which defines the baseline electrical state of neuronal cells (Furukawa et al., 1996; Vierbuchen et al., 2010). Neurons receive thousands of individual inputs (Hawkins & Ahmad, 2016; Palay, 1956) from the axons of other neurons along their dendritic arbors (axo-dendritic), cell bodies (axo-somatic), and axons (axo-axonic). These inputs are principally mediated by chemical junctions of < 20 nm (width), known as synaptic clefts (Clements, et al., 1992). A synapse is an interface wherein pre-synaptic cells (senders) exocytose packets of chemical signals, or neurotransmitters, by vesicular fusion with the plasma membrane at the axon terminal (Bark & Wilson, 1994). Post-synaptic cells (receivers), in turn, become stimulated by the neurotransmitters within the synaptic cleft by means of receptor proteins embedded within the post-synaptic plasma membrane. Upon ligand-receptor binding, ionotropic and metabotropic (G-protein coupled) receptors are activated, potentiating ion transport through the plasma membrane, changing the membrane potential of the cell (Kew & Kemp, 2005).

Two types of input drive deviations from resting membrane potential: excitatory (EPSPs) and inhibitory post-synaptic potentials (IPSPs). EPSPs, which drive post-synaptic cells to depolarize (i.e., increase positive or decrease negative charge within the cell) can summate at the cell soma like a series of signals filtering in to activate a “switch” (Huguenard, 1996). When the resting membrane potential of the neuron is shifted sufficiently (from -70 mV to -55 mV), voltage-gated ion channels at the axon hillock (the point between the cell soma and axon) open, allowing for a mass depolarization (120 mV action potential) of the cell which propagates down the axon barrel at a velocity between 10 and 100 m/s on average (Zalc & Colman, 2000). The velocity remains constant due to saltatory conduction (Bodian, 1951) whereby the action potential “jumps” between Nodes

of Ranvier – clustered patches of ion channels separated intermittently by sections of the axon barrel insulated by the myelin of surrounding glial cells (e.g., oligodendrocytes). As the action potential propagates toward the axon terminal, Ca^{2+} channels mediate a series of vesicular events (e.g., priming, docking, and membrane-fusion) which ultimately potentiate neurotransmitter release into the synaptic cleft (Neher & Sakaba, 2008). This final step completes the cycle of signal propagation.

This simple electrochemical signal transduction method is thought to mediate the brain function with the exception of electrotonic signaling between cells via gap-junctions (Kumar & Gilula, 1996) which will not be described here in detail. The brain is thought to generate function by way of internally-regulated electrochemical gradients. Signals are generated within, transmitted through, and received by other subsections of the brain – a closed computational system. By shuffling ions between the extracellular and intracellular spaces surrounding neurons, brains perform inordinately complex computations. However, brain functions can be elicited by the application of external forces including ultrasound and electromagnetic fields (EMFs) (Ueno, Matsuda & Fujiki, 1990). This is largely unsurprising given the brain generates a bioelectric field which can be measured by magnetoencephalographs (Vrba & Robinson, 2001). Endogenous EMFs, generated by neurons, are even known to drive local brain activity by means outside of the classical synaptic model (McFadden, 2007; Persinger, 2014; Persinger & Koren, 2007). The brain is therefore an electromagnetic organ as much as it is a chemical organ and is sensitive to fields surrounding it. If we are to study the potential functions of post-mortem brains, we must consider their capacity to transduce external energies such as electromagnetic fields (Eder et al., 2012; Kirschvink, Walker & Diebel, 2001). After all, in the absence of

metabolic activity, the brain's energy supply nets zero. If post-mortem brains interact with electromagnetic fields, they could process information by structural filtration rather than active electrochemical signal propagation – a property which would not require endogenous energy sources, molecular or otherwise.

Fundamentals of Electromagnetism

A field is a coherent array of points within space-time made up of discrete, quantitative values. The quality of the field is determined by the nature of the point identity where electromagnetic fields are determined by discretized point-charges (Born, 1934). The electric field component is determined by stationary charge points (Nunez & Srinivasan, 2006) whereas positional translocation (movement) determines the magnetic component. Interactions between matter and electromagnetic fields are mediated by exchanges of packets of energy or photons with particular wavelengths and frequencies (Quigg, 1985). Photons are quanta of pure energy which express properties of frequency and wavelength proportional to their total energy and are related by Planck's equations (1901). These interactions define a considerable subset of the total set of force-matter interactions in nature. One of the most fundamental and readily observable phenomena throughout the cosmos is the change in energy state of an atom associated with the absorption or emission of a photon (Strömgren, 1939).

Electromagnetic fields of force are composed of two types of charges, positive and negative, which exist in symmetry. Their quantitative values are +1 and -1 respectively but are arbitrary in isolation. That is, their values as electric charges are only relevant insofar as they exist simultaneously and are therefore, in all senses, relative. "Positive"

and “negative” charges are nominal referents referring to symmetrical opposition of force. In contrast to gravitational fields which are only defined by positive masses (as opposed to negative masses) which attract, positive (+) and negative (-) electric charges interact bi-directionally: like-charged particles are repellent whereas unlike-charged particles are attractive. Charged objects (or particles) express flux lines (of force) which move out from the center of the object indefinitely (Nunez & Srinivasan, 2006). Flux density, or the amount of flux per unit cubed of space, decreases as a function of the distance from the charged object or particle. Objects consisting of two poles with opposite charges form flux lines that intersect and follow common paths from the negative to the positive poles. This is the basis of electrical polarity – a property observed ubiquitously throughout nature, even in cells and tissues.

Bioelectromagnetism

All cells display basic polar properties. The most evident example of cellular polarity is that of the resting membrane potential which has been described elsewhere. However, there are several other cellular phenomena which have been tied to polarity. M-phase of the cell cycle is dependent upon structural segregation of microtubules and other organelles along a dipole (Tuszyński et al., 1995). Tissue patterning, including left-right asymmetry, is also due to basic cell-cell polar interactions (Aw & Levin, 2009). Indeed, the regenerative capacities of planarian worms are due to a polar configuration of cells surrounding the blastema which are correlated with bioelectric tissue events (Oviedo et al., 2010). Cells, in addition to molecular factories, are polar objects.

As was eluded to elsewhere, polarity is generated by structural inequalities over space. As such, organs which are non-symmetrical in three-dimensional space (i.e., not perfect spheres) can display electrically polar properties. Indeed, the brain's polar properties are many-fold. Its concentric shell organization, rostro-caudal and left-right asymmetries (e.g., different ratios of gray-to-white matter), and complex topology (i.e., gyrification) produce the ideal conditions for polar interactions across the organ proper.

Several papers published by Saroka and Persinger (Persinger et al., 2013; Saroka, Caswell, Lapointe & Persinger, 2014; Saroka, Dotta, & Persinger, 2013) have demonstrated that electric potentials over the surface of the human scalp are intimately related to signals which permeate the electromagnetic field of the planet Earth. The Schumann resonance, a low-frequency electromagnetic signature produced largely by interactions between the Earth's electromagnetic field and equatorial lightning, has been observed to systematically vary with the electroencephalographic profiles of human participants. To summarize years of research surrounding this phenomenon, the primary locus which has been demonstrated to reliably respond to variations in geomagnetic activity and to the Schumann signal is the parahippocampal gyrus (Saroka & Persinger, 2014; Saroka, Vares, & Persinger, 2016). It is unknown whether the major signalling frequency of the hippocampus (~7 – 8 Hz) is related to the Schumann mode (~7 – 8 Hz) by causation or correlation alone, however brain-ionospheric interactions have been predicted by calculating the resonance frequency of the skull (Nunez & Cutillo, 1995; Nunez & Srinivasan, 2006). Alternative approaches have derived the same frequency from permittivity and inductance of gray matter (Tsang, Koren, & Persinger, 2004).

Experiments have repeatedly demonstrated that brains reliably respond to both natural and laboratory-controlled (synthetic) electromagnetic fields (Blackman et al., 1988; Floderus et al., 1993; Persinger, Ludwig & Ossenkopp, 1973). The mechanism by which this interaction is mediated is unknown though there are several hypotheses which are regularly referenced. The most common explanation points to simple induction of current within the wire-like axons of neurons (Marg & Rudiak, 1994). Other explanations range from transduction by magnetite-coupled neurons (Kirschvink, Walker & Diebel, 2001) to resonance interactions (Cherry, 2003). These mechanism presuppose that electromagnetic fields must interact physiologically with cells in order to induce changes in organic function. Though there is evidence to suggest that electromagnetic fields can act upon receptors directly, the most fundamental interactions in nature involving matter and electromagnetic fields do not require molecules at all. The atom is sufficient to transduce electromagnetic fields, or rather its carrier-particle: the photon.

Electromagnetism and Receptors

In the biomolecular sciences, it is customary to describe “pathways” in relation to a series of interacting molecules or matter-matter interactions. Indeed, molecules can be observed to form chains of interaction events such that A affects B, which affects C and so on. In general, the surface charge profile of one molecule must be optimally organized or “fit” the surface charge profile of its molecular counterpart in order to potentiate downstream action. The degree to which molecules “fit” determines the degree to which they will potentiate a given physiological event. Stated alternatively, degrees of structural parity determine degrees of function. Affinity, whether describing the strength of attraction between receptors and ligands or enzymes and substrates, is fundamental to the function

of molecular machines. This basic relationship has been classically described using metaphors such as “lock and key” which emphasize the importance of stimulus-receiver complementarity (Koshland, 1995).

Affinity is a fundamental property in physics due to intrinsic structural symmetries in the Universe. Take the neutral hydrogen atom, for instance. The energy level of an electron in orbit around the hydrogen atom (as is the case with any atom) is determined by discrete orbits that are energetically indivisible. That is, an electron can “jump” from one orbit to another but cannot occupy space (or hold energy values) between orbits. In the case of neutral hydrogen, electrons at the first energy level (n= 1) can be observed to hold energy values of -13.6 Ev. Higher levels are associated with higher energy values. To pass from the second energy level (n=2) to the first energy level (n=1), energy must be lost so that the electron can exist within a state of -13.6 eV. This net loss of 10.2 eV is emitted as a spontaneously generated photon whose wavelength can be calculated using the equation $E= hc/\lambda$. Re-arranging the equation to $\lambda = hc/E$ such that wavelength can be determined by the known energy value of 10.2 eV yields a wavelength of 1.21×10^{-7} m. This ultraviolet-range photon must be emitted by neutral hydrogen when the electron jumps from n= 2 to n= 1. Similarly, absorption of this and only this wavelength of light can induce the n=1 to n=2 jump. Shorter or longer wavelengths will not do – the precise wavelength is required to induce the jump. This relationship between precise energy values and precise changes to a system, for all practical purposes, describes the relationship between a ligand and its receptor. In the case of neutral hydrogen, degrees of affinity do not exist – the lock either fits or doesn’t. Molecules are much more forgiving in this regard, where deviations from optimal “keys” can still affect “locks” and vice versa.

That is, they express degrees of affinity where non-optimal ligands can still affect receptors.

It is therefore possible that even in the absence of normal cell function, electromagnetic energies could induce changes within post-mortem brain tissue, filtered by brain structure at a physical rather than biological level. All that would be required to induce these effects would be structural stasis at the tissue-level, however, the brain decomposes rapidly after death. Fortunately, centuries of neuroanatomical study have produced several reliable methods by which brain structure can be preserved after death.

Chemical Fixation of Brain Structure

When cells fail to maintain a sufficiently impermeable boundary between their inner contents and their environments, they become electrically and chemically unstable. Resisting entropy is one of the cell's most fundamental functions – if the discrete microenvironment of the cell becomes destabilized by excess ions, particulate matter, metals, microorganisms, or heat sources, it becomes disorderly and ultimately dies. A complete absence of nutrient- and oxygen-rich blood supply following cardiovascular death potentiates a series of cellular events which promote decomposition. Exposing the dying brain to microorganisms accelerates this process wherein brains fully disintegrate over the course weeks post-mortem (Vass, 2001). Anatomists have therefore employed techniques to preserve the structures of organs, including brains, for years to decades – even centuries after death. There are five principle methods which accomplish this goal: cryogenics (Cameron et al., 1997), vitrification (Pichugin, Fahy & Morin, 2006), saponification (Sledzik & Micozzi, 1996), mummification (Radanov et al., 1992), and

chemical fixation (Kiernan, 2000; Bjorksten, 1951). I will only discuss chemical fixation as it is most relevant to our questions concerning post-mortem brain function and for the purposes of brevity.

Immersing brain tissue in ethanol forces the water-content of cells and the extracellular spaces to be replaced by the perfused solution (Brandtzaeg, 1974). Serially increasing concentrations of ethanol in water will systematically de-hydrate brain material sufficiently to inhibit cellular breakdown and most infiltrating microorganisms. Aldehyde-based fixatives are typically used either in combination with ethanol, water, or alone where 10% buffered formalin (pH 6.8) is most common (Klinger & Ludwig, 1957). Aldehyde-based fixatives preserve cell and tissue structure by insertion of protein cross-links or -CH_2- (methylene) bridges into adjacent polypeptide structures (Kiernan, 2000; Bjorksten, 1951). The net result is a structurally static cell where proteins are thought to be relatively non-functional though continue to remain within three- and two-dimensional folding structures. Aldehyde-based fixatives are also known to produce considerable DNA damage, even in low concentrations (Douglas & Rogers, 1998). Cells and tissues perfused by aldehyde-based fixatives are therefore considered to be non-viable. Indeed, cyto- and histo-chemical techniques employ the same solutions to induce membrane pores within cells to render these structures permeable to dyes and anti-body tags (Farr & Nakane, 1981). Fixed, post-mortem brains are not considered viable organs which are in any sense functional under our modern biological paradigm. Nevertheless, I have described why functions might persist due to material-like properties of the tissue within electromagnetic fields.

Post-Mortem Brain Function

This brief introduction should serve to address the fundamentals of brain structure and function as they relate to electromagnetism so that a hypothesized model of post-mortem brain function can be conceived. The argument, which has been hinted at here, challenges the assumption of total and irreversible loss of brain function after cessation of neurophysiology and motor responses. Instead, it will be proposed that brains are both biological organs with metabolically-driven functions as described in detail above, as well as material aggregates which can perhaps draw upon environmental sources of energy (e.g., electromagnetic fields) to elicit signal processing functions (or filtrations) which challenge the underlying implications of death as applied to the brain. The brain's active (metabolic) and passive (non-metabolic) functions are, here, hypothesized to interact in such a way that together they produce synergistic functions. Death, however, strips the brain of its active functions entirely, leaving a passive filter in its wake with heretofore uncharacterized potential.

Thesis Hypothesis and Objectives

Hypothesis

I hypothesize that post-mortem brains, preserved chemically by process of fixation, will elicit basic functions insofar as their structural integrity is maintained. The hypothesis is based upon the general principle of anatomy and physiology which posits that structure determines function. Fixed post-mortem brains, by dint of their structural integrity alone, are likely able to interact with electromagnetic fields (and electric current applied directly) non-trivially, eliciting regionally-dependent microvolt fluctuations at the tissue-level which may or may not be modulated by chemical probes applied to the surface of the

specimens. The proposed hypothesis treats fixed, post-mortem neural tissue as a material substrate rather than a reanimated biological organ. That is, fixed brains are hypothesized to represent static though structurally complex objects which filter signals by way of intact, three-dimensional pathways which can perhaps be ordered by conductance or properties of “least-resistance”.

Objectives

The objective of this work is to develop a method by which residual functional capacities can be detected in post-mortem brains which have been preserved chemically. We will apply regional injections of alternating current, patterned electromagnetic fields, neurochemical probes, ionic manipulations (pH), and other energetic stimuli to elicit regional changes to the frequency-dependent microvolt fluctuations within preserved brain specimens. We will have achieved success if we can 1) demonstrate meaningful signals in the tissue which respond to external applications of stimuli, 2) demonstrate cytoarchitectural preservation by unique regional output of microvolt fluctuations, 3) demonstrate the brain’s capacity to selectively filter electrical and chemical probes, 4) isolate conditions or regions of the brain which are less affected by our manipulations than others, 5) demonstrate “responses” which can be correlated to behaviour or events during the life of the organism, and 6) demonstrate the brain’s capacity to interact with or draw upon environmental, electromagnetic energy – to function by filtration in the absence of endogenous energy production: an antenna that once could think.

References

American Clinical Neurophysiology Society (2006). Guideline 3: minimum technical standards for EEG recording in suspected cerebral death. Journal of Clinical Neurophysiology. 23:97-104.

Amunts, K., Kedo, O., Kindler, M., Pieperhoff, P., Mohlberg, H., Shah, N. J., ... & Zilles, K. (2005). Cytoarchitectonic mapping of the human amygdala, hippocampal region and entorhinal cortex: intersubject variability and probability maps. Anatomy and embryology, 210(5-6), 343-352.

Aw, S., & Levin, M. (2009). Is left-right asymmetry a form of planar cell polarity?. Development, 136(3), 355-366.

Azevedo, F. A., Carvalho, L. R., Grinberg, L. T., Farfel, J. M., Ferretti, R. E., Leite, R. E., ... & Herculano-Houzel, S. (2009). Equal numbers of neuronal and nonneuronal cells make the human brain an isometrically scaled-up primate brain. Journal of Comparative Neurology, 513(5), 532-541.

Bailey, P., & Davis, E. W. (1942). Effects of Lesions of the Periaqueductal Gray Matter in the Cat∗. Proceedings of the Society for Experimental Biology and Medicine, 51(2), 305-306.

Bark, I. C., & Wilson, M. C. (1994). Regulated vesicular fusion in neurons: snapping together the details. Proceedings of the National Academy of Sciences, 91(11), 4621-4624.

Bartelmann, M., & Schneider, P. (2001). Weak gravitational lensing. Physics Reports, 340(4), 291-472.

Bjorksten, J. (1951). Cross linkages in protein chemistry. Advances in Protein Chemistry, 6, 343-381.

Blackman, C. F., Benane, S. G., Elliott, D. J., House, D. E., & Pollock, M. M. (1988). Influence of electromagnetic fields on the efflux of calcium ions from brain tissue in vitro: A three-model analysis consistent with the frequency response up to 510 Hz. Bioelectromagnetics, 9(3), 215-227.

Blanke, O., Landis, T., Spinelli, L., & Seeck, M. (2004). Out-of-body experience and autoscopy of neurological origin. Brain, 127(2), 243-258.

Blatt, G. J., Pandya, D. N., & Rosene, D. L. (2003). Parcellation of cortical afferents to three distinct sectors in the parahippocampal gyrus of the rhesus monkey: an anatomical and neurophysiological study. Journal of Comparative Neurology, 466(2), 161-179.

Bliss, T. V., & Collingridge, G. L. (1993). A synaptic model of memory: long-term potentiation in the hippocampus. Nature, 361(6407), 31.

Bodian, D. (1951). A note on nodes of ranvier in the central nervous system. Journal of Comparative Neurology, 94(3), 475-483.

Born, M. (1934). On the quantum theory of the electromagnetic field. Proceedings of the Royal Society of London. Series A, Containing Papers of a Mathematical and Physical Character, 143(849), 410-437.

Braak, H., & Braak, E. (1992). The human entorhinal cortex: normal morphology and lamina-specific pathology in various diseases. Neuroscience research, 15(1), 6-31.

Brandtzaeg, P. (1974). Mucosal and glandular distribution of immunoglobulin components: immunohistochemistry with a cold ethanol-fixation technique. Immunology, 26(6), 1101.

Cameron, D. F., Othberg, A. I., Borlongan, C. V., Rashed, S., Anton, A., Saporta, S., & Sanberg, P. R. (1997). Post-thaw viability and functionality of cryopreserved rat fetal brain cells cocultured with Sertoli cells. Cell transplantation, 6(2), 185-189.

Carpenter, M. B., & Sutin, J. (1983). Chapter 19: The Cerebral Cortex. In Human neuroanatomy. Williams & Wilkins, Baltimore, MD, 643-706.

Cherry, N. J. (2003). Human intelligence: the brain, an electromagnetic system synchronised by the Schumann Resonance signal. Medical Hypotheses, 60(6), 843-844.

Churchland, P. M. (1985). Reduction, qualia, and the direct introspection of brain states. The Journal of Philosophy, 82(1), 8-28.

Clements, J. D., Lester, R. A., Tong, G., Jahr, C. E., & Westbrook, G. L. (1992). The time course of glutamate in the synaptic cleft. SCIENCE-NEW YORK THEN WASHINGTON-, 258, 1498-1498.

Creutzfeldt, O. D. (1977). Generality of the functional structure of the neocortex. Naturwissenschaften, 64(10), 507-517.

Crosby, E. C., Humphrey, T., & Lauer, E. W. (1962). Correlative anatomy of the nervous system, Ch 7, Telencephalon, Pt 2, Subcortical telencephalic nuclei. pp. 356-393.

Douglas, M. P., & Rogers, S. O. (1998). DNA damage caused by common cytological fixatives. Mutation Research/Fundamental and Molecular Mechanisms of Mutagenesis, 401(1), 77-88.

Eder, S. H., Cadiou, H., Muhamad, A., McNaughton, P. A., Kirschvink, J. L., & Winklhofer, M. (2012). Magnetic characterization of isolated candidate vertebrate magnetoreceptor cells. Proceedings of the National Academy of Sciences, 109(30), 12022-12027.

Facco, E., & Agrillo, C. (2012). Near-death experiences between science and prejudice. Frontiers in human neuroscience, 6, 209.

Farr, A. G., & Nakane, P. K. (1981). Immunohistochemistry with enzyme labeled antibodies: a brief review. Journal of immunological methods, 47(2), 129-144.

Floderus, B., Persson, T., Stenlund, C., Wennberg, A., Öst, Å., & Knave, B. (1993). Occupational exposure to electromagnetic fields in relation to leukemia and brain tumors: a case-control study in Sweden. Cancer Causes and Control, 4(5), 465-476.

Furukawa, K., Barger, S. W., Blalock, E. M., & Mattson, M. P. (1996). Activation of Kpositive channels and suppression of neuronal activity by secreted beta-amyloid-precursor protein. Nature, 379(6560), 74.

Gibson, K. R. (1988). Brain size and the evolution of language. The genesis of language: A different judgement of evidence, 149-72.

Hawkins, J., & Ahmad, S. (2016). Why neurons have thousands of synapses, a theory of sequence memory in neocortex. Frontiers in neural circuits, 10.

Huguenard, J. R. (1996). Low-threshold calcium currents in central nervous system neurons. Annual review of physiology, 58(1), 329-348.

Kew, J. N., & Kemp, J. A. (2005). Ionotropic and metabotropic glutamate receptor structure and pharmacology. Psychopharmacology, 179(1), 4-29.

Kiernan, J. A. (2000). Formaldehyde, formalin, paraformaldehyde and glutaraldehyde: what they are and what they do. Microscopy Today, 1(5).

Kirschvink, J. L., Walker, M. M., & Diebel, C. E. (2001). Magnetite-based magnetoreception. Current opinion in neurobiology, 11(4), 462-467.

Klinger, H. P., & Ludwig, K. S. (1957). A universal stain for the sex chromatin body. Stain technology, 32(5), 235-244.

Koshland, D. E. (1995). The key–lock theory and the induced fit theory. Angewandte Chemie International Edition in English, 33(23-24), 2375-2378.

Kumar, N. M., & Gilula, N. B. (1996). The gap junction communication channel. Cell, 84(3), 381-388.

Llinas, R., Ribary, U., Contreras, D., & Pedroarena, C. (1998). The neuronal basis for consciousness. Philosophical Transactions of the Royal Society of London B: Biological Sciences, 353(1377), 1841-1849.

Lutz, A., & Thompson, E. (2003). Neurophenomenology integrating subjective experience and brain dynamics in the neuroscience of consciousness. Journal of consciousness studies, 10(9-10), 31-52.

Marg, E., & Rudiak, D. (1994). Phosphenes induced by magnetic stimulation over the occipital brain: description and probable site of stimulation. Optometry & Vision Science, 71(5), 301-311.

McFadden, J. (2007). Conscious electromagnetic (CEMI) field theory. NeuroQuantology, 5(3).

Morth, J. P., Pedersen, B. P., Toustrup-Jensen, M. S., Sørensen, T. L. M., Petersen, J., Andersen, J. P., ... & Nissen, P. (2007). Crystal structure of the sodium–potassium pump. Nature, 450(7172), 1043-1049.

Nagel, T. (1974). What is it like to be a bat?. The philosophical review, 83(4), 435-450.

Neher, E., & Sakaba, T. (2008). Multiple roles of calcium ions in the regulation of neurotransmitter release. Neuron, 59(6), 861-872.

Norton, L., Gibson, R. M., Gofton, T., Benson, C., Dhanani, S., Shemie, S. D., ... & Young, G. B. (2016). Electroencephalographic Recordings During Withdrawal of Life-Sustaining Therapy Until 30 Minutes After Declaration of Death. Canadian Journal of Neurological Sciences, 1-7.

Nunez, P. L., & Cutillo, B. A. (Eds.). (1995). Neocortical dynamics and human EEG rhythms. Oxford University Press, USA.

Nunez, P. L., & Srinivasan, R. (2006). Electric fields of the brain: the neurophysics of EEG. Oxford University Press, USA.

Oviedo, N. J., Morokuma, J., Walentek, P., Kema, I. P., Gu, M. B., Ahn, J. M., ... & Levin, M. (2010). Long-range neural and gap junction protein-mediated cues control polarity during planarian regeneration. Developmental biology, 339(1), 188-199.

Palay, S. L. (1956). Synapses in the central nervous system. The Journal of biophysical and biochemical cytology, 2(4), 193.

Papez, J. W. (1956). Central reticular path to intralaminar and reticular nuclei of thalamus for activating EEG related to consciousness. Electroencephalography and clinical neurophysiology, 8(1), 117-128.

Parvizi, J., & Damasio, A. (2001). Consciousness and the brainstem. Cognition, 79(1), 135-160.

Persinger, M. A. (2014). Quantitative convergence between physical-chemical constants of the proton and the properties of water: implications for sequestered magnetic fields and a universal quantity. International Letters of Chemistry, Physics and Astronomy, 2, 1-10.

Persinger, M. A., Dotta, B. T., Saroka, K. S., & Scott, M. A. (2013). Congruence of energies for cerebral photon emissions, quantitative EEG activities and~ 5 nT changes in the proximal geomagnetic field support spin-based hypothesis of consciousness. Journal of Consciousness Exploration & Research, 4(1).

Persinger, M. A., & Koren, S. A. (2007). A theory of neurophysics and quantum neuroscience: implications for brain function and the limits of consciousness. International Journal of Neuroscience, 117(2), 157-175.

Persinger, M. A., Ludwig, H. W., & Ossenkopp, K. P. (1973). Psychophysiological effects of extremely low frequency electromagnetic fields: a review. Perceptual and motor skills, 36(3 suppl), 1131-1159.

Pichugin, Y., Fahy, G. M., & Morin, R. (2006). Cryopreservation of rat hippocampal slices by vitrification. Cryobiology, 52(2), 228-240.

Planck, M. (1901). On the law of distribution of energy in the normal spectrum. Annalen der Physik, 4(553), 1.

Radanov, S., Stoev, S., Davidov, M., Nachev, S., Stanchev, N., & Kirova, E. (1992). A unique case of naturally occurring mummification of human brain tissue. International journal of legal medicine, 105(3), 173-175.

Rodrıguez, F., López, J. C., Vargas, J. P., Broglio, C., Gómez, Y., & Salas, C. (2002). Spatial memory and hippocampal pallium through vertebrate evolution: insights from reptiles and teleost fish. Brain research bulletin, 57(3), 499-503.

Saroka, K. S., Caswell, J. M., Lapointe, A., & Persinger, M. A. (2014). Greater electroencephalographic coherence between left and right temporal lobe structures during increased geomagnetic activity. Neuroscience Letters, 560, 126-130.

Saroka, K. S., Dotta, B. T., & Persinger, M. A. (2013). Concurrent photon emission, changes in quantitative brain activity over the right hemisphere, and alterations in the proximal geomagnetic field while imagining white light. International Journal of Life Science and Medical Research, 3(1), 30.

Saroka, K. S., Vares, D. E., & Persinger, M. A. (2016). Similar spectral power densities within the Schumann resonance and a large population of quantitative electroencephalographic profiles: supportive evidence for Koenig and Pobachenko. PloS one, 11(1), e0146595.

Saroka, K. S., & Persinger, M. A. (2014). Quantitative evidence for direct effects between earth-ionosphere Schumann resonances and human cerebral cortical activity. International Letters of Chemistry, Physics and Astronomy, 20.

Shewmon, D. A., Holmes, G. L., & Byrne, P. A. (1999). Consciousness in congenitally decorticate children: developmental vegetative state as self-fulfilling prophecy. Developmental Medicine & Child Neurology, 41(6), 364-374.

Sledzik, P. S., & Micozzi, M. S. (1996). Autopsied, Embalmed, and Preserved Human Remains. In Forensic Taphonomy: The Postmortem Fate of Human Remains. CRC Press.

Strömgren, B. (1939). The Physical State of Interstellar Hydrogen. The Astrophysical Journal, 89, 526.

Stuss, D. T., Picton, T. W., & Alexander, M. P. (2001). Consciousness, self-awareness, and the frontal lobes.

Tart, C. T. (1972). States of consciousness and state-specific sciences. Science, 176(4040), 1203-1210.

Tsang, E. W., Koren, S. A., & Persinger, M. A. (2004). Power increases within the gamma range over the frontal and occipital regions during acute exposures to cerebrally counterclockwise rotating magnetic fields with specific derivatives of change. International Journal of Neuroscience, 114(9), 1183-1193.

Tuszyński, J. A., Hameroff, S., Satarić, M. V., Trpisova, B., & Nip, M. L. A. (1995). Ferroelectric behavior in microtubule dipole lattices: implications for information processing, signaling and assembly/disassembly. Journal of Theoretical Biology, 174(4), 371-380.

Ueno, S., Matsuda, T., & Fujiki, M. (1990). Functional mapping of the human motor cortex obtained by focal and vectorial magnetic stimulation of the brain. IEEE Transactions on Magnetics, 26(5), 1539-1544.

Vass, A. A. (2001). Beyond the grave-understanding human decomposition. Microbiology today, 28, 190-193.

Vierbuchen, T., Ostermeier, A., Pang, Z. P., Kokubu, Y., Südhof, T. C., & Wernig, M. (2010). Direct conversion of fibroblasts to functional neurons by defined factors. Nature, 463(7284), 1035-1041.

Vrba, J., & Robinson, S. E. (2001). Signal processing in magnetoencephalography. Methods, 25(2), 249-271.

Watt, D. F. (2000). The centrecephalon and thalamocortical integration: neglected contributions of periaqueductal gray. Consciousness & Emotion, 1(1), 91-114.

Whittall, K. P., Mackay, A. L., Graeb, D. A., Nugent, R. A., Li, D. K., & Paty, D. W. (1997). In vivo measurement of T2 distributions and water contents in normal human brain. Magnetic Resonance in Medicine, 37(1), 34-43.

Zalc, B., & Colman, D. R. (2000). Origins of vertebrate success. Science, 287(5464), 271-271.

Zola-Morgan, S., Squire, L. R., & Amaral, D. G. (1986). Human amnesia and the medial temporal region: enduring memory impairment following a bilateral lesion limited to field CA1 of the hippocampus. Journal of Neuroscience, 6(10), 2950-2967.

Zola-Morgan, S., Squire, L. R., Amaral, D. G., & Suzuki, W. A. (1989). Lesions of perirhinal and parahippocampal cortex that spare the amygdala and hippocampal formation produce severe memory impairment. Journal of Neuroscience, 9(12), 4355-4370.

Chapter Transition: Quantifying Death

As discussed throughout the Introduction, one major impediment of neuroscientific research concerning phenomena surrounding brain death has been a comprehensive quantification of the death state. In order to measure the absence of something, it is often necessary to infer its boundaries by making observations at the periphery of the phenomenon or void. As such, we endeavoured to measure electric potential differences over the scalp of a human subject using electroencephalography and comparing these measurements to electric potentials obtained over analogous regions within a fixed, post-mortem brain. Needle-electrodes were inserted directly into superficial gyri along the convexities of an unsectioned human brain. Microvolt potentials were obtained and transformed to observe spectral content (i.e., the periodicity or frequency of the signal over time). Our quantitative approach indicated that the charge-based energy differential between the two systems is estimated to approach $2 \cdot 10^{-23}$ J – a value which is proximal to cosmic microwave background. Further calculations based upon the measurements indicated that this energy applied over the universal hydrogen line – a ubiquitous emission line observed throughout the cosmos due to hydrogen atom phenomena – produces a power value of 10^{-12} $W \cdot m^{-2}$. This value has been observed as ultra-weak photon emissions in countless living biological specimens. Our approach indicates that the death state can be quantified energetically and related to physical phenomena tied to living cells. We also provide support for theories of consciousness which rely upon background forces by process of induction rather than endogenous expression.

Chapter 2:

Spatial-Temporal Quantitative Global Energy Differences Between the Living and Dead Human Brain

(Original Research)

Published in Journal of Behavioural and Brain Sciences,

Vol. 6, pp. 475 – 484, 2016

Nicolas Rouleau & Michael A. Persinger

DOI: 10.4236/jbbs.2016.612043

(Open Access)

Abstract

The dynamic differences between a living human brain and a clinically dead (fixed) human brain were measured over international Quantitative Electroencephalographic (QEEG) sites for 1 Hz increments between 1 Hz and 50 Hz. Although the expected greater power ($\mu V^2 \cdot Hz^{-1}$) for the living brain was apparent, the difference was particularly obvious for theta and low beta bands. The integrated square root values over the entire band indicated the difference in intrinsic charge-based energy between the living (higher) and dead brain was $\sim 2 \cdot 10^{-23}$ J. This quantity is remarkably proximal to the Cosmic Background Microwave value and would be consistent with the Hameroff-Penrose definition of consciousness that suggests a permeating presence derived from discrete physical events. A power value obtained by multiplying this increment of energy by the frequency of the universal hydrogen line resulted in $\sim 10^{-12}$ $W \cdot m^{-2}$ when applied to the surface area of the human cerebrum. This value is the median flux density that has been measured from human brains during cognition and defines the ultra-weak photon emissions displayed by cells, tissue, and organisms. These results suggest that modern technology may now be sufficiently precise to discern the critical parameters that differentiate the living brain from the fixed “dead” brain. This information might be useful for future designs of virtual consciousness and simulations within cerebral space.

Introduction

One of the basic principles of neuroscience is that structure determines function. The physical parameters that differentiate between the living human brain and the fixed, post-mortem human brain have not been explored thoroughly. Once the human brain is removed and fixed it is assumed to be “dead” and without the potential for dynamic properties. Recent technologies have allowed, for the first time, access to quantitative measures of sufficient density to assess these potential differences (Rouleau & Persinger, 2015; Rouleau & Persinger, 2016; Rouleau, Lehman & Persinger, 2016). In most sciences the contribution of a process or experimental manipulation requires a reference (a “control” group). We designed an experiment that would produce relatively artifact- free quantitative differences between the intrinsic electroencephalographic properties of a representative fixed human brain and that obtained from a representative living brain.

Historically the aggregate or field of electromagnetic patterns and the mosaic of chemical processes that define or can be employed to describe the living brain and its properties have not measured the quantitative differences between living and dead states from a holistic perspective. However if one approached the problem in a manner similar to the measurement of spontaneous photons where the actual measurements are subtracted from the dark counts that define the intrinsic circuitry of the photomultiplier unit (Persinger, Dotta, Karbowski & Murugan, 2015) then the actual increments of dynamic energy can be inferred. Here we demonstrate for the first time in the published literature that differences in potentials over the 1 Hz successive increments of the contemporary quantitative electroencephalography (QEEG) between a living and a dead human brain reveals a quantity of energy that might be central to understanding the universal values

that define “living and consciousness”. These quantities may have philosophical significance as well as application to the synthetic creation of simulated or virtual living and consciousness states.

Methods

The aim of the study was to investigate the frequency-dependent electric potential differences (μV) between gyri of a post-mortem, chemically fixed human brain and its basilar artery. Needle-electrodes were inserted into all major gyri of a post-mortem human brain. Power densities (PDs) measured in $\mu V^2 \cdot Hz^{-1}$ and compared to equivalent measures from the QEEG of a living brain. Relatively equal PDs as a function of frequency defines white noise. The measurements presented here are unevenly distributed across frequency bands and respond dynamically to applications of stimuli (Rouleau, Lehman & Persinger, 2016).

Fixed Human Brain Specimen

A human brain that had been maintained in ethanol-formalin-acetic acid for over 20 years was selected from a collection of specimens held within the Neuroanatomy Laboratory at Laurentian University. The full, unsectioned brain featured an intact brain stem, a complete cerebellum, and partially preserved vasculature. Major neuroanatomical features including typical fissures and lobular demarcations were well preserved. All of the major cerebral gyri and sulci outlined by Crosby, Humphrey, and Lauer (1962) were ap-parent. For the purposes of the study, only gyri which could be probed by the unimpeded insertion of a needle electrode (n= 52) were included in the analysis. Gyri of the human cerebrum can extend over considerable spatial distances. In this experiment

probes were only inserted into one point along a given gyrus. The fixed human brain, for the purposes of simplicity, was labelled the “Non-Living” and the person’s brain was labelled “Living”.

Measurement Device

A Mitsar 201 amplifier unit, typically used in quantitative electroencephalography, was coupled to five needle-electrodes. Four of the probes, which were inserted into the basilar artery of the human brain fixed in EFA, collectively served as the electrical reference point. The remaining probe was inserted serially into most gyri over the surface of the human brain. Electric potential differences (μV) were obtained and subsequently con-verted to spectral power densities ($\mu V^2 \cdot Hz^{-1}$) within SPSS v19 for segmentation into discrete bands: delta (1.5 Hz – 4 Hz), theta (4 Hz – 7.5 Hz), alpha (7.5 Hz – 14 Hz), beta1 (14 Hz – 20 Hz), beta2 (20 Hz – 30 Hz), and gamma (30 Hz – 40 Hz). The device was set to measure with a sampling rate of 250 Hz. Low- (1.5 Hz) and high-cut (50 Hz) filters were applied to reduce extraneous sources of electrical noise. An additional notch filter was applied to remove 60 Hz electrical artifacts.

Human QEEG Reference Point

QEEG data extracted from the brain of a living human participant was used as a reference point for the analysis. The case was selected from a database of QEEG profiles containing hundreds of individuals’ electroencephalograms (Saroka, Vares & Persinger, 2016) which were collected by the Neuroscience Research Group at Laurentian University. This Living brain met criteria which indicated that it was representative of the database. The mean normalized (z-scored) power densities within

all bands during QEEG recordings while the subject's eyes were closed did not exceed z = 2.00. There was no reported history of head injury or neuropathology. QEEG channels for the Living brain were those typically associated with the 10-20 International system of electrode placement. However, only channels which were situated over gyri which were probed within the Non-Living brain were retained for the analysis. The pairs are not perfectly superimposed in space, though their positions are proximal to within < 1 cm.

Protocol

Non-Living brain measurements consisted of 30 second recordings of raw microvolt potentials. Each measurement was preceded by a surface primer application of 10% EFA to prevent tissue from drying. Raw potentials were extracted and transferred to SPSS v19 for subsequent processing. Signals were z-transformed and spectral analysed. Data were then segmented into frequency bins.

Analysis

In addition to simple tests of differences between the magnitude of band-specific PDs between the Non-Living human brain and the Living brain, two other analyses were employed. The first analysis involved dimensional reduction. Factor analyses with varimax rotation were explored by loadings of all gyrus- (Non-Living) and channel-sourced (Living) PD profile time series. With maximum iterations set to 25, the factor analyses were performed within each QEEG band (i.e. delta, theta, alpha, beta1, beta2, and gamma). These analyses facilitated plotting of the numbers of factors which cumulatively explained the most amount of variance within each frequency band for both the Non-Living and Living brains.

The second analysis involved correlating time-independent, band-specific PDs obtained over left and right hemispheric homologous areas. Living and Non-Living brain data obtained at different times (T1 and T2) were extracted for contralateral pairs of channels and needle-electrodes. Data were normalized by z-transformation and spectral analysed. Power profiles for contralateral pairs of channels (Living) and needle-electrodes (Non-Living) were correlated within typical QEEG frequency bands (i.e. delta, theta, alpha, beta1, beta2, and gamma) as well as low- and high-frequency case-controlled (n= 254) band ranges (i.e. 1.5 Hz – 10 Hz and 31.5 Hz – 40Hz). We reasoned that strong correlations would indicate time-independent PD profile parity for contralateral pairs. This is an implicit measure of PD stability between hemispheric homologues over time. Alternatively, any reliable strong correlation between time-independent PD profiles for contralateral pairs could be considered as an indicator of high signal redundancy for the paired structures being directly probed or over which QEEG channels were positioned.

Results

Increased power densities ($\mu V^2 \cdot Hz^{-1}$) within all frequency bands were observed in the Living brain relative to those obtained within the needle-probed Non-Living brain with effect sizes (r^2) ranging between .26 and .90 (Figure 1A). On the other hand within the delta-band (1.5 Hz – 4 Hz) PDs of equivalent amplitudes were observed when parieto-occipital sources for Living (i.e. O1, O2, P3, and P4) and Non-Living (i.e. left and right occipital poles and superior parietal lobules) brains [$t(6)= -1.10$, $p= .31$] were compared as show in Figure 1B. These differences indicate that measurements obtained within the Living and Non-Living brains could be effectively discriminated based upon frequency-

dependent signal amplitudes. The exception was the caudal aggregates. The primary sources of variance were differences within theta, alpha, and beta1 bands.

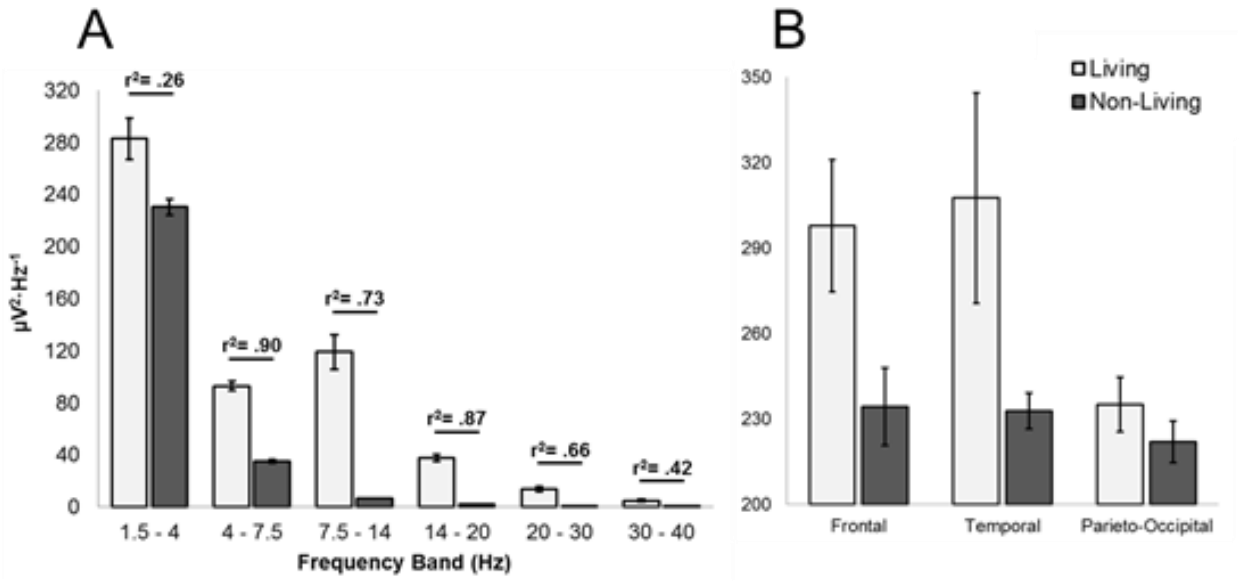

Figure 1. Living (light) and Non-Living (dark) PD differences as a function of frequency band for an aggregate of all channel-electrode matched measurements (A) as well as delta-band PDs for lobular aggregates (B).

When brain-surface-matched PD sources (e.g. Fp1 and the left superior frontal gyrus) were extracted into separate factor analyses for the Living and Non-Living brain, the resulting dimensional reduction profiles revealed a major distinction. The Living brain PD sources underwent less, relatively frequency-independent dimensional reduction as compared to the Non-Living brain (Figure 2A). In contrast, the Non-Living brain ex-pressed frequency-dependent dimensional reduction magnitudes where higher frequency PDs were associated with increased dimensional reduction. When all PD sources or gyri (n= 52) were entered into the factor analysis, a conspicuous, strong

positive relationship emerged between frequency and factors (r= .95, p<.005, rho = .93, p<.01), which is presented in Figure 2B.

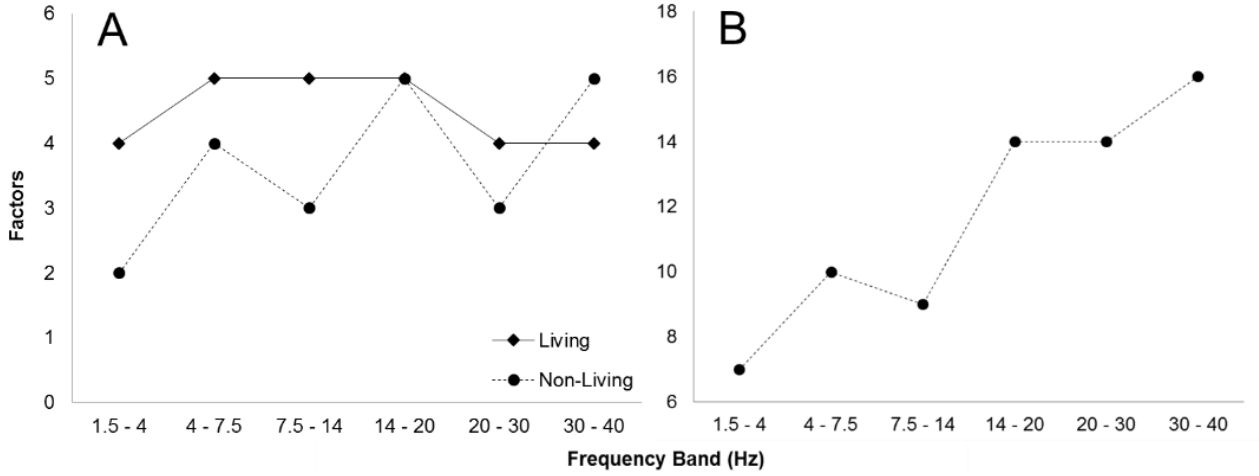

Figure 2. Living (squares) and Non-Living (circles) channel-electrode matched PD source (n= 14) factors within all frequency bands (A) as well as Non-Living PD source factors for all probed gyri (n= 52) within all frequency bands (B).

To eliminate the confounding factor of cases associated with each frequency band, factor analyses were performed within the 1.5 Hz – 10 Hz, 16.5 Hz – 25 Hz, and 31.5 Hz – 40 Hz. The three band ranges were case-matched (n= 254). They generated 4, 13, and 16 factors, respectively. This supported the anticipated positive relationship. These results suggest that for the Non-Living human brain, more factors were required to satisfy classification of PD sources at higher relative to lower frequencies – which points to greater spatially independent signal spectra as frequency increases. The gyri of the Non-Living brain displayed less spectral overlap with other gyri at higher frequencies within magnitudes comparable to the Living brain. Stated alternatively, the Living Brain

exhibited more spectral coherence within the higher electroencephalographic frequencies over larger (more integrative) cerebral areas.

The low-frequency (1.5 Hz – 10 Hz) case-controlled band range demonstrated in-creased correlations relative to the high-frequency (31.5 Hz – 40 Hz) range for both Living and Non-Living brains. However, correlations for the Living brain were (in a majority of cases) significantly weaker than those associated with the Non-Living brain when low-frequencies ($Fz > 1.96$, $p<.001$) were examined. One conspicuous overlapping feature consisted of clusters of strong correlations ($r > .80$) centering upon the fronto-temporal operculum for both the Living and Non-Living low-frequency bands. They were eliminated ($r \simeq 0$) at higher frequencies. It was apparent that the Living brain was subject to incidences of non-correlation over spatially diffuse regions within the high-frequency band (Figure 3). In contrast, the Non-Living brain expressed primarily fronto-temporal incidences of non-correlation (Figure 4). These representational maps suggest some gross overlap of time-independent PD profiles for paired sensors across hemispheres. Both the Living and Non-Living brains shared a degree of spatially clustered signal stability which was contingent, in both cases, upon frequency.

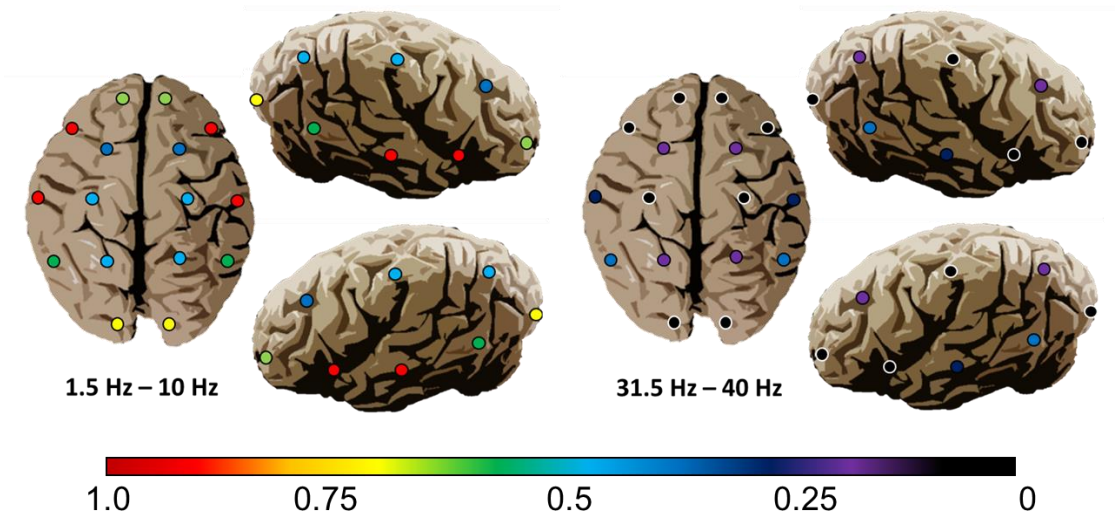

Figure 3. Representational maps of time-independent PD correlations (Pearson r) between contralateral homologous sensor pairs in a Living human brain for the 1.5Hz – 10 Hz and 31.5 Hz – 40 Hz bands. Non-correlations (p>.05) are indicated by black markers with white borders.

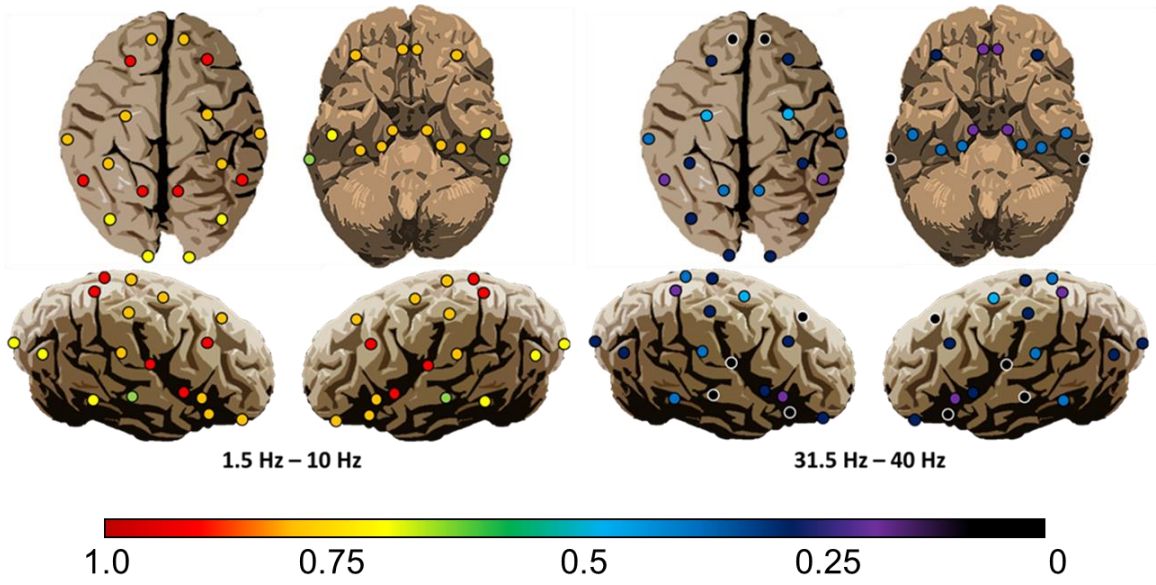

Figure 4. Representational maps of time-independent PD correlations (Pearson r) between contralateral homologous sensor pairs in a Non-Living human brain for the 1.5Hz

– 10 Hz and 31.5 Hz – 40 Hz bands. Non-correlations ($p>.05$) are indicated by black markers with white borders.

Discussion

The employment of a single test case representative of one population (a dead brain) compared to a case that is representative of another population (a living brain) might be considered anecdotal. However, this would not be the first instance in the history of neuroscience where a single case is representative. Classic examples include Broca's patient who demonstrated expressive aphasia and Alzheimer's female patient who exhibited the pre-senile manifestations of dementia. We suggest that the specific nature of the quantitative differences in power densities over different regions of the cerebrum and frequency bands in the present study may represent a real phenomenon separate and distinct from noise.

One of the advantages of physical sciences and quantitative measurements is that values can be obtained that reflect the phenomenon being studied. When the difference between the total power ($\mu V^2 \cdot Hz^{-1}$) for the Living and Non-Living (dead) brain were obtained a significant energy was apparent. The square root of the sum of the products of the averaged μV^2 per Hz multiplied by the numbers of 1 Hz integers within each frequency band for each band shown in Figure 1A results in 78 μV for the band between 1.5 Hz and 50 Hz.

When the differences for the powerful source from the 0.5 to 1.5 Hz band was added (26 μV), the Living brain was 104 μV higher over the 0.5 Hz to 50 Hz band compared to the dead brain. This would be similar to the transcerebral availability of 0.1

mV which is within the range of a miniature EPSP (Excitatory Postsynaptic Potential) (Suzue, Wu & Furukawa, 1987). Like photon measurements where direct photon counts are subtracted from background (dark) counts, this value could be considered the actual phenomena when the differences be-tween the two electrodynamic aggregates are obtained. Because the dead brain dis-played effectively similar values to those from other brains in our library (Rouleau & Persinger, 2016; Rouleau, Lehman & Persinger, 2016) and the Living brain was representative of the data base from living populations the quantitative value can be considered reliable.

If this assumption is valid, then the energy difference associated with “living and consciousness” relative to the “dead” organic substrate of fixed brains can be estimated. The product of $1.04 \cdot 10^{-4}$ V and $1.6 \cdot 10^{-19}$ A·s is $1.7 \cdot 10^{-23}$ J for the aggregate of process distributed over the 1 to 50 Hz band for the cerebrum. This energetic unit is significant from two perspectives. First, it is within error measurement of the cosmic background microwave (CBM) energy derived from temperature that permeates the universe (Penzias & Wilson, 1965). We speculate that the convergence of the energy associated with the difference between the living and dead brain and the CBM value could support the (Hameroff & Penrose, 1996) definition of conscious-ness. They have stated that “consciousness results from discrete physical events; such events have always existed in the universe as non-cognitive, proto-consciousness events, these acting as part of precise physical laws not yet fully understood” (Hameroff & Penrose, 2014). Contemporary consensus assumes CBM energy permeates the universe. If, as Mach’s principle indicates, any part of the Cosmos is determined by all of its parts (Sing, 1961), then some representation might be residual within the appropriately fixed cerebral matter.

There is some experimental evidence (Costa & Persinger, 2016) that might support this interpretation. In other words, background electromagnetic fields likely interact with brain matter in non-random ways.

The Hameroff-Penrose model of consciousness assumes a pervasive physical force which orders molecular as well as other biologically-relevant events and which can be measured as changing brain states. There is evidence to suggest that human brains are influenced by subtle environmental factors including perturbations in the Earth's electromagnetic field (Allahverdijev, Babayev, Khalilov & Gahramanova, 2001). Radiofrequency-induced calcium ion efflux has also been measured in brain tissue (Blackman, Elder, Weil, Banane, Eichinger & House, 1979). Hinrikus et al. (2005) demonstrated that microwave stimulation, known to induce vibration of charged particles and cellular membranes, produced in-creased EEG energy levels within human brains, particularly within the beta 1 band. The effects were non-thermal. The observations presented here indicated a discrete energetic difference between pre- and post-mortem brains which was within error term of CBM. Our hypothesis requires further substantiation by independent observers with similar or greater resources. The important discovery presented here is that modern electrophysiological technology and statistical methods might reveal hidden relationships that previously could not be systematically examined.

Several models and calculations have indicated the pervasiveness of a physical substrate to Hameroff and Penrose's depiction of consciousness would require a universal integrator. The most likely candidate is the neutral hydrogen line or precision frequency of the hydrogen atom which constitutes about 90% of the universe (Cameron, 1973). When the living-dead brain difference value of $1.7 \cdot 10^{-23}$ J for the energy difference

from the electrodynamics we measured here is multiplied by the hydrogen frequency ($1.42 \cdot 10^{9}$ s^{-1}), the result is ~$1.2 \cdot 10^{-14}$ W. When this power is divided by typical estimates of the cerebral cortical area (Van Essen & Drury, 1997), which is in the order of 10^{-2} m^2, the flux power density is 10^{-12} $W \cdot m^{-2}$.

Approximately one picoWatt per meter squared is the consistent value for photon flux density measured by many researchers as the central value from living systems that include bacteria, cells, hippocampal slices, and whole brain sections (Gurwitsh, 1988; Persinger, 2016). The potential connection to cognition was reported by Dotta et al (2012) who instructed volunteers who were sitting in very dark rooms to think about white light or mundane ideation over several trials. Photonic energy was measured either as flux density by analogue photo-multiplier tubes or numbers of photons by digital photomultiplier units placed approximately 15 cm from the right hemisphere at the level of the temporal lobe. The quantitative relationships between this magnitude of photon flux density and energies intrinsic to action potentials and related physical substrates to "consciousness" have been consistently convergent (Persinger, 2015).

When the subjects were engaging in imagery and imagination the increased output of photon flux density from the right hemisphere was ~10^{-12} $W \cdot m^{-2}$. The magnitude of the output was correlated >0.9 with the higher frequency QEEG power from the left prefrontal region. Subsequent experiments by Costa et al (2016) strongly suggested that the gradient of photon emissions from the human brain were temporally coupled to mediation through the thin (400 to 800 nm) axons within the corpus callosum. Although we would expect substantial complexity in the physical substrates of the living human brain and consciousness the fact that quantitative values for the simple difference

between the living brain and the dead brain can be measured so simply may open new perspectives.

One experiment, which would serve as verification of our measurements and provide a detailed understanding of the intermediates between the living and post-mortem brain states presented here, would involve the measurement of fresh human brains after autopsy with subsequent longitudinal measures including data collection post-fixation. We do not possess the facilities or equipment to conduct the serial measurements on fresh cadavers, though human brains can be substituted for animal models assuming common mechanisms.

References

Allahverdijev, A. R., Babayev, E. S., Khalilov, E. N., & Gahramanova, N. N., (2001). Possible space weather influence on functional activity of the human brain. In Proc. Space Weather Workshop: Looking towards a European Space Weather Programme (pp. 17-19).

Blackman, C.F., Elder, A., Weil, C.M., Benane, S.G., Eichinger, D.C., & House, D.E., (1979). Induction of calcium-ion efflux from brain tissue by radio-frequency radiation: Effects of modulation frequency and field strength. Radio Science, 14(65), 93-98.

Cameron, A. G., (1973). Abundances of the elements in the solar system. Space Science Reviews, 15(1), 121-146.

Costa, J. N., Dotta, B. T. & Persinger, M. A., (2016). Lagged coherence of photon emissions and spectral power densities between the cerebral hemispheres of human subjects during rest conditions: phase shift and quantum possibilities. World Journal of Neuroscience, 6, 119-125.

Costa, J. N. and Persinger, M. A., (2016). A possible flux density value of 10^{-12} $W \cdot m^{-2}$ for “spontaneous” photon emissions in fixed human brain tissue: was Spinoza correct? Research in Neuroscience, 5, 10-14.

Crosby E.C., Humphrey T., Lauer E.W., (1962). Chapter 7 Telecephalon, Part 1-Gross structure of the telencephalon, Correlative anatomy of the nervous system, New York: Macmillan, 343-355.

Dotta, B. T., Saroka, K. S., & Persinger, M. A., (2012). Increased photon emission from the head while imagining light in the dark is correlated with changes in electroencephalographic power: Support for Bókkon's Biophoton Hypothesis. Neuroscience Letters, 513(2), 151-154.

Gurwitsch, A. A., (1988). A historical review of the problem of mitogenetic radiation. Experientia, 44(7), 545-550.

Hameroff, S., & Penrose, R., (2014). Consciousness in the universe: A review of the ‘Orch OR’theory. Physics of life reviews, 11(1), 39-78.

Hameroff, S., & Penrose, R., (1996). Orchestrated reduction of quantum coherence in brain microtubules: A model for consciousness. Mathematics and Computers in Simulation, 40(3), 453-480.

Hinrikus, H., Bachmann, M., Tomson, R., & Lass, J., (2005). Non-thermal effect of microwave radiation on human brain. Environmentalist, 25(2-4), 187-194.

Penzias, A. A., & Wilson, R. W., (1965). A Measurement of Excess Antenna Temperature at 4080 Mc/s. The Astrophysical Journal, 142, 419-421.

Persinger, M. A., (2016). Spontaneous photon emissions in photoreceptors: potential convergence of Arrhenius reactions and the latency for rest mass photons to accelerate to Planck unit energies. Journal of Advances in Physics, 11, 3529-3537.

Persinger, M. A., (2015). The Prevalence and Significance of~ 10^{-20} J and~ 10^{-12} W* m^{-2} as Convergent/Divergent Nodal Units In the Universe. International Letters of Chemistry, Physics and Astronomy, 61, 94-100.

Persinger, M. A., (2013). Experimental evidence that Hubble's parameter could be reflected in local physical and chemical reactions: support for Mach's Principle of Imminence of the Uni-verse. International Letters of Chemistry, Physics and Astronomy, 11, 86-92.

Persinger, M.A., Dotta, B.T., Karbowski, L.M., and Murugan, N.J. (2015). Inverse relationship between photon flux densities and nanoTesla magnetic fields over cell aggregates: quantitative evidence for energetic conversion. FEBS OpenBio, 5, 413-418.

Rouleau, N., Lehman, B., & Persinger, M.A. (2016). Focal attenuation of specific electroencephalographic power over the right parahippocampal region during

transcerebral copper screening in living subjects and hemispheric asymmetric voltages in fixed brain tissue. Brain Research, 1644, 267-277.

Rouleau, N. & Persinger, M.A. (2015). Enhancement of Theta and Gamma Activity Power Within Fixed Sections of Human Brains Stimulated by Sean Harribance's Electroencephalographic Configuration: Is He Equivalent to a "Universal Donor" for Entanglement?. NeuroQuantology, 13(4).

Rouleau, N. & Persinger, M.A. (2016). Differential responsiveness of the right parahippocampal region to electrical stimulation in fixed human brains: Implications for historical surgical stimulation studies?. Epilepsy & Behavior, 60, 181-186.

Saroka, K. S., Vares, D. E., & Persinger, M. A., (2016). Similar Spectral Power Densities Within the Schumann Resonance and a Large Population of Quantitative Electroencephalographic Profiles: Supportive Evidence for Koenig and Pobachenko. PloS one, 11(1).

Singh, J., (1961). Great ideas and theories of modern cosmology. Dover: N.Y.

Suzue, T., Wu, G. B., & Furukawa, T., (1987). High susceptibility to hypoxia of afferent synaptic transmission in the goldfish sacculus. Journal of Neurophysiology, 58(5), 1066-1079.

Van Essen, D. C., & Drury, H. A., (1997). Structural and functional analyses of human cerebral cortex using a surface-based atlas. The Journal of Neuroscience, 17(18), 7079-7102.

Chapter Transition: Electrical Asymmetry

The previous chapter indicated that electric potentials could be obtained from fixed, post-mortem human brain tissue and systematically compared to values obtained from living, human participants. The following chapter explores the role of specific subsections of the tissue to expressions of left-right electrical asymmetry of proportions of signal periodicity as well as a mechanism by which quantitative electroencephalographic signals can be attenuated using transcerebral copper screening. The chapter demonstrates that living human “brain waves” are subject to suppressed magnitude when the space surrounding the electrodes are covered in a copper mesh. The data also indicate that the right parahippocampal region was most affected by the screening method. Coronal sections of fixed, post-mortem brain tissue were then measured to highlight intrinsic discrepancies between the left and right hemispheres as a function of periodic signal expression. We noted that the right parahippocampal region was most anomalous and that general rostro-caudal, left-right full brain anisotropies could be detected. These fixed electrical states are discussed in terms of their relevance to brain structure and function in general. Our observations are consistent with other studies which suggest that the right parahippocampal region is sensitive to extra-cerebral sources of electromagnetic energy. The copper mesh screening method demonstrates that there are environmental contributions of noise to either the electroencephalograph as a tool or the object of measurement – though the latter is most probable as regions of tissue are unequally affected. These experiments highlight further avenues which can be pursued with respect to the structure and function of post-mortem brain tissue.

Chapter 3:

Focal Attenuation of Specific Electroencephalographic Power Over the Right Parahippocampal Region During Transcerebral Copper Screening in Living Subjects and Hemispheric Asymmetric Voltages in Fixed Coronal Sections

(Original Research)

Published in Brain Research, Vol. 1644, pp. 267 – 277, 2016

Nicolas Rouleau, Brendan Lehman,

& Michael A. Persinger

DOI: 10.1016/j.brainres.2016.05.034.

Abstract

Covering the heads of human volunteers with a toque lined with copper mesh compared to no mesh resulted in significant diminishments in quantitative electroencephalographic power within theta and beta-gamma bands over the right caudal hemisphere. The effect was most evident in women compared to men. The significant attenuation of power was verified by LORETA (low resolution electromagnetic tomography) within the parahippocampal region of the right hemisphere. Direct measurements of frequency-dependent voltages of coronal section preserved in ethanol-formalin-acetic acid from our human brain collection revealed consistently elevated power (0.2 $\mu V^2 \cdot Hz^{-1}$) in right hemispheric structures compared to left. The discrepancy was most pronounced in the grey (cortical) matter of the right parahippocampal region. Probing the superficial convexities of the cerebrum in an unsectioned human brain demonstrated rostrocaudal differences in hemispheric spectral power density asymmetries, particularly over caudal and parahippocampal regions, which were altered as a function of the chemical and spatial contexts imposed upon the tissue. These results indicate that the heterogeneous response of the human cerebrum to covering of the head by a thin conductor could reflect an intrinsic structure and unique electrical property of the (entorhinal) cortices of the right caudal hemisphere that persists in fixed tissue.

Introduction

One of the basic assumptions for biological systems and of the human brain as a subset of these systems is that structure dictates function and hence microstructure determines microfunction. As quantitative precision and instruments have evolved over the centuries the presumed homogeneity of structure within the cerebral volume has been modified to accommodate this “complex heterogeneity”. For example with the development of flat-mapping and the application of non-linear geometries to the sulcal and gyral patterns, the relative absence of geometric similarity between the left and right hemispheres of the human cerebrum was visualized. In 1997 Van Essen and Drury showed that of the ~80 “folding patterns” discernable in both hemispheres only four (pairs): the central sulcus, Sylvian fissure on the lateral side, the calcarine fissure on the medial side and the cingulate sulcus, were in similar locations. The others exhibited asymmetries. For example the posterior inferior temporal sulcus showed a y-shaped pattern in the right hemisphere but a single linearity in the left. With such propensity for structural anisotropy one would expect a geometric-based potential difference (voltage) that is likely to be frequency-dependent.

Quantitative electroencephalograph (qEEG) and the complex algorithms applied to these data have reiterated the heterogeneity of power densities for inferences of potential differences (voltages) measured a few cm over the cerebral surface as well as the time-dependent alterations in those patterns. The slightly larger voltage measures within the alpha frequency (8-13 Hz) range over the caudal right hemisphere compared to other brain regions which were evident in the days of strip-chart recordings (Morgan, McDonald & Macdonald, 1971), has been enhanced and differentiated. The

enhancements can occur over larger regions of the cerebral surface. For example the trans-surface microstate analyses described by Lehmann (1990) and developed by Koenig et al (2002) revealed the remarkable stability of these states, some of which are hemispherically asymmetric or “diagonally connected”, over people’s lifetimes. Inferences of three dimensional dynamic structure, as inferred by LORETA (low resolution electromagnetic tomography), have allowed discernment of intrinsic differences in regional displays of current density coupled to specific frequency bands.

Although there has been substantial documentation concerning the quantitative properties of cerebral structure and function during rest states or those associated with cognitive challenges, the response of cerebral activity to proximal physical boundaries such as conductors has been less frequently pursued. However metallic helmets and other containments for the human head could potentially affect not only measurements but cerebral function. Here we present evidence that when normal people wear a head-covering lined with copper mesh compared to the same covering without copper mesh, a local attenuation of power within specific frequency bands occurred only over the right caudal area. LORETA analyses indicated the region involved was centralized around and within the right parahippocampal region.

This region is very significant because it contains the entorhinal cortices (Pruessner et al., 2002) which is the primary input to the hippocampal formation whose function is important for the initial stages of representation of experiences or memory (Van Strien, Cappaert & Wittler, 2009; Witter, 1993). The area is known structurally for its multimodal integration of information from and to the entire neocortices and for the unusual stellate cells (the stratum stellar of Stephan) that contains pace-maker neurons

that continually generate 8 Hz oscillations with peak-to-peak changes of a few mV (Alonso & Klink, 1993). Interestingly, the energy associated with this increment is remarkably congruent with Landauer's threshold when 1 bit of information is dissipated to entropy or two operations converge (Saroka & Persinger, 2014). This region is also the area that has been directly correlated or inferred to be associated with weak increases in geomagnetic activity as well as simulations of that activity within the laboratory (Saroka, Caswell, Lapointe, & Persinger, 2014).

In this article we present the results that show electrophysiological activity within the right caudal hemisphere differentially responds to trans-cerebral "shielding". In addition, we found that direct measurements of coronal sections of human brains which had been maintained in ethanol-formalin-acetic acid for decades exhibited visible integrity of general cytological structure within the cerebral cortex revealed a consistent hemispheric anisotropy in potential difference with specific EEG related frequency bands. These increments included potential within the theta (4-7 Hz) band, sufficient to reflect resonance "circuits", within the grey matter (cortices) of the right parahippocampal region. Finally, and in consideration of the intra-cranial environment, we identified rostrocaudal asymmetries in frequency-dependent hemispheric spectral power density as well as spatial-chemical discriminant factors in a whole, unsectioned fixed brain.

Results

QEEG While Wearing Copper Screen-Line Toque

The presence of plates or surgical metals in some of our patients over the years produced conspicuous changes in strip-chart amplitudes and some frequency

modulation over the sites of implant. However the effects of covering the entire scalp with a conductor and then placing more modern sensor caps over the copper lining has not been employed routinely. A priori, one would expect some difference over the right caudal hemisphere in light of the well-known enhancement of alpha power over this region.

To test this hypothesis we custom-constructed two cloth coverings shaped like toques. One was lined with 28 gauge copper mesh such that when it was placed on the head the entire brain would be covered. The second identical toque contained no mesh. Following approval by the university's human ethics committee and signed consent a total of twelve men and women from university classes were recruited. Each subject sat within a comfortable arm chair that was housed within an acoustic chamber that was also a Faraday cage (13 m^3). The resultant geomagnetic field within the space was reduced from 45,000 nT to 20,000 nT (Persinger, Dotta, Karbowski, & Murugan, 2015). For the first or second half of the measurements each subject wore the wire lined toque or the control toque. The order was counterbalanced.

A Mitsar 19-channel Quantitative Electroencephalography (qEEG) system connected to a Lenovo ThinkPad laptop running Windows 7 logged electric potential difference from the surface of the scalp referenced to an average of sensors placed on the ears. The qEEG cap contained sensors positioned according to the 10 – 20 International System of Electrode Placement. A sodium-based electrogel was applied in order to establish a cap-scalp interface. Data were collected for 1 min when the subject's eyes were closed and for 1 min while the eyes were opened. Data were extracted as spectral power densities and uploaded to SPSS v20. All recording equipment was outside

the closed chamber and the only contact with the subject during the recording was through a lapel microphone.

The results were quantitatively evident. Aggregated potentials from the right caudal sensors (T6, P4, and O2) displayed a decrease in global power spectral density ($\mu V^2 \cdot Hz^{-1}$) during the copper-lined condition (M= 5.16, SE= 1.85) relative to the control condition (M= 5.98, SE= 2.08) when the participants' eyes closed, $t(11)=2.18$, $p=.05$. This was not measured for other cerebral regions and was not apparent in the right caudal sensors when the participants' eyes were open ($p>.05$).

To discern a specific frequency-band source for this effect, global power was separated into low frequency (1.5Hz – 14Hz) and high-frequency (14Hz – 40Hz) band ranges. The right caudal sensor cluster displayed a decrease in high-frequency $\mu V^2 \cdot Hz^{-1}$ during the copper-lined condition (M= 1.59, SE= .73) relative to the control condition (M= 1.91, SE= .81) when the participants' eyes were closed, $t(11)= 2.89$, $p<.05$. The contralateral sensor cluster (T5, P3, and O1) also demonstrated a comparable decrease of ~ 0.33 $\mu V^2 \cdot Hz^{-1}$ during the copper-lined condition relative to the control condition when for this band of high-frequencies, $t(11)= 2.37$, $p<.05$.

Inspection of the data revealed a conspicuous gender effect. When the females were removed from the analyses the significant decreases in power spectral densities observed during the copper-lined condition were effectively eliminated. Male subjects did not demonstrate decreases in power as a function of cap type within any sensor or band ($p>.05$). Average decreases of 0.60 $\mu V^2 \cdot Hz^{-1}$ within the high-frequency bands were observed for females during the copper-lined condition relative to control condition, $t(5)=4.41$, $p<.01$, $r^2= .80$. In other words for the female subjects wearing or not

wearing the copper toque accommodated 80% of the variance in the power variation within the high frequency band.

In addition a specific decrease in theta power over O2 was noted for females only during the copper-lined condition relative to control condition, $t(5)= 2.58$, $p=.05$. This decrease was equivalent to ~ 0.80 $\mu V^2 \cdot Hz^{-1}$. To discern if there was a finer increment of frequency, spectral frequencies within the theta band (4Hz – 7.5Hz) for the O2 sensor were split into 0.5 Hz increments. A significant decrease in spectral densities within the 5.5 Hz increment were noted during the copper-lined condition, $t(6)=5.41$, $p<.005$. The same 5.5 Hz increment was associated with a decrease in spectral densities over T6 during the copper-lined condition, $t(6)= 3.13$, $p<.05$. In summary a theta power diminishment occurred simply because copper mesh covered the entire skull in a region that is traditionally and frequently associated with indicators of changes in activity within the right parahippocampal region. Consequently we explored source-localization.

S-LORETA Measurements

Standardized low-resolution electromagnetic tomography (sLORETA) was employed as a neuroimaging technique in order to source-localize any potential differences between experimental conditions. Raw data were extracted in 15 second segments from WinEEG, converted to individual cross-spectral files, and further to sLORETA files. Within-subject comparisons were performed with 5000 randomizations and a variance smoothing parameter of 0. Current source densities (CSD) were computed within sLORETA software and uploaded to SPSS v20.

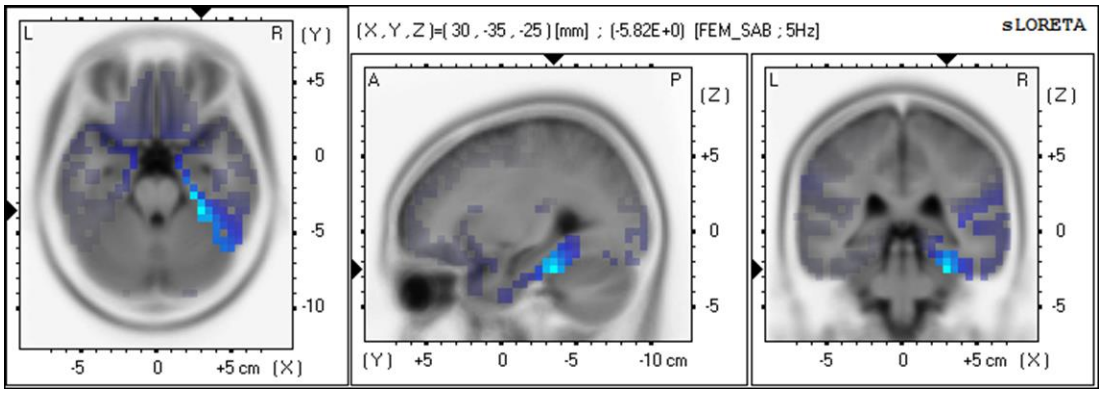

Figure 5. sLORETA tomogram showing decreased beta2 signals localized to the right fusiform gyrus. MNI coordinates (X,Y,Z): 30, -35, -25.

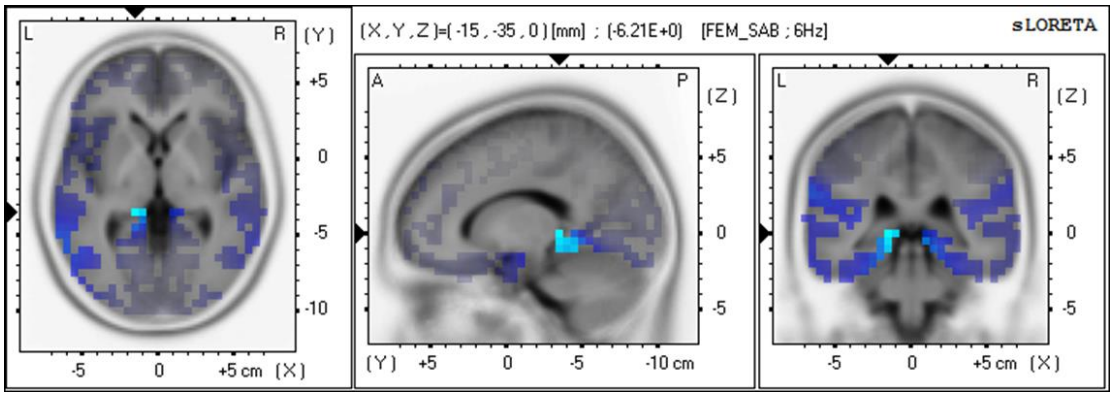

Figure 6. sLORETA tomogram showing decreased beta3 signals localized to the left parahippocampal gryus. MNI coordinates (X,Y,Z): -15, -35, 0.

sLORETA source-localized a decrease in beta2 and beta3 power for females only within the right fusiform gryus (Figure 5) and within the left parahippocampal gyrus (Figure 6) for the copper-lined condition relative to the control condition. Talairach Client Version 2.4.3 demonstrated the equivalent co-ordinates (X,Y,Z) were -15, -35, 0 corresponding to gray matter of Brodmann area 27. Whereas Brodmann area 27 is classically representative of the presubiculum, the low spatial resolution of sLORETA (~5 mm) would indicate involvement of the adjacent parahippocampal gyrus. Co-ordinates

30, -35, -25 were identified within a cubic range (± 4mm) of right parahippocampal gray matter. The bilateral decreases occurred within the identical position on the Y or rostrocaudal axis (-35). CSD values were extracted for MNI coordinates 30,-35,-25 (right fusiform gyrus) and -15,-35, 0 (left parahippocampal gyrus) from all participants in order to quantify differences as a function of the experimental condition. Descriptive statistics revealed an average CSD value of 5.63 for the control cap condition and a value of 3.90 for the copper-lined cap condition.

Potential Differences from Coronal Brain Sections

The results suggested that there may be something intrinsically unusual about the right parahippocampal region. This region shows unique surface topography that was labeled by Klinger according to Pierre Gloor (1997) as “verrucae gyri hippocampi”. They are repeated protrusions along the surface of the rostral component of this region that is primarily entorhinal cortices and are visualized histologically as lozener-shaped close clusters of cells with relatively cell free intermittent zones within Layer II. The stellate cells in this layer give rise to thick descending axons that form the principal component of the perforant pathway. The structure and connectivity of the entorhinal cortices is considered to be unique and different from any other cortical area.

As a component of the Advanced Human Neuroanatomy Laboratory for the Behavioural Neuroscience Program we have had about 9 human brains maintained in ethanol-formalin-acid acid (EFA) for the last 30 years. Six of these brains were obtained from North Carolina Biological Supply before the moratorium on sale of human tissue while another 3 were obtained from anonymous donors. Consequently there was no

specific information regarding the genders, the ages (although this can be inferred) or the times of termination of the specimen. Each brain was transferred immediately upon its arrival to its own plastic (Tupperware) container and immersed within EFA where it remained.

EFA stock consists of 75% ethanol, 15% distilled water, 5% formaldehyde, and 5% acetic acid. We have found that EFA is less harsh with the tissue over protracted periods than formalin only. In addition, histological analyses of cortical sections indicate that the cellular structures are intact even decades later. Figure 7 illustrates that the integrity of the fixed tissue stored in EFA for sample frontal cortical and hippocampal sections stained with toluidine blue O. Images A and C (400 x) show preserved polar orientation of the neural parenchyma while images B and D (1000 X oil) reveal a relatively gross preservation of cytomorphology including that of the nucleus with heavy staining of the nucleolus for most cells.

Coronal sections from three of the most intact brains were selected from our collection of human neuroanatomical tissue. It was critical that each slice should contain residual vasculature that remained structurally connected (for qEEG referencing) to the cerebrum. One hundred and six (n=106) anatomical features were probed using a single needle-probe. The probe was inserted into the locus of interest referenced to 4 needle-probes coupled to one of the major arterial offshoots of the Circle of Willis where electric potential differences were obtained. Two sections were referenced to the basilar artery and the third was referenced to the middle cerebral artery (MCA). Impedance values from vascular references were regulated to < 5kΩ. Sixty seconds of raw electric potential differences were obtained from each locus of interest. Recordings were classified by type

of matter (grey or white), hemisphere (left or right), and longitudinal position (rostral or caudal). All measurements were in the Neurochemistry/Neuroanatomy Laboratory.

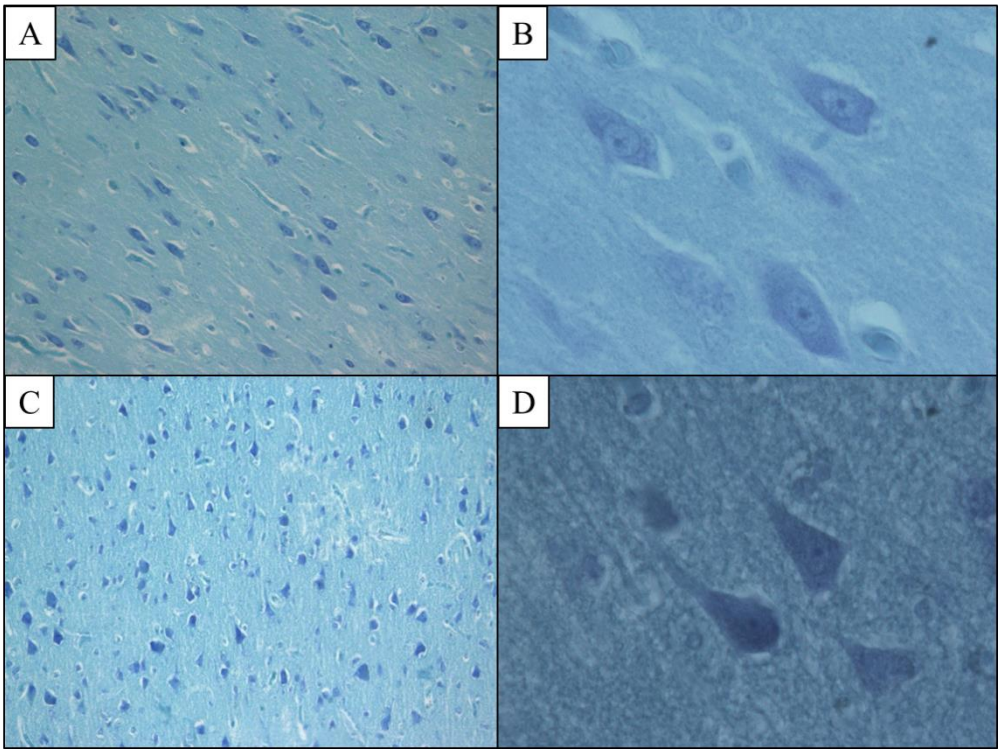

Figure 7. Cortical section from the frontal cortex at 400 (A) and 1000 (B) times magnification as well as hippocampal grey matter at 400 (C) and 1000 (D) times magnification. These human brains had been fixed in EFA after arrival from the source for more than 25 years before histological processing.

The results of the measurements between the left and right hemispheric structures are shown in Table 1. Increased power spectral density equivalent to 0.20 $\mu V^2 \cdot Hz^{-1}$ on average within the gamma band was identified within the right hemisphere (M= 1.31, SE= .10) relative to the left hemisphere (M=1.10, SE= .03), $t(82)= 2.01$, $p<.05$, $r^2= .05$. Other bands did not demonstrate similar hemispheric disparity ($p>.05$). Discriminant analysis involving power spectral density within all frequency bands predicting

longitudinal position accurately classified 67% of cases in a cross-validated model Λ=.77, $\chi 2(1)=18.14$, $p<.001$, canonical $R^2=.48$. Increased classification accuracy (69%) was noted if white matter structure were eliminated from the analysis.

Differences in power spectral density associated with all structures between coronal slices were identified within the delta ($p<.001$) and theta ($p<.005$) bands. Examining only white matter structures eliminated these differences. Only increases in delta power remained when isolating grey matter structures, $F(2,50)= 7.66$, $p=.001$.

Table 1. Left (L) and Right (R) Hemispheric General Structure Power Spectral Density ($\mu V^2 \cdot Hz^{-1}$) and Voltage (μV)

	Spectral Power Density ($\mu V^2 \cdot Hz^{-1}$)				Voltage (μV)			
	Gen - L (N= 44)		Gen - R (N=40)		Gen - L (N=44)		Gen - R (N=40)	
Band	Mean	SD	Mean	SD	Mean	SD	Mean	SD
Delta	132.11	33.75	131.17	35.40	18.17	9.19	18.11	9.41
Theta	38.55	10.62	38.59	10.68	11.62	6.10	11.62	6.11
Alpha	17.17	3.84	17.91	3.31	10.56	5.00	10.79	4.64
Beta1	4.63	1.80	5.21	2.97	5.27	3.29	5.59	4.22
Beta2	3.06	1.16	3.55	3.08	5.53	3.41	5.96	5.55
Gamma	1.10	0.22	1.31	0.66	3.32	1.48	3.62	2.57
Global	32.77	6.99	32.96	7.50	35.52	16.40	35.62	16.99

Left-right Parahippocampal Gyrus

Three (n=3) caudal coronal sections stored in EFA, each derived from a separate brain, containing an intact basilar artery, and clearly defined parahippocampal structures were selected in order to systematically investigate this region of interest. For all practical

purposes, the sections were structurally identical in their representation of gross neuroanatomy, angle of the cut, thickness (1-2 cm), and age of preservation. The basilar artery, which served as the electrical reference, was truncated at its caudal end and anchored to the cerebrum by the bilateral remnants of the posterior cerebral arteries (PCA). A total of n=24 recordings were obtained from these sections. Figure 8 shows the position of needle probes within a coronal slice.

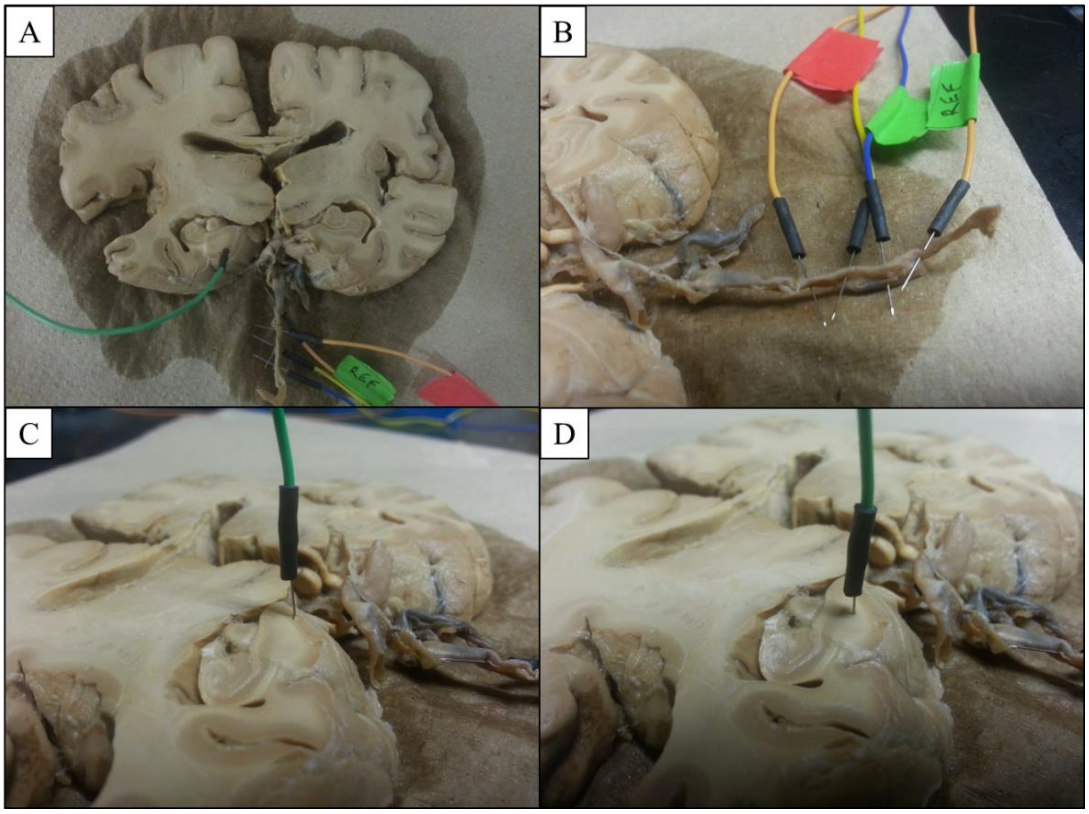

Figure 8. Experimental setup (A) demonstrating a needle probe inserted into grey (C) and white (D) matter of the parahippocampal gyrus referenced to the basilar artery (B).

Increased $\mu V^2 \cdot Hz^{-1}$ within the theta band was noted for right parahippocampal grey matter (M= 72.06, SE= 8.12) relative to left parahippocampal grey matter (M= 51.58, SE= 4.32), t(10)= 2.23, p= .05, r^2= .33. This increase was equivalent to ~20 $\mu V^2 \cdot Hz^{-1}$ on

average. Neither other bands nor parahippocampal white matter displayed this effect ($p>.05$). A discriminant analysis involving theta-range power spectral density accurately classified 83% of left-right hemisphere group membership for gray matter only in a cross-validated model $\Lambda=.67$, $\chi^2(1)=3.82$, $p=.05$, canonical $R^2=.58$.

Differences in theta power associated with parahippocampal structures were identified across coronal slices, $F(2,23)= 5.24$, $p<.05$. Power spectral densities within grey matter structures did not differ as a function of coronal slice ($p>.05$); however, white matter within the parahippocampal region did demonstrate differences in theta power as a function of coronal section, $F(2,11)= 10.90$, $p<.005$.

Table 2. Left (L) and Right (R) Hemispheric Parahippocampal (PHG) Grey Matter Power Spectral Density ($\mu V^2 \cdot Hz^{-1}$) and Voltage (μV)

	Spectral Power Density ($\mu V^2 \cdot Hz^{-1}$)				Voltage (μV)			
	PHG - L (N= 12)		PHG - R (N=12)		PHG - L (N=12)		PHG - R (N=12)	
Band	Mean	SD	Mean	SD	Mean	SD	Mean	SD
Delta	228.05	90.02	273.43	92.16	23.88	15.00	26.15	15.18
Theta	51.58	10.59	72.07	19.90	13.44	6.09	15.88	8.34
Alpha	20.95	4.29	21.07	5.62	11.67	5.28	11.70	6.04
Beta1	6.13	1.71	4.60	1.73	6.06	3.20	5.25	3.22
Beta2	3.17	0.62	3.03	0.90	5.63	2.49	5.50	3.00
Gamma	1.37	0.28	1.15	0.27	3.70	1.67	3.39	1.64
Global	51.88	15.33	62.56	13.69	44.69	24.29	49.08	22.96

Potential Differences from an Unsectioned Brain

The conspicuous rostrocaudal as well as hemispheric differences, which were most evident for the parahippocampal gyri, indicated structure-function anisotropy within the coronal slices. Whereas sectioned tissue samples represent practical sources of investigation, the spatial limits imposed upon the slices represent a degree of separation from the intact organ whose activity is typically measured using qEEG sensors applied over the scalp. Our previous research (Rouleau & Persinger, 2014) that measured a simulated human cerebral cortex composed of dough (flour, salt, water, and citric acid) showed a remarkable concordance of spectral power profiles between the dough when shaped like the human cortices and normal healthy brain activity across the fundamental band (1 to 40 Hz) when the ambient pH was within a narrow band between 2.47 and 2.52. Slight differences in the concentration resulted in a marked reduction of the coherence with normal EEG activity. The concordance occurred primarily within the higher frequencies (20 to 40 Hz) and around 8 Hz. Similarly the shape of the dough and its positioning within a skull also facilitated the congruence.

So as to approximate the spatial and chemical contexts within which the brain typically operates, it was necessary to design an experiment in consideration of the intra-cranial environment. To this end, an unsectioned brain which included all telencephalic, diencephalic, and brainstem structures was utilized. The brain was immersed in EFA or distilled H_2O for 20 minutes prior to measurement. Once removed from the liquid, the brain was placed on a flat surface, within a human replica skull (Figure 9), or within a polystyrene foam box (Figure 10). The volume of both "enclosures" was ~ 0.003 m^3. In addition to highlighting the importance of optimal pH, any relevant differences between the spatial conditions could confirm, as Nunez (1995) has previously demonstrated, that

the cranial vault is a non-trivial space which contributes to the amplification of specific harmonic frequencies.

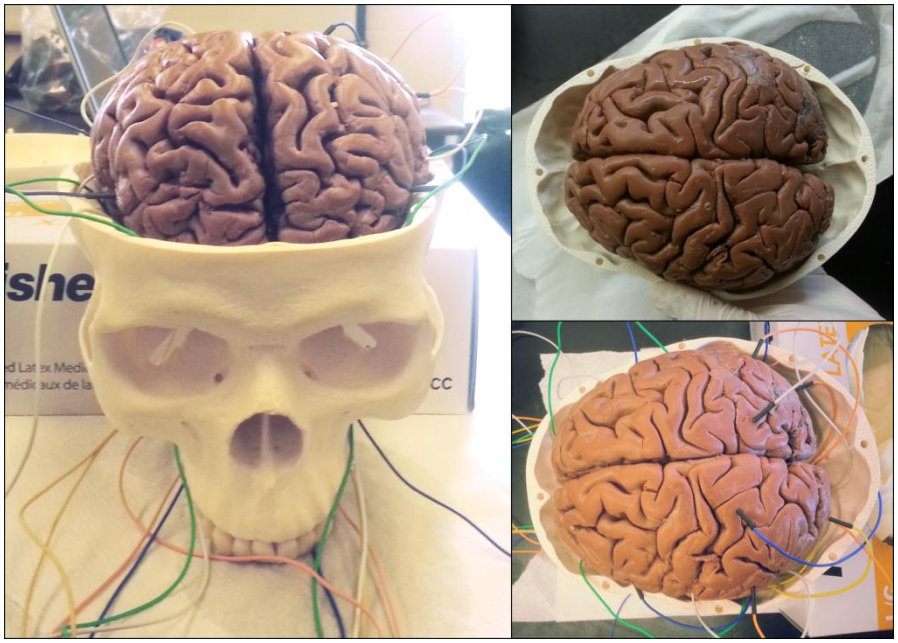

Figure 9. The brain is equipped with a needle probe array and inserted into the skull. A skull cap (not pictured) encloses the cerebrum within an artificial cranial vault.

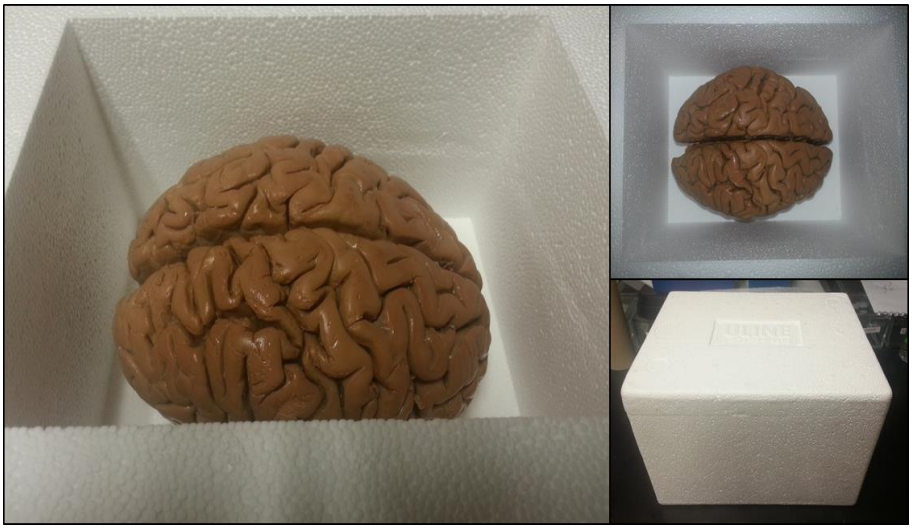

Figure 10. A polystyrene foam box was employed as a control enclosure within which the brain is placed during recording of electric potential differences.

Applied to the unsectioned brain were 14 needle-probes inserted into gyri distributed over the surface of the cerebrum. Probes were inserted into the orbiotofrontal (Fp1, Fp2), inferior frontal (F7, F8), parahippocampal (T3, T4), insular (C3, C4), supramarginal (T5, T6), superior parietal (P3, P4), and lateral occipital gyri (O1, O2). Odd numbers referred to probes inserted into the left hemisphere whereas even numbers referred to probes inserted into the right hemisphere. Potential differences between probed loci and reference cup sensors clamped to the ears of n=2 human participants were obtained. A sodium-based electrogel was applied to the cup sensors in order to establish an interface with the reference point (i.e. ear lobe), a procedure which is commonplace in qEEG measurement of human participants.

It became apparent that two distinct clusters of sensors could be isolated by dimensional reduction. Spectral power density values for all probes were entered into a factor analysis. A loading coefficient of .80 was selected due to the highly redundant signals shared between probes. A rotated component matrix revealed 2 factors, which cumulatively explained 93% of the variance. Probes T3, T4, T5, C3, C4, and P3 loaded on the first factor, explaining 87% of the variance, while Fp1, Fp2, O1 and O2 loaded on the second factor, explaining ~6% of the variance. The first factor consisted of loci which were spatially distributed between the rostral and caudal poles of the cerebrum whereas the second factor consisted of rostral (Fp1, Fp2) and caudal (O1, O2) polar structures. Spectral power densities were averaged across the respective sensor clusters into new variables: Polar and non-polar. Significant differences between these distinct factors as a function of reference sources – the human participants' earlobes – were not noted ($p>.05$).

Polar structures were unique in that spectral power densities obtained from within these convexities varied as a function of the signal frequency, $F(5, 143)= 27.83$, $p<.001$, $\eta^2= .50$. Homogenous subsets isolated common groups using Scheffe's method ($p<.05$), partitioning the 6 groups into 3 equal increments of frequency which were significantly different: low (1.5Hz – 7.5 Hz), middle (7.5Hz – 20Hz), and high (20Hz – 40Hz). Figure 11 demonstrates these differences. Frequency and polar structure spectral power densities were positively correlated, $r= .68$, $p<.001$. Non-polar structures demonstrated an analogous relationship with frequency ($r= .22$, $p<.005$); however, a Fisher z-transformation revealed the latter strength of the association was significantly reduced compared to the former, $z = 5.08$, $p<.001$. Spectral power densities within non-polar structures did not differ as a function of frequency ($p>.05$).

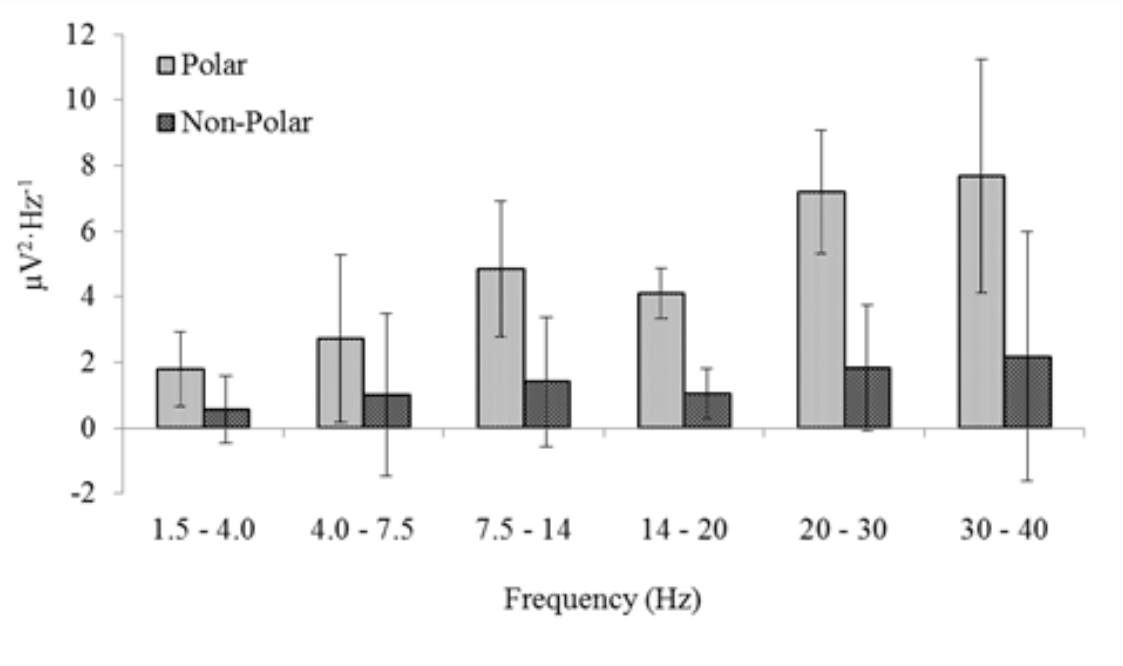

Figure 11. Spectral power density of polar and non-polar structures as a function of frequency. Means and standard deviations are presented.

A discriminant analysis accurately classified 60% of cases as a function of whether polar or non-polar structures within the replica human skull were immersed in EFA or H_2O Λ=.87, $\chi^2(2)$=6.05, p<.05, canonical R^2=.36. Discriminant functions were not generated if the brain was placed on a flat surface or within the polystyrene foam box (p>.05). That is, spectral power densities within combined polar and non-polar structures could only be discriminated as a function of the antecedent chemical condition if the brain was placed within a replica human skull. Increased global power within non-polar structures while inside the polystyrene foam box (M= 5.52, SE= .61) relative to polar structures within the context of the replica skull (M= 4.30, SE= .31) or the flat surface (M= 4.34, SE= .31) were noted, F(2,143)= 2.55, p= .01, η^2= .06.

As was the case for coronal sections, rostrocaudal differences were reliably present in the data. Paired t-tests examining differences in spectral power density as a function of hemisphere demonstrated conspicuous disparity along the rostrocaudal axis. Orbitofrontal, inferior frontal, and parahippocampal pairs demonstrated increased left hemispheric global power relative to contralateral pairs (p<.001) whereas insular, supramarginal, superior parietal, and lateral occipital pairs demonstrated increased right hemispheric power relative to contralateral pairs (p<.001). Figure 12 illustrates the left-rostral, right-caudal topography.

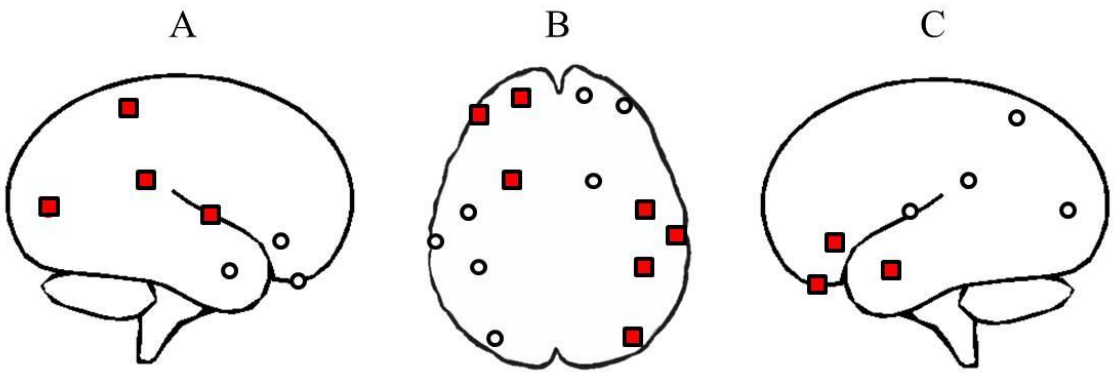

Figure 12. Right hemispheric (A), dorsal (B), and left hemispheric (C) perspectives of needle-probe (sensor) placement demonstrating rostrocaudal differences in hemispheric spectral power densities where red squares indicate a relative increase compared to the contralateral sensor (circles).

A conspicuous overlap in left-right spectral densities is noted when the brain is contained within a human replica skull. The parahippocampal (T3-T4) and lateral occipital gyri (O1-O2) show a complete absence of left-right differences in spectral power densities within all frequency bands when contained within the human replica skull ($p>.05$). This was not the case for the polystyrene foam box condition or when the brain was placed on a flat surface. An absence of difference in voltage is indicative of increased homogeneity between the sensors. Tables 3 through 5 demonstrate these differences in spectral power density across the sensor pairs as a function of the space of containment.

Table 3. Differences in Spectral Power Density Between Paired-Sensors for Recordings of the Brain Placed on a Flat Surface

Spectral Power Density Difference ($\mu V^2 \cdot Hz^{-1}$)							
	Fp1-Fp2	F7-F8	T3-T4	C3-C4	T5-T6	P3-P4	O1-O2
Delta	-0.05	0.39	0.01	-0.05	-1.31	-0.48*	-0.04
Theta	0.30*	0.96*	0.09*	-0.12*	-1.12	-0.71*	-0.11
Alpha	0.77*	2.04*	0.26*	-0.18	-5.45	-1.41*	-0.15
Beta1	0.59*	1.85*	0.23*	-0.22*	-2.3	-1.25*	-0.24*
Beta2	1.11*	3.24*	0.43*	-0.3	-2.74*	-2.28*	-0.53*
Gamma	1.14*	3.45*	0.44*	-0.34*	-2.72*	-2.37*	-0.54*

* indicates significant differences between paired sensors ($p<.05$)

Table 4. Differences in Spectral Power Density Between Paired-Sensors for Recordings of the Brain Placed Inside a Human Replica Skull

Spectral Power Density Difference ($\mu V^2 \cdot Hz^{-1}$)							
	Fp1-Fp2	F7-F8	T3-T4	C3-C4	T5-T6	P3-P4	O1-O2
Delta	0.01	0.46	0	-0.04	-1	-0.46*	0.01
Theta	0.33*	0.99*	0.11	-0.08	-0.80*	-0.68*	-0.11
Alpha	0.31	1.64*	0.06	-0.15	-8.61	-1.20*	0.04
Beta1	0.43	1.67*	0.09	-0.21*	-3.07	-1.16*	-0.13
Beta2	1.07*	3.26*	0.27	-0.33	-3.13	-2.00*	-0.32
Gamma	1.14*	3.33*	0.3	-0.29	-3.14	-2.11*	-0.35

* indicates significant differences between paired sensors ($p<.05$)

Table 5. Differences in Spectral Power Density Between Paired-Sensors for Recordings of the Brain Placed Inside a Polystyrene Foam Box

Spectral Power Density Difference ($\mu V^2 \cdot Hz^{-1}$)							
	Fp1-Fp2	F7-F8	T3-T4	C3-C4	T5-T6	P3-P4	O1-O2
Delta	0.33*	0.72*	0.09*	-0.13*	-1.44	-0.55*	-0.11*
Theta	0.38*	1.07*	0.12*	-0.17*	-2.46	-0.73*	-0.17*
Alpha	0.70*	1.95*	0.23*	-0.30*	-4.22	-1.45*	-0.30*
Beta1	0.66*	1.91*	0.21*	-0.26*	-2.29	-1.33*	-0.28*
Beta2	1.16*	3.38*	0.35*	-0.47*	-3.22	-2.32*	-0.49*
Gamma	1.12*	3.27*	0.17	-0.67	-2.54*	-2.43*	-0.55*

* indicates significant differences between paired sensors ($p<.05$)

Discussion

The visible heterogeneity of structures between the two human cerebral hemispheres for specific sub-regions, even when accounting for individual differences, has been frequently documented (Good et al., 2001; Raz et al., 2004; Watkins et al., 2001). However, heterogeneity in brain space for electroencephalographic response to a homogenous surface of an applied conductor is less well known. Our measurements of diminished topographical voltages over only the right caudal hemisphere would suggest, at its simplest, either a decrease in current or a decrease in resistivity within this region. Either condition should be associated with a specific pattern or tissue density within this region that is different from most other structures. As a result the properties of the copper mesh (with apertures between 1 and 5 mm, depending upon stretch) specifically diminished the fields emerging from the scalp. Gloor's (1997) interpretation was that this region is unique because "its structure and connections differ from any other cortical area".

The electroencephalographic region defined by T6, O2, and P4 revealed a specific diminishment of voltage within the 14 to 40 Hz band when subjects wore the copper mesh toque relative to the toque without lining. In addition the theta power within O2 was also diminished specifically within the 5.5 Hz to 6 Hz increment within this region and T6. We find this interesting for two reasons. First, one of the most defining neurophysiological features of the hippocampal-entorhinal-trans-cerebral cortical configuration is the powerful theta band upon which a higher "40 Hz" frequency is superimposed (Buzsáki, 2002). The superposition has been considered by many researchers, such as Bear (1996) as evidence of the mechanisms by which initially coded "hippocampal memory" can be distributed throughout the cerebral cortical volume for "long-term" representation. This juxtaposition is also consistent with the supposition that "consciousness" requires a significant "memory" component, that is, the reiterative processing of representations of experience within the recursive rostral-caudal electroencephalographic waves coupled to consciousness (Crick & Koch, 1990; Llinas & Ribary, 1993; Meador et al., 2002).

Secondly, "temporal binding" factors in large areas of cerebral activity are considered to be an important condition for consciousness (Crick & Koch, 2003; Joliot, Ribary & Llinas, 1994). The most frequent candidate is the "40" Hz band which is reflective of the approximately 20 to 25 ms recursive rostral-caudal transcerebral fields measured by Llinas and his colleagues many years ago (1991; 1993). While quantifying the derivatives from differences of lagged value, Persinger (1999) calculated that the higher variations that could sequester the 20 to 25 ms ("40 Hz") "point durations" of consciousness occurred between 5 Hz and 6 Hz for the lag of a lag condition. For these calculations the actual duration (in ms) of each integer frequency from 1 to 60 Hz was

calculated and lagged by one case. The difference between adjacent lags was calculated and lagged. The emergent duration for 20 to 25 ms was between 5.5 and 6 Hz.

LORETA analyses indicated that the most likely source location for this differential activity when (particularly female) subjects were wearing the toque lined with the copper mesh or not was the right parahippocampal region. Most of the decrease occurred within the higher frequency beta band. These algorithms verified our interpretations that there is some conductive feature within the right ventral caudal hemisphere that is differentially affected (compared to other areas) by the placement of copper mesh over the head.

Differential responsiveness of women's right temporal lobes to the application of burst-firing fields was reported by Richards et al (1992) who were attempting to discern processes associated with "panics". The significant interaction between gender and hemisphere of stimulation (left vs right) was due to the marked elevation of reports of fear (e. g., responding affirmatively to post-exposure items such as "I experienced fear or terror" by women who received the right hemispheric stimulation for only 20 min. Covariance for clusters of items that are similar to complex partial epileptic signs did not eliminate the interaction suggesting the effect was a direct effect upon structure rather than electrical state.

The other possibility is that this region (as a physiological aggregate), unlike other cerebral cortical areas, responds differentially to the presence of copper mesh. We (Dotta et al., 2014) have shown that cells may respond to reflective features of coverings. Direct measurements of photon emissions (by photomultiplier units) from cancer cells covered by different optical filters (10 nm increments) produced more photon flux density than if there had been no filters. Because the filters are actually micromirrors we concluded that

reflection of emitting photons that did not pass through the filter back onto the source stimulated the cells to enhance photon emission. Whether or not cortical cells, the primary source of electroencephalographic power, can respond to the presence of proximal conductors like copper must still be established.

Although our sample was relatively small (6 men, 6 women) the gender effect was conspicuous and suggested a right hemispheric specificity. Good et al (2001) who employed a voxel-based morphometric analysis of 465 normal adult human brains observed the expected asymmetry of cerebral white and grey matter in the occipital, frontal, and (petalia) temporal lobes as well as the hippocampus. In addition, females displayed increased grey matter with minimal asymmetry in the cortical mantle, parahippocampal gyri, the banks of the calcarine sulci, the cingulate region as well as increased neuronal density and numbers of cells within the temporal cortices. The very specific increase in grey matter within the left parahippocampal gyrus (-15, -34, -4) for females was almost exactly the same coordinates as our MNI values, which also approximates Talairach space, demonstrated for females who wore the copper mesh lined toque.

If our results are coupled to actual structures then they should complement more traditional morphometric studies. Insausti et al (1998) who examined MR volumetry from healthy volunteers and autopsy cases indicated significantly large volumes for the entorhinal and perirhinal cortices for the right compared to the left hemisphere. The mean number of 2-mm MR imaging sections for the right and left entorhinal cortices which is most of the parahippocampal gyrus was 11.9 and 11.3, respectively.

The ratio of the difference is about 1.05. If we assume the ranges reported in their data reflected 95% of the population, then the standard deviations would be about 1.5 sections. Consequently hemispheric differences would account for about 8 to 10% of the variance. During our measurements with volunteers the difference (attenuation of power) over the right caudal hemisphere was about 0.3 $\mu V^2 \cdot Hz^{-1}$ compared to the typical 6 $\mu V^2 \cdot Hz^{-1}$ which is a comparable ratio. This would be consistent with but not a demonstration that the attenuation effect was simply coupled to volume. One possible explanation is the greater the “volume voltage” the greater the current and hence the differential induction by the covering copper mesh that resulted in the attenuated qEEG. However the effect was frequency band-specific which suggests the effect was not a simple D.C. (steady potential) response.

The measurement of a cerebral asymmetry in fixed coronal sections for potential differences between the right and left hemisphere in general and specifically for the parahippocampal region strongly suggests an intrinsic structural feature that is not coupled to living brain or to the metabolic processes such as blood flow. The slightly elevated voltage (0.2 μV) in the right compared to the left hemispheric structures and the conspicuously elevated (2 μV) potential in the right compared to the left parahippocamapal grey matter within the theta range in fixed coronal sections suggests there may be relatively resilient structural properties within this region. This greater discrepancy of potential difference in the parahippocampal grey on average compared to general hemispheric asymmetry would be consistent with Insausti et al (1998) who found a larger volume for the entorhinal cortices in the right hemisphere compared to the left.

Higher intrinsic potential for power densities could contribute to more current density that would allow greater initial voltage potentials from this region. When interacting with the copper mesh the resultant current and magnetic field would potentially attenuate the source. Although surface qEEG is not easily accessible to a ventral temporal lobe structure such as the entorhinal cortices, Gloor (1997) has emphasized that auditory area 22, visual area 20, and the caudal third of the parietal region 7a, send major afferents to this region. These areas are either directly under or very proximal to the sensors (O2, T6, P4) from which we discerned the largest attenuation of power density for the qEEG and power density as inferred by LORETA when the wire mesh toque was being worn.

Although the measurement of any potential difference might be considered unlikely even with the appropriate referencing to an artery within the section, the EFA solution was distinctly acetic. Consequently there would be sufficient protons within the aqueous-ethanol environment that could have produced the potential difference assuming there was a disparity of charge. A disparity of charge usually requires some structural impedance that prevents homogenous distribution.

This intrinsic (micro) structure appeared to encourage a type of resonance with or the emission of frequencies within the theta and higher beta and gamma bands. According to empirical measurements (Tsang, Koren & Persinger, 2004) the inductance per meter (permeability) of cortical grey matter at 1 kHz (the approximate duration average action potentials, i.e., 1 ms) is about 10^{-2} Henrys. The permittivity for grey matter is ~$2 \cdot 10^{-1}$ Farads per m. Application of the classic formula for a circuit where resonance

frequency is $f=1/2(2\pi\cdot(LC)^{-1/2})$, L is inductance, and C is capacitance, the solution is about 7 Hz.

Although these measures are based upon fresh tissue within physiological level pH (in the order of 7.4 to 7.0), the calculated pH within 10 nm of cell membranes is more likely to be 2.5 to 3.0. This is within the range of the pH of the EFA solution in which the brain sections had been maintained and the present measures were collected. The average pH of EFA is about 3.45 which is similar to that when the sensor was immediately adjacent to the tissue surface. The study of simulated cortex by Rouleau & Persinger (2014) demonstrated the relevance of narrow-band pH as a potential regulator of human-coherent qEEG spectra.

Together, the data indicate that structural features which are preserved in fixed post-mortem tissue contribute to non-homogeneity of electric potential differences when referenced to a common point. Rostrocaudal and interhemispheric differences as a function of spectral power density revealed topographies which are perhaps intrinsic to the structure of the brain involved. The extent to which these findings are generalizable is unknown; however, the convergent findings presented here do suggest that some properties of living and non-living human brains overlap. The parahippocampal gyrus consistently demonstrated anomalies relative to structures within the same brain-space.

Materials & Methods

Mitsar QEEG System, sLORETA, & WinEEG Software

All qEEG measurements were completed with the use of a Mitsar qEEG system. For human participants, a 19-channel system was employed which was connected to a

Lenovo ThinkPad laptop running Windows 7. The qEEG cap contained sensors positioned according to the 10 – 20 International System of Electrode Placement. A sodium-based electrogel was applied in order to establish cap-scalp and ear-sensor interfaces. For fixed tissue, needle-probes were inserted into the fixed brains directly. Electric potential differences were logged within WinEEG Version 2.93.59 (07.2013). Impedance values for all sensors were regulated to < 5kΩ. A sampling rate of 250Hz remained consistent across all experiments.

Spectral power densities were extracted in 30 s segments with 8 s epochs, and imported to SPSS v.20. For narrow-band investigation, raw data were extracted in 30 s segments from WinEEG as ASCII files, imported to SPSS v.20, standardized, and spectral analyzed. LORETA current spectral densities were obtained by first generating Talairach Electrode Coordinates which, when applied with the appropriate transformation matrix, allows the user to navigate voxels in 3D space and query the system for CSD values.

Copper Screen-Line Toque & Procedure

A black acrylic knit cap was retrofitted with a dual-layer of 28-gauge copper mesh wire lining (i.e. Copper Blocker). The mesh matrix consisted of evenly-distributed 5mm squares that could expand by 1-2 mm in any direction, providing flexibility. The elasticity of the weave and mesh lining were such that head sizes up to 60 cm in circumference could be accommodated. An identical cap that was not retrofitted served as a control. Each individual was fitted with a qEEG electrode cap which rested beneath either the copper-lined or control cap. Participants were asked to sit quietly within the chamber and

remain relaxed. Low-light levels were maintained throughout the experiment. Baseline qEEG data were collected with the participant's eyes open and closed. Subsequent to baseline recordings, the experimenter informed the participant that an adjustment to the equipment was necessary in order to continue the experiment. During said time, the cap was switched to either a copper-lined or control cap. All participants were exposed to both cap conditions which were counterbalanced to eliminate order-effects. The procedure was approved by Laurentian University's Research Ethics Board.

Needle-Probe Placement

The current methods specified for the measurement of voltage from fixed human brain tissue are similar to those employed by Saroka et al. (2015) in order to measure the electrical and spectral properties of tumors within mice. In their study, the reference consisted of the animal's tail. In the current study, the reference consisted of vasculature.

For coronal sections of human brain tissue, needle-probes were placed within the following areas which were always recorded in both hemispheres and included adjacent white matter for cortical loci: anterior cingulate, posterior cingulate, genu of corpus callosum, septum pellucidum, gyrus rectus, orbital gyrus, septal nucleus, head of the caudate nucleus, claustrum, putamen, globus pallidus (I & II), anterior commissure, posterior commissure, fibers of the internal capsule, corona radiata, nucleus accumbens, olfactory tubercle, amygdala, superior frontal gyrus, middle frontal gyrus, inferior frontal gyrus, CA fields (1-3), parahippocampal gyrus, insular gyrus, superior temporal gyrus, middle temporal gyrus, inferior temporal gyrus, pillars of fornix, medial geniculate nucleus, lateral geniculate nucleus, sublenticular component of the posterior arm of the internal

capsule, transverse temporal gyrus, fusiform gyrus, crus of fornix, substantia nigra, crus cerebri, red nucleus, pulvinar, tail of caudate nucleus, superior parietal lobule, columns of fornix, hypothalamus, mamillothalamic tract, anterior nucleus of the thalamus, ventral anterior nucleus of the thalamus, body of fornix, extreme capsule, external capsule, alveus, supramarginal gyrus, optic chiasm, optic nerve, optic tract, periaqueductal grey, and the cerebral peduncle. Measurements were performed sequentially and were counterbalanced with respect to factors such as hemisphere and type of tissue.

The unsectioned brain was equipped with 14 sensors which recorded simultaneously. Probes were inserted into the orbiotofrontal (Fp1, Fp2), inferior frontal (F7, F8), parahippocampal (T3, T4), insular (C3, C4), supramarginal (T5, T6), superior parietal (P3, P4), and lateral occipital gyri (O1, O2). Placement of each needle probe was performed with reference to adjacent landmark structures. Orbitofrontal probes were placed within the center of the most rostral convexity of the orbital gyri which bordered the clearly defined orbital sulci. Inferior frontal probes were placed within the center of the pars triangularis bordered by the anterior ascending ramus (caudally) and anterior horizontal ramus (rostrally). Parahippocampal probes were placed within the parahippocampal gyrus at a midway point along the rostrocaudal axis between the rhinal fissure and collateral sulcus. Insular probes were inserted into the anterior gyri breves. Supramarginal probes were placed within the caudal component of the supramarginal gyrus where the posterior ascending limb of the lateral fissure formed a rostral border. Superior parietal probes were inserted into the superior parietal lobule at the dorsal-most extent of this convexity and at a half-way point between the postcentral fissure and the parieto-occipital fissure along the rostrocaudal axis. Lateral occipital probes were inserted

at a point between the lateral occipital sulcus and the occipital pole, ventral to the intraparietal fissure.

References

Alonso, A., & Klink, R., (1993). Differential electroresponsiveness of stellate and pyramidal-like cells of medial entorhinal cortex layer II. Journal of Neurophysiology, 70(1), 128-143.

Bear, M.F., (1996). A synaptic basis for memory storage in the cerebral cortex. Proceedings of the National Academy of Scicences. 93, 13453-13459.

Buzsáki, G., (2002). Theta oscillations in the hippocampus. Neuron, 33(3), 325- 340.

Crick, F., & Koch, C., (1990). Towards a Neurobiological Theory of Consciousness. Seminars in the Neurosciences, 2, 263-275.

Crick, F., & Koch, C., (2003). A framework for consciousness. Nature Neuroscience, 6(2), 119-126.

Dotta, B. T., Murugan, N. J., Karbowski, L. M., Lafrenie, R. M., & Persinger, M. A., (2014). Shifting wavelengths of ultraweak photon emissions from dying melanoma cells: their chemical enhancement and blocking are predicted by Cosic's theory of resonant recognition model for macromolecules. Naturwissenschaften, 101(2), 87-94.

Good, C. D., Johnsrude, I., Ashburner, J., Henson, R. N., Friston, K. J., & Frackowiak, R. S., (2001). Cerebral asymmetry and the effects of sex and handedness on

brain structure: a voxel-based morphometric analysis of 465 normal adult human brains. Neuroimage, 14(3), 685-700.

Gloor, P., (1997). The Temporal Lobes and Limbic System. Oxford Press, Oxford

Insausti, R., Juottonen, K., Soininen, H., Insausti, A. M., Partanen, K., Vainio, P., ... & Pitkänen, A., (1998). MR volumetric analysis of the human entorhinal, perirhinal, and temporopolar cortices. American Journal of Neuroradiology, 19(4), 659-671.

Joliot, M., Ribary, U., & Llinas, R., (1994). Human oscillatory brain activity near 40 Hz coexists with cognitive temporal binding. Proceedings of the National Academy of Sciences, 91(24), 11748-11751.

Koenig, T., Prichep, L., Lehmann, D., Sosa, P. V., Braeker, E., Kleinlogel, H., ... & John, E. R., (2002). Millisecond by millisecond, year by year: normative EEG microstates and developmental stages. Neuroimage, 16(1), 41-48.

Lehmann, D., (1990). Brain electric microstates and cognition: the atoms of thought. In Machinery of the Mind (pp. 209-224). Birkhäuser Boston.

Llinas., R., & Pare, D., (1991). Of dreams and wakefulness. Neuroscience. 44, 521-535.

Llinas., R. & Ribary, U., (1993). Coherent 40-Hz oscillation characterizes dream state in humans. Proceedings of the National Academy of Science. 90, 2078-2081.

Meador, K. J., Ray, P. G., Echauz, J. R., Loring, D. W., & Vachtsevanos, G. J., (2002). Gamma Coherence and Conscious Perception. Neurology, 59, 847-854.

Morgan, A. H., McDonald, P. J., & Macdonald, H., (1971). Differences in bilateral alpha activity as a function of experimental task, with a note on lateral eye movements and hypnotizability. Neuropsychologia, 9(4), 459-469.

Nunez, P.L., (1995). Neocortical Dynamics and Human EEG Rhythms. Oxford University Press, New York.

Persinger, M. A., Dotta, B. T., Karbowski, L. M., & Murugan, N. J., (2015). Inverse relationship between photon flux densities and nanotesla magnetic fields over cell aggregates: quantitative evidence for energetic conservation. FEBS Open Bio.

Persinger, M. A., (1999). Is there more than one source for the temporal binding factor for human consciousness?. Perceptual and Motor Skills, 89(3f), 1259-1262.

Pruessner, J. C., Köhler, S., Crane, J., Pruessner, M., Lord, C., Byrne, A., ... & Evans, A. C., (2002). Volumetry of temporopolar, perirhinal, entorhinal and parahippocampal cortex from high-resolution MR images: considering the variability of the collateral sulcus. Cerebral Cortex, 12(12), 1342-1353.

Raz, N., Gunning-Dixon, F., Head, D., Rodrigue, K. M., Williamson, A., & Acker, J. D., (2004). Aging, sexual dimorphism, and hemispheric asymmetry of the cerebral cortex: replicability of regional differences in volume. Neurobiology of aging, 25(3), 377-396.

Richards, P. M., Koren, S. A., & Persinger, M. A., (1992). Experimental stimulation by burst-firing weak magnetic fields over the right temporal lobe may facilitate apprehension in women. Perceptual and motor skills, 75(2), 667-670.

Rouleau, N., & Persinger, M., (2014). Cerebral Networks of Interfacial Water: Analogues of the Neural Correlates of Consciousness in a Synthetic Three-Shell Realistic Head Model. Journal of Signal and Information Processing, 5(4), 143.

Saroka, K. S., Caswell, J. M., Lapointe, A., & Persinger, M. A., (2014). Greater electroencephalographic coherence between left and right temporal lobe structures during increased geomagnetic activity. Neuroscience letters, 560, 126-130.

Saroka, K. S., Karbowski, L. M., Murugan, N. J., & Persinger, M. A., (2015). Evidence of "trapped" voltage spectrum residuals within mouse melanoma tumors for about 30 minutes following brief exposures to treatment-related, physiologically-patterned magnetic fields. Archives in Cancer Research, 3(29), 1-5.

Saroka, K. S., & Persinger, M. A., (2014). Quantitative Evidence for Direct Effects Between Earth-Ionosphere Schumann Resonances and Human Cerebral Cortical Activity. International Letters of Chemistry, Physics and Astronomy, 20.

Tsang, E. W., Koren, S. A., and Persinger, M. A., (2004). Power increases within the gamma range over the frontal and occipital regions during acute exposures to cerebrally counterclockwise rotating magnetic fields with specific derivatives of change. Int. J. Neurosci. 114, 183–194.

Van Essen, D. C., & Drury, H. A., (1997). Structural and functional analyses of human cerebral cortex using a surface-based atlas. The Journal of Neuroscience, 17(18), 7079-7102.

Van Strien, N. M., Cappaert, N. L. M., & Witter, M. P., (2009). The anatomy of memory: an interactive overview of the parahippocampal–hippocampal network. Nature Reviews Neuroscience, 10(4), 272-282.

Watkins, K. E., Paus, T., Lerch, J. P., Zijdenbos, A., Collins, D. L., Neelin, P., ... & Evans, A. C., (2001). Structural asymmetries in the human brain: a voxel-based statistical analysis of 142 MRI scans. Cerebral cortex, 11(9), 868- 877.

Witter, M. P., (1993). Organization of the entorhinal—hippocampal system: A review of current anatomical data. Hippocampus, 3(S1), 33-44.

Chapter Transition: Predicting Pathology

In the previous chapter, fixed, post-mortem human brain tissue was examined to determine if left-right asymmetries could be detected. The following chapter applies the same principles and methods to rat brains in order to attempt to discriminate between specimens which, during their lifetime, were induced to seize or not. We ask the question: Is it possible to tell if a rat brain had been seized during its lifetime 20 years after the electrical event using only electric potential differences? Our results indicate that a relationship between the mass of the brain and low-frequency signal periodicities within the left ventral quadrant of seized brains could be identified which was highly indicative of difference from controls. Our measurements demonstrate that other quadrants were not predictive of pathology. The experimental results suggest that events during the brain's living state remain encoded within microstructural subsections of the tissue sufficient to suppress periodic signals which can be readily differentiated from controls. Though it has been assumed that preserved brain structure correlates to some degree with acquired experiences over the organ's antecedent lifetime, the following chapter demonstrates a dynamic correlate which can discriminate a binary variable: seizure or no seizure. The results are consistent with histological reports published previously using the same sample which demonstrated profound hippocampal and parahippocampal ablations subsequent to an injection of lithium-pilocarpine. The theta rhythms which were suppressed within the less massive seized brains are hypothesized to be related to cell populations within the entorhinal cortices which, under living conditions, pace-make at the same firing frequency.

Chapter 4:

Functional Neuroimaging of Post-Mortem Tissue: Lithium-Pilocarpine Seized Rats Express Reduced Brain Mass and Proportional Reductions of Left Ventral Cerebral Theta Spectral Power

(Original Research)

Published in Heliyon, Vol. 2, pp. 1 – 10, 2016.

Nicolas Rouleau, Brady S. Reive,

& Michael A. Persinger

DOI: 10.1016/j.heliyon.2016.e00181

Abstract

Structural imaging tools can be used to identify neuropathology in post-mortem tissue whereas functional imaging tools including quantitative electroencephalography (QEEG) are thought to be restricted for use in living subjects. We are not aware of any study which has used electrophysiological methods decades after death to infer pathology. We therefore attempted to discriminate between chemically preserved brains which had incurred electrical seizures and those that did not using functional imaging. Our data indicate that modified QEEG technology involving needle electrodes embedded within chemically fixed neural tissue can be used to discriminate pathology. Forty (n= 40) rat brains preserved in ethanol-formalin-acetic acid (EFA) were probed by needle electrodes inserted into the dorsal and ventral components of the left and right cerebral hemispheres. Raw microvolt potentials were converted to spectral power densities within classical electroencephalographic frequency bands (1.5 Hz to 40Hz). Brain mass differences were shown to scale with left hemispheric ventral theta-band spectral power densities in lithium-pilocarpine seized rats. This relationship was not observed in non-seized rats. A conspicuous absence of pathological indicators within dorsal regions as inferred by microvolt fluctuations was expected given the known localization of post-ictal damage in lithium-pilocarpine seized rats. Together, the data demonstrate that post-mortem neuroimaging is both possible and potentially useful as a means to identify neuropathology without structural imaging techniques or dissection.

Introduction

Post-mortem neuroimaging is currently performed by the use of structural imaging tools such as MRI (Griffiths, Paley & Whitby, 2005). These techniques have even been used to image ancient tissues preserved by mummification (Karlik, Bartha, Kennedy & Chhem, 2007). Functional neuroimaging tools such as quantitative electroencephalography (QEEG), however, are used exclusively in living subjects. Rouleau & Persinger (2016) have recently demonstrated that a modified QEEG technique using needle electrodes and a vascular electrical reference can be used to identify intrinsic laterality of frequency-dependent microvolt fluctuation power in coronal sections of human brain tissue. The experiments also demonstrated that select areas including the parahippocampal gyrus could be "reactivated" by frequency-modulated 2 μV pulsed current applied directly to the brain. These results indicate that post-mortem tissue can be measured by use of functional imaging technologies and that structural-functional relationships can be investigated post-mortem in chemically fixed tissue specimens. Whether or not this method is of any practical consequence with respect to pathological analysis or autopsy can now be considered.

For more than three decades we (Persinger, Makarec & Bradley, 1988; Persinger, Bureau, Kostakos, Peredery & Falter, 1993) explored the structural bases of epilepsy as well as the multiple means of chemical-procedures by which seizures could be induced in rats. During that period both quantitative and semi-quantitative measurements of the proportion of neuronal dropout within the approximately 150 Paxinos and Watson structures within the telencephalon and diencephalon of hundreds of rats were documented (Peredery, Persinger, Parker & Mastrosov, 2000). Most of the severe

neuronal damage occurred within ventral structures that included the pyriform lobe, CA1 of the hippocampus, portions of the amygdala and directly connected thalamic structures. The mosaics of those proportions of damage were found to be correlated with the animals' subsequent histories of developing spontaneous seizures and unusual behaviours (St-Pierre & Persinger, 2005) as well as blood chemistry and alterations in specific organ weights (George et al., 2009). We hypothesized that structural changes at the level of the cerebrum would be paired with quantifiable fluctuations of electric potential differences within the fixed tissue samples. If, as Rouleau & Persinger (2016) demonstrated, the normal human brain's regional structure is intimately tied to unique, spatially-specific microvolt potential fluctuations, the pathological rat brains should display an equivalent structural-electrical relationship. Here we present evidence that long after brains have been removed and fixed there are residual, site-specific electrophysiological anomalies that reflect the history of the animals. This novel approach might be considered a technique for first screening of the potential anomaly within a brain before the costly and labour-intense histopathological analyses are pursued.

Methods & Materials

Specimens

Forty (n=40) rat brains (Wistar, albinos), which were extracted within 5 min after death (usually decapitation) and preserved in ethanol-formalin-acetic acid (EFA) at various points over the course of the past 20 years, were utilized for the present study. The brains were sequestered in compliance with ethical standards outlined by Laurentian University's Research Ethics Board. Five (n=5) were laboratory teaching specimens, and

thirty-five (n=35) were involved in one of 12 experiments supervised by Dr. Michael A. Persinger (primary investigator) and conducted by the Neuroscience Research Group at Laurentian University between 1996 and 2008. Data presented by Michon & Persinger (Michon & Persinger, 1997) as well as Peredery and colleagues (Peredery, Persinger, Parker & Mastrosov, 2000) are examples of the primary studies from which the tissue collection protocols were originally approved by the University Research Ethics Board. Of the preserved specimens, eight (n=8) were known females and nine (n=9) were known males. Within the full sample, thirteen (n=13) brains had been extracted from rats in which seizures had been induced by a single system injection of lithium-pilocarpine. Twenty three (n=23) were not seized and four (n=4) were excluded from the analysis due to group uncertainty. The brains shared common gross morphology and were structurally unremarkable by visual detection without the assistance of histological tools. Behavioural metrics and identifying characteristics associated with each animal including weight and sex were included as part of the data analysis. Brain wet weights were collected and included as part of the analysis.

Quantitative Electroencephalography

A quantitative electroencephalography (QEEG) electrical amplifier (Model 201) by Mitsar was coupled to a series of 5 needle electrodes (probes). Four probes were inserted into the brainstem where the average microvolt value was computed and served as an electrical reference. The fifth probe was inserted directly into 1 of 4 regions of interest which will be discussed in a later section. Measurements were recorded from an HP ENVY laptop computer running Windows 8. WinEEG software version 2.93.59 (07.2013) was employed for data collection. Gain was set to 150 µV while low- (1.6 Hz) and high-

cut (50 Hz) filters were applied in addition to a notch filter (50 Hz – 70 Hz and 110 Hz – 130 Hz) to exclude electrical artefacts. Each measurements was preceded by a surface clearing of the tissue with 10% EFA to avoid tissue damage and changes of conductivity associated with the electrophysiological measurement device.

Procedure

Brains were probed directly by the modified electrophysiological measurement device (QEEG). A similar procedure has been previously applied to human tissue (Rouleau & Persinger, 2016). Microvolt fluctuations within brains were measured by insertion of 1/3 of the needle probe (6.6 mm) into the dorsal or ventral surface of the left and right hemispheres of the rat cerebrum (Figure 13). The dorsal probes were inserted dorso-ventrally at equidistance between the rostral- and caudal-most poles of the cerebrum and at its apex on the dorsal surface. Ventral probes are inserted caudo-rostrally at the caudal- and ventral-most extension of the cerebrum anterior to the cerebellum and inferior to the rhinal fissure which included the pyriform region involving the entorhinal cortices and underlying hippocampal formation. The reference consisted of an average of probes inserted into the spinal cord. If the spinal cord was not spared during extraction from the animal, the medulla or pons served as the reference point and these exceptions were noted within the dataset. Each brain was washed with 10% EFA and measured by QEEG for 40 seconds. The order of measurements was counterbalanced so that confounding factors of time could be eliminated.

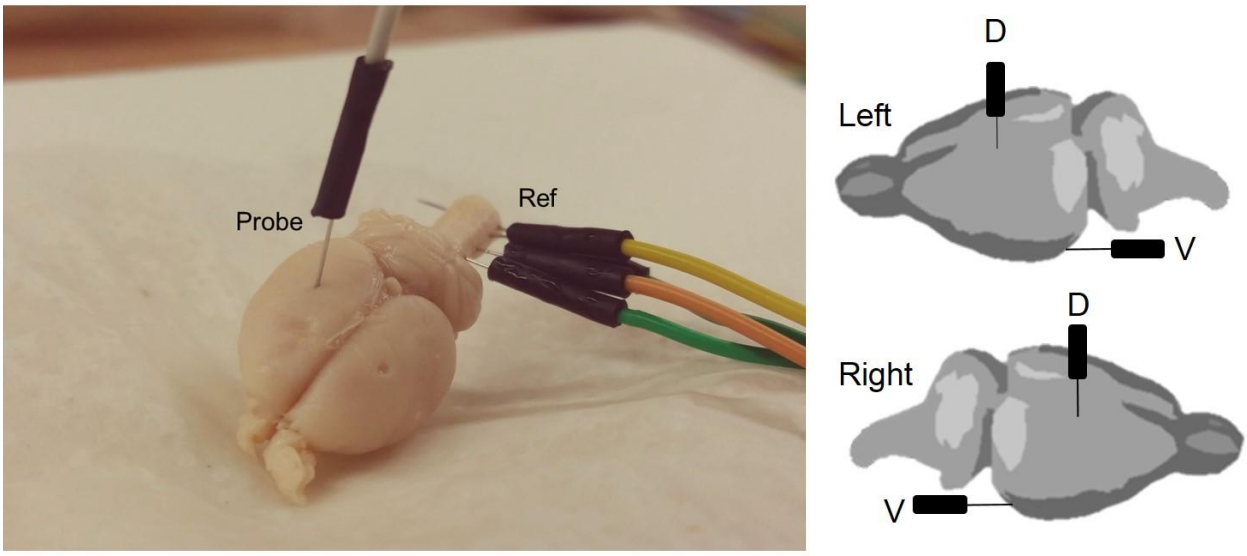

Figure 13. A probe, referenced to the spinal cord, is inserted 6.6 mm into the dorsal (D) or ventral (V) surface of the left or right cerebral hemisphere.

Analysis

Spectral power densities (SPDs) derived from QEEG microvolt fluctuations were extracted directly from WinEEG, computed from 30 second segments of raw microvolt fluctuations with 4 second epochs. Classic electroencephalographic bands were selected: Delta (1.5 Hz – 4 Hz), theta (4 Hz – 7.5 Hz), alpha (7.5 Hz – 14 Hz), beta1 (14 Hz – 20 Hz), beta2 (20 Hz – 30 Hz), gamma (30 Hz – 40Hz). Data were entered into an SPSS v19 dataset with all relevant experimental and quasi-experimental variables obtained from laboratory logs. Sex, age of the rat, time elapsed since death, whether the rat was seized or not, and brain wet weight were included into the analysis. Basic differences were computed by the use of t-tests as well as parametric and non-parametric correlational analyses. Equality of variances were satisfied. Measures of effect sized were

included to demonstrate the relative magnitude of each finding beyond the simple presence of differences between groups.

Results

The results were surprisingly robust and site-specific suggesting minimal contribution from generalized measurement epiphenomena. As expected the weight of the male brains (M= 2.01 g, SEM= 0.02 g) were significantly heavier than female brains (M= 1.83 g, SEM= 0.01 g) [$t(14)= 3.94$, $p<.001$, $r^2= .53$]. This difference was equivalent to a proportion of 9% or approximately 200 mg. This is within the range expected for general sexual dimorphism. However the brains of rats in which seizures had been induced by a single, systemic injection of lithium-pilocarpine demonstrated lighter brains (M= 1.81 g, SEM= 0.04 g) compared to non-seized rats (M= 1.91, SEM= 0.02) [$t(32)= -2.20$, $p<.05$, $r^2= .13$ (Figure 14A)]. The difference was equivalent to about 5% or 100 mg.

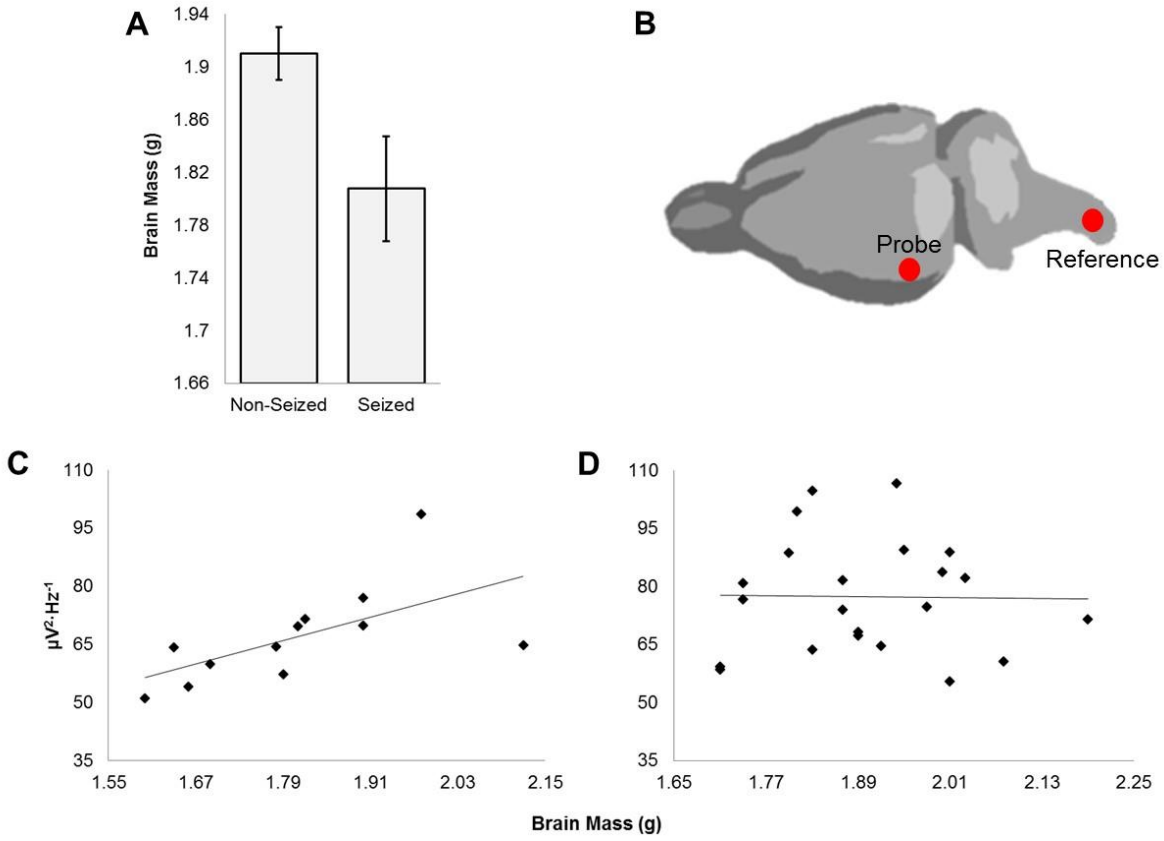

Figure 14. Seized rats demonstrated a statistically significant ($p < 0.05$) 5% decrease in brain mass relative to non-seized rats (A). Theta-band spectral power densities obtained by probing the left hemispheric ventral component of the rat cerebrum (B) demonstrated a linear relationship with brain mass in seized rats (C) which was not observed for non-seized rats (D).

Theta-band (4 Hz – 7.5 Hz) spectral power densities were decreased in seized (M= 66.37, SEM= 1.56) rat brain measurements relative to non-seized (M= 73.22, SEM= 2.10) rat brain measurements [$t(142)= 2.26$, $p<.05$, $r^2=.03$]. Those which were obtained within the left ventral quadrant of seized rat cerebra (Figure 14B) expressed theta-band SPDs which positively correlated with brain mass, $r= .61$, $p<.05$, $rho= .81$, $p<.001$ (Figure 14C). As the brain weight decreased in seized brains, so did the left hemispheric ventral

theta rhythms. Non-seized rat cerebra did not display an analogous relationship within the left ventral quadrant (r=.02, p=.94, rho=.04, p=.85). These results are shown in Figure 14D. There were no differences observed as a function of the electrical reference point (p>.05).

Discussion

The results demonstrate that voltage potential differences obtained from deceased, chemically fixed brains can be used to discriminate between animals which displayed a history of seizure activity and those that did not whilst alive. The average decrease of 5% cerebral mass compared to normal rats would be equivalent to ~10^8 neurons and other cells assuming about 50% of the space is occupied by cells immersed in interstitial fluid. This is estimated by assuming each cell with a width of 10 μm and a density of water would weigh about $5 \cdot 10^{-10}$ g and 5% decreased weight would be about 10^{-1} g (100 mg).

There is quantitative evidence that numbers of cells associated with that mass (volume) of brain tissue could have contributed to the shift in electroencephalographic power. The slope from Figure 2C was 25.2 $\mu V^2 \cdot Hz^{-1}$. The theta band included 3.5 Hz; as a result the total potential change was $9.4 \cdot 10^{-6}$ V (the square root of 88.2 μV^2). The numbers of water molecules with a charge (such as H+) at a pH of ~5 within $5.6 \cdot 10^{-3}$ M (0.1 cc) would be $3.4 \cdot 10^{14}$ charges. About 10^6 charges (static) are functionally associated with the resting plasma membrane potential of a neuron (Persinger, 2010). Consequently the shift would be equivalent the integrated loss of ~10^8 cells. This is the same order of magnitude as the estimated loss of neurons inferred from the brain mass differences

between the seized and non-seized rats. Alternatively, 10^{14} charges multiplied by the unit charge ($1.6 \cdot 10^{-19}$ A·s) per s (1 Hz) would be $5.4 \cdot 10^{-5}$ A. Considering the enhanced conductivity of the fixative (~10^{-1} Ω) the voltage equivalence would be within the microvolt range.

The measurements showed that only the power within theta band was significantly correlated with the weight of the brains if the animals had histories of seizures. Other QEEG bands did not display this relationship. In addition, the normal, non-seized brains did not display any differential shift in theta power density as a function of brain weight. That brain tissue, specifically grey matter, in mammals may display an intrinsic resonance within the theta range has been suggested by the calculations of Tsang et al. (2004). Employing a LC (impedance-capacitance) formula for these values for grey matter they found that the intrinsic resonance frequency was about 7 Hz. If this frequency band is a material property of brain matter, within nature or fixed environments, then its ubiquitous presence within structures such as the hippocampal formation-entorhinal cortices might be accommodated. It may also explain one possible advantage for gamma ripples to be superimposed upon this fundamental theta rhythm and for the pervasive neocortical connections and influences that originate from the entorhinal cortices.

The occurrence of the brain weight-theta power within the left lower caudal quadrant (pyriform region) for the seized brains would be expected because of the relatively greater proportion of grey matter and hence the greater range of decimation from the progressive consequences of the seizures. Hemispheric asymmetries have been well established for both function and structure. For example Adamec and Morgan (1993) found that right hemispheric kindling within the basolateral amygdale increased

behaviours consistent with anxiety in rats while left hemispheric kindling of this structure diminished these behaviors. Schubert et al (2005) demonstrated differential effects in plasticity within the rat amygdala and hippocampus following theta pulse stimulation that reflected hemispheric differences. Asymmetrical compromise of the blood brain barrier can be induced by seizures according to Kutlu et al. (2002). The observation by Kawakami et al. (2003) that strong asymmetrical distributions of epsilon 2 subunits of NMDA receptors that strongly influenced if not determined the differential plasticity between the left and right hippocampus. This might have the capacity to produce subtle changes in intrinsic theta elicitation when activated by specific proton donors such as EFA.

Left ventral cerebral theta power scaled with the mass of seized rat brains where decreases in mass would have been associated with linear decreases in power. This relationship could be relevant to entorhinal-hippocampal connections. Peredery and colleagues (Peredery, Persinger, Parker & Mastrosov, 2000) reported that neuronal dropout following lithium-pilocarpine seizures in the rat were most evident within CA1 fields of the hippocampus and the piriform cortex in addition to select thalamic regions. The distribution of said structures is skewed toward the ventral half of the cerebrum. The entorhinal cortex, which is localized to the ventral components of the rat cerebrum, is known to both project to CA1 fields and generate theta rhythms (Alonso & Garcia-Austt, 1987). Neuronal loss within the CA1 field could have promoted afferent degeneration, resulting in mass-scaled theta power dropout. However, it remains unclear as to why this relationship was only present within the left hemisphere. It may be relevant that we (Persinger & Dupont, 2004) found that the amount of damage within the left dentate gyrus

was the driving factor for the numbers of spontaneous monthly seizures subsequent to induction of lithium-pilocarpine epilepsy.

References

Adamec, R. E. & Morgan, H. D. (1993). The effect of kindling of different nuclei in the left and right amygdala on anxiety in the rat, Physiology and Behavior. 55, 1-12.

Alonso, A., & Garcia-Austt, E. (1987). Neuronal sources of theta rhythm in the entorhinal cortex of the rat, Experimental Brain Research. 67, 493-501.

George, K. R., Rico, T., St-Pierre, L. S., Dupont, M. J., Blomme, C. G., Mazzuchin, A., ... & Persinger, M. A. (2009). Large differences in blood measures, tissue weights, and focal areas of damage 1 year after postseizure treatment with acepromazine or ketamine. Epilepsy & Behavior, 15, 98-105.

Griffiths, P. D., Paley, M. N. J., & Whitby, E. H. (2005). Post-mortem MRI as an adjunct to fetal or neonatal autopsy, The Lancet. 365, 1271-1273.

Karlik, S. J., Bartha, R., Kennedy, K., & Chhem, R. (2007). MRI and multinuclear MR spectroscopy of 3,200-year-old Egyptian mummy brain, American Journal of Roentgenology, 189, W105-W110.

Kawakami, R., Shinohara, Y., Kato, Y., Sugiyama, H., Shigemoto, R., & Ito, I. (2003). Asymmetrical allocation of NMDA receptor ε2 subunits in hippocampal circuitry, Science. 300, 990-994.

Kutlu, N., Vatansever, H. S., Bayazit, T. O., Ekerbicer, N., & Tan, U. (2002). Blood brain barrier in right-and left-pawed female rats assessed by a new staining method, International Journal of Neuroscience. 112, 1037-1046.

Michon, A. L., & Persinger, M. A. (1997). Experimental simulation of the effects of increased geomagnetic activity upon nocturnal seizures in epileptic rats. Neuroscience Letters, 224, 53-56.

Peredery, O., Persinger, M. A., Parker, G., & Mastrosov, L. (2000). Temporal changes in neuronal dropout following inductions of lithium/pilocarpine seizures in the rat. Brain Research, 881, 9-17.

Persinger M. A. (2010). 10^{-20} Joules as a neuromolecular quantum in medicinal chemistry: an alternative approach to myriad molecular pathways. Current Medicinal Chemistry. 17, 3094-3098.

Persinger, M. A., Bureau, Y. R., Kostakos, M., Peredery, O., & Falter, H. (1993). Behaviors of rats with insidious, multifocal brain damage induced by seizures following single peripheral injections of lithium and pilocarpine, Physiology & Behavior. 53, 849-866.

Persinger, M. A., & Dupont, M. J. (2004). Emergence of spontaneous seizures during the year following lithium/pilocarpine-induced epilepsy and neuronal loss within the right temporal cortices. Epilepsy & Behavior, 5, 440-445.

Persinger, M. A., Makarec, K., & Bradley, J. C. (1988). Characteristics of limbic seizures evoked by peripheral injections of lithium and pilocarpine. Physiology & Behavior, 44, 27-37.

Persinger, M. A., Stewart, L. S., Richards, P. M., Harrigan, T., O'Connor, R. P., & Bureau, Y. R. J. (2002). Seizure onset times for rats receiving systemic lithium and pilocarpine: sources of variability, Pharmacology Biochemistry and Behavior, 71, 7-17.

Rouleau, N. & Persinger, M.A. (2016). Differential Responsiveness of the Right Parahippocampal Region to Electrical Stimulation in Fixed Human Brains: Implications for Historical Surgical Stimulation Studies?. Epilepsy & Behavior, 60 181-186.

Schubert, M., Siegmund, H., Pape, H. C., & Albrecht, D. (2005). Kindling-induced changes in plasticity of the rat amygdala and hippocampus. Learning & Memory, 12, 520-526.

St-Pierre, L. S., & Persinger, M. A. (2005). Extreme obesity in female rats following prepuberal induction of lithium–pilocarpine seizures and a single injection of acepromazine, Epilepsy & Behavior. 7, 411-418.

Tsang, E. W., Koren, S. A., & Persinger, M. A. (2004). Power increases within the gamma range over the frontal and occipital regions during acute exposure to cerebrally counter clockwise rotating magnetic fields with specific derivatives of change, International Journal of Neuroscience. 114, 1183-1193.

Chapter Transition: Electrical Stimulations

The previous chapter demonstrated that suppressions of low-frequency electric potential fluctuations within subsections of fixed, post-mortem rat brain tissue were predictive of seizure pathology and related to brain mass. The following chapter is an attempt to experimentally assess coronal sections of fixed, human brain tissue by injecting patterned current into neuroanatomical loci and observing electrical output. The study involves applying sine-, square-, and spike-waveforms into the tissue at a constant 2 μV intensity in order to assess regional differential expression of output signals. The results indicate that the right parahippocampal and hippocampal regions were most receptive to the stimulation protocol as inferred by marked amplifications and that spike-wave inputs were most potent overall. Stimulus-dependent theta (low-frequency) and gamma (high-frequency) signal outputs were observed within the right mesial temporal region. A general response was observed as increased high-frequency power within the hippocampus which was not dependent upon the frequency of the applied current. However, the right parahippocampus responded to the narrow-band 7 Hz frequency by increasing mid-frequency (8-30 Hz) power output. These results are indicative of intrinsic or “hard-wired” differences within the fixed tissues which are unique in their receptivity to applied electrical stimuli. In other words, the tissues filter signals differently as a function of area and these are most pronounced within a small area of the right hemisphere when the applied signal closely approximates living-like waveforms and frequencies.

Chapter 5:

Differential Responsiveness of the Right Parahippocampal Region to Electrical Stimulation in Fixed Human Brains: Implications for Historical Surgical Stimulation Studies?

(Original Research)

Published in Epilepsy & Behaviour,

Vol. 60, pp. 181 – 186, 2016

Nicolas Rouleau & Michael A. Persinger

DOI: 10.1016/j.yebeh.2016.04.028

Abstract

If structure dictates function within the living human brain, then the persistence of specific responses to weak electric currents in fixed, deceased brains could reflect “hardwired” properties. Different key structures from the left and right hemispheres of brains that had been fixed for over 20 years with ethanol-formalin-acetic acid were stimulated with either 1 Hz, 7 Hz, 10 Hz, 20 Hz, or 30 Hz, sine-wave, square-wave or pulsed currents while needle-recorded quantitative electroencephalographic responses were obtained. Differential responses occurred only within the right hippocampus and parahippocampal gyrus. The right hippocampus displayed frequency-independent increases in gamma power relative to the left hemispheric homologue. The parahippocampal region responded exclusively to 7 Hz pulsed currents with wide band (8-30 Hz) power. These profiles are consistent with dynamic connections associated with memory and consciousness and may partially explain the interactions resultant of pulse type and hemisphere for experiential elicitations during the golden age of surgical stimulations. The results also indicate there may be an essential “hardwiring” within the human brain that is maintained for decades when it is fixed appropriately.

Introduction

A primary assumption in neuroscience specifically and science in general is that structure dictates function and therefore microstructure dictates microfunction. There is no a priori reason to presume that specific structures are homogenously distributed within the volume in which they are located. There is also no evidence that every intrinsic physical property of the human brain ceases to persist when the post-mortem tissue is maintained for several years in fixative. The history of direct surgical stimulation of the human brain has produced revealing characteristics of contiguous experiences and how cerebral electrical activity and complex cognition might be correlated (Gloor, Olivier, Quesney, Andermann, & Horowitz, 1982; Horowitz & Adams, 1970; Kubie, 1953; Mahl, Rotherberg, Delgado, & Hamlin, 1964; Williams, 1956). Very early in this research several critical properties about the human brain and the electrical parameters required to elicit experiences or paroxysmal cortical activity became apparent. First the mesiobasal portions of the temporal lobes were particularly responsive to direct electrical stimulation (Bancaud, Brunet-Bourgin, Chauvel, & Halgren, 1994; Gloor, 1972; Halgren, Walter, Cherlow, & Crandal, 1978). Second, square-wave electrical patterns with specific durations appear to have been either simply preferred by neurosurgeons or maximally effective (Babb, Wilson, & Isokawa-Akesson, 1987; Isokawa-Akesson, Wilson, & Babb, 1987; Lieb, Hoque, Skomer, & Song, 1987; Mahl, Rotherberg, Delgado, & Hamlin, 1964; Steven, Mark, Erwin, Pacheco, Suematsu, 1969; Weiser, 1983). The effects were implicitly attributed to the dynamic living brain. Here we present evidence that specific properties in response to electrical stimulation that was optimal for surgical stimulation in

living human brains within specific regions of right temporal (parahippocampal) region may persist for decades if the cerebral tissue has been fixed appropriately.

Materials & Methods

Specimens and Histology

The fixed human whole brains and sections were obtained from the Behavioural Neuroscience Laboratory's collection. The brains had been obtained from North Carolina Biological Supply or anonymous donors between 10 and 25 years ago. There was no information available about the history of the brains. Upon arrival at the laboratory the brains were removed from the packing solutions and placed within ethanol-formalin-acetic acid (EFA) where they had been maintained. The EFA was refreshed every year. This fixative is routinely employed in our laboratory for human and rodent brain research (Persinger, 1979) because following processing and paraffin embedding the sections by microtome are reliable, deliver protracted "ribbons", and produce homogenous staining. In addition we have found that EFA fixative allows, following chemical reconstitution, staining of some enzyme related indicators.

Examples of the integrity of the human brain tissue that had been maintained in EFA for more than 25 years are shown in Figure 15. Small approximately 2 cc (2 g) cubic sections had been sampled from the cortices or hippocampal formations of various specimens. All sections were stained with Toluidine blue O. The presence of somas in the temporal cortices and hippocampus are clearly evident. Even the nuclei of glial cells were clearly discernable. Although the sections did not display the sharp acuity typical of

rat brains that had been removed and placed in EFA within about 4 to 5 min, the human sections indicated remarkable integrity.

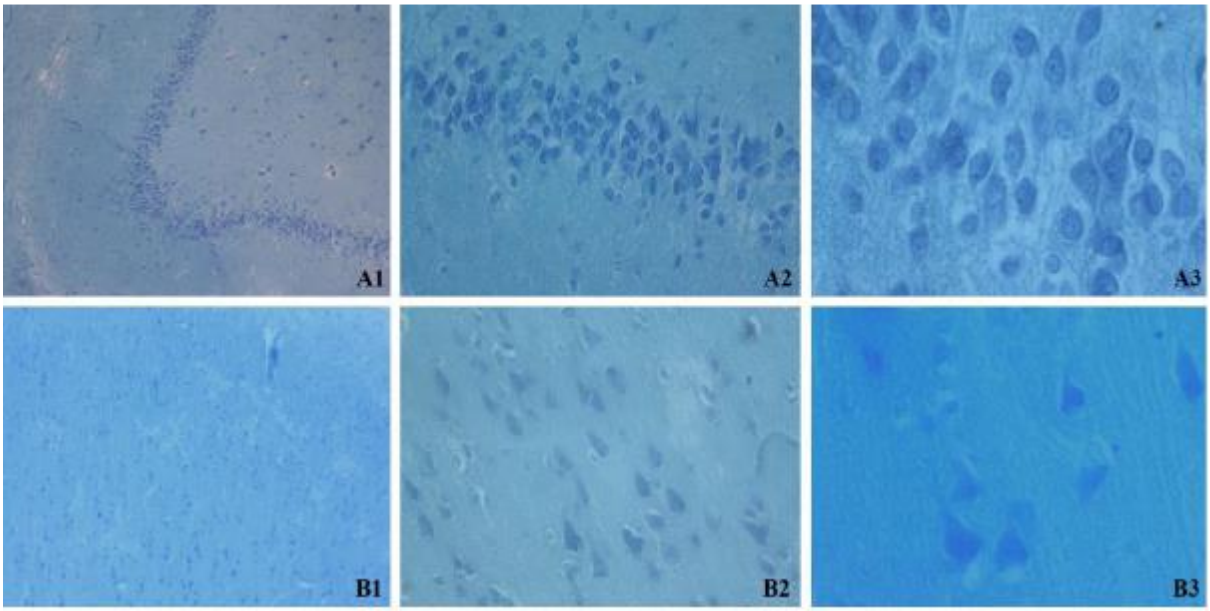

Figure 15. The Fixed Brain: Histological sections (Toluidine blue O) of human brain tissue that had been fixed in EFA for over 20 years. The source tissues were measured for signal responses in the present experiment. A1-A3 is hippocampus at 100 x, 400 x and 1,000 x. B1 to B3 is temporal cortex at 100 x, 400 x, and 1000 x.

Generating Signals & Output

The signal processing capacities of coronal sections of chemically fixed human brain tissue were investigated by applying patterned current and examining local electric potential differences as a function of the probed locus and signal type. Three (3) simple wave types were utilized: sine waves, square waves, and spike waves. Square and sine waves with associated frequencies of 1Hz, 7Hz, 10Hz, 20Hz, and 30Hz were generated within Audacity 2.0.5 audio editing software at the 44, 100Hz (default) sampling rate. The

signals were generated as pure tones where the amplitude was defined as 0.8 of the potential maximum 1.

Spike waves were generated by first coding a 7Hz square wave pattern within Arduino 1.0.6 software. Output was directed to an Arduino UNO R3 microcontroller coupled to a toroidal coil. The electromagnetic field generated within the center of the toroid was measured using a telephone pickup device that measured amplitude changes in electromagnetic fields. The rise and fall of the square wave signal, once transduced by the coil, resulted in positive and negative spike-potentials which were recorded within Audacity 2.0.5. For each square-wave cycle, two spikes were generated: One spike associated with the rise of the square wave and one was associated with the fall (decay). In order to generate analogous 1Hz – 30Hz wave patterns, fall-spikes were removed from the record, leaving rise-spike potentials which were frequency-matched to sine and square wave signals.

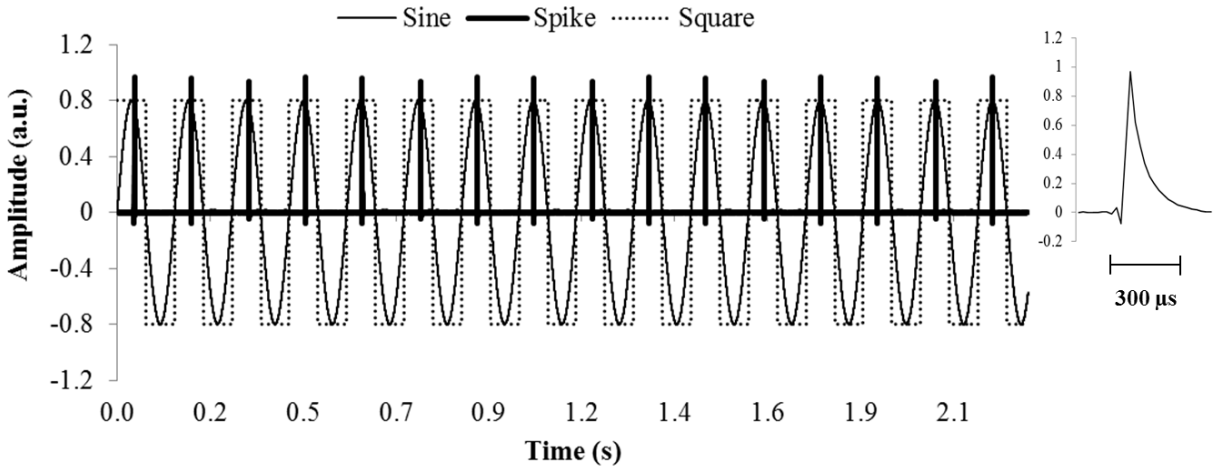

Figure 16. Electrical Stimuli: Sine, spike, and square stimulus waveforms with matched 7Hz frequency. The spike potential is displayed within a finer increment of time (300 µs).

Sine waves displayed frequency-dependent signal rise-fall times which ranged between 18ms for the highest frequency and 500ms for the lowest. Square waves displayed a consistent rise-fall time of 23 µs. Spike-potentials, however, were associated with rise times of 45 µs and fall times of 320 µs. These signals can be visualized in Figure 16 for 7 Hz waveforms.

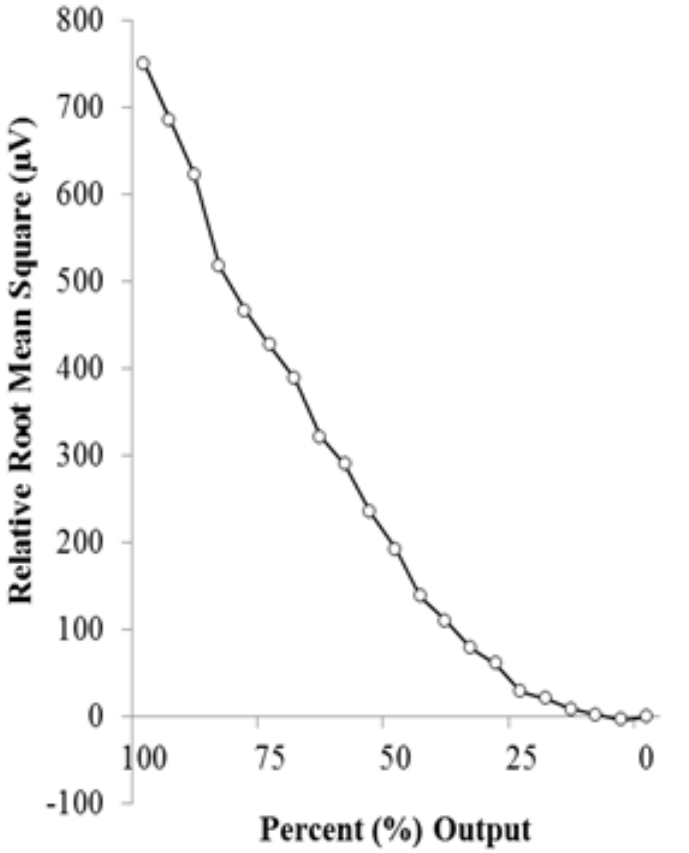

Figure 17. Output Curve: Root mean square of voltage increase relative to baseline measurements plotted by percentage of maximum intensity output from the laptop computer. Each point represents a 5% decrease in output amplitude.

Output of signals to the tissue was accomplished by coupling a coaxial cable to the soundcard of an HP Envy laptop computer running a Windows 8 operating system.

Signals were loaded into Audacity 2.0.5 in 30s segments to be displayed to the tissue sequentially. Figure 17 shows the intensity curve associated with the 7Hz sine wave stimulus when applied to the tissue as a function of percentage of maximum output of the laptop computer via the soundcard-coaxial cable. Audio output was reduced to 10% of maximum amplitude for the purposes of the experiment, resulting in 2μV potentials. The order of each signal was counterbalanced across trials.

Electric Potential Difference

A Mitsar electroencephalography system was used to measure electric potential differences between selected loci within coronal sections (n=3) of brain tissue relative to a common reference point. Needle-probes were inserted into 1 of 7 potential areas: parahippocampal gyrus, corona radiata, caudate nucleus, hippocampus, temporal stem, insular grey, or internal capsule. Left and right hemispheric neuroanatomical analogues were probed independently. The basilar artery served as the electrical reference. The stimulating and recording probes were always separated by 4 mm. This configuration of needle probes can be visualized in Figure 18.

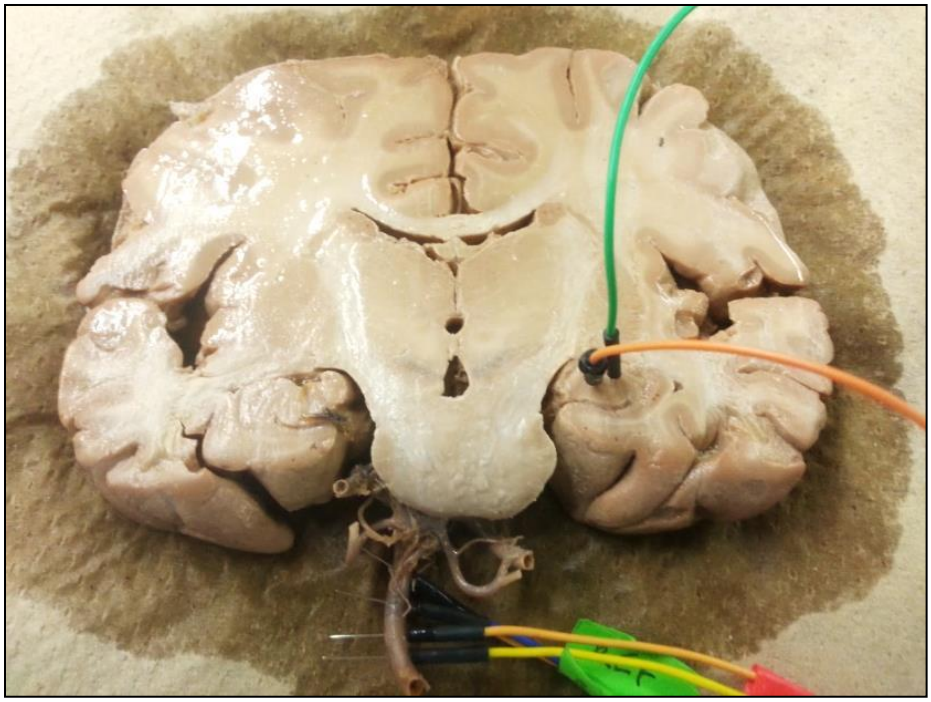

Figure 18. Human Coronal Sections: Coronal section receiving signal input (orange) to the right hippocampal body during simultaneous recording of electric potential difference between adjacent hipoocampal tissue (green) and the basilar artery (REF).

WinEEG software was used as a recording platform. The system was set to sample at 250Hz with a notch filter applied to exclude electrical artifacts between 50Hz and 70Hz as well as 110Hz and 130Hz. Low- and high-cut filters of 1.6Hz and 50Hz were applied to the record. Frequency bins for spectral power density (SPD) extraction such as delta (1.5Hz – 4Hz), theta (4Hz – 7.5Hz), alpha (7.5Hz – 14Hz), beta1 (14Hz – 20Hz), beta2 (20Hz – 30Hz), and gamma (30Hz – 40Hz) bands were defined. Data extraction consisted of sequestered 30 second segments of raw data with 2 second epochs.

Procedure

Ethanol-formalin-acetic acid (EFA) was applied to the sections prior to each trial. A 30 second baseline recording of intrinsic electric potential differences was obtained, after which the sequence of signals was initiated. For any given trial, all frequencies were displayed within one of the wave conditions. Each signal was displayed to the tissue for 30 seconds. Each trial lasted 180 seconds consisting of baseline, and 5 frequencies generated in sequence. Signal sequences were counterbalanced to eliminate confounding factors.

Results

Spectral power densities (SPDs) obtained within the probed loci were compared across the aforementioned conditions. ANOVAs revealed a hemisphere by matter by wave interaction for theta, alpha, and beta1 power with weak effect sizes of ~1%. Spike trains ubiquitously produced increased power across spectral frequency bands relative to sine and square waves ($p<.05$). However, grey matter within the right hemisphere generated the only significant “split” of the waveforms such that three distinct and independent homogeneous subsets were identified, $F(2, 214)= 16.21$, $p<.001$, $\eta^2=.13$ (Figure 19). The SPDs obtained within alternative combinations of collective loci as classified by hemisphere and matter type did not display similar signal processing characteristics ($p>.05$).

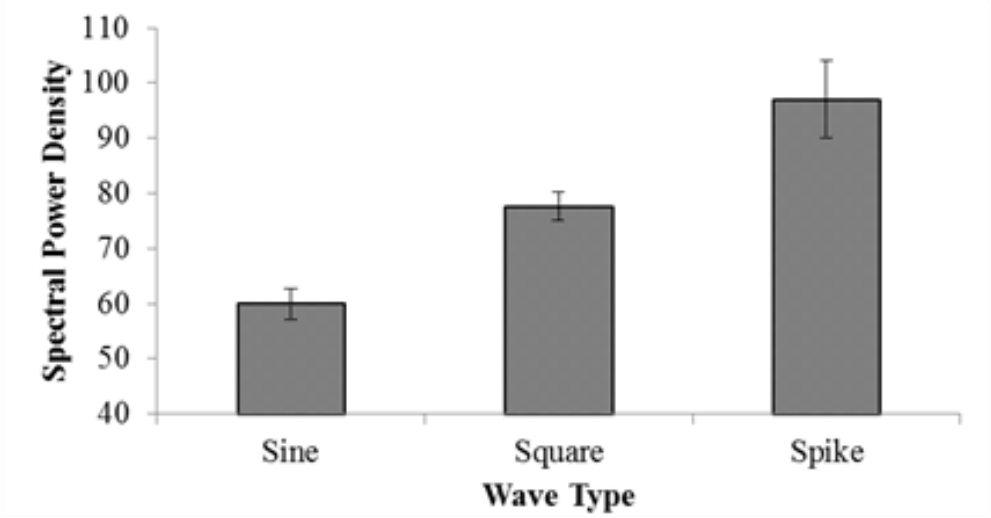

Figure 19. Spike-Theta Effect: Theta power within right hemispheric grey matter as a function of the wave type of the stimulus.

An ANOVA revealed a locus by hemisphere interaction upon SPDs if the tissue was stimulated, $F(6,627)= 2.61$, $p<.05$, $\eta^2= .02$. This effect did not depend upon the type of stimulation. SPD differences as a function of loci within the left hemisphere were not identified across any of the QEEG frequency bands ($p>.05$). However, significant theta power differences were identified as a function of the locus of the probe within the right hemisphere, $F(6,313)= 2.73$, $p<.05$, $\eta^2= 0.01$. Homogeneous subsets identified that the source of the variance was due to significantly increased theta power within the parahippocampal gyrus relative to the internal capsule ($p<.05$). Other frequencies of intrinsic power were not affected as a function of general stimulation ($p>.05$).

Isolating the parahippocampal gyrus, hemispheric differences in theta power were identified if the tissue received some form of stimulation wherein right hemispheric expression of theta ($M= 92.47$, $SE= 8.97$) increased relative to the left hemispheric analogue ($M= 67.91$), $t(88)= -2.51$, $p<.05$, $r^2=.07$. Theta power differences as a function

of hemisphere were not identified for any of the alternative loci (p>.05). These data are presented in Figure 20.

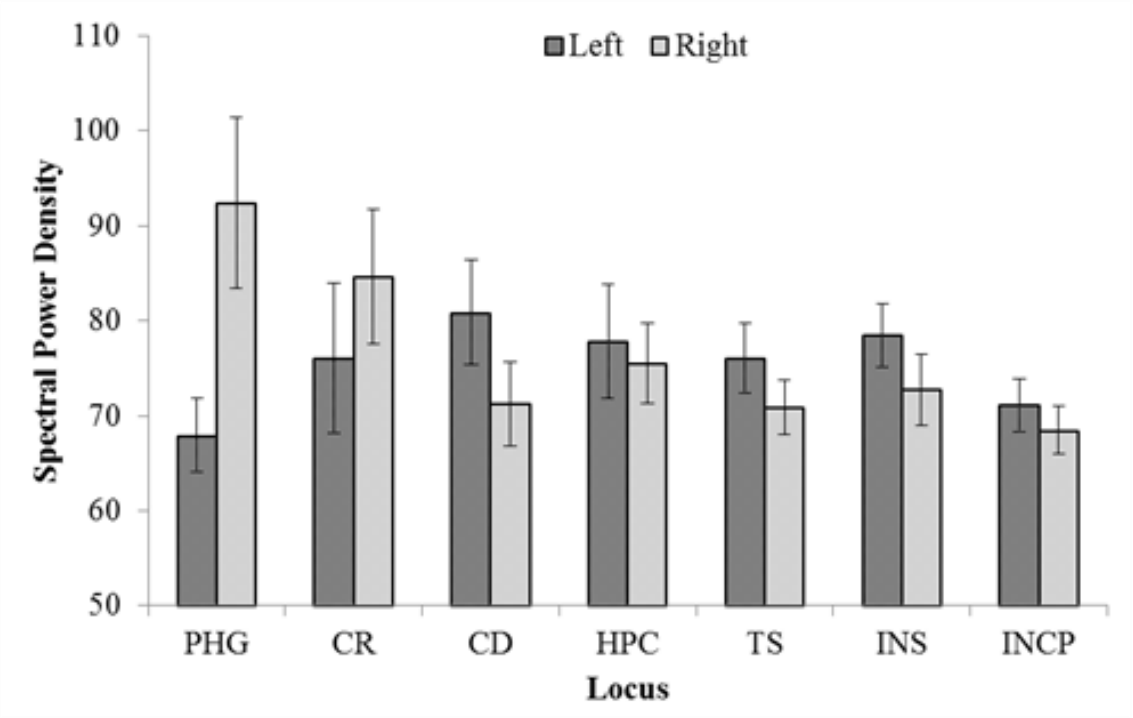

Figure 20. Interhemispheric Parahippocampal Theta-Effect: Theta power differences upon stimulation of tissue as a function of hemisphere for the parahippocampal gyrus (PHG), corona radiata (CR), caudate nucleus (CD), hippocampus (HPC), temporal stem (TS), insular grey (INS), and internal capsule (INCP).

In order to focus upon the precise stimulus which optimally generated hemispheric differences in expressed theta power within the parahippocampal gyri, analyses were conducted controlling for wave type. Right parahippocampal theta power effectively doubled (M= 138.75, SE= 25.50) relative to left parahippocampal theta power (M= 74.47, SE= 4.15) when the stimulus was a spike-train, $t(22) = 2.49$, $p<.05$, $r^2= .22$. Significant differences in theta power as a function of hemisphere could not be identified when

examining only sine- or square-wave-stimulated tissue (p>.05). The hippocampus was the only other locus which responded differentially to wave types as a function of hemisphere. Significantly increased gamma-band SPD were identified within the right (M= 1.62, SE= .08) relative to the left (M= 1.37, SE= .06) hippocampal body when spike train stimuli were applied to the tissue, t(28)= 2.61, p<.05, r^2=.20. These effects were not observed when comparing left and right measurements obtained within the corona radiata, caudate nucleus, temporal stem, insular grey, or internal capsule (p>.05). Figures 21 and 22 illustrate this unique feature of spike train stimuli.

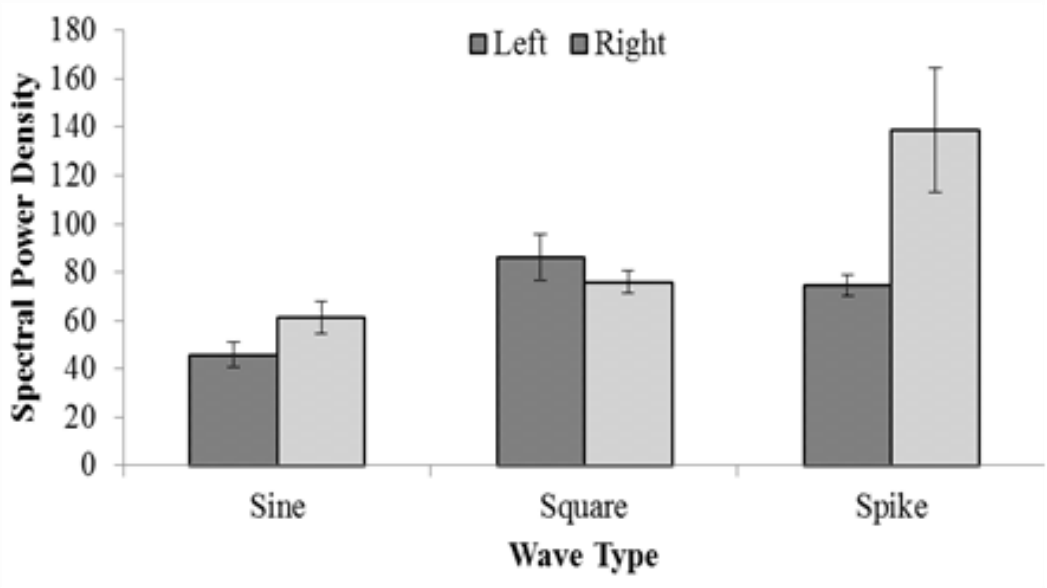

Figure 21. Interhemispheric Spike-Theta Effect: Parahippocampal theta power differences as a function of hemisphere for each stimulus wave type condition.

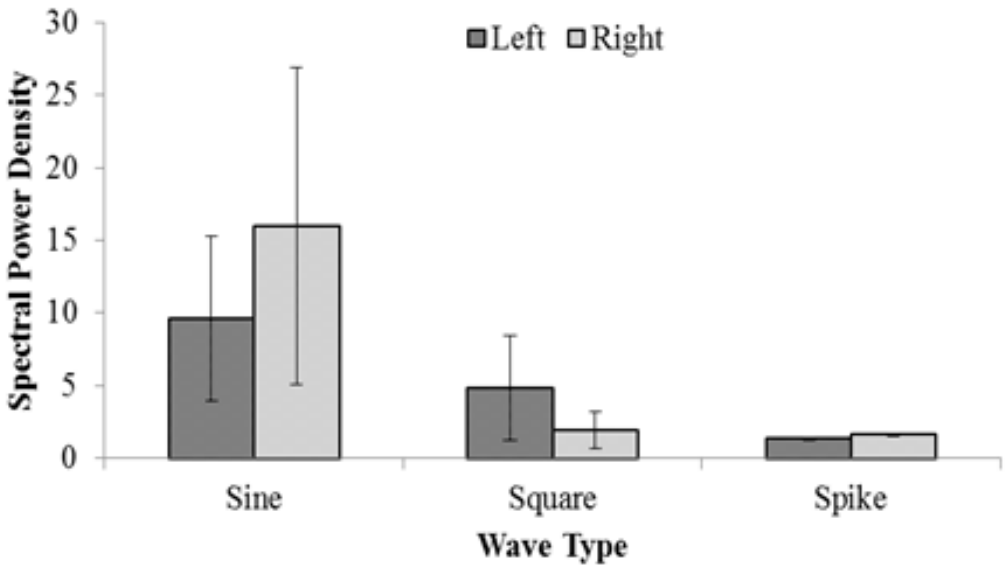

Figure 22. Interhemispheric Spike-Gamma Effect: Hippocampal gamma power differences as a function of hemisphere for each stimulus wave type condition.

When the parahippocampal gyrus was stimulated with a 7Hz spike train, right hemispheric alpha-, beta1-, and beta2-band SPD increased significantly relative to the left hemisphere ($p<.05$) with effect sizes ranging between 66% and 75%. This lateralized activation was not identified for the left hemispheric anatomical homolog or any other locus receiving 7Hz spike train stimulation ($p>.05$). Spike trains with associated frequencies of 1Hz, 10Hz, 20Hz, or 30Hz did not generate similar effects within the right parahippocampal gyrus ($p>.05$).

Discussion

The results of these direct measurements of fixed human brain tissue employing quantitative measurements of potential differences in response to different signal shapes to discern the tissue's response to these patterns indicate residual differences in response potential decades following death and fixation. As would be expected for a

heterogeneous mass the spectral density profiles exhibited non-specific enhancements from the injection of electrical energy to very localized, frequency, and pulse form-specific response profiles to only one of the frequencies (7 Hz) compared to frequencies below (1 Hz) or above (10 Hz, 20 Hz, 30 Hz) this value. This might be considered strong evidence that cerebral microstructures were still intact to some degree despite the absence of vitality and prolonged fixation. It might also suggest the presence of a fundamental base structure of the human brain that could accommodate its interesting features such as sensory-limbic hyperconnectionism (Bear, 1979).

In this study, we have treated the brain as a type of electroconductive material. If subcomponents of the brain can be conceptualized as partially isolated circuits, it is sensible that given the heterogeneity of neural connections certain areas of the brain would process the same signal differently. Variable forms of processing do not necessarily require physiological parameters observed in living tissue. Rather, the microstructure of the neural environment provides sufficiently variable structural gradients with electrically-relevant characteristics such as resistance which alter the passage of current. Our results suggest that the material of the brain, sectioned and chemically fixed, demonstrates non-uniform responses to applied electrical signals.

These results must be viewed within the context of certain key factors. The tissue samples were fixed in ethanol-formalin-acetic acid (EFA). A comprehensive review of the various types of actions performed upon proteins by the constituent factors of this fixative solution is provided by Harrison (Harrison, 1984). In addition to conformational changes and coagulation of protein complexes, the primary mechanism by which fixation is maintained is protein cross-linking – a putative function of aldehyde-based fixatives. The

structural surfaces of proteins, which express spatially distinct surface charge gradients, are altered as a function of any of these modifications and therefore represent sources of variance when considering the electrical properties of the brain as a material. In the context of our study, however, we have maintained the solution as a constant and instead have experimentally demonstrated local differences in signal processing of common signals.

The right hemispheric grey matter responded with wide-band power increases to all three forms of stimulation. The most efficacious signal shape was the pulse or spike signal (300 μs) followed by the square wave and sine wave patterns. There was also no specific effect within the areas that were measured for the stimulation frequencies 1 Hz, 7 Hz, 10 Hz, 20 Hz, and 30 Hz. When the tissue sampled from the right hemispheric grey matter was measured there was a specific increase in power within the theta range. The amplitude was about double that of the left hemisphere. Closer inspection of the data indicated that the primary source of variance was from the right parahippocampus compared to the internal capsule.

Specificity of response occurred only in the hippocampus and parahippocampal area. Only the *spike trains* but not the square wave or sine wave sequences produced increased power changes and these occurred only in the *right hippocampus* and specifically for the *gamma range*. The only tissue to respond to a specific frequency was the *parahippocampal region*. It responded only to the *7 Hz spike pattern* with increased generalized power across the alpha bands to the higher beta range, that is, 8 Hz to 30 Hz. This conspicuous increase in wide band power did not occur for the frequencies below

(1 Hz) or above (10 Hz, 20 Hz, and 30 Hz) the 7 Hz spike trains and was not evident within the left parahippocampal region.

The elicitation of theta power from the hippocampus in response to any frequency stimulation between 1 Hz and 30 Hz and the importance of pulsed stimulation (rather than sine waves or square waves) and the specific enhancements of 8 to 30 Hz within the right parahippocampal region to only 7 Hz is significant for several reasons. Recently, Fernandez, Malerba, Bressloff, and White (Fernandez, Malerba, Bressloff, & White, 2013) measured a distinct "preference" for stellate cells in the entorhinal cortices for spike phase-locking to theta inputs. They found this phase-locking was robust and was displayed over a range of background fluctuations in plasma membrane fluctuations.

The 7 to 8 Hz fundamental of the entire cerebrum was shown also by Nunez (1995) to be a quantitative solution with realistic bulk velocities (~4.5 m/s) of rostral-caudal axonal activity for a typical living cerebrum with a circumference of about 60 cm. He also showed that the shift in lower alpha frequencies was associated with skull circumference. The time required for a coherent bulk velocity field to move along the rostral caudal axis would be about 25 ms whose frequency equivalent is "40 Hz". The seminal work by Llinas and Ribary (1993) and Llinas and Pare (1991) have shown theta coherent 40 Hz oscillations characterize the waking state and the dream state in human brain activity.

That this frequency peak is not completely a dynamic process but directly predictable by assuming that brain tissue exhibits the properties of a LC circuit was calculated by Tsang, Koren, and Persinger (2004). Employing measures of inductance (permeability) of cortical grey matter at 1 kHz (to simulate the action potential duration) the value was 10^{-2} Henrys. The permittivity for grey matter was 2×10^{-1} F. Application of

the formula f (resonance frequency)=1/(2π (LC)$^{-1/2}$) solves for a resonance or standing resonance of about 7 Hz. The persistence of this frequency band either as responses to generalized stimulation or generalized responses from specific stimulation suggests that the microstructure or general metrics of the human brain is more resonant with this oscillation.

The experimentally-induced specific changes in the right temporal lobe from applied currents in fixed human brain tissue were consistent with the current understanding of the relationship between the hippocampus and parahippocampal cortices. Theta trains spontaneously generated as a function of state could be argued to actually define hippocampal dynamics. Buzsaki (2002) found that 40 Hz ripples were superimposed upon these large amplitude theta patterns generated from the hippocampus. In the living brain theta-gamma synchronization has been measured during visual working memory tasks (Holtz, Glennon, Prendergast, & Sauseng, 2010). The review by Whitman, Ward, and Woodword (2013) indicated that the amplitudes of the gamma oscillations are modulated by the theta phase. In a set maintained in working memory each 40 Hz gamma cycle within a 7 Hz theta cycle corresponded to an organization of one item. The results of the present study indicate that this bimodal power frequency may be a feature of intrinsic structures within the brain that remain after being fixed, and, that they can be re-activated.

In the present experiments there was enhancement of power within the gamma range in response to only the spike trains. The single duration of these spikes was 364 μs (rise time: 35 μs, dissipation time: 320 μs) or about 0.5 ms which is within the duration time for the peak component of the action potential. The corresponding frequency

equivalence would be a factor of 2 to 4 of that involved with the optimal elicitation of long-term potentiation (LTP) in hippocampal slices (Greenough, 1984; Rose, Diamond, Pang, & Dundwiddie, 1988; Whitlock, Heynen, Shuler, & Bear, 2006). However this duration is well within the range of the fast frequency discharges recorded from both human and rat epileptic brain (Bragin, Engel, Wilson, Fried, & Buzsaki, 1999; Bragin, Wilson, Staba, Reddick, Fried, & Engel, 2002).

The major output from (as well as input to) the hippocampus is the entorhinal cortex within the parahippocampal gyrus. Only this region responded to the specific 7 Hz spike stimulation. The response was wide band and ranged from 8 to 30 Hz. This effect would be consistent with the role of the parahippocampal gyrus as the major input to the entire neocortex (Gloor, 1997). The intimate connection between the hippocampus and neocortex through the 40 Hz ripples superimposed upon the 7 Hz fundamentals of the hippocampus was hypothesized by Bear (1996) to be the condition that allows memory and awareness to converge potentially into consciousness. Our measurements in the present study suggest that these propensities may be more “hardwired” than previously assumed.

The differential response of the right hemispheres of fixed brains, specifically portions of the temporal lobe, to the experimental currents suggests that some feature of living structures remained for decades following fixation. The histological staining verified there was substantial gross integrity. The right hemisphere is not sufficiently different in volume from the left hemisphere to explain these effects (Goldberg et al., 2013; Good, Johnsrude, Ashburner, Henson, Friston, & Frackowiak, 2001). There is an estimated 10% greater proportion of white matter in the right compared to the left hemisphere. Clinical

approaches (Bear, 1986) indicate that the left hemisphere is more “module organized” while the right hemisphere is more diffuse and “field-like”. Consistent with this traditional approach is the recent evidence that “space” and the units within it may be encoded within the parahippocampal cortices (Giocomo & Roudi, 2012).

Recently we (Rouleau, Lehman, & Persinger, 2016) found the right caudal hemisphere which would include the temporal region uniquely displays attenuation of power when a copper screen is placed over the person’s head while he or she is wearing the EEG sensor cap. In living brains, quantitative electroencephalograph (QEEG) power profiles were correlated with increases in global geomagnetic activity (Mulligan, Hunter, & Persinger, 2010), an effect that can be produced experimentally by imitating geomagnetic variations (Mulligan & Persinger, 2012). One of the frequency bands that “shifted” was theta range. Whether or not the results of this experiment require a re-evaluation of the explanation of the subjective experiences produced during surgical stimulation over the last decades might only be a philosophical issue. That is, in light of what we hypothesized are conserved intrinsic structural features within the brain which selectively process specific types of signals, the shared experiences of individuals that have historically undergone surgical stimulations (Gloor, Olivier, Quesney, Andermann, & Horowitz, 1982; Horowitz & Adams, 1970; Kubie, 1953; Mahl, Rotherberg, Delgado, & Hamlin, 1964; Williams, 1956) are now subject to analyses of phenomenology. However, if structure dictates function then intrinsic organizations in the human brain that are so potent they produce dynamic quantitative effects to appropriate electrical stimulation long after the brain no longer lives may be worthy of further investigation.

References

Babb T.L., Wilson C.L., & Isokawa-Akesson M. (1987). Firing patterns of human limbic neurons during stereoencephalography (SEEG) and clinical temporal lobe seizures. Electroencephal Clin Neurophysiol. 66, 467-482.

Bancaud J., Brunet-Bourgin F., Chauvel P., & Halgren E. (1994). Anatomical origin of déjà vu and vivid “memories” in human temporal lobe epilepsy. Brain, 117, 71-90.

Bear D.M. (1986). Hemispheric asymmetries in emotional function: a reflection of lateral specialization in cortical-limbic connections. In Doane BK, Livingston KE (eds). The limbic system: functional organization and clinical disorders. N.Y., Raven, pp. 29-42.

Bear D.M. (1979) Temporal lobe epilepsy- a syndrome of sensory-limbic hyperconnectionism. Cortex, 15, 357-384.

Bear M.F. (1996). A synaptic basis for memory storage in the cerebral cortex. Proc Natl Acad Sci USA, 93, 13453-13459.

Bragin A., Engel J., Wilson C.L., Fried I., & Buzaski G. (1999). High-frequency oscillation in human brain. Hippocampus, 9, 137-142.

Bragin A., Wilson C.L., Staba R.J., Reddick M.S., Fried I., & Engel J. (2002). Interictal high-frequency oscillations (80 to 500 Hz) in the human epileptic brain: entorhinal cortex. Ann Neurol, 52, 407-415.

Buzsaki G. (2002). Theta oscillations in the hippocampus. Neuron, 33, 325-340.

Fernandez F.R., Malerba P., Bressloff P.C., & White J.A. (2013). Entorhinal stellate cells show preferred spike phase-locking to theta inputs that is enhanced by correlations in synaptic activity. J Neurosci, 33, 6027-6040.

Giocomo L.M. & Roudi Y. (2012). The neural coding of space in the parahippocampal cortices. Frontiers in Neural Circuits, Vol 6, Article 53.

Gloor P. (1972). Temporal lobe epilepsy: its possible contribution to the understanding of the functional significance of the amygdala and its interaction with neocortical-temporal mechanisms. In Eleftherion BE (ed) Advances in Behavioral Biology: The Neurobiology of the Amygdala, Plenum Press, N.Y.

Gloor P. (1997). The temporal lobe and limbic system, Oxford University Press, Oxford.

Gloor P., Olivier A., Quesney L.F., Andermann F., & Horowitz S. (1982). The role of the limbic system in experiential phenomena of temporal lobe epilepsy. Ann Neuro, 12, 129-144.

Goldberg E., Roediger D., Kucukboyaci N.E., Carlson C., Devinsky O., Kuzniecky R., Halgren E., & Thesen T. (2013). Hemispheric asymmetries of cortical volume in the human brain. Cortex, 49, 200-210.

Good C.D., Johnsrude I., Ashburner J., Henson R.N.A., Friston D.J., & Frackowiak S.J. (2001). Cerebral asymmetry and the effects of sex and handedness on brain structure: a voxel-based morphometric analysis of 465 normal adult brains. NeuroImage, 14, 685-700.

Greenough W.T. (1984). Structural correlates of information storage in the mammalian brain: a review and hypothesis. Trends in Neurosci, 7, 229-233.

Holtz E.M., Glennon M., Prendergast K., & Sauseng P. (2010). Theta-gamma phase synchronization during memory matching in visual working memory. NeuroImage, 52, 326-335.

Horowitz M.J., Adams J.E. (1970). Hallucinations on brain stimulation: evidence for revision of the Penfield hypothesis. In Keup W (ed) Origins and mechanisms of hallucinations. N.Y. Plenum, pp 12-20.

Halgren E., Walter R.D., Cherlow D.G. & Crandal P.H. (1978). Mental phenomena evoked by electrical stimulation of the human hippocampal formation and amygdala. Brain, 101, 83-117.

Harrison P.T.C. (1984). An ethanol-acetic acid-formol saline fixative for routine use with special application to the fixation of non-perfused rat lung. Laboratory Animals, 18(4), 325-331.

Isokawa-Akesson M., Wilson C.L., Babb T.L. (1987). Structurally stable burst and synchronized firing in human amygdaloid neurons: autocorrelation analyses in temporal lobe epilepsy. Epilep Res, 1, 17-34.

Kubie L.S. (1953). Some implications for psychoanalysis of modern concepts of the organization of the brain. Psychoanaly Quart, 22, 21-68.

Lieb J.P., Hoque K., Skomer C.E., & Song X.-W. (1987). Interhemispheric propagation of human mesial temporal lobe seizures: a coherence/phase analysis. Electroenceph Clin Neurophysiol, 67, 101-119.

Llinas R.R. & Pare D. (1991). Of dreaming and wakefulness. Neurosci, 44, 521-535.

Llinas R. & Ribary U. (1993). Coherent 40-Hz oscillation characterizes dream state in humans. Proceed Natl Acad Sci, 90, 2078-2081.

Mahl G.F., Rothenberg A., Delgado J.M.R., & Hamlin H. (1964). Psychological responses in the human to intracerebral electrical stimulation. Psychosomat Med, 26, 337-368.

Mulligan B.P., Hunter M.D., & Persinger M.A. (2010). Effects of geomagnetic activity and atmospheric power variations on quantitative measures of brain activity: replication of Azerbijani studies. Adv Space Res, 45, 940-948.

Mulligan B.P. & Persinger M.A. (2012). Experimental simulation of the effects of sudden increases in geomagnetic activity upon quantitative measures of human brain activity: validation of correlational studies. Neurosci Lett, 516, 54-56.

Nunez P.L. (1995). Towards a physics of the neocortex: in Nunez PL (ed) Neocortical dynamics and human EEG rhythms, Oxford University Press, Oxford.

Persinger M.A. (1979). Brain mast cells in the albino rat: sources of variability. Behav and Neural Biol, 25, 380-386.

Rose G.M., Diamond D.M., Pang K., & Dundwiddie T.V. (1988). Primed burst potentiation: lasting synaptic plasticity invoked by physiologically patterned stimuli. In Haas HL,

Buzsaki G (Eds) Synaptic plasticity in the hippocampus, Springer-Verlag, Berlin, pp. 96-98.

Rouleau, N., Lehman, B., & Persinger, M.A. (2016). Focal Attenuation of Specific Electroencephalographic Power Over the Right Parahippocampal Region During Transcerebral Copper Screening in Living Subjects and Hemispheric Asymmetric Voltages in Fixed Coronal Sections. Brain Research. 1644, 267-277.

Tsang E.W., Koren S.A., & Persinger M.A. (2004). Power increases within the gamma range over the frontal and occipital regions during acute exposures to cerebrally counterclockwise rotating magnetic fields with specific derivatives of change. Int. J. Neurosci. 114, 1183-1193.

Whitlock J.R., Heynen A.J., Shuler M.G., & Bear M.F. (2006). Learning induces long-term potentiation in the hippocampus. Science, 313, 1093-1098.

Whitman J.C., Ward L.M., Woodward T.S. (2013). Patterns of cortical oscillations organize neural activity in whole-brain functional networks evident in the fMRI BOLD signal. Front Human Neurosci, 7, Article 80.

Williams D. (1956). The structure of emotions reflected in epileptic experiences. Brain, 79, 29-67.

Stevens J.R., Mark V.H., Erwin F., Pacheco P., Suematsu K. (1969). Deep temporal stimulation in man. Arch Neurol, 21, 157-169.

Weiser H.G. (1983). Depth recorded limbic seizures and psychopathology. Neurosci Biobehav Rev, 7, 427-440.

Chapter Transition: A Filter Function

The previous chapter indicated that coronal sections of fixed, post-mortem human brain tissue filtered applied current differentially as a function of the neuroanatomical locus where the signal was applied. In the following chapter, we further test this “filtration” hypothesis by immersing brain tissue within electromagnetic fields. As field exposures are global immersions and inductions of current were anticipated within the conductive brain material, we expected to observe regional, punctate responses to the field patterns if said loci in particular were receptive to the signal. This is equivalent to testing the tuning frequency of particular antennas immersed within an array of antennas. Our results present two key findings. First, geomagnetic storms produce right-hemispheric amplifications of power spectra within coronal sections of fixed, post-mortem human brain tissue. Second, an unsectioned human brain was induced to express right-hemispheric but not left-hemispheric responses when exposed to electromagnetic fields within the laboratory setting. The applied fields, which were patterned to simulate physiological events (with appropriate control conditions), induced optimal expressions of power within the right orbital gyrus and uncus. These structures are intimately connected by the uncinate fasciculus, a tract system which governs reciprocal inhibition and excitation of the frontal-temporal region to modulate emotion, memory retrieval, and other brain functions. The observed phenomena are in line with historical data indicating geomagnetic disturbances are associated with changes in human cognition and behaviour related to aggression.

Chapter 6:

Neural Tissues Filter Electromagnetic Fields: Investigating Regional Processing of Induced Current in ex vivo Brain Specimens

(Original Research)

Published in Biology and Medicine, Vol. 9, pp. 1 – 7, 2017

Nicolas Rouleau & Michael A. Persinger

DOI: 10.4172/0974-8369.1000392

(Open Access)

Abstract

As has been demonstrated experimentally, the living brain responds to pulsatile electromagnetic fields. Our aim was to investigate the capacities of *ex vivo* neural tissue to process and filter induced current generated by naturally occurring and laboratory-controlled electromagnetic fields. Microvolt potentials within the chemically fixed post-mortem brains were collected throughout the field exposures. During strong geomagnetic storms there was a significant increase in power spectra within the 7.5 Hz to 14 Hz range within the right but not the left parahippocampal gyrus compared to days with relatively quiet geomagnetic activity. This finding indicated that ambient electromagnetic fluctuations from natural sources were processed differentially as a function of subsections of the post-mortem tissue. Exposing a whole, fixed human brain to two physiologically patterned magnetic fields that have been associated with powerful subjective experiences reported by hundreds of human volunteers in the laboratory setting elicited increased power within the 7.5 Hz to 20 Hz range. The effects required 10 to 20 s to emerge and were represented primarily represented within tissue subsections of the right amygdala and orbitofrontal gyri. Other fields such as a simple sine-wave (20 Hz) patterns of comparable intensity (2 to 10 μT) did not elicit the same configuration of changes. The results indicate that neural tissues filter electromagnetic fields non-randomly.

Introduction

The development of living systems from single cell to multicellular organisms occurred within the geomagnetic field. As Dubrov et al. (1978) succinctly summarized, there are large numbers of correlational studies that indicate all organisms respond to some component of geomagnetic activity. As reviewed by Persinger (1980), the correlations between increased geomagnetic activity and changes in various measures of behavior for human and animal populations usually accommodate 15% to 30% of the variability in these measures. The strongest correlations between changes in geomagnetic activity and behavioral or physiological variables occur within the same day or with changes one to three days previously. The median threshold of intensity for the activity is about 15 to 20 nT, although biological systems can exhibit thresholds below or above this value. One experiment involving more than 100 human subjects individually tested within a quiet, darkened chamber over several years demonstrated a conspicuous global geomagnetic activity threshold of about 20 nT above which the report of vestibular experiences were enhanced during a specific experimental manipulation. This magnitude was similar to that which disrupted homing behavior in pigeons.

That the geomagnetic effect is likely responsible for these correlations rather than the multiple temporally contiguous stimuli (e.g., cosmic rays, Alfven waves) or secondary effects have been shown experimentally. Inspired by the moderate strength correlations between global geomagnetic activity and convulsive seizures in human patients reported by Rajaram and Mitra (1981) Michon and Persinger (1997) demonstrated that the magnitude of the correlation between spontaneous seizures in epileptic rats and geomagnetic activity during the same intervals was experimentally reproducible when the

rats were exposed to a simulated “magnetic storm” pattern that was generated within the laboratory. Mulligan et al (2010) partially replicated the correlations reported by Babayev and Allahverdiyeva (2007) between global geomagnetic activity and specific frequency bands within the quantitative electroencephalographic (QEEG) measures of human volunteers. This included alterations in theta activity (4 Hz to 8 Hz) over the right parietal region. Mulligan and Persinger (2012) simulated the geomagnetic activity experimentally and found that after 10 to 15 min of whole body exposure to 20 nT variations there was enhancement of spectral power for theta activity over the right parietal region.

Saroka and his colleagues (2014) measured the electroencephalographic coherence between the left and right temporal lobes of 184 volunteers over a three year period while they sat within a quiet, darkened chamber. They found significantly increased coherence between the caudal temporal lobes for the 11 Hz band when the global geomagnetic activity increased above 8 to 10 nT. Source localization as inferred by sLORETA (Low Resolution Electromagnetic Tomography) revealed that the (right) parahippocampal region contributed significantly to the interhemispheric temporal lobe coherence. Within 1 Hz increments between 1 and 40 Hz, the most significant peaks in spectral power occurred at 7.5 Hz and 19.5 Hz. Although intuitions might dictate that direct effects of geomagnetic variations upon the cerebral volume may be too weak to be effective, the energy available according to the classic equation:

$$J=B^2 \cdot (2\mu)^{-1} m^3 \qquad (1),$$

where B is the strength of the field, μ is magnetic permeability ($1.26 \cdot 10^{-6}$ $N \cdot A^{-2}$) and m^3 is the volume might be significant.

Assuming a cerebral volume of $1.3 \cdot 10^{-3}$ m^3, a shift of 20 nT would be associated with ~10^{-13} J. Considering that each action potential ($1.2 \cdot 10^{-1}$ V) exerts upon a unit charge ($1.6 \cdot 10^{-19}$ As) an energy of 10^{-20} J (Persinger, 2010) this means that approximately 10^7 neurons could be affected. Rouleau and Dotta (2014) have argued that this aggregate of neurons is within the magnitude of the numbers of neurons involved with experiences of a percept. When the work of Cheng-yu et al. is (2009) considered, who showed that only one neuron is required to change the electrophysiological state of a (rat) brain, then energies induced within the brain volume from geomagnetic activity may not be trivial. Even single neurons in the prefrontal cortex encode abstract rules (Wallis and Kennerley 2011) and in rats, stimulation of a single neuron in the somatosensory cortex affects response detection (Houwelling and Brecht, 2007).

The most intuitively obvious explanation for the correlations between geomagnetic activity (including threshold effects) and specific frequency bands within the human electroencephalogram presumes the role of dynamic processes associated with the living brain. However if structure dictates function and the rudimentary microstructures of human brains remain after clinical death, assuming the tissue is appropriately fixed, then the energies within the volume of the brain during geomagnetic activity should be sufficient to alter the spectral power densities in a subtle but quantifiable manner. As reported by Tsang et al (2004) the inductance and capacitance of fresh brain tissue when stimulated with action potential related durations (1 kHz) is in the order of 7 Hz. The quantitative estimates and imaginative models by Nunez (2006) indicates that the intrinsic resonance of bulk velocity of action potentials along the rostral-caudal course of the living

cerebrum (Llinas and Ribary, 1993) every approximately 20 to 25 ms (“40 Hz”) divided by the typical cerebral circumference solves for a value in the theta range.

Direct application of physiologically patterned magnetic fields with intensities between 1 and 5 μT across the temporal lobes of volunteers has been reported to be associated with a continuum of subjective experiences including the “sensed presence” (Persinger and Healy, 2002). One of the most effective protocols to induce the latter experience has been the application of a decelerating complex pattern with slightly higher strength over the right hemisphere for 30 min followed by more bilateral stimulation of an accelerating complex patterned magnetic field once every 3 to 4 s across both hemispheres at the level of the temporal lobes (St-Pierre and Persinger, 2006) for 30 min. The latter pattern was shown to produce analgesia in rats (Martin et al, 2004). Saroka and Persinger (2013), employing LORETA methodology for source localization supported the hypothesis that enhanced stimulation of the right hemisphere followed by bilateral stimulation across the temporal lobes was associated with the most frequent reports of a sensed presence. Here we report for the first time that fixed human tissue during specific stimulation displayed significant enhancement with geomagnetic activity and the effect was prominent within the right hemisphere. In addition we demonstrate that the specific patterns of physiologically patterned magnetic fields that are most effective for producing powerful subjective experiences also elicited the greatest response from the fixed brain tissue.

Material and Methods

The present study was based upon the observation that geomagnetic storm conditions influenced microvolt fluctuations within coronal sections of fixed human brain tissue. An experiment was designed to test the hypothesis that electromagnetic fields were processed differentially as a function of spatial loci within the brain. The experimental procedure involved exposing a full (non-sectioned) chemically fixed human brain to different physiologically-patterned electromagnetic fields. Microvolt fluctuations induced by electromagnetic fields were measured within neuroanatomical regions of interest. Analyses were performed to determine whether different electromagnetic field patterns were amplified or attenuated by tissue subsections.

Investigative Analysis

Baseline spectral power densities (SPD) derived from electrical potential difference measurements which were obtained from coronal sections (n= 3) of fixed human brain tissue from four (n= 4) independent experiments completed between May 6, 2015 and April 8, 2016 were aggregated into a database. The only structures from which SPD data were abundantly available were the parahippocampal and hippocampal regions bilaterally. Consequently, the responses from these structures were utilized. These data were coded by date and Kp-index values indicative of geomagnetic storm conditions. They had been retrieved from the National Oceanic and Atmospheric Administration (NOAA) Space Weather online database (www.ngdc.noaa.gov). Kp 24 hour maxima were retrieved, which ranged between 1 and 5 on days of testing. A “storm” binary variable was coded where Kp values less than three (Kp < 3) were classified as “no storm” and Kp

values greater than three (Kp > 3) were classified as “storm”. Data analyses were performed to discern any potential relationship between geomagnetic field disturbances and spectral power fluctuations derived from microvolt measurements within coronal sections of fixed human brain tissue.

Human Brain Tissue

A full human brain, unsectioned and preserved for over 15 years in ethanol-formalin-acetic acid, served as the tissue specimen which was exposed to different patterned electromagnetic fields. The brain was ethically obtained from an anonymous donor and its use was approved by the institution’s research ethics board. The brain was neuroanatomically unremarkable, featuring all major gyri and sulci outlined by Crosby, Humphrey, and Lauer (1962). The anterior, middle, and posterior cerebral arteries were intact and partially affixed to the cerebrum and brainstem. This was important as previous electrophysiological measurements involving post-mortem fixed human brain tissue has involved the use of vasculature as the electrical reference point (Rouleau and Persinger, 2016; Rouleau, Lehman and Persinger, 2016).

The measurement procedure, similar to previous studies, involved a Mitsar 201 amplifier typically used for human quantitative electroencephalography (QEEG). Instead of the typical multi-sensor cap used in living human studies, five needle electrodes were coupled to the amplifier box. The first four sensors served as references and were directly inserted into the basilar artery of the brain. The average of the sensors constituted the electrical reference point. The fifth sensor was inserted into regions of interest where

microvolt fluctuations relative to the reference point were obtained during experimental manipulations.

Six neuroanatomical loci were selected as points of measurement wherein the needle electrode was inserted directly: the amygdala (by way of the uncus), middle frontal gyrus, orbital frontal gyrus, occipital pole, superior parietal lobule, and the parahippocampal gyrus. Both the right and left hemispheric structural equivalents were probed. All measurements were performed with the brain resting on its dorsal surface which rendered both the reference and probe sites accessible. Raw microvolt (μV) potentials were collected using WinEEG (2.93.59) and subsequently converted to SPD ($\mu V^2 \cdot Hz^{-1}$) within delta (1.5 Hz – 4Hz), theta (4 Hz – 7.5 Hz), alpha (7.5 Hz – 14 Hz), beta1 (14 Hz – 20 Hz), beta2 (20 Hz – 30 Hz), and gamma (30 Hz – 40 Hz) bands. Filters were applied to exclude 60 Hz ambient noise, 120 Hz harmonics, as well as periodicities below 1.6 Hz and above 50 Hz. All data collection and analyses were performed within SPSS v20 on an HP ENVY laptop computer with a Windows 8 operating system.

Exposure Device

Electromagnetic field patterns were delivered to a custom coil by a Zenith-386 compute (Model ZF-148-41, Zenith Data Systems, Benton Harbor, MI, USA) computer. The patterns were created by converting strings of programmable numbers (0 to 256, with 127=0) into voltage values between -5 and +5 V which were delivered by the complex software© (Professor Stanley A. Koren) to the coils through a digital-to-analogue converter (DAC). The current was then delivered to the coil from which the magnetic fields were generated (see Martin et al, 2004 for details). The “point durations” or discrete

application pulses within each pattern were selected based upon previous studies which identified specific field effects. Six patterns were selected: Burst X (3000, 3), Burst X (3, 3), Thomas (3000, 3), Thomas (3, 3), LTP (4500, 1), and a 20 Hz Sine (3000, 3). The first number within parentheses refers time (in ms) between repetitions of the pattern. The second number refers to the point duration that is the duration each voltage equivalent of the numbers between 0 and 256 were generated in ms. The LTP pattern disrupts memory consolidation in rats by potentially competing with Long Term Potentiation (Mach and Persinger, 2009). The sine-wave pattern is self-explanatory and was employed to discern the potential differential effectiveness of a physiologically-patterned field that contains a 20 Hz component from the redundant presentation of a symmetrical 20 Hz input. The total numbers of points in Burst, Thomas, LTP and sine patterns were 239, 859, 225 and 200, respectively. Figure 23 includes representations of the complex field patterns.

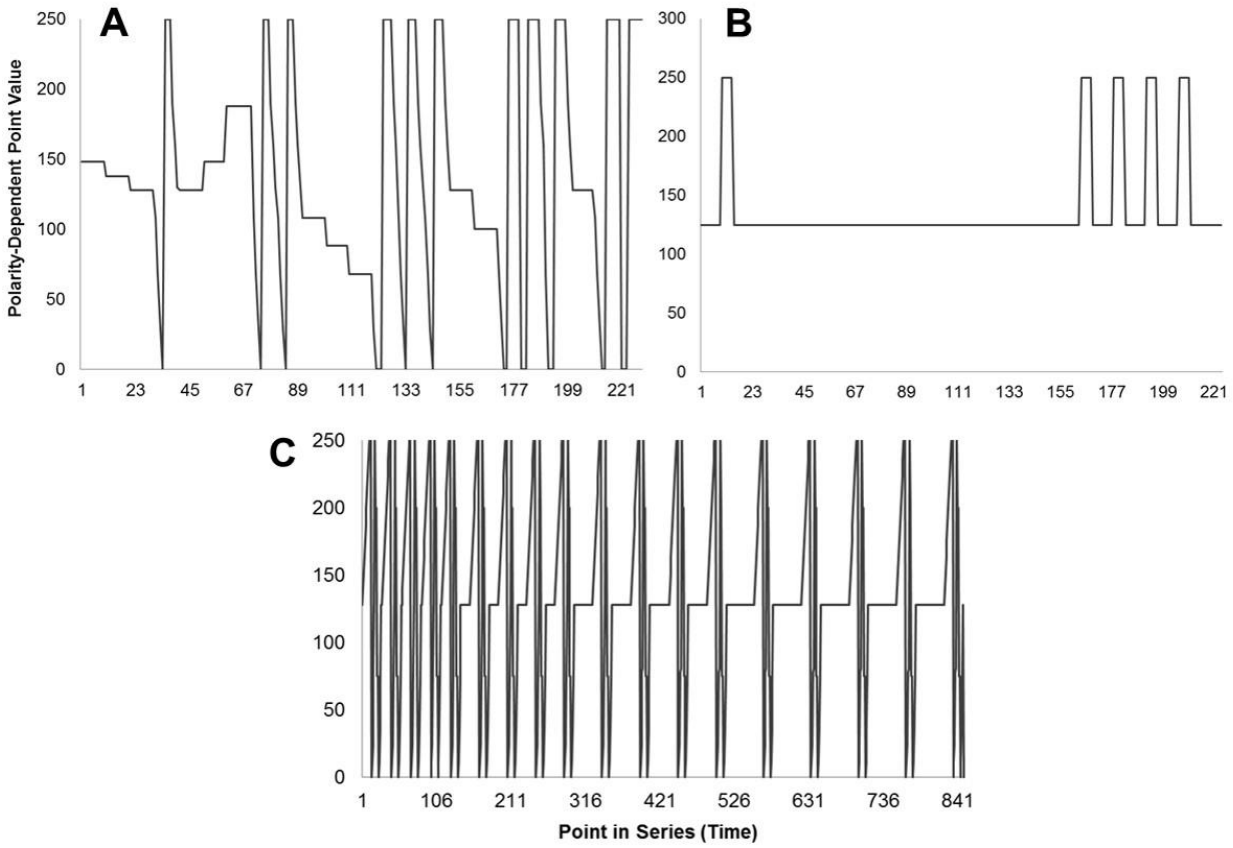

Figure 23. The Burst X (A), LTP (B), and Thomas (C) electromagnetic field patterns. The Y-axes represent polarity-dependent point values ranging between 0 and 250 whereas the X-axes represent the points within each series or, implicitly, time.

A coil, built by wrapping 305 m of a single layer of 30 AWG (Belden 9978) wire around a 38 cm × 33 cm × 27 cm milk crate (Figure 24), served as the electromagnetic field exposure device. This was the same coil employed by Murugan et al (2015). The crate was placed face-down over the tissue such that the wire was wrapped along the horizontal plane perpendicular to the surface of the testing table. The strength of the fields ranged between 2-10 μT. The tissue was exposed to one of the time-varying, complex electromagnetic fields for 60 seconds per trial. Each trial involved measurement of a single neuroanatomical locus. Experimental manipulations were counterbalanced to

avoid order-dependent confounding factors. There were a total of three replicates per pattern. Each trial was 60 s in duration.

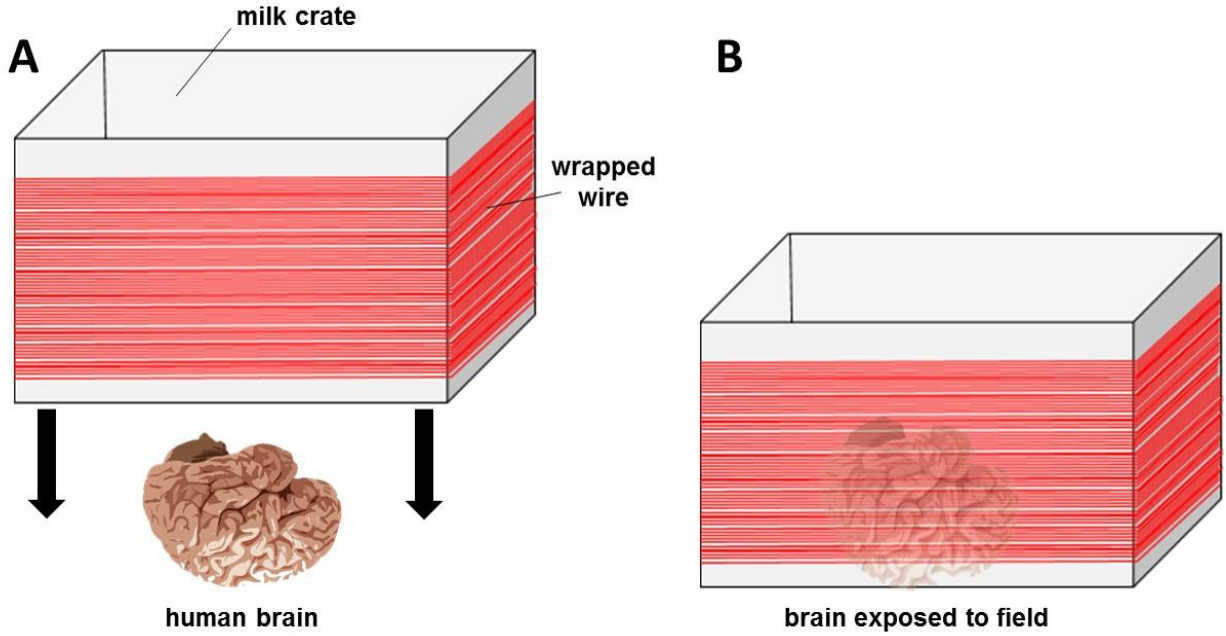

Figure 24. The coil was placed over the human brain (A), exposing the brain to a complex, time-varying electromagnetic field (B).

Analysis

SPDs (1.5 Hz – 40 Hz) were extracted from WinEEG as 60 second segments with 4 second epochs. Data were imported to SPSS v.20 and coded by condition. In addition to the classical EEG bands, averages of periodically adjacent bands were computed including theta-alpha (theta + alpha/2) and alpha-beta1 (alpha + beta1/2). Simple tests of mean differences were computed.

Results

Investigative Analysis

The geomagnetic values were coded for storm (Kp= 4 or 5) and non-storm (Kp =1 or 2). Statistically significant increases of alpha power (7.5 Hz – 14 Hz) were noted within the right but not the left parahippocampal gyrus during “storm” conditions, $t(12)= 2.56$, $p<.05$, $r^2=.35$ (Figure 25). Other frequencies were unaffected by daily Kp-index 24 hour maxima ($p>.05$). Hippocampal SPD differences were not statistically significant ($p>.05$) These data indicate that right parahippocampal but not hippocampal or left hemispheric background microvolt fluctuation periodicities were affected by geomagnetic storm conditions within fixed human brain tissue. Based upon these observations, experimental applications of electromagnetic fields to brain tissue were performed.

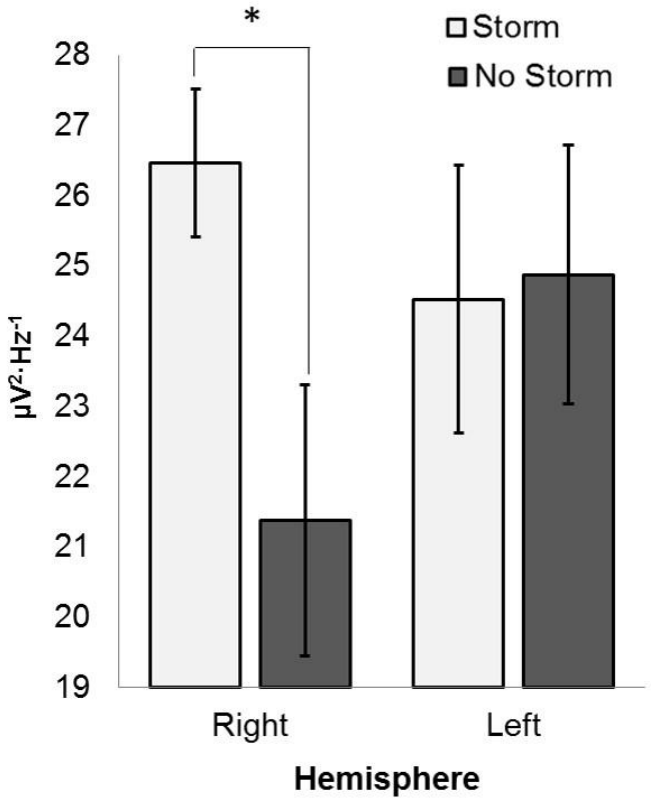

Figure 25. Mean alpha (7.5 Hz – 14 Hz) power within the right and left parahippocampal gyri of fixed human brain sections (coronal) obtained within a 24 hour period within which

the daily maximum geomagnetic perturbation (Kp index) value was indicative of storm conditions (Kp > 3) or not (Kp < 3).

Experimental Electromagnetic Field Exposures

Regardless of the pattern of the magnetic field, when the fixed, unsectioned human brain was exposed, right hemispheric structures (M= 15.83, SEM= 0.79) displayed increased alpha-beta1 (7.5Hz – 20Hz) power relative to left hemispheric structures (M= 13.97, SEM= 0.48), $t(214)= 2.02$, $p<.05$. The effect size was very weak ($r^2= .02$). The effects were relatively immediate but not instantaneous. The contribution of each field to the overall effect was then investigated systematically. Burst X (3000, 3) and Thomas (3, 3) patterns elicited increased alpha-beta1 power within aggregates of right hemispheric structures relative to the equivalent aggregates from the left hemisphere, explaining 14% and 12% respectively (Figure 26). Burst X and Thomas fields generated with the other point duration parameters did not produce equivalent hemispheric asymmetries ($p>.05$). Similarly, LTP and Sine (20Hz) patterns did not produce any statistically significant changes in power as a function of hemisphere ($p>.05$). The 20 Hz Sine pattern produced, non-specific statistically significant increases of alpha-beta1 power within all structures relative to all other conditions.

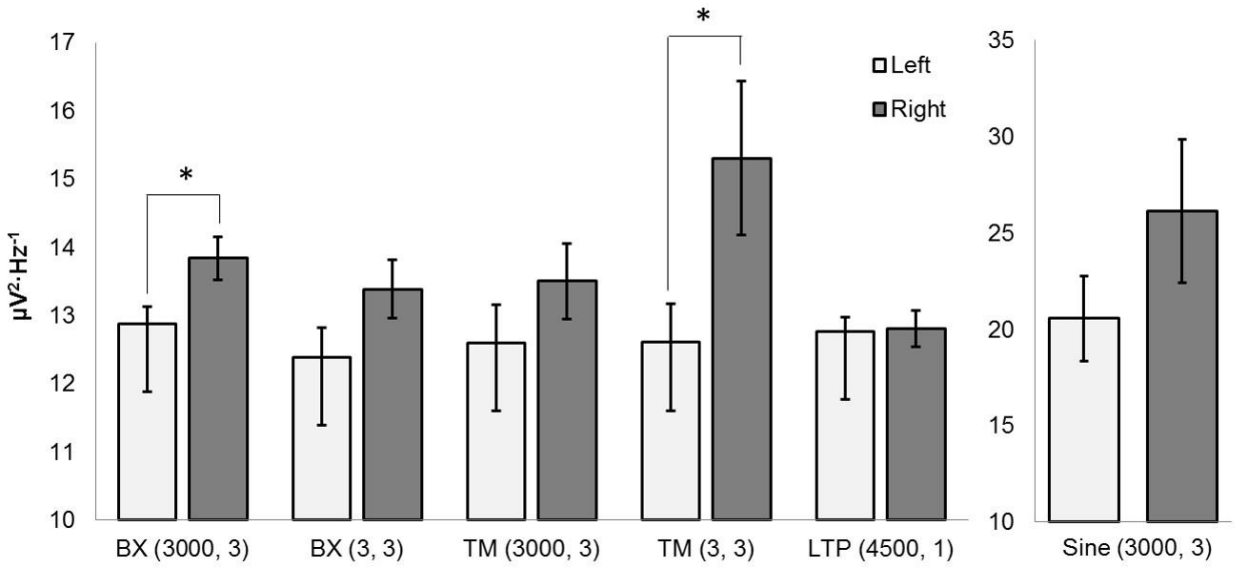

Figure 26. Alpha-beta1 (7.5 Hz – 20 Hz) power within the left and right hemisphere of a full, unsectioned human brain as a function of the electromagnetic field exposure pattern. Burst X (BX), Thomas (TM), long-term potentiation (LTP), and sine (Sine) patterns are shown where significant differences between hemispheres are indicated ($p<.05$).

Further analyses revealed that the right hemispheric increases of alpha-beta1 power observed in the fixed, unsectioned human brain during exposures to Burst X (3000, 3) were due to one neuroanatomical locus. The right amygdala, accessed by way of the uncus, generated increased alpha-beta1 power within the right hemisphere (M= 15.32, SEM= 0.54) relative to the left hemisphere (M= 12.52, SEM= 0.66), $t(4)= 3.30$, $p<.05$, $r^2=.73$ (Figure 27). This right-left difference emerged within 10 to 20 s after the onset of the field exposures ($p <.05$). ANOVAs revealed statistically significant alpha-beta1 power differences across structures within the right hemisphere, $F(5,17)= 3.56$, $p<.05$, $\eta^2= .60$. Homogeneous subsets revealed the major source of the variance was due to a difference between the right amygdala and right orbital frontal gyrus ($p<.05$). There were no statistically significant changes in the left hemispheric structural differences after

accommodating for multiple comparisons. Power differences within other frequency bands were not significant during exposures to the Burst X (3000, 3) pattern. Together, these results suggested that the right amygdala was most responsive to the Burst X (3000, 3) electromagnetic field pattern relative to its contralateral paired structure in a fixed, unsectioned human brain.

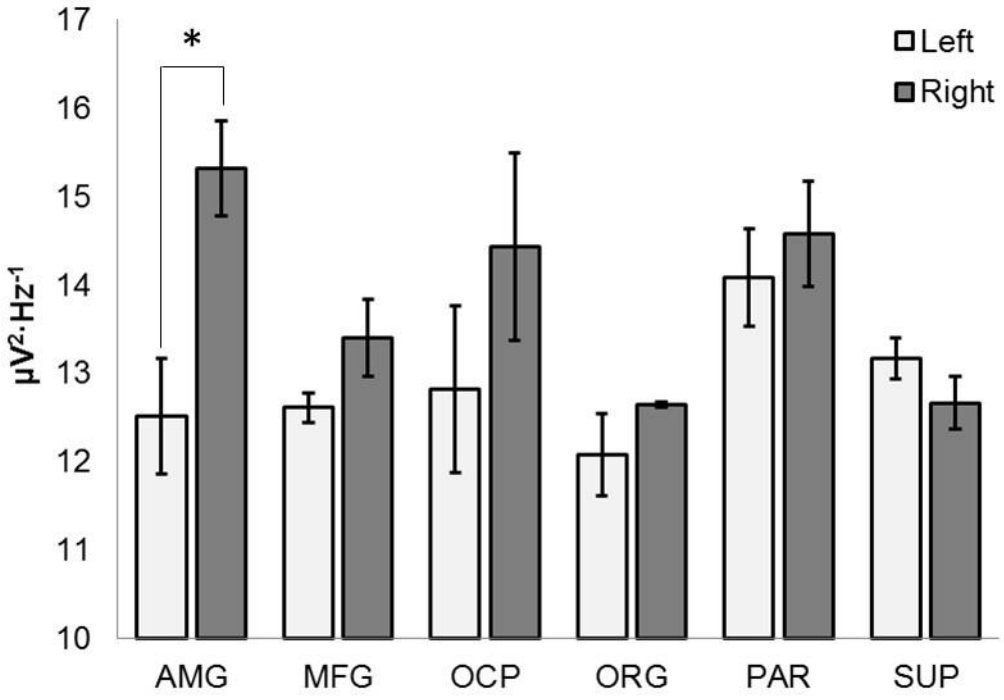

Figure 27. Alpha-beta1 (7.5 Hz – 20 Hz) power within the left and right amygdala (AMG), middle frontal gyrus (MFG), occipital pole (OCP), orbital gyrus (ORG), parahippocampal gyurs (PAR), or superior parietal lobule (SUP) while exposed to Burst X (3000,3). Significant differences are indicated ($p<.05$).

When exposed to the Thomas (3, 3) pattern, two neuroanatomical loci that were not differential responsive to Burst-X responses demonstrated statistically significant hemispheric differences. During exposure, the right orbital frontal gyrus displayed

increased theta-alpha (4 Hz – 14Hz) power relative to the contralateral locus, $t(4)= 3.02$, $p<.05$, $r^2=.70$ (Figure 28). Although the effects were evident within the 60 sec trial periods, subsequent analyses revealed the onset of the left-right difference emerged between 10 and 20 s after the onset of the field. Similarly, the right superior parietal lobule displayed increased theta-alpha power relative to the left superior parietal lobule, $t(4)= 3.34$, $p<.05$, $r^2=.74$.

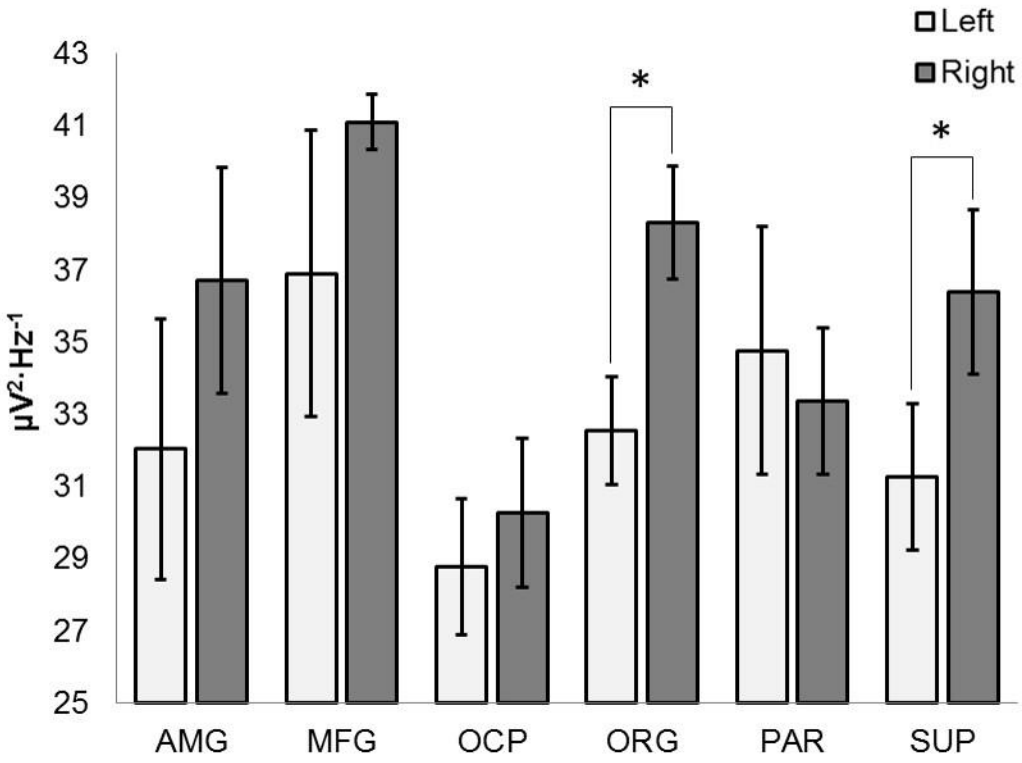

Figure 28. Theta-alpha (4 Hz – 14 Hz) power within the left and right amygdala (AMG), middle frontal gyrus (MFG), occipital pole (OCP), orbital gyrus (ORG), parahippocampal gyurs (PAR), or superior parietal lobule (SUP) while exposed to Thomas (3,3). Significant differences are indicated ($p<.05$).

Whereas orbital frontal effects were discernable between 10 and 20 s after the onset of the field changes within the superior parietal lobule were manifested within 10 s. Exposure to the Thomas (3, 3) pattern was also associated with theta-alpha differences between neuroanatomical loci within the right hemisphere, $F(5, 17)= 3.26$, $p<.05$, $\eta^2= .58$. Homogeneous subsets isolated the power differences between the right middle frontal gyrus and the right occipital polar region as the major sources of variance ($p<.05$). Structure-dependent SPD differences within the left hemisphere were not evident $F(5, 17)= .95$, $p>.05$. These results suggested that the orbital frontal and superior parietal structures of the right hemisphere as well as the middle frontal gyrus were particularly response to the Thomas (3, 3) field pattern.

Discussion and Conclusion

The moderate correlations between brain activity, such as epileptic seizures, or behaviors related to cerebral sensitivity have been reported for decades (Persinger, 1980). The statistically significant and conspicuous effects of experimentally generated weak magnetic fields within the 0.02 (20 nT) to 10 microTesla range, particularly when applied as physiologically-simulated patterns, upon human behaviour, subjective experiences and current densities within the human cerebrum suggest that the brain volume may be more responsive to these stimuli than classically assumed. The energies associated with this level of magnetic field strength within the human cerebrum would be equivalent to at least the energy from action potentials from about a million neurons each discharging around 10 Hz.

The results of the present experiments indicate that fixed human brain tissue has the capacity to differentially respond to both increases in geomagnetic activity as well as the application of different physiologically patterned magnetic fields. Two major findings were common across the investigative and experimental results. First, the geomagnetic effects as well as the experimentally generated physiologically-patterned electromagnetic field effects were most pronounced within specific right hemispheric structures. Differential hemispheric effects have been shown for living brain. Applications of physiologically-patterned magnetic fields over the left or the right hemisphere produced differential electrophysiological effects within about 15 min (Persinger, 1999). The enhanced sensitivity of the right hemisphere, particularly within the temporal and parahippocampal regions, for geomagnetic activity has been reported by several researchers (Babayev and Allahverdiyeva, 2007; Booth, Koren and Persinger, 2005; Sandyk, 1995). These conclusions have been derived from direct measurements or inferred by right-lateralized experiences reported by participants including visual flashes or phenomena within the upper left peripheral visual fields.

Second, where there were spectral power differences, the alpha band (7.5 Hz – 14 Hz) was always involved. Though SPD differences were observed within the 4 Hz – 20 Hz band, the overlapping alpha signature was conspicuous. The enhancement of the alpha band during increased geomagnetic activity compared to less intense periods suggests that the effects of the applied electromagnetic fields were not artefacts. In addition, some patterns did not evoke significant changes in SPD and each pattern differentially induced changes within different structures. The anisotropy of the response profile would be consistent with differential structural properties rather than non-specific

artefacts. Left hemispheric structures reliably demonstrated uniform spectral power across all frequency bands when exposed to both different perturbation levels of the background geomagnetic field or applied electromagnetic fields within the laboratory setting.

Not all regions that were measured within the human brain responded in the same manner. Those areas that differentially responded to very specific patterns of the applied fields displayed the changes relatively quickly, typically within about 10 to 20 s. This latency is much longer than effects produced by spurious induction artefacts. Over the last few decades we have observed and measured multiple electroencephalographic phenomena that were artefacts. All of them occurred within 1 s of the field application. In addition, we found that some areas such as the superior parietal lobule displayed even shorter latencies. The most parsimonious explanation for the requirement for 10 to 20 s exposure to the fields to elicit the changes in a specific band of electrophysiological activity within only some brain regions would involve a property like reluctance or inductance (latency) that is different within those regions particularly within the right hemisphere.

This 10 to 20 latency is much shorter than the usual latency of 15 min to 30 min that is required for the living brain to respond to these same fields. The latter is not likely to be an impedance effect from the skull because direct measurements of simulated skull thickness and salinity did not attenuate the penetration of these fields (Persinger and Saroka, 2013). This discrepancy might be employed to estimate the “intertia” of the neuronal fields within the living brain that must be accommodated by the applied, physiologically patterned magnetic fields. We have suggested that one mechanism by

which weak, applied, physiologically-patterned magnetic fields influence the dynamic brain is through the hydronium ion. Murugan et al (2014) showed that experimental application of the same field patterns that were effective in this study produced quantitative shifts in the pH of spring water that reflected the intrinsic energies from the applied fields.

We have assumed that the fundamental dynamics associated with cell membrane dynamics that contributes to cognition and to consciousness occurs within the 10 nm space extending from the membrane. This is the functional width from which the resting membrane potential emerges (Persinger, 2010). The volume associated with this thin shell is about $0.8 \cdot 10^{-12}$ cc. Assuming there are about 10^{12} neurons and glial cells within the volume that would be equivalent to ~ 1 cc. This volume is $5.5 \cdot 10^{-2}$ M and considering there are $6.02 \cdot 10^{23}$ molecules per mole and at pH 7.4 the concentration of available protons would be $4.8 \cdot 10^{-8}$ M the number of protons would be $159 \cdot 10^{13}$. If the duration of each hydronium ion is 10^{-12} s (De Coursey, 2014), then approximately 1600 s would elapse before potentially the vast majority of protons would be affected. This is equivalent to about 30 min which is the same order of magnitude of exposure required to produce demonstrable changes in electroencephalographic activity in live human exposures. Because the response from the fixed tissue was about one thousandths of that value, this would suggest either a modified functional volume around the cells or a slightly more acidic pH associated with the fixative. We have measured such values. These calculations do not prove this mechanism is the origin of the differential latency for fixed and live human brains to respond to physiologically-patterned magnetic fields. However the physical-chemical perspective may encourage alternative interpretations and

approaches to intrinsic residual properties within significant human tissue in response to weak, time-varying magnetic fields.

References

Babayev, E.S. and Allahverdiyeva, A.A. (2007). Effects of geomagnetic activity variations on the physiological and psychological state of functionally healthy humans: some results of Azerbaijani studies. Advances in Space Research, 40(12), 1941-1951.

Booth, J.N., Koren, S.A. and Persinger, M.A. (2005). Increased feelings of the sensed presence and increased geomagnetic activity at the time of the experience during exposures to transcerebral weak complex magnetic fields. International Journal of Neuroscience, 115(7), 1053-1079.

Cheng-yu, T.L., Poo, M.M. and Dan, Y. (2009). Burst spiking of a single cortical neuron modifies global brain state. Science, 324(5927), 643-646.

DeCoursey, T.E. and Hosler, J. (2014). Philosophy of voltage-gated proton channels. Journal of The Royal Society Interface, 11(92), 20130799.

Dubrov, A.P. and Brown, F.A. (1978). The geomagnetic field and life: Geomagnetobiology (p. 318). New York: Plenum Press.

Houweling, A.R. and Brecht, M. (2007). Behavioural report of single neuron stimulation in somatosensory cortex. Nature, 450(7172), 65-69.

Llinas, R. and Ribary, U. (1993). Coherent 40-Hz oscillation characterizes dream state in humans. Proceedings of the National Academy of Sciences,90(5), 2078-2081.

Mach, Q.H. and Persinger, M.A. (2009). Behavioral changes with brief exposures to weak magnetic fields patterned to stimulate long-term potentiation. Brain research, 1261, 45-53.

Martin, L.J. and Persinger, M.A. (2004). Thermal analgesia induced by 30-min exposure to 1 μT burst-firing magnetic fields is strongly enhanced in a dose-dependent manner by the α 2 agonist clonidine in rats. Neuroscience Letters, 366(2), 226-229.

Michon, A.L. and Persinger, M.A. (1997). Experimental simulation of the effects of increased geomagnetic activity upon nocturnal seizures in epileptic rats. Neuroscience letters, 224(1), 53-56.

Mulligan, B.P. and Persinger, M.A. (2012). Experimental simulation of the effects of sudden increases in geomagnetic activity upon quantitative measures of human brain activity: validation of correlational studies. Neuroscience letters, 516(1), 54-56.

Murugan, N.J., Karbowski, L.M., and Persinger, M.A. (2014). Serial pH Increments (~ 20 to 40 Milliseconds) in Water during Exposures to Weak, Physiologically Patterned Magnetic Fields: Implications for Consciousness. Water, 6, 45-60.

Murugan, NJ, Karbowski, LM, Lafrenie, RM, et al. (2015). Maintained Exposure to Spring Water but Not Double Distilled Water in Darkness and Thixotropic Conditions to Weak (~ 1 μT) Temporally Patterned Magnetic Fields Shift Photon Spectroscopic Wavelengths: Effects of Different Shielding Materials. Journal of Biophysical Chemistry, 6(01), 14-28.

Nunez, P.L. and Srinivasan, R. (2006). Electric fields of the brain: the neurophysics of EEG. Oxford University Press, USA.

Persinger, M.A. (1980). The weather matrix and human behavior. Praeger Publishers.

Persinger, M.A. (2010). 10^{-20} Joules as a Neuromolecular Quantum in Medicinal Chemistry: An Alternative Approach to Myriad Molecular Pathways?. Current Medicinal Chemistry, 17(27), 3094-3098.

Pierre, L.S. and Persinger, M.A. (2006). Experimental facilitation of the sensed presence is predicted by the specific patterns of the applied magnetic fields, not by suggestibility: re-analyses of 19 experiments.International Journal of Neuroscience, 116(19), 1079-1096.

Persinger, M.A. (1999). Increased emergence of alpha activity over the left but not the right temporal lobe within a dark acoustic chamber: differential response of the left but not the right hemisphere to transcerebral magnetic fields. International Journal of Psychophysiology, 34(2), 163-169.

Persinger, M.A. and Healey, F. (2002). Experimental facilitation of the sensed presence: Possible intercalation between the hemispheres induced by complex magnetic fields. The Journal of nervous and mental disease,190(8), 533-541.

Persinger, M.A. and Saroka, K.S. (2013). Minimum Attenuation of Physiologically-Patterned, 1 μTesla Magnetic Fields through Simulated Skull and Cerebral Space. Journal of Electromagnetic Analysis and Applications,5(04), 151-156.

Rajaram, M. and Mitra, S. (1981). Correlation between convulsive seizure and geomagnetic activity. Neuroscience letters, 24(2), 187-191.

Rouleau, N. and Dotta, B.T. (2014). Electromagnetic fields as structure-function zeitgebers in biological systems: environmental orchestrations of morphogenesis and consciousness. Frontiers in integrative neuroscience, 8(84) 1-9.

Rouleau, N., Lehman, B. and Persinger, M.A. (2016). Focal attenuation of specific electroencephalographic power over the right parahippocampal region during transcerebral copper screening in living subjects and hemispheric asymmetric voltages in fixed brain tissue. Brain research, 1644, 267-277.

Rouleau, N. and Persinger, M.A. (2016). Differential responsiveness of the right parahippocampal region to electrical stimulation in fixed human brains: Implications for historical surgical stimulation studies?. Epilepsy & Behavior,60, 181-186.

Sandyk, R. (1995). Improvement of right hemispheric functions in a child with Gilles de la Tourette's syndrome by weak electromagnetic fields.International Journal of Neuroscience, 81(1-2), 199-213.

Saroka, K.S. and Persinger, M.A. (2013). Potential production of Hughlings Jackson's “parasitic consciousness” by physiologically-patterned weak transcerebral magnetic fields: QEEG and source localization. Epilepsy & Behavior, 28(3), 395-407.

Saroka, K.S., Caswell, J.M. and Lapointe, A., et al. (2014). Greater electroencephalographic coherence between left and right temporal lobe

structures during increased geomagnetic activity. Neuroscience Letters,560, 126-130.

Tsang, E.W., Koren, S.A. and Persinger, M.A. (2004). Power increases within the gamma range over the frontal and occipital regions during acute exposures to cerebrally counterclockwise rotating magnetic fields with specific derivatives of change. International Journal of Neuroscience, 114(9), 1183-1193.

Wallis, J.D. and Kennerley, S.W. 2011. Contrasting reward signals in the orbitofrontal cortex and anterior cingulate cortex. Annals of the New York Academy of Sciences, 1239(1), 33-42.

Chapter Transition: Post-Mortem Neurochemistry

The previous chapter validated the hypothesis that the fixed, post-mortem human brains could filter electromagnetic signals non-randomly with a right-hemispheric and temporal lobe bias. The following chapter serves to demonstrate the relevant role of applied chemical probes to the post-mortem tissues and their regional effects upon microvolt fluctuations. The experimental procedures presented throughout the chapter detail a series of assays which involve injecting different concentrations of brain-relevant compounds to the surface of coronal sections of fixed, post-mortem human brain tissue. Nicotine, 5-HTP, L-Glutamate, and Ketamine were employed, eliciting differential effects. Most notable, agonist-like and antagonist-like responses with reverse proportionalities of high-frequency power were observed for glutamate and ketamine respectively within the same neuroanatomical region (left parahippocampal region) and paired to reliable photon emissions. Habituation-like power curves over repeated exposure to similar concentrations with effective regions were observed. Supplemental experiments demonstrated that Heschl's gyrus, a tonotopically organized tissue section along the surface of Sylvian's fissure which mediates primary auditory reception, expressed electrical outputs which could be used to discriminate between different frequency inputs of current. In general, the data support the claim that the tissues remain responsive to chemical probes decades after death and chemical fixation. The data also indicate that microstructure is maintained from a functional perspective and that receptor processes could contribute to some subset of the variance.

Chapter 7:

When is the Brain Dead? Living-Like Electrophysiological Responses and Photon Emissions From Applications of Neurotransmitters in Fixed Post-Mortem Human Brains

(Original Research)

Published in PLoS One, Vol. 11, e0167231, 2016

Nicolas Rouleau, Nirosha J. Murugan, Lucas W.E. Tessaro,

Justin N. Costa, & Michael A. Persinger

DOI: 10.1371/journal.pone.0167231

(Open Access)

Abstract

The structure of the post-mortem human brain can be preserved by immersing the organ within a fixative solution. Once the brain is perfused, cellular and histological features are maintained over extended periods of time. However, functions of the human brain are not assumed to be preserved beyond death and subsequent chemical fixation. Here we present a series of experiments which, together, refute this assumption. Instead, we suggest that chemical preservation of brain structure results in some retained functional capacity. Patterns similar to the living condition were elicited by chemical and electrical probes within coronal and sagittal sections of human temporal lobe structures that had been maintained in ethanol-formalin-acetic acid. This was inferred by a reliable modulation of frequency-dependent microvolt fluctuations. These weak microvolt fluctuations were enhanced by receptor-specific agonists and their precursors (i.e., nicotine, 5-HTP, and L-glutamic acid) as well as attenuated by receptor-antagonists (i.e., ketamine). Surface injections of 10 nM nicotine enhanced theta power within the right parahippocampal gyrus without any effect upon the ipsilateral hippocampus. Glutamate-induced high-frequency power densities within the left parahippocampal gyrus were correlated with increased photon counts over the surface of the tissue. Heschl's gyrus, a transverse convexity on which the primary auditory cortex is tonotopically represented, retained frequency-discrimination capacities in response to sweeps of weak (2 μV) square-wave electrical pulses between 20 Hz and 20 kHz. Together, these results suggest that portions of the post-mortem human brain may retain latent capacities to respond with potential life-like and virtual properties.

Introduction

The fundamental principle that integrates anatomy and physiology can be effectively summarized as “structure dictates function”. This means the functional capacities of biological substrata are determined by the chemical composition, geometry, and spatial orientation of structural subcomponents (Persinger & Koren, 2007; Persinger, Saroka, Koren, & St-Pierre, 2010). As the heterogeneity of structure increases within a given organ, so does the functional heterogeneity. Nowhere is this more evident than in the human brain. It can be described as a collection of partially-isolated networks which function in concert to produce consciousness, cognition, and behaviour. It also responds to its multivariate, diversely energetic environment by producing non-isotropic reflections within its micrometer and nanometer spaces. The specific spatial aggregates of these dendritic alterations result in processes that have been collectively described as memory: the representation of experience.

When structures of the brain undergo changes sufficient to terminally disrupt these functional processes and the individual is ultimately observed to lose the capacity to respond to stimuli (Wijdicks, 2010), the brain is said to be clinically dead. This state has been assumed to be largely irreversible. It should be noted that the specific criteria which must be achieved in order to ascribe death to an individual are not universal and exhibit a significant degree of non-consensus (Wijdicks, 2002). The precise point beyond which the brain is no longer “living”, a threshold which remains unidentified, is perhaps less definite than has been historically assumed. Without life support systems, either endogenously in the form a cardiovascular network or exogenously in the form of mechanical aids, the brain degenerates progressively until full decomposition and

dissolution. Complete loss of structure is strongly correlated with the complete loss of function. When the brain is dead and the tissue has lost its structural integrity, the individual is assumed to no longer be represented within what remains of the organ.

If, however, the brain is immersed within certain chemical solutions before degeneration and decomposition, the intricate and multiform structures of the human brain can be preserved (Fox, Johnson, Whiting & Roller, 1985; Hopwood, 1972; Kiernan, 2000) for decades or perhaps centuries. The gyri and sulci which define the convex and concave landscapes of the brain's outer surface as well as the cytoarchitectural features of the cerebral cortex remain structurally distinct. The deep nuclei and surrounding tract systems remain fixed in space, unchanging in time. Though structurally intact, the functions of the brain are, however, still considered to be absent. It has been assumed that the chemical microenvironment (e.g., pH, nutrient content, ionic gradients, charge disparities, etc.) of both cells and tissues within the preserved brain must be altered to such a degree to prevent degradation that these spaces no longer represent those which underlie the cellular processes which give rise to normal human cognition and behaviour.

The principle of anatomy and physiology which describes the relationship between structure and function would hold that in the presence of structural integrity so too must there be a functional integrity. If the structure-function relationship is a physical determinant, functional capacities should scale with structural loss and vice versa. Therefore the maintenance of structure subsequent to clinical death by chemical fixation could potentially regain some basic function of the tissue to the extent to which structure and function are intimately related. Here we present lines of evidence that indicate brains preserved and maintained over 20 years in ethanol-formalin-acetic acid (EFA) (Harrison,

1984), a chemical fixative, retain basic functions as inferred by microvolt fluctuations and paired photon emissions within the tissue. They are both reliably induced and systematically controlled by the display of electrical and chemical probes which include the basic inhibitory and excitatory neurotransmitters or their precursors. Each of these profiles exhibit dosage-dependence and magnitude dependences that are very similar to those displayed by the living human brain.

Materials & Methods

Tissue Samples

Human brain tissue samples fixed in EFA (72% ethanol, 18% dH_2O, 5% acetic acid, 5% formaldehyde) were subjected to a series of experimental procedures. The aim was to elicit stimulus-response patterns characteristic of structure-function relationships observed in the living human central nervous system. Three (n=3) caudal coronal sections and four (n=4) hemispheric sections severed within the midline sagittal plane along the medial longitudinal fissure at the level of the corpus callosum were used throughout the course of the study. Coronal sections were selected based upon exclusionary criteria including the presence of the basilar artery, Ammon's horn, and the parahippocampal gyrus. Of the four sagittal sections, two were left hemispheres and two were right hemispheres. All samples were originally obtained from separate full human brain specimens and were therefore independently sourced. All specimens had been obtained from anonymous donors or from accredited companies (North Carolina Biological Supplies) over 20 years ago. The brains had been stored in secure areas and handled appropriately and respectfully.

Measurement Device: Quantitative Electroencephalography

A Mitsar quantitative electroencephalography (QEEG) amplifier was equipped with needle electrodes which were inserted directly into the brain tissue (Figure 29). Weak microvolt fluctuations (μV) were measured within WinEEG software throughout the course of all experiments outlined here using an HP ENVY laptop computer running Windows 8. Each experiment involved specific needle electrode placement and referencing procedures which were contingent upon the type of sample. In all cases, notch filters were applied to exclude voltage fluctuations whose frequency spectra were sourced between 50 and 70 Hz as well as 110 and 130 Hz in order to reduce environmental noise. Low and high cut filters of 1.6Hz and 50Hz were applied. Electrode impedance was regulated to <5kΩ. Data were extracted as power densities (PDs) in 30 second segments with 2 second epochs. Each extraction consisted of power measures within delta (1.5Hz – 4Hz), theta (4Hz – 7.5Hz), alpha (7.5Hz – 14Hz), beta1 (14Hz – 20Hz), beta2 (20Hz – 30Hz), and gamma (30Hz – 40Hz) band ranges.

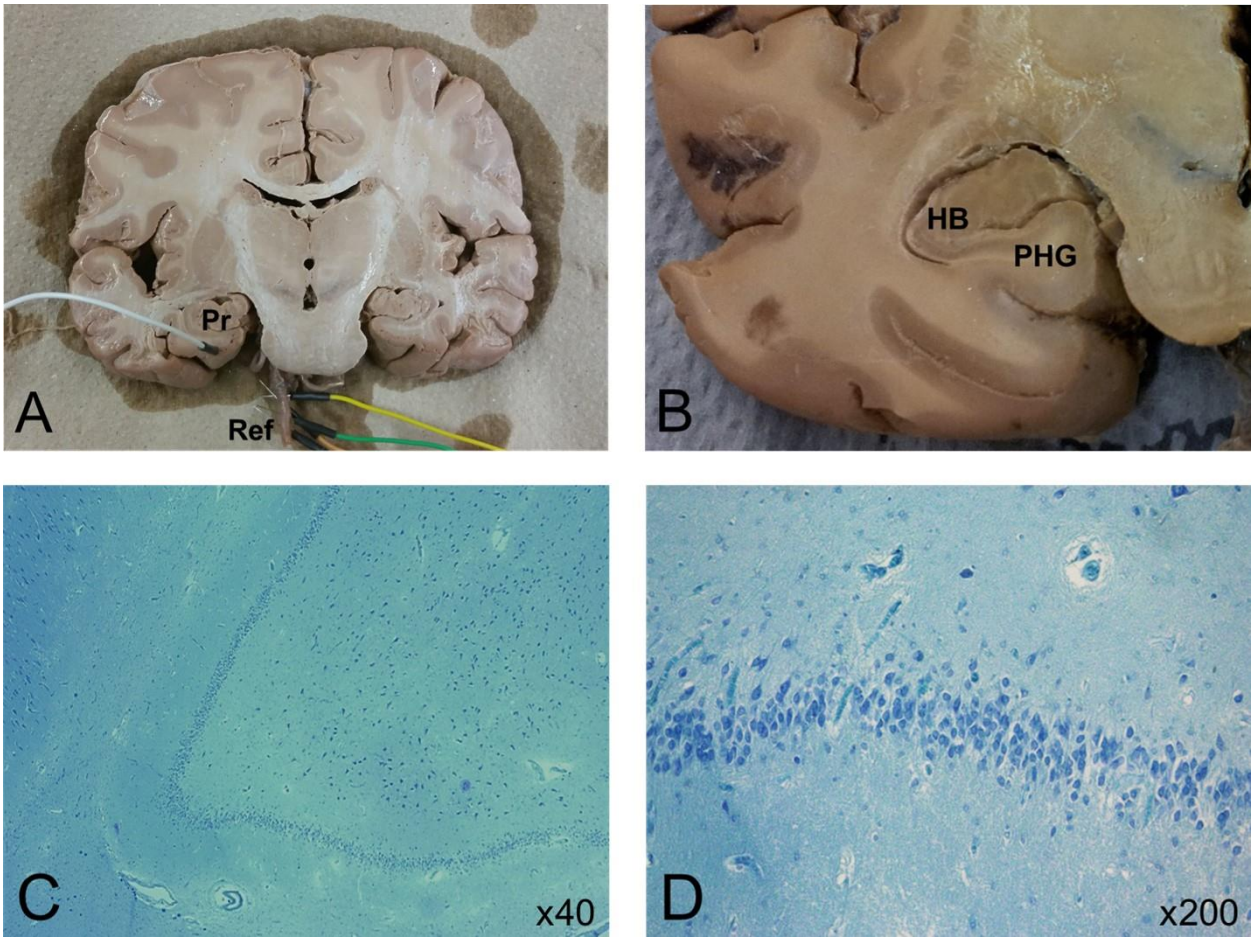

Figure 29. Coronal sections of human brain tissue fixed in EFA. Each section was equipped with a needle electrode inserted into the grey matter of the left parahippocampal gyrus (Pr) referenced (Ref) to the basilar artery (A). The hippocampal body (HB) and parahippocampal gyrus (PHG) served as the regions of interest (B). Cytoarchitecture of the hippocampal body fixed in EFA can be visualized under x40 (C) and x200 (D) magnification in stained (Toluidine Blue-O) sections.

In the case of coronal sections, needle electrodes were inserted into the basilar artery which served as an electrical reference (Figure 29). A single electrode was then inserted into the region of interest. The left and right parahippocampal gyri and hippocampal bodies served as the areas of interest throughout the course of the study.

Only one structure was ever probed for a given trial due to limitations of the referencing procedure. This means that it was not possible to infer in real-time whether or not hemispheric analogues or adjacent structures were simultaneously responding to the same stimulus. Once the needle electrode was inserted into the region of interest and was referenced to an average of electrodes inserted into the basilar artery, microvolt fluctuations could be recorded. Sagittal sections of fixed human brain tissue were probed similarly. The basilar artery always served as the electrical reference point. In the case of the sagittal sections, the primary loci of interest were the transverse temporal gyri. Needle electrodes were inserted directly into the transverse temporal gyri within both the postero-medial and antero-lateral subdivisions. The precise stimulation procedure carried out over the course of electrophysiological measurement is outlined elsewhere

Measurement Device: Photomultiplier Tube

Photon measures were obtained within a darkened chamber concurrently with QEEG for trials involving applications of glutamate to the brain. Raw photon counts were recorded using a single photomultiplier tube (PMT) that was suspended 10cm above the brain specimen. The PMT was a DM0090C model from Sens-Tech Sensor Technologies, with a spectral response range between 300-850 nm (visible light). Sens-Tech Counter timer software recorded digital output from the photomultiplier tube at a 50 Hz sampling rate for 3000 readings (20 msec data points for 60 seconds) on a Lenovo ThinkPad laptop that was positioned outside of the enclosed chamber via USB output cables. To remove the contributions from dark counts (i.e., those associated with the intrinsic photoelectric circuitry), counts measured when the brain tissue was present were subtracted from baseline conditions when no tissue was present. It was determined that the use of

equipment measuring electric potential differences (QEEG) and photon counts over time would serve as a measure of internal validity, confirming the presence of systematic response patterns which could be observed by both measurement devices independently.

Procedures

Chemical Application

Within the context of the living brain, chemical signals in the form of neurotransmitters are transduced at the level of the receptor into miniature inhibitory and excitatory post-synaptic potentials or IPSPs and EPSPs (Hasenstaub, Shu, Kraushaar, Duque, & McCormick, 2005). They undergo summation within the post-synaptic cell resulting in further propagation of electrochemical signals. The proximal cause of ionic inflow to the cell is receptor-modulated by agonistic and antagonistic ligands interacting at the level of the plasma membrane. Here, we have designed a series of experiments which involved the application of neurotransmitters, their precursors, or known modulators of receptors within the central nervous system to coronal sections of human brain tissue fixed in EFA. L-glutamic acid (glutamate), 5-Hydroxy-L-tryptophan (5-HTP), (−)-nicotine, and ketamine were obtained from Sigma-Aldrich (USA) and serially diluted into various concentrations ranging between 1 M and 1 nM.

Experiments involving the application of chemical compounds to the tissue were associated with a specific injection protocol. Each injection was preceded by washing the surface of the coronal slice with 10% ethanol-formalin-acetic acid (EFA) which was followed by a 30 second baseline condition during which electrophysiological recordings were obtained. A 1 mL aliquot of the solution was injected on to the surface of coronal

slices at the parahippocampal-hippocampal interface. The point of injection was therefore crudely distributed over both regions of interest. Therefore, upon injection of the compound, any changes in microvolt fluctuations observed within either the parahippocampal gyrus or hippocampal body was not necessarily due to stimulation of the probed area alone. Instead, adjacent regions, whose efferent and afferent connections likely contributed to local activity, should be considered as potential sources of any differences in addition to the probed area.

Electrical Stimulation

The human primary auditory cortex is localized within the medial two-thirds of the transverse temporal gyrus or Heschl's gyrus (HG) whereas the antero-lateral component is designated as an adjacent, non-primary region (Rivier & Clarke, 1997). Morphometric analyses have revealed the reliable presence of tonotopic subfields along HG which run perpendicular to the classical postero-medial-to-antero-lateral cytoarchitectonic organizational divisions (Da Costa, 2011). These "tonotopic maps" are frequency-representing gradients within the tissue which process primary auditory information received by way of the medial geniculate nucleus of the thalamus. An experimental verification of preserved frequency-discrimination within the postero-medial component of Heschl's gyrus in chemically fixed brain specimens could support a structural-functional model in post-mortem tissue.

Square and sine wave-forms were generated using Audacity's (2.0.5) tone-generating tool on an HP ENVY laptop running Windows 8. Each signal consisted of 30 seconds of a square or sine wave with an associated frequency of 20 Hz, 100 Hz, 500

Hz, 1 kHz, 2 kHz, 5 kHz, 10 kHz, 12 kHz, 15 kHz, or 20 kHz. We selected the 20 Hz – 20 kHz range to reflect the operating range of the human auditory pathways. Though the relationship between pressure waves and their transduced electrical equivalents is not 1:1, the large band range would accommodate our practical, methodological needs to demonstrate frequency-dependent discrimination. Amplitude of the signal within Audacity was set to 0.8 (a.u.). The signal output was regulated to 10% of maximum audio card output. A coaxial cable coupled to an electronic breadboard jumper cable by an alligator clip served as a stimulating probe which was inserted into the tissue. The voltage equivalent at the level of the needle probe positioned within ~2 mm adjacent to the stimulating probe, 2 μV, was measured directly by the electrophysiological recording device (Rouleau & Persinger, 2016).

The measurement procedure involved inserting both the data collecting needle probe from the electrophysiological recording device and the stimulating probe into either the postero-medial or antero-lateral division of the right or left HG. The needle probes were separated by ~ 2 mm where the stimulating probe was always the lateral-most probe. Each trial consisted of a 30 second baseline followed by 270 seconds of stimulation. The 270 second stimulation period was further divided into 9 periods, each with an associated frequency. Frequencies were counterbalanced to eliminate order effects.

Methods of Analysis

Power densities (PDs) were extracted from WinEEG 2.93.59 (07.2013) and imported to SPSS v19 for subsequent analysis. The spectral analysis technique and

resulting power values were selected so as to isolate frequency-dependent signatures from the overall signal. Alternative signal processing techniques of raw data extractions were employed when analyzing the tissue's response to electrical stimulation so as to infer information processing disparities as a function of the probed region. Fractal geometry, when applied to statistical analyses, refers to a method of generating a ratio which represents an index of complexity – how the detail in the pattern or signal under analysis changes with respect to the scale or level of discourse at which it is being measured and examined. The Higuchi Fractal Dimension (HFD) algorithm is one such method of determining statistical complexity and was employed in the present study involving electrical stimulation of HG as has been employed in other studies which have examined electroencephalographic complexity (Accardo, Affinito, & Carrozzi, 1997). Additional data processing was conducted prior to the HFD analysis. It was assumed that the effect of the stimulus on the tissue as inferred by the recorded QEEG signal would be best illustrated if a difference was taken between each of the segments corresponding to the periods of frequency-specific stimulation and the baseline electrophysiological recordings from the fixed brain. Thus each of the segments underwent the following transform prior to HFD analyses:

$$ND = (RS_{xy} - RS_{BL})$$

Where *ND* is the new data file generated, RS_{xy} is the raw signal segment for frequency *xy*, and RS_{BL} is the raw signal baseline (no frequency), for each individual trial.

Results

Surface Injections of Nicotine

Analyses of variance (ANOVAs) revealed statistically significant three-way interactions between structure, hemisphere, and concentration for differences of theta (4Hz – 7.5Hz) and alpha (7.5Hz – 14Hz) PDs. Alpha effects were weak, and were eliminated when accounting for multiple comparisons. The three-way theta power interaction was conspicuous [$F(10,130)= 4.06$, $p<.001$, $\eta^2= .22$]. Right parahippocampal theta power differed as a function of concentration [$F(10,32)= 8.02$, $p<.001$, $\eta^2= .78$] (Figure 30). The effect was dose-dependent with a general linear increase ($r= .60$). The effect was not present for the immediately adjacent hippocampal body ($p>.05$) or contralateral structures ($p>.05$) which was the major source of the interaction. The control (water) condition was associated with differences in power as a function of structure; however, there were no within-structure differences in theta power as a function of hemisphere ($p>.05$).

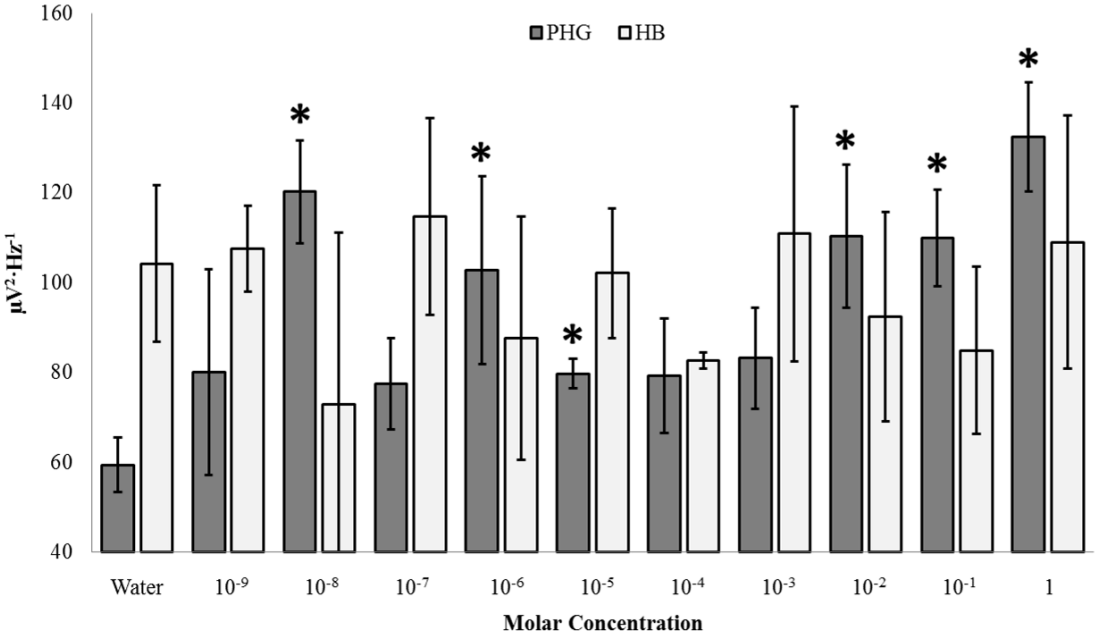

Figure 30. Nicotine Response. Theta (4Hz – 7.5Hz) PDs as a function of nicotine concentration within the right parahippocampal gyrus (PHG) and hippocampus (HB). Significant differences from sham (Water) after correction (α = .005) are indicated.

The primary sources of variance associated with increases in theta power within the right parahippocampal gyrus following surface injections of nicotine were between sham condition (M= 59.43, SEM = 3.49) and a number of concentrations, namely: 10 nM (M= 120.20, SEM= 6.63), 1 uM (M= 102.77, SEM = 12.03), 10 uM (M= 79.70, SEM= 1.90), 1 mM (M= 83.23, SEM= 6.48), 10 mM (M= 110.33, SEM= 9.21), 100 mM (M= 109.93, SEM= 6.19), and 1 M (M= 132.47, SEM= 7.00). Effect sizes ranged between 75% and 96%. Theta power was also observed to linearly increase as a function of concentration, r= .53, p<.001; rho= .50, p<.005 (Figure 31). This relationship was strengthened when removing trials involving the peak 10 nM concentration (r= .71, p<.001). In fact, power fluctuations were essentially non-linear below concentrations of 1 µM after which the relationship strengthened markedly. After Bonferonni correction for multiple comparison (α = .005), three concentration ranges could be discerned, each defined by a “peak” wherein the average was visually increased as seen in Figure 30. Three concentrations, 10 nM, 1 uM, and 1M, were selected across the range of the set

for further experimentation where the time-course of theta fluctuations would be monitored post-injection.

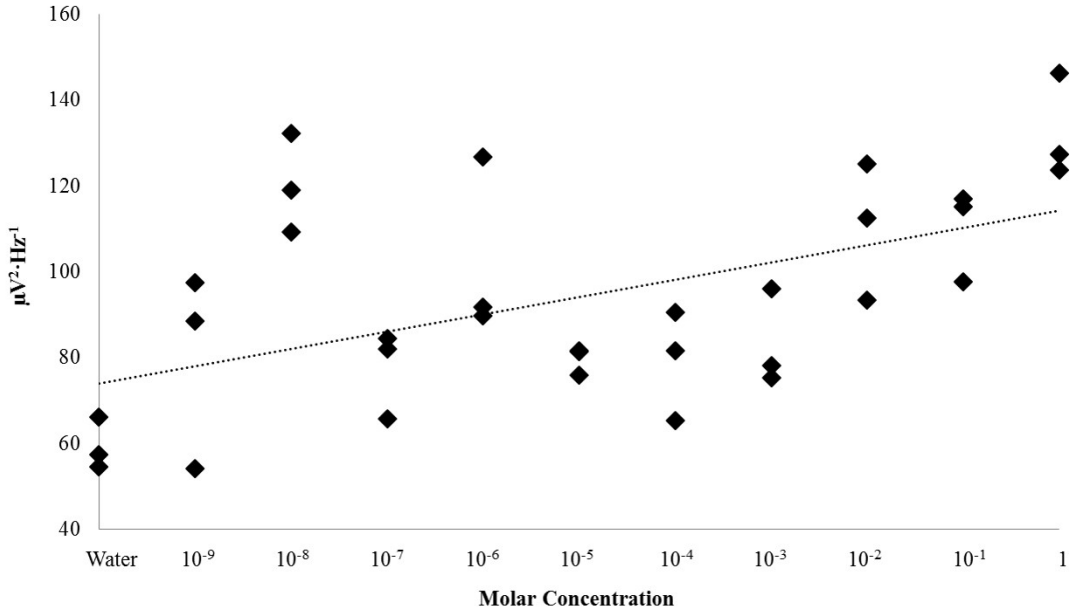

Figure 31. Concentration Dependence: Nicotine. Theta (4Hz – 7.5Hz) PDs within the right parahippocampal gyrus as a function of the concentration of nicotine injected over the surface of the tissue.

A grand mean of the "peak" concentration theta power responses to surface injections of nicotine (M= 95.06, SEM= 7.47) were increased relative to baseline conditions (M= 78.41, SEM= 3.34) [$t(34)= 2.04$, $p=.05$, $r^2= .11$]. An ANOVA revealed that 10 nM injections over the surface of the parahippocampi induced time-dependent fluctuations in theta power, $F(5,35)= 2.60$, $p<.05$, $\eta^2=.30$. These disparities were likely driving the differences observed with the grand-means. Other concentrations did not demonstrate robust time-dependent effects ($p>.05$). Homogeneous subsets identified two groups wherein the major sources of variances were between theta power 20 minutes

post-injection (which was indistinguishable from baseline theta power) and the 1 minute immediately following injection (r^2= .27, p<.05). These differences in theta power within the PHG are visualized in Figure 32A. A clear initial increase was noted, followed by a decrease to baseline levels over time.

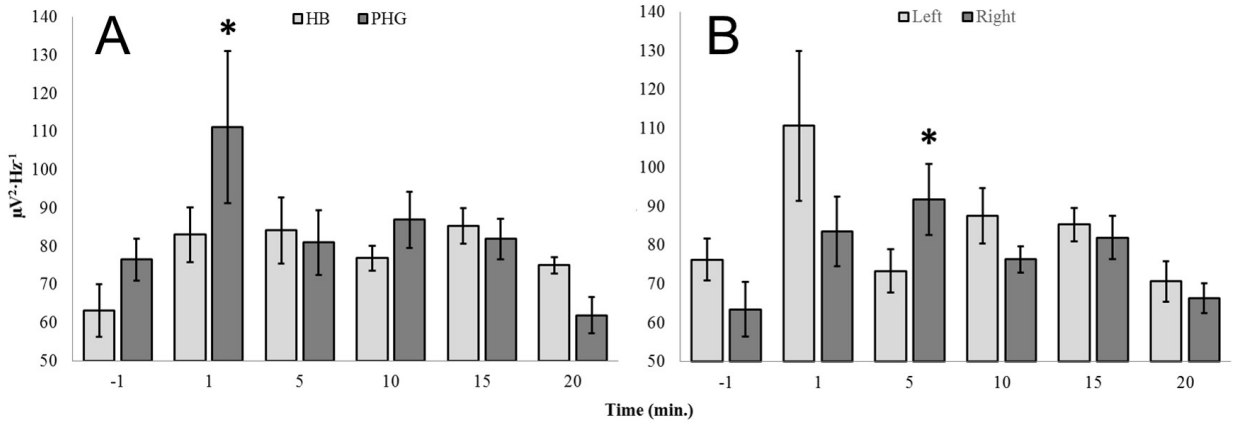

Figure 32. Time Dependence: Nicotine. Theta (4Hz – 7.5Hz) PDs as a function of time (min) from injection (time = 0 or between -1 and 1) of 10 nM nicotine for hippocampal (HB) and parahippocampal (PHG) loci (A) as well as between left (Left) and right (Right) hemispheres (B).

Further analysis of hemispheric effects indicated that theta power increased significantly within right hemispheric structures (parahippocampal gyri and hippocampal bodies) 5 minutes post-injection of 10 nM nicotine (M= 91.75, SEM= 9.08) relative to baseline conditions (M= 63.43, SEM= 7.04), t(10)= 2.46, p<.05, r^2= .38 (Figure 32B). The effect was specific to the theta band and did not generalize to left hemispheric structures [t(10)= .38, p>.05]. Left hemispheric structures did not demonstrate time-dependent changes relative to baseline. As is apparent in Figure 32B, the high degree of variability

associated with left hemispheric theta power 1 minute post-injection may have masked an early-phase homologous effect.

PDs collected serially over several weeks of experimentation were plotted over time in order to discern any long-term effects associated with repeated and protracted exposures to surface injections of various concentrations of nicotine. Time, in this case, was represented by trial order. Investigating linear relationships between band-specific power and trial order (implicitly time) within the tissue revealed a negative correlation for the theta-band PDs during the sham condition ($r= -.62$, $p<.05$). The relationship is plotted in Figure 33. Selecting for the first and last three sham trials, a significant decrease in theta power was observed, $t(4)= 5.40$, $p= .006$, $r^2= .88$. Three conspicuous trials can be seen in Figure 33 which can be interpreted as “peaks” within the negative trend which are represented at points 5, 8 and 9. Each trial was determined to have originated from separate coronal slices (n=3). Trials 8 and 9 were preceded by injections of 10 mM nicotine. Considering that conditions associated with each trial were randomized and order-effects were unlikely due to chance alone, this observation could be relevant.

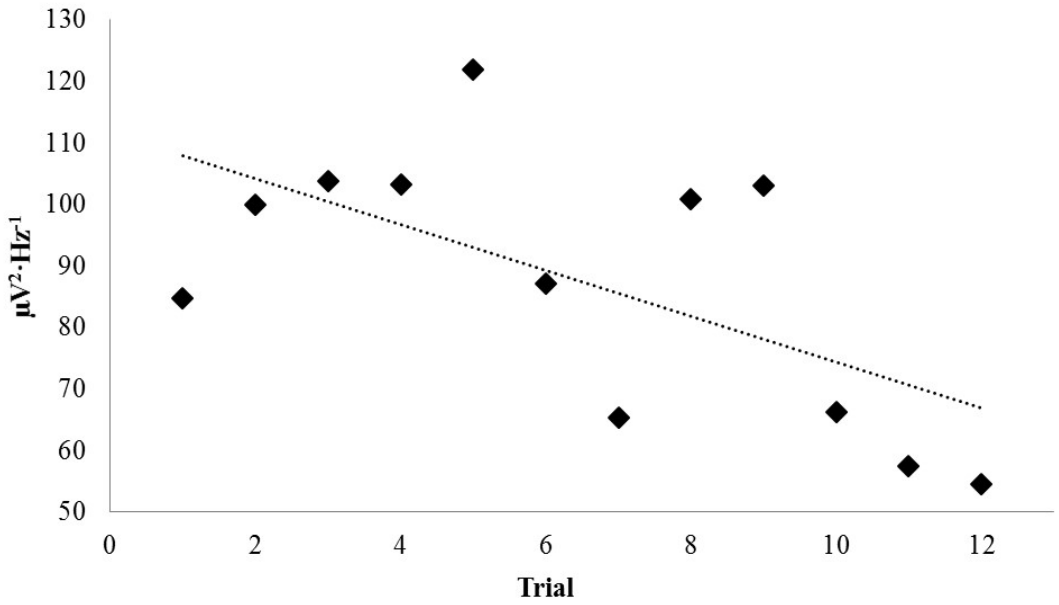

Figure 33. Repeated Exposure: Nicotine. Theta (4Hz – 7.5Hz) PDs upon injection of water (control) as a function of time.

Surface Injections of 5-Hydroxy-L-trypotophan

Applications of various concentrations of 5-HTP to the coronal sections revealed a number of features. Significant increases in theta (4Hz – 7.5Hz) PDs within the right hippocampal body were noted for the 100 nM (M= 82.67, SEM= 10.81) and 100 µM (M= 81.53, SEM= 10.21) concentrations relative to the water control (M=39.47, SEM= 5.32) where $p<.05$ and effect sizes were 76% and 77% respectively (Figure 34). Other frequencies were unaffected and the contralateral hippocampal body did not demonstrate similar response patterns ($p>.05$).

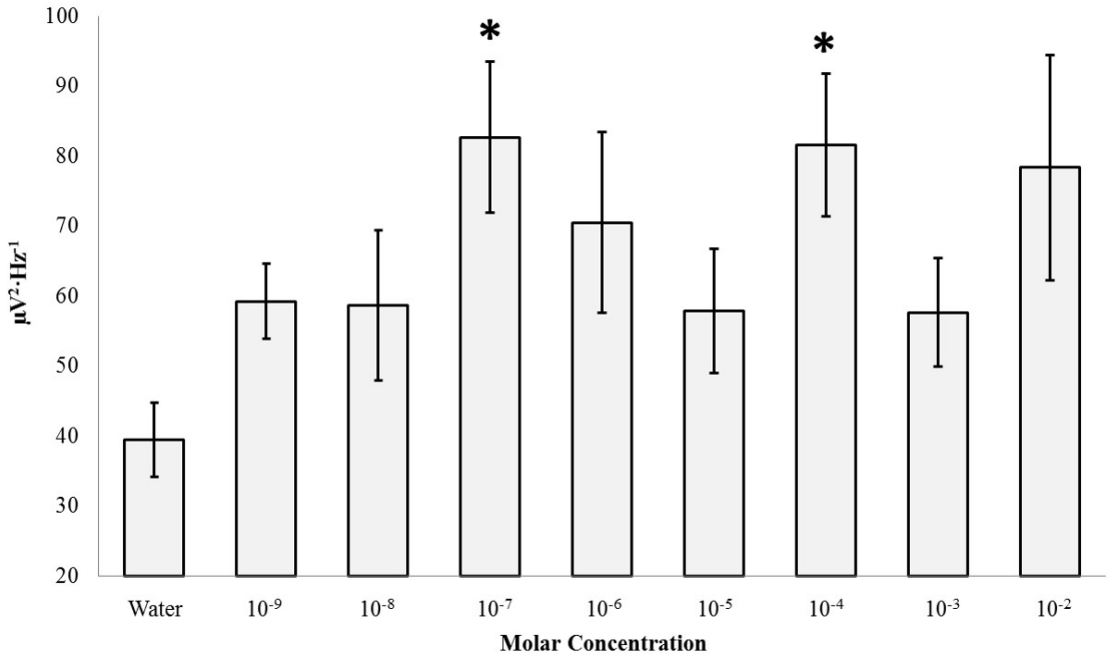

Figure 34. 5-HTP Response: Right Hippocampus. Theta (4Hz – 7.5Hz) PDs within the right hippocampal gyrus as a function of the molar concentration of 5-HTP applied to the surface of coronal sections of human brain tissue. Significant differences are indicated (p>.05).

The right parahippocampal gyrus displayed increased gamma (30Hz – 40Hz) activity upon injection of 10 nM 5-HTP (M= 1.58, SEM= .06) relative to water control [(M= 1.23, SEM= .03), t(4)= 4.98, p=.008, r^2=.86 (Figure 35)]. The contralateral parahippocampal gyrus did not express similar differences as a function of any concentrations of 5-HTP (p>.05). Other frequency-specific microvolt fluctuations remained unaffected by surface injections of 5-HTP applied to the right parahippocampal gyrus (p>.05). Dose-dependent linear relationships or changes in microvolt potentials over time could not be identified for coronal sections exposed to 5-HTP. This feature was observed for all of the other applied chemical compounds.

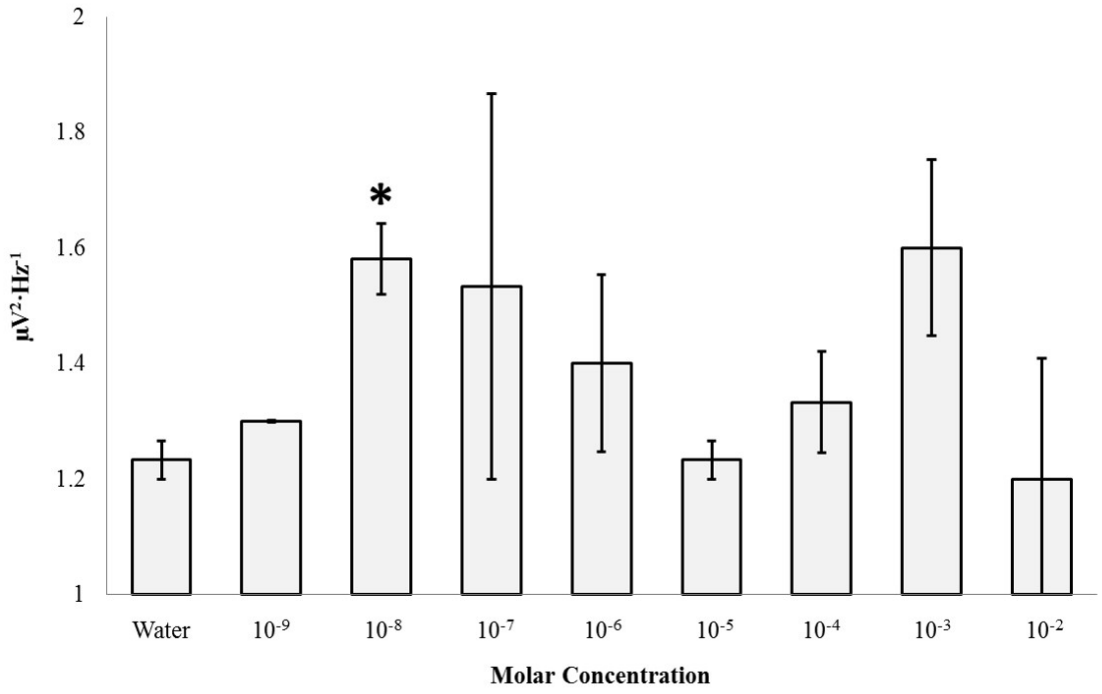

Figure 35. 5HTP Response: Right Parahippocampal Gyrus. Gamma (30Hz – 40Hz) PDs within the right parahippocampal gyrus as a function of the molar concentration of 5-HTP applied to the surface of coronal sections of human brain tissue. Significant differences are indicated (p>.05).

Surface Injections of Glutamate

An ANOVA revealed a three-way interaction between structure, hemisphere, and concentration for global (1.5 Hz – 40 Hz) PDs [$F(8, 107)= 3.02$, $p<.01$, $\eta^2= .20$]. Selecting for the left parahippocampal gyrus, global power (1.5Hz – 40Hz) increased upon injection of concentrations of 100 nM (M= 108.76, SEM= 6.07) of glutamate relative to water (sham) control [(M= 70.23, SEM= 2.49) [$t(4)= -5.88$, $p<.005$, $r^2= .90$ (Figure 36)]. This effect was largely due to increases in delta (1.5Hz – 4Hz) activity between the same conditions [$t(4)= -4.99$, $p<.01$, $r^2=.86$]. Conspicuous high-frequency modulations by

nanomolar-range glutamate can be observed in Figures 36 and 37. The left parahippocampal gyrus demonstrated increased theta band PDs upon surface injections of 10 µM concentrations (M= 89.37, SEM= 1.29) of glutamate relative to the sham condition [(M= 69.20, SEM= 4.10), $t(4)= -4.70$, $p<.01$, $r^2=.85$]. Finally, increases of 0.3 to 0.5 $\mu V \cdot Hz^{-1}$ were observed for probed left parahippocampi within the gamma band upon surface injections of 10 mM and 1 mM glutamate respectively with associated effect sizes of 68% and 70%. The anatomically adjacent left hippocampal body did not display significantly different spectral power upon surface injections of any concentration of glutamate relative to the sham condition ($p>.05$).

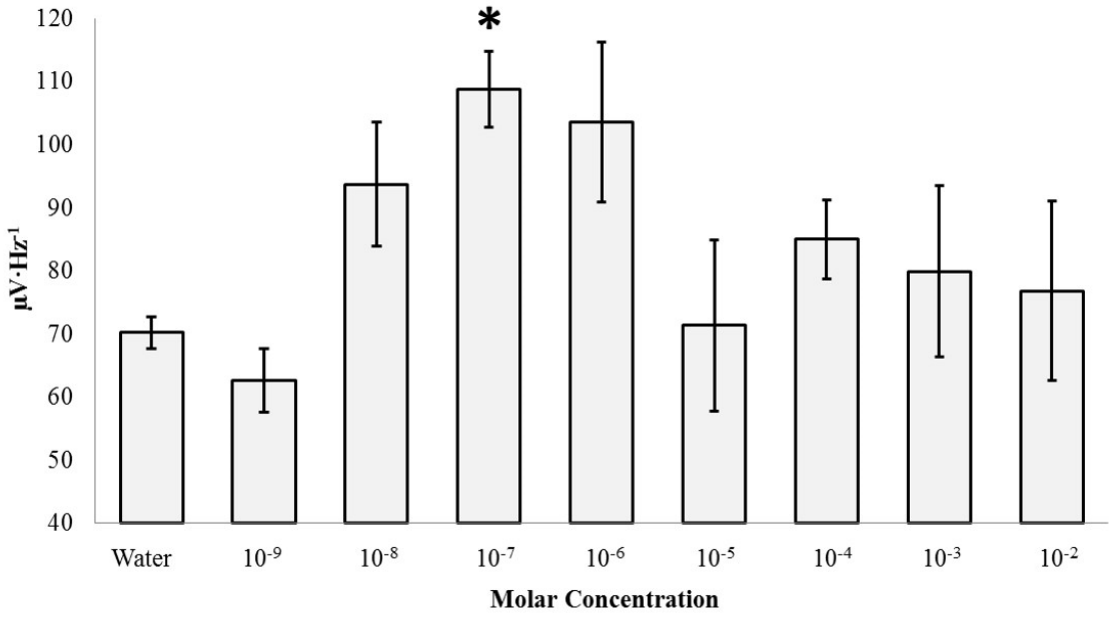

Figure 36. Glutamate Response. Global power (1.5Hz – 40Hz) within the left parahippocampal gyrus as a function of concentration of glutamate. A significant increase

in mean global power after Bonferonni correction (α = .006) is indicated.

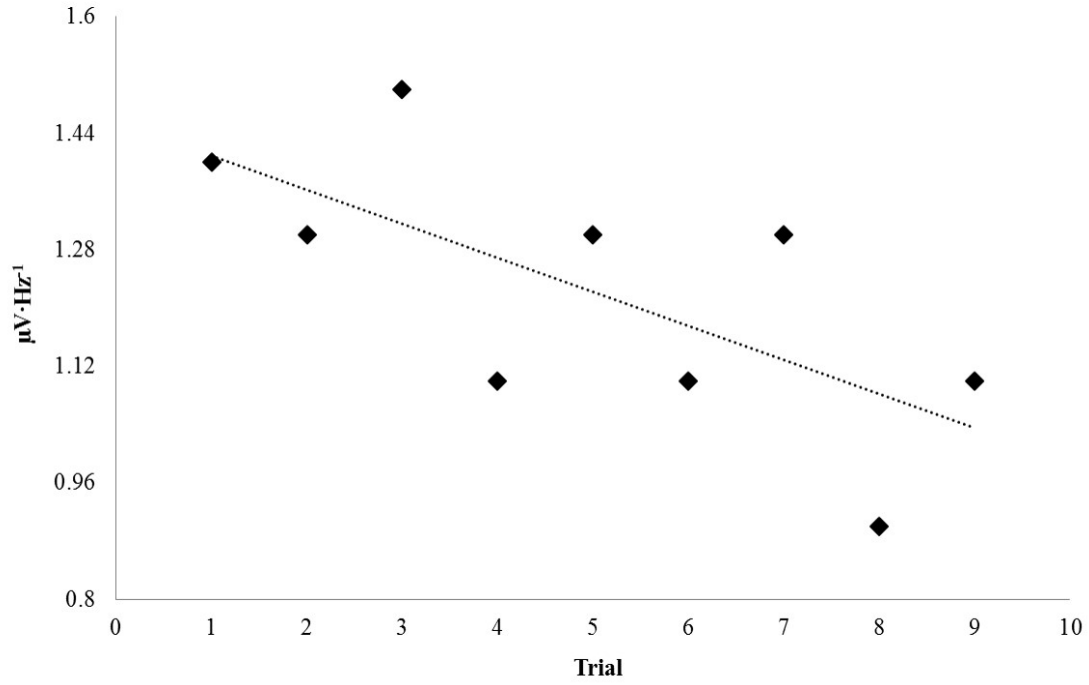

Figure 37. Concentration Dependence: Glutamate. Gamma (30Hz – 40Hz) power within the left parahippocampal gyrus plotted as a function of concentration of the injected material.

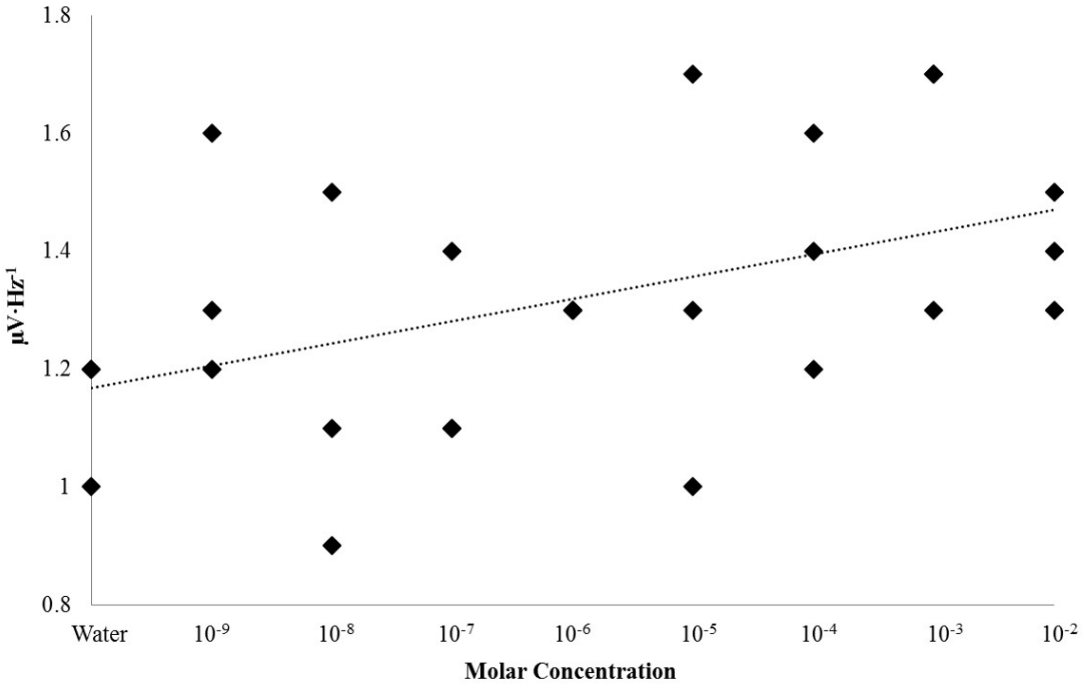

Figure 38. Repeated Exposure: Glutamate. Gamma (30Hz – 40Hz) power within the left parahippocampal gyrus for trials involving surface injections of 10^{-8} to 10^{-6} M glutamate as a function of trial order, or implicitly, time.

A conspicuous linear relationship between gamma activity within the left parahippocampal gyrus and the concentration of the injected material was also observed [r= .45, p<.05; rho= .47, p<.05 (Figure 37)]. Linear relationships between concentration of the injected material and spectral power within any band could not be identified within alternative structures (p>.05). Selecting for concentrations between 10^{-8} to 10^{-6} M glutamate, conditions which produced the greatest magnitude shifts in computed global power relative to the water control, a strong negative correlation was observed between trial order and gamma power [r= -.73, p<.05; rho= -.71, p<.05 (Figure 38)]. This relationship indicates that gamma power linearly decreased as a function of time upon injections of the same concentrations of glutamate which transiently increased gamma

power activity. This relationship was not observed when plotting trial order with gamma power independent of selective concentration bands ($p>.05$). In other words, the negative relationship was only maintained when narrow-band concentrations which induced maximal responses relative to control conditions were selected.

Two minor right hemispheric effects were noted. First, an increase in delta power (1.5Hz – 4Hz) within the right parahippocampal gyrus was noted upon injection of 1 mM ($M= 401.97$, $SEM= 14.67$) glutamate relative to the sham condition ($M= 351.70$, $SEM= 9.27$), $t(4)= -2.90$, $p<.05$, $r^2= .68$. When considering a computed global average of spectral power differences the effect size associated with significant differences between 1 mM and the sham condition increased to 73%. Second, an increase in gamma power (30Hz – 40Hz) within the right hippocampal body was noted upon surface injections of 10 nM ($M= 1.63$, $SEM= .07$) glutamate relative to the sham condition ($M= 1.27$, $SEM= .09$) [$t(4)= 3.32$, $p<.05$, $r^2= .73$].

Having identified the "peak" concentration of 10^{-7} M, which optimally induced gamma power increases within the left parahippocampal gyrus, a series of trials were completed in order to plot the time-course of glutamate power over 20 minutes (Figure 39). An ANOVA revealed significant differences in gamma power over time, $F(5, 17)= 4.25$, $p<.05$, $\eta^2= .64$. No other frequency band was affected ($p>.05$). *Post-hoc* tests revealed two homogeneous subsets with the 1 minute post-injection condition loading separately from all other time conditions. The increase in power was equivalent to ~ 0.7 $\mu V \cdot Hz^{-1}$ on average.

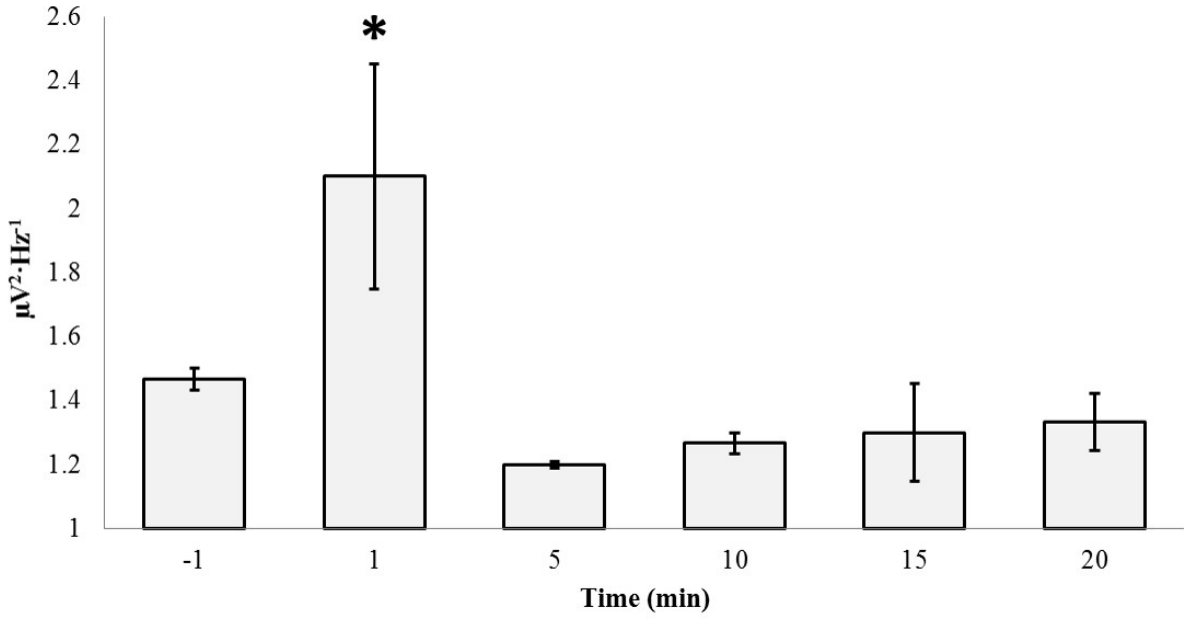

Figure 39. Time Dependence: Glutamate. Gamma (30Hz – 40Hz) power within the left parahippocampal gyrus as a function of time elapsed from the point of surface injections of 100 nM (10^{-7} M) glutamate.

Surface Injections of Ketamine

Dose-dependent curves of high-frequency PDs identified within the left parahippocampal gyrus occurred from exposure to a narrow band of molar concentrations of glutamate. We investigated the potential mechanisms governing the effects. A focused experimental procedure was designed whereby left hemispheric hippocampal bodies and parahippocampal gyri were exposed to various concentration of ketamine, an N-methyl-D-aspartate (NMDA) receptor antagonist (Newcomer et al., 1999). It was hypothesized that decreases in high-frequency PDs within the parahippocampus but not the hippocampus would result if the operating mechanism was common to that which was underlying the glutamate effects.

A one-way ANOVA selecting for the parahippocampal gyrus revealed that beta1 PD differences from the pre-injection period (i.e., a 30 second period immediately preceding the injection) to the post-injection period (i.e., a 30 second period immediately following the injection) differed as a function of concentration of ketamine [$F(4,14)= 4.09$, $p<.05$, $\eta^2=.62$ (Figure 40A)]. Homogeneous subsets revealed the primary source of variance was a difference between the 1 nM condition and the water control ($p<.05$). *Post-hoc* t-tests confirmed this difference marked by a decrease in power after injection [$t(4)=3.63$, $p<.05$, $r^2=.77$]. A proportionally similar decrease was also noted when using an average of beta1 and gamma activity [$t(4)= 2.86$, $p<.05$, $r^2= .67$ (Figure 40B)]. Concentration effects were not noted for the hippocampal body across any spectral power band ($p>.05$). That high-frequency activity was enhanced by glutamate and suppressed by ketamine suggests a common site of action and reduces the probability that the effects were simple artifacts of injections. That both of these phenomena were observed within the parahippocampal gyrus but not the hippocampus indicates internal consistency.

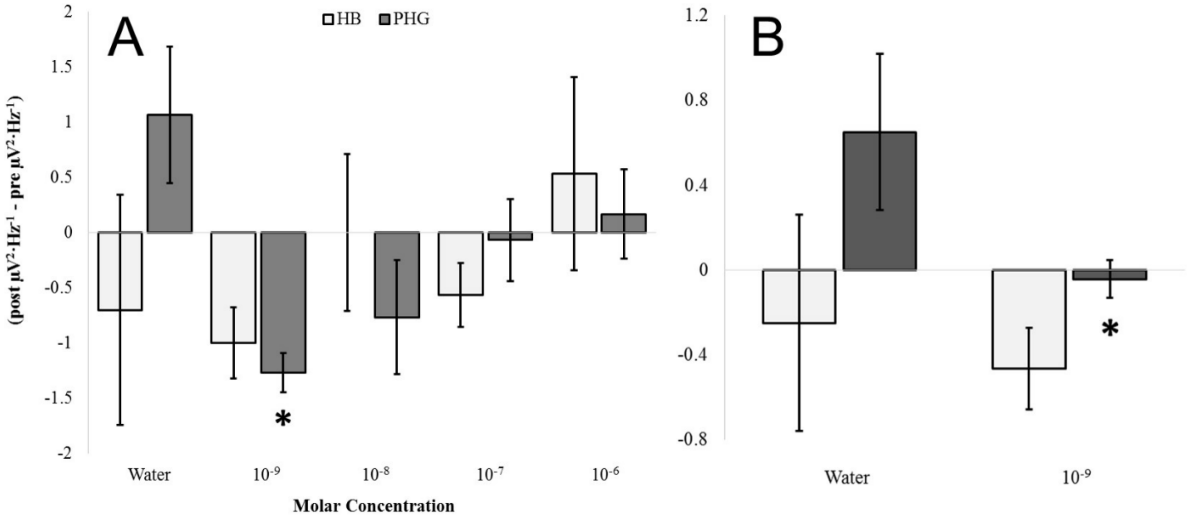

Figure 40. Ketamine Response. Beta1 (14Hz – 20Hz) SPD differences from the pre-injection period to the post-injection period for left hemispheric hippocampal bodies (HB) and parahippocampal gyri (PHG) exposed to various concentrations of ketamine (A). High frequency PDs computed from an average of beta1 (14Hz – 20Hz) and gamma (30Hz – 40Hz) SPD differences from the pre-injection period to the post-injection period for left hemispheric hippocampal bodies (HB) and parahippocampal gyri (PHG) exposed to 1nM ketamine compared to sham injection (B). Significant differences are indicated ($p<.05$).

A non-parametric correlation was identified between low-frequency (delta to alpha) but not high-frequency (beta1 to gamma) SPD differences within the left parahippocampal gyrus from pre- to post-injection periods and the molar concentration of ketamine administered ($rho=.60$, $p<.05$). These differences were primarily due to an underlying positive correlation between delta PD differences from pre- to post-injection periods and molar concentrations of ketamine, $rho= .56$, $p<.05$ (Figure 41). The adjacent hippocampal body did not demonstrate any statistically significant relationships between expressed power density differences from pre- to post-injection periods and drug concentration ($p>.05$). Figure 42 demonstrates the non-relationship observed between delta-band PD differences from pre- to post- injection periods and molar concentration for the hippocampal body ($rho= -.10$, $p=.73$) which was in stark contrast to that which is displayed in Figure 41 for the parahippocampal gyrus.

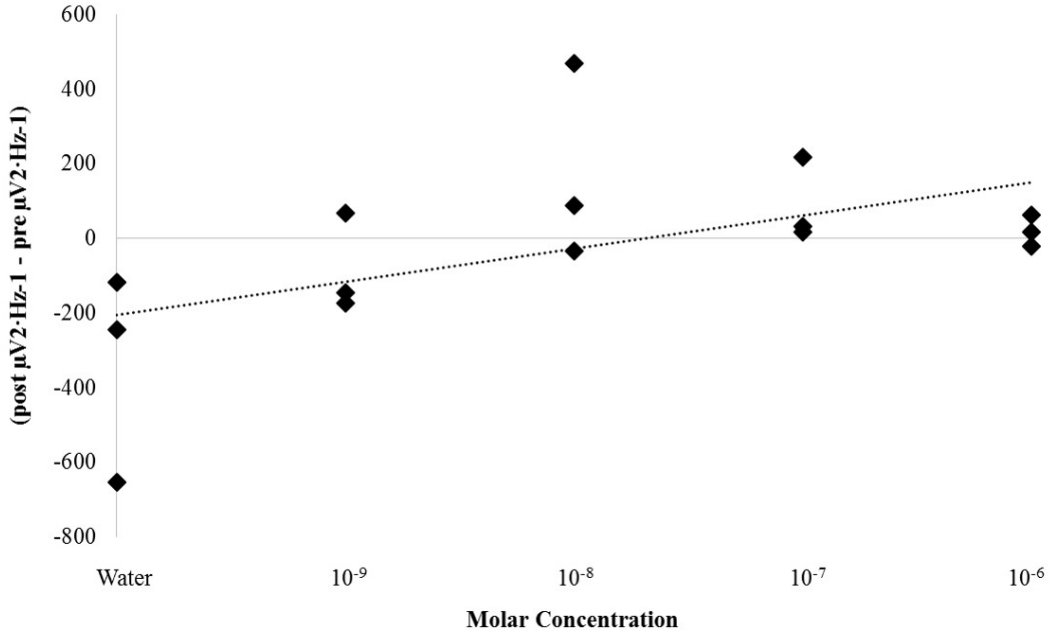

Figure 41. Concentration Dependence: Ketamine. Non-parametric correlation between delta (1.5Hz – 4Hz) SPD differences from the pre-injection period to the post-injection period and molar concentration of ketamine for the left parahippocampal gyrus. A significant correlation was identified (rho= .60, p<.05).

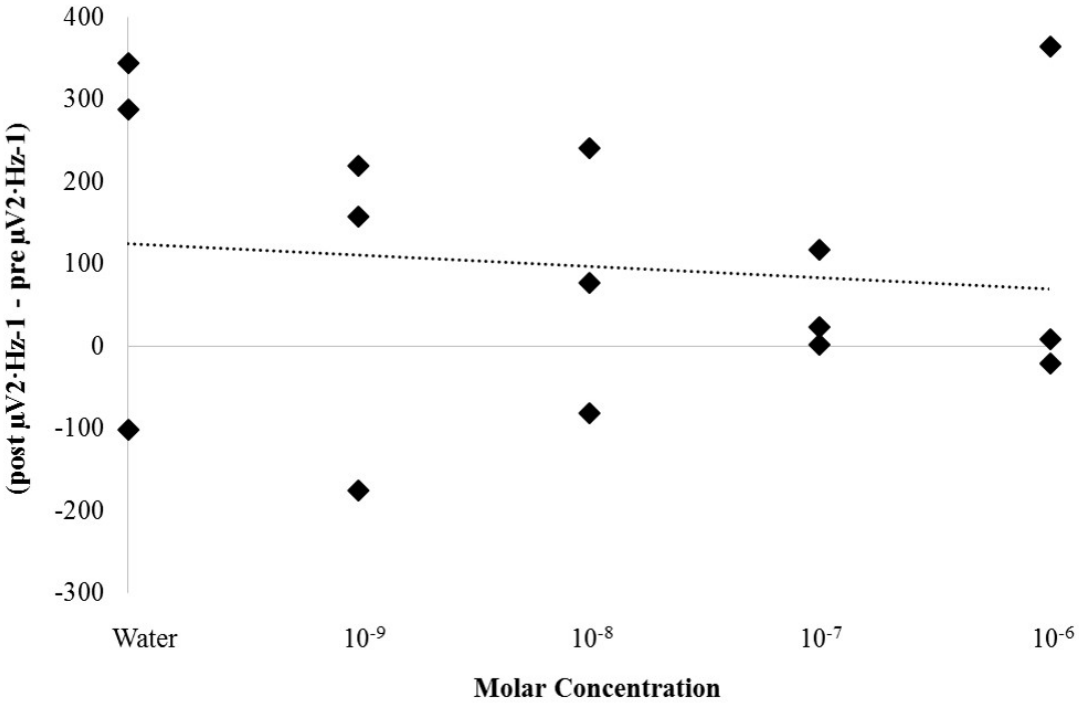

Figure 42. Null Hippocampal Effect: Ketamine. Non-parametric correlation between delta (1.5Hz – 4Hz) SPD differences from the pre-injection period to the post-injection period and molar concentration of ketamine for the left hippocampal body. No significant correlation was identified ($p>.05$).

In order to substantiate the potential receptor-mediated mechanisms governing increases in high-frequency microvolt fluctuations associated with NMDA receptor agonist glutamate and similar decreases associated with NMDA receptor antagonist ketamine, mixed solutions were generated. Left parahippocampi were exposed to surface injections of water, a mixed solution of 10^{-7} M glutamate and 10^{-9} M ketamine (i.e. the optimal concentrations which modulated high-frequency microvolt fluctuations), or a mixed solution of 10^{-5} M glutamate and 10^{-7} M ketamine which served as an alternative control. No significant differences between injection conditions were noted for beta1,

beta2, and gamma PDs (p>.05). Figure 43 demonstrates the mutual nullification of glutamate- and ketamine-mediated high-frequency effects within the left parahippocampal gyrus.

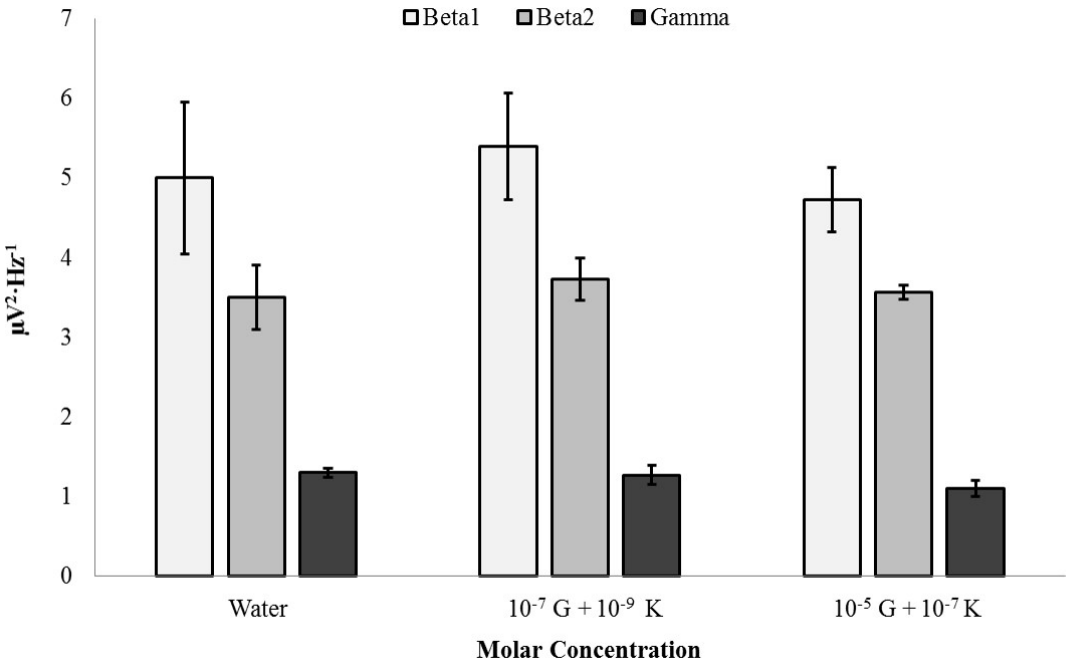

Figure 43. Glutamate-Ketamine Response. Beta1 (14Hz – 20Hz), beta2 (20Hz – 30Hz), gamma (30Hz – 40Hz) PDs within the left parahippocampal gyrus exposed to surface injections of water (Water), 10^{-7} M glutamate and 10^{-9} M ketamine (10^{-7} G + 10^{-9} K), or 10^{-5} M glutamate and 10^{-7} M ketamine (10^{-5} G + 10^{-7} K). No significant differences were observed (p>.05).

Glutamate-Induced Microvolt Fluctuations And Coupled Photon Emissions

Within a darkened environment, injections of 100 nM glutamate applied to the surface of coronal sections placed in the darkened environment produced increased post-injection (M= 4.60, SEM= .45) beta2 PDs relative to the pre-injection (M=3.10, SEM=.31)

period for the left parahippocampal gyrus [$t(6)= 2.73$, $p<.05$, $r^2=.55$ (Figure 44A)]. This response was not noted for the right parahippocampal gyrus, nor was it observed when water was applied to the tissue (Figure 44B). The mean photon raw count when the glutamate was applied over the left parahippocampal region was 241.2 per 20 ms and 225.3 per 20 ms when water was applied. The difference (16 photons) per second (50 Hz sampling) was 800 counts. Assuming a typical peak range photon for the equipment to be associated with $4.22 \cdot 10^{-19}$ J the increased photon flux density from the tissue after glutamate was applied compared to when only water was applied would have been $3.38 \cdot 10^{-16}$ Watts (Joules per s). Because the aperture of the PMT was about $2.25 \cdot 10^{-4}$ m^2, the photon flux power density increase would have been $1.5 \cdot 10^{-12}$ $W \cdot m^{-2}$.

The regression equation relating the change in power density for the beta2 band to the numbers of photons was 0.0394 multiplied by the number of photons (plus 4.314, the constant). This means that for an increase of every ~10 photons per s over the left parahippocampal region after glutamate application the corresponding beta2 band power increased by 0.39 $\mu V^2 \cdot Hz^{-1}$. When applied over the 10 Hz increment of beta2 (20 to 30 Hz) this would be 3.9 μV^2 or about 2 μV.

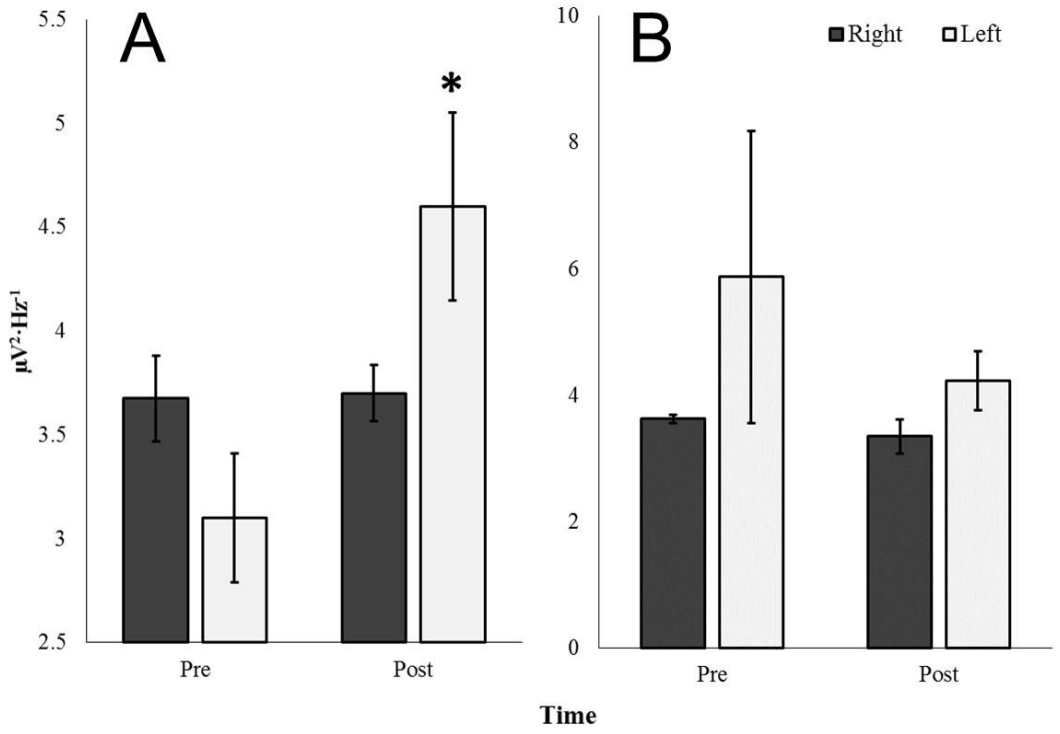

Figure 44. Glutamate Response in a Darkened Environment. Beta2 (20Hz – 30Hz) PDs for periods of pre- and post-injection for right (dark) and left (light) parahippocampal gyri exposed to 1 mL surface injections of 100 nM glutamate (A) and water (B). A significant difference from pre-to-post-injection periods for the left parahippocampal gyrus was revealed ($p<.05$).

A bivariate non-parametric correlational analysis was performed with beta2 PDs and raw photon counts obtained 10 cm over the tissue within the vertical plane. Spearman rho values indicating the relationship between beta2 and raw photon counts were examined for hemisphere-, compound-, and time-dependent differences. An ANOVA revealed a three-way interaction of these factors [$F(1,31)= 8.38$, $p=.008$, $\eta=.23$]. The primary source of variance was identified as a difference in rho values associated with the pre-injection period ($M= -.44$, $SEM= .18$) and the post-injection period ($M= .30$,

SEM=.20) for the left parahippocampal gyrus [t(6)= 2.61, p<.05, r^2=.53]. Figure 45 demonstrates this difference which was not noted for the right parahippocampal gyrus. Alternative PD-photon relationships (e.g. delta PD-photon, theta PD-photon, etc.) were not observed (p>.05).

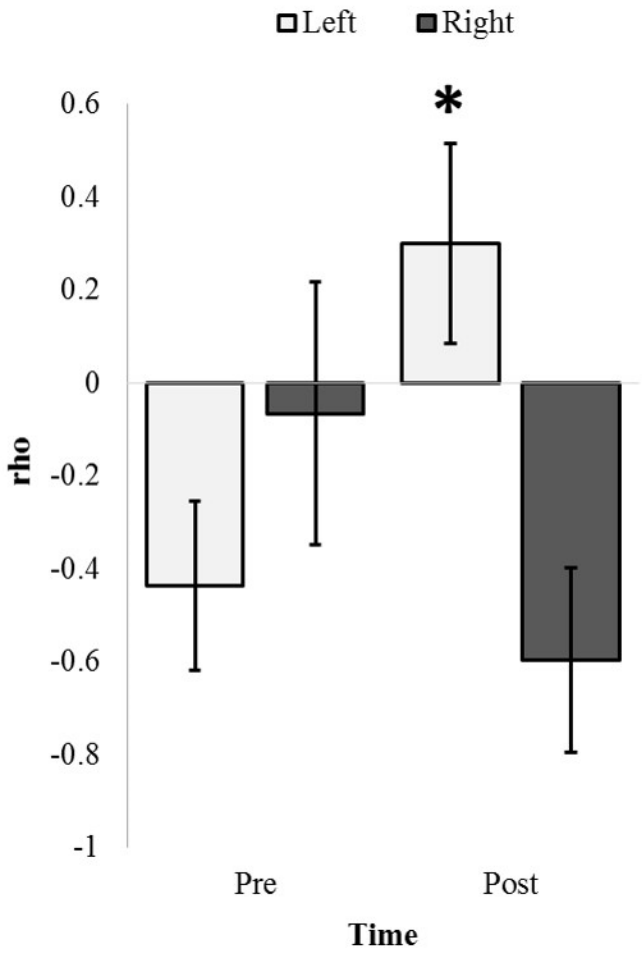

Figure 45. Glutamate Induced Microvolt-Photon Pairings. Non-parametric correlations (Spearman rho values) between beta2 (20Hz – 30Hz) PDs within and raw photon counts over the left (light) and right (dark) parahippocampal gyri for the 25 seconds preceding (Pre) and proceeding (Post) injections of 100 nM glutamate applied to the

surface of the coronal sections. Significant differences in non-parametric correlations from pre-to-post-injection periods is noted for the left parahippocampal gyrus ($p<.05$).

Signal Complexity and Frequency Discrimination: Heschl's Gyrus

HFDs were calculated for each transformed segment of EEG data, including the baseline condition, using MatLab. The results of Kolmogorov-Smirnov tests for normalcy were significant, thus non-parametric methodologies were employed. Significant effects for hemisphere (Mann-Whitney U, $p=0.017$) and waveform (Mann-Whitney U, $p=0.008$), but not location of sensor were found and directed further analyses. Selecting for each individual hemisphere and waveform condition revealed significant differences in the HFDs of the EEG data recorded during the right sine wave condition (KW $\chi^2(9)=17.927$, $p=0.036$). Subsequent *post-hoc* analyses revealed three groups (average HFDs = 1.38, 1.40, 1.42) where the HFD for 20 Hz (1.425) was largest and different from all other conditions, including baseline (1.398) (Figure 46).

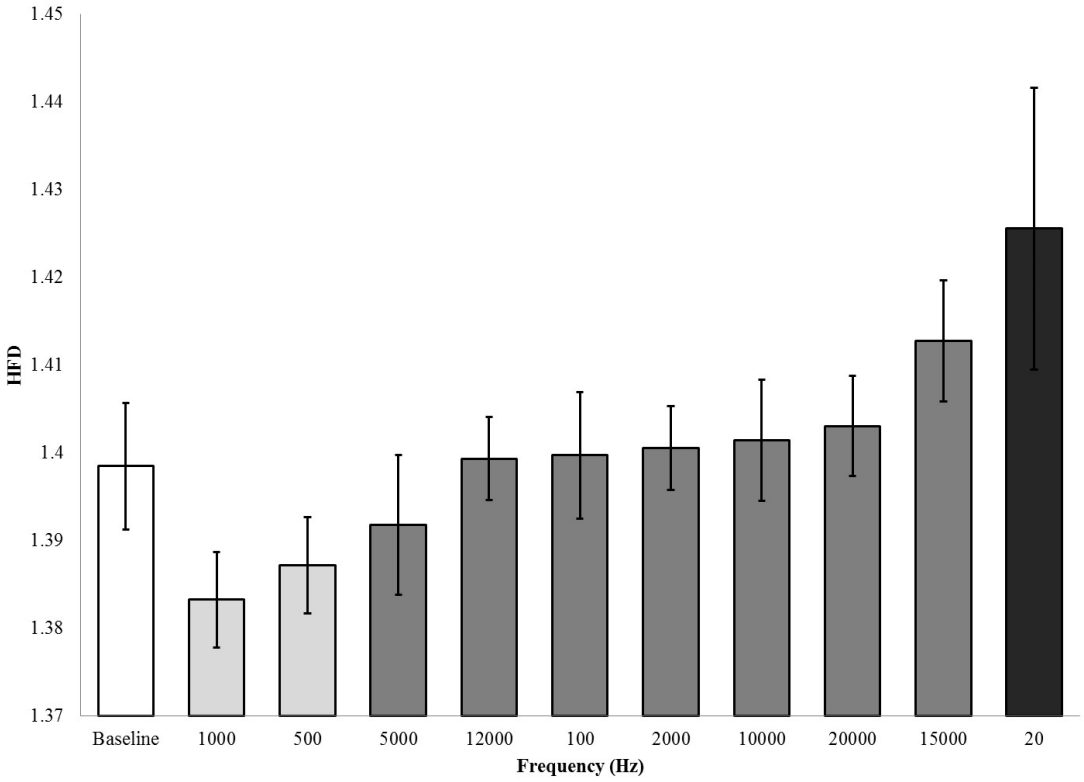

Figure 46. Fractal Dimensions by Frequency: Heschl's Gyrus. Results of the Higuchi Fractal Dimension (HFD) Kruskall-Wallis test. Groups as revealed by post-hoc Mann-Whitney U tests are indicated by shading of bars, with the exception of the baseline (error bars = SEM).

ANOVAs revealed that delta (η^2= .30), theta (η^2= .28), and beta2 (η^2= .28) PDs differed as a function of frequency for square-wave stimuli presented to the medial aspect of HG within left hemispheric sagittal sections ($p<.05$). Differences were not identified as a function of the frequency of the stimulus for all combinations of factors within the right hemisphere, for presentations to the antero-lateral aspect of HG within the left hemisphere, or for sine wave signals ($p>.05$). It was strictly a square-wave effect. Applying the Bonferonni method, a corrected alpha level (α = .016) was selected as a

conservative threshold beyond which differences were considered significant. Frequency-dependent differences in theta band spectral power (4.0 Hz – 7.5 Hz) remained significant after Bonferonni correction ($p<.016$). Differences within delta and beta2 bands did not meet this threshold. The primary sources of variance were identified to be differences between 20Hz (M= 89.52, SEM= 5.88) and 5,000Hz (M= 64.60, SEM= 4.01), 20 Hz (M= 89.52, SEM= 5.88) and 20,000 Hz (M= 65.02, SEM= 2.64), as well as 100Hz (M= 77.97, SEM= 2.12) and 20,000 Hz (M= 65.02, SEM= 2.64) which are visualized in Figure 47A. The effect sizes (r^2) associated with each significant difference were .55, .59, and .59 respectively. In contrast, Figure 47B demonstrates the overlap between frequency-responses within the right hemisphere.

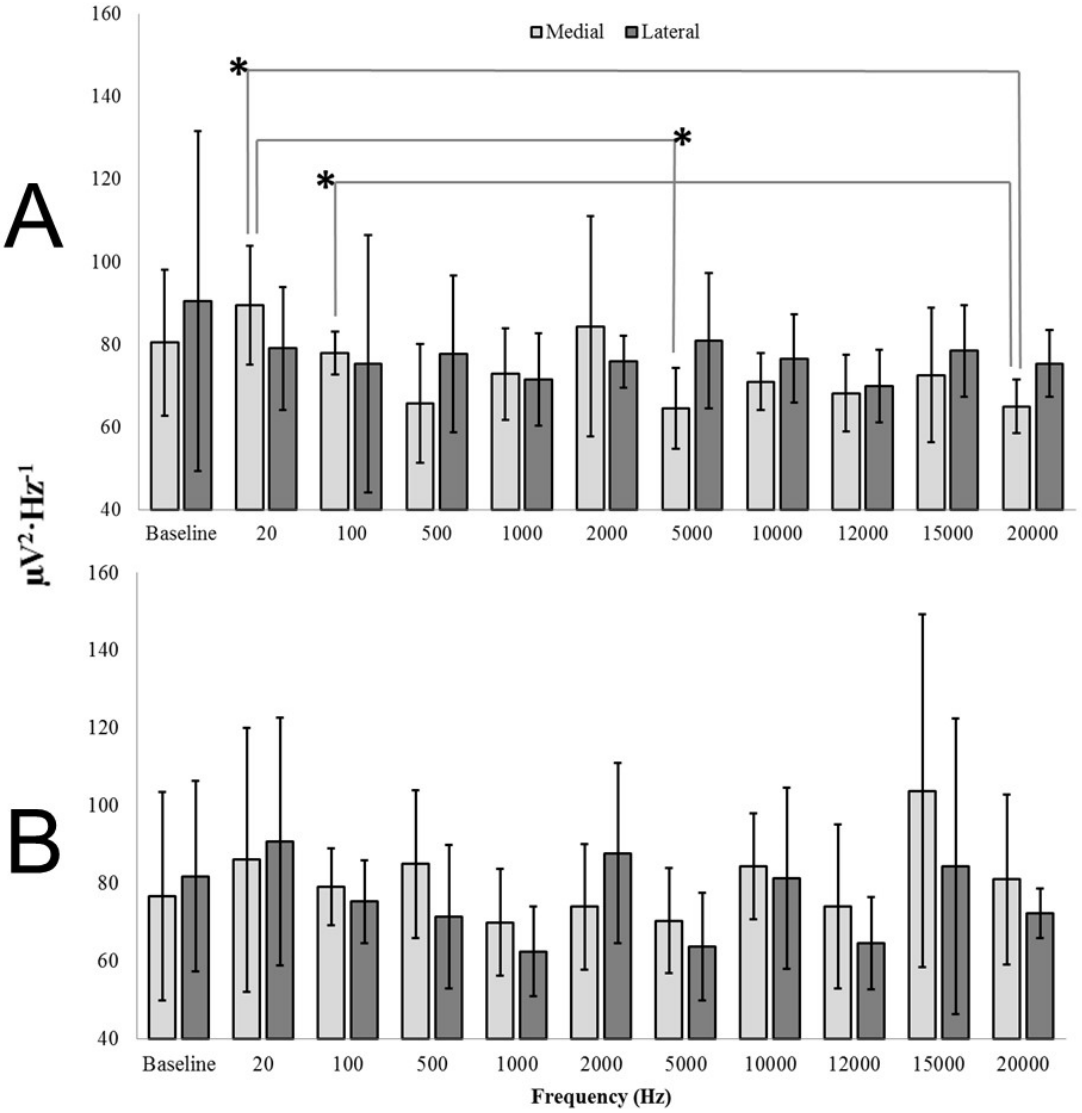

Figure 47. Frequency Discrimination. Theta (4Hz – 7.5Hz) PDs within the postero-medial (Medial; light) and antero-lateral (Lateral; dark) aspect of Heschl's Gyrus within the left (A) and right (B) hemispheres as a function of square-wave signals with frequencies ranging between 20Hz to 20, 000 Hz. Significant differences after correction (α = .005) are indicated.

A discriminant analysis revealed that wide-band PDs (1.5Hz – 40Hz) derived from the postero-medial aspect of HG within the left hemisphere upon stimulation by square-wave 20Hz and 20,000Hz signals successfully classified 100% of cases in a corrected model [(n=12), Λ =.09, $\chi^2(6)=16.64$, $p<.01$, canonical $R^2= .95$]. No other combination of factors, including those selecting for the antero-lateral aspect of the same gyrus, could reproduce a successful classification of cases when attempting to discriminate 20Hz and 20,000Hz ($p>.05$). The same confluence of factors (i.e. postero-medial, left hemisphere, square waves) generated 100% classification of cases when discriminating 20Hz and 5,000Hz, [Λ =.10, $\chi^2(6)=16.27$, $p<.05$, canonical $R^2= .95$]. Together, these results suggest that the posterior and medial aspects of HG within the left hemisphere but not the adjacent anterior and lateral components maintain frequency discrimination capacities long after death in EFA-fixed human brain tissue – a property unobserved within analogous areas of the right hemisphere.

Discussion

One of the most important perspectives afforded by the pursuit of knowledge through systematic and scientific methods is to assume nothing. Axioms, self-evident truths, and (most frequently) designation by decree of authority or unchallenged faith in traditions have often been major impedances to the types of discoveries that lead to shifts in paradigms and a more accurate or at least a different perspective of the human condition. As neuroscientists we have been taught or have assumed that the fixed human brain is an unresponsive mass of organic residual that has replaced what was once a

vital, complex structure that served as the physical substrate for thought, consciousness, and awareness. The results of the present experiments strongly suggest we should at least re-appraise the total validity of that assumption.

Histological analyses indicated that there was general neuronal conservation that is discernable by routine light microscopy (Figure 29). Although neuronal (soma) Nissl-dominant stains do not discern the integrity of the fields of dendrites or the fidelity of their spines, we have found in unpublished studies with rat brains that those fixed in EFA for protracted periods (years) and later processed through modified Fox-Golgi (zinc chromate) methods exhibited some remarkable integrity of dendritic-spine processes. EFA had been selected based upon experimental comparisons as the primary mode of long-term fixation in our laboratory many years ago (Persinger, 1979) regardless of the initial post-mortem immersion (for human brains), because of the cytological detail it retained, its compatibility with a multitude of different stain types, and more recently because of its capacity to express immunochemical properties following specific “rejuvenating” pre-treatments.

If some proportion of the living microstructure remains with the potential to be activated, then electrophysiological patterns similar to those in the living brain should be elicited by physiologically-appropriate concentrations of classic neurotransmitters that would influence primarily only particular frequency bands. We selected the parahippocampal region as the primary focus because of the central role of this structure in human cognitive phenomena. First, it is the primary locus for the initial representation of experience (“memory”) as indicated by the marked decrement in this capacity following loss or lesions such as the cases of HM (Scoville & Milner, 1957) and RB (Zola-Morgan,

Squire, & Amaral, 1986). Secondly, as demonstrated by the precision of Pierre Gloor's (1997) micro- and macro-anatomical analyses this region directly accesses and reciprocally receives input and output respectively from the entire cerebral cortical manifold. Third, this region, particularly in the right hemisphere, is remarkably sensitive in the living state (Saroka, Caswell, Lapointe, & Persinger, 2014) as well as the fixed state (Costa, Rouleau, & Persinger, 2016) to ambient geomagnetic activity to which all human beings are usually immersed.

During the late 19th century portions of the hippocampal region were argued by anti-Darwinian debaters as the unique feature that discriminated human brains (and presumably the special nature of this species) from other primates (Jensen, 1988). It has been known for decades that temporal lobectomies as a treatment for intractable epilepsy eliminated the psychotrophic and hallucinogenic effects of LSD (Serafetinides, 1965). The central role of the parahippocampal region and its decreased connectivity from the retrosplenial cortex during hallucinatory experiences induced by LSD (Carhart-Harris et al., 2016) also highlights the potentially unique feature of this structure. Carhart-Harris et al (2016) found that the functional disconnectivity was strongly correlated with the rating of ego "dissolution" that was inferred to reflect the importance of this circuit to maintain the sense of self. Tagliazucchi et al. (2016), employing a slightly different approach, noted that the LSD effects enhanced global between-module interactions within those regions rich in 5-HT$_{2a}$ receptors.

Within the fixed dead human brain increases in theta power within the right hippocampal body was observed after application of 100 nM and 100 μM concentrations of serotonin. Unlike the living brain the serotonin immediately and directly apposed the

tissue upon application and was not diluted by either the multiple blood-brain barriers or the catabolising environment of enzymes. The double peak suggests two receptor subtypes that are consistent with those reported within the hippocampus (Pazos, Gonzalez, Waeber, & Palacios, 1991). The elicitation of gamma power within an even smaller concentration (10 nm) from the right parahippocampus region suggests an intrinsic separation of some remaining infrastructure that differentiates 4-7 Hz and 30-40 Hz patterns. This is important simultaneity in light of the common observation that gamma ripples are superimposed upon the massive theta activity within this region (Belluscio, Mizuseki, Schmidt, Kempter, & Buszaki, 2012; Sirota, Montgomery, Fujisawa, Isomura, Zugaro, & Buzsaki, 2008; Quilichini, Sirota, & Buszaki, 2010). This intrinsic association has been argued by Bear (1996) to be a primary electrophysiological correlate by which consciousness and awareness are coupled to memory. That this structure in the right but not the left hemisphere displayed the effect indicates the responses were specific and that there may be some particular residual within the right hemisphere. Rouleau and Persinger (1979) on the bases of similar results have suggested that the implications of the massive historical data base of surgical stimulation of patients and the interpretation of the etiology of their colourful experiences might be reconsidered.

Glutamate is considered the major excitatory neurotransmitter of the brain and is a major correlate of the processes that contribute to long-term potentiation (LTP) which are the first phases of memory consolidation (Bashir et al., 1993). The peak power density within the gamma range over the left parahippocampal region also suggested that some residual of two receptor subtypes remained with affinities in the nanoMolar and milliMolar range. The increase in power within the gamma range after the applications of

these two concentrations was between 0.3 and 0.5 $\mu V^2 \cdot Hz^{-1}$ which is within the range of shifts in cerebral cortical activity that we have measured to be associated with consciousness and specific tasks (Persinger & Saroka, 2015; Saroka, Vares, & Persinger, 2016). The laterality of the effect was clearly indicated. In contrast the right parahippocampal region displayed power increases that were primarily evident across the gross band of activity; this occurred for the milliMolar range. That the effects were dynamic and not passive was indicated by the transience of the peak response (Figure 37) and the gradual "habituation" or diminishment with repeated trials (Figure 38).

Glutamate has been shown to induce biophotonic activities (Tang & Dai, 2014) in neural circuits. Several authors have suggested that biophoton patterns may be central to neural information processing and decoding that may depend upon quantum brain mechanisms (Baars & Edelman, 2012; Persinger, Dotta, & Saroka, 2013; Tegmark, 2000). The left parahippocampal gyrus responded significantly to surface applications of 100 nM of glutamate solutions by increasing the power spectra within the 20 to 30 Hz range by about 1.5 $\mu V^2 \cdot Hz^{-1}$ compared to the previous baseline conditions while in the darkened environment. This was not observed for the right equivalent region. There were also moderately strong correlations between the numbers of photons emitted after the injection (but not before) and the power density for 30 to 40 Hz, the gamma range but not for other PD frequency bands.

The mean numbers of photons per s was equivalent to a photon flux density of about 10^{-12} $W \cdot m^{-2}$ which is the same order of magnitude as those generated in rat hippocampal slices when coupled to theta activity (Kovayashi et al., 1999). This flux density is the same order of magnitude that was measured from the right hemispheres

(at the level of the temporal lobe) when people sitting in very dark rooms engaged in vivid imagination about white light compared to mundane thoughts (Dotta, Saroka, & Persinger, 2012). Finally, the presence of a temporal discrepancy between the left and right temporal lobes for the spectral flux density of photon emissions while human beings sat with their eyes closed in a dark room has been measured for this magnitude (Dotta & Persinger, 2011). In other words, by simply applying glutamate at concentrations typically encountered within living brain tissue photons were emitted from human tissue that had been fixed in EFA for decades. The flux densities were comparable to that associated with specific cognitions generated by the living brain.

The physical bases to "consciousness" and cognition with the implication of a more ubiquitous property that may occur throughout the universe would be consistent with the philosophy of Spinzoa (Grene, 1978) and the concept of Ernst Mach (1919) that the behaviour of any part of the universe ("cosmos") is determined by all of its parts. Similar, more recent approaches have been expanded and quantified by Hameroff and Penrose (2014) and Persinger and St-Pierre (2015). We have operated upon the assumption that either gravity or electromagnetism – or both as these are not mutually exclusive – represent physical candidates which could satisfy these parameters. Our approach has favoured the photon (Persinger & St-Pierre, 2015) and therefore electromagnetism. The photon may be the fundamental process that relates complex phenomena over large distances of space and time and would be unimpeded by restrictions of speed assuming non-local photon-photon interactions. If this were valid, then an integrating factor must be present such as the commonality of the most dominant constituent, the hydrogen atom and the neutral hydrogen line of 1.42 GHz (Hummel, Dettmar, & Wielebinski, 1986). It

may be relevant (but also potentially spurious) that the average spectral power density produced by the application of glutamate (~$2 \cdot 10^{-12}$ $W \cdot m^{-2}$ or $kg \cdot s^{-3}$) divided by the change in microvoltage associated with that application (~$2 \cdot 10^{-6}$ V) results in 10^{-6} $A \cdot m^{-2}$. Applied across the area of the PMT aperture that would be the equivalent of 10^{-10} A associated with the application of the glutamate compared to water. When this current is divided by the unit charge value of 10^{-19} $A \cdot s$, the residual frequency is 10^{9} Hz or GHz which is well within the range of the neutral hydrogen line. In the absence of a strong hypothetical mechanism which explains how long-deceased biological material could systematically emit photons, this convergence of numbers should be further considered even if with caution.

Systematic injections of different concentrations of two “psychotropic” compounds, nicotine and ketamine, also showed natural, living brain-like responses in terms of both latency and concentration. Again there were anisotropic hemispheric responses within the regions of interest. Enhanced theta power associated with nicotine would be consistent with the memory-enhancing capacity of this cholinergic-stimulating compound (Huerta & Lisman, 1995). It may be relevant that nicotinamide adenine dinucleotide (NAD), which contains the molecular structure nicotinic acid, is a major source of electrons in living biochemical systems. The purine component of that molecule is synthesized from glutamate, aspartate and glycine. Tryptophan is the precursor of the nicotinamide moiety of NAD and NADP and contributes to the creation of nicotinic acid. From this perspective the similarity of the theta-band enhancement for the right hippocampal regions for both serotonin and nicotine would be expected. These patterns suggest the possibility that a residual of the intrinsic signatures that reflected the complex

biochemical reactions within brain tissue may still be present in fixed post-mortem tissue and might be “reactivated”. That the same sites and frequencies were either enhanced by glutamate or suppressed by ketamine at realistic physiological dosages would support this possibility.

Whereas electrophysiological studies are regularly conducted with still-living tissue explants, there are a few notable methodological differences between the aforementioned and what we have presented. First, tissue preparations, whether measured by single electrodes or multi-electrode arrays, are usually no thicker than 1 mm where slices of ~400 µm are typical (Oka, Shimono, Ogawa, Sugihara, & Takenati, 1999). Second, measurements of tissue preparations such as those of hippocampal slices are typically conducted within 24 hours of decapitation and within a nutrient-rich medium which is supplemented in various ways to inhibit rapid tissue deterioration (Egert et al., 1998; Oka, Shimono, Ogawa, Sugihara, & Takenati, 1999). During this period, and despite mitigation efforts, a significant proportion of the cells usually die as inferred by staining procedures (Egert et al., 1998). The tissue explants are normally maintained at physiological temperature and immobilized to reduce mechanically-induced damage. Our specimens are chemically fixed, much thicker (> 1cm), older, maintained at room temperature, and not supplemented in any way. It is therefore curious that in both cases, fluctuations in electric potential differences can be observed. Multi-electrode array recordings of tissue explants are known to register spike values of up to 600 µV, though the typical range of fluctuations are within 10 – 100 µV (Oka, Shimono, Ogawa, Sugihara, & Takenati, 1999). Our measurements of post-mortem, fixed tissue have revealed typical fluctuations within

1 – 80 μV with some high-magnitude transients (Rouleau & Persinger, 2016). In this respect, our measurements are consistent with those observed by others.

Finally, the persistence of essential microstructure was evident by the remaining signal complexity and frequency discrimination that was still apparent within the transverse temporal gyrus. A remarkable frequency dependence for maximum responsivity according to our measures occurred at the lower boundary of the threshold for hearing in the human brain. Compared to baseline measurements, the largest discrepancy occurred around 20 Hz. As recently reviewed by Persinger (2014) this is the classic transition between infrasound and regular sound discernment by the human brain. What is less known is that human auditory system does respond to < 20 Hz sound (mechanical vibrations). However, these regions of the system are less expansive and have few afferents to regions of the cortices involved with awareness. This structural substrate appears to remain after death in appropriately fixed brains.

Merker (2013) presented an argument that gamma synchrony, rather than representing a cognitively-significant correlate, is more likely an indicator of generic infrastructural control at the level of the tissue. That is, the cognitive correlate of cortical gamma synchrony is really just a necessary co-occurrence rather than a central operator of cognitive states. If one assumes that the brain is “dead” and therefore categorically can’t be conscious, Merker’s (2013) interpretation could hold true as we’ve observed a degree of gamma activations which could be indicative of synchrony. However, as self-report methods which require sensory inputs and motor outputs are unavailable to the post-mortem specimens, consciousness and cognitive states cannot be measured without inference by electroencephalography. Therefore, the assumption of an absence

of consciousness would be based upon an absence of evidence. From this perspective, if Merker's interpretation is incorrect and gamma synchrony is in fact cognitively-significant beyond mere activation, the post-mortem brain which displays subtle cortical oscillations, particularly within the theta and gamma bands as demonstrated here, could express some capacity for cognitive activation.

References

Accardo, A., Affinito, M., Carrozzi, M., & Bouquet, F. (1997). Use of the fractal dimension for the analysis of electroencephalographic time series. Biological cybernetics, 77(5): 339-350.

Baars, B.J. & Edelman, D.B. (2012). Consciousness, biology and quantum hypotheses. Phys Life Rev. 9(3), 285-294.

Bashir, Z.I., Bortolotto, Z.A., Davies, C.H., Berretta, N., Irving, A.J., Seal, A.J. et al. (1993). Induction of LTP in the hippocampus needs synaptic activation of glutamate metabotropic receptors. Nature. 363: 347-350.

Bear, M.F. (1996). A synaptic basis for memory storage in the cerebral cortex. Proc Nat Acad Sci. 93(24): 13453-13459.

Belluscio, M.A., Mizuseki, K., Schmidt, R., Kempter, R., & Buzsáki, G. (2012). Cross-frequency phase–phase coupling between theta and gamma oscillations in the hippocampus. J Neuro. 32(2): 423-435.

Carhart-Harris, R.L., Muthukumaraswamy, S., Roseman, L., Kaelen, M., Droog, W., Murphy, K. et al. (2016). Neural correlates of the LSD experience revealed by multimodal neuroimaging. Proc Nat Ac Sci. 113(17): 4853-4858.

Costa, J., Rouleau, N., & Persinger, M.A. (2016). Differential spontaneous photon emissions from cerebral hemispheres of fixed human brains: Asymmetric coupling to geomagnetic activity and potentials for examining post-mortem intrinsic photon information. Neuro Med. 7(2): 49-59.

Da Costa, S., van der Zwaag, W., Marques, J.P., Frackowiak, R.S., Clarke, S., & Saenz, M. (2011). Human primary auditory cortex follows the shape of Heschl's gyrus. J Neurosci. 31(40): 14067-14075.

Dotta, B.T., & Persinger, M.A. (2011). Increased photon emissions from the right but not the left hemisphere while imagining white light in the dark: The potential connection between consciousness and cerebral light. J Con Exp Res. 2(10): 1463-1473.

Dotta, B.T., Saroka, K.S., & Persinger, M.A. (2012). Increased photon emission from the head while imagining light in the dark is correlated with changes in electroencephalographic power: Support for Bókkon's Biophoton Hypothesis. Neuro Let. 513(2): 151-154.

Egert, U., Schlosshauer, B., Fennrich, S., Nisch, W., Fejtl, M., Knott, T., ... & Hämmerle, H. (1998). A novel organotypic long-term culture of the rat hippocampus on substrate-integrated multielectrode arrays. Brain Research Protocols. (4): 229-242.

Fox, C.H., Johnson, F.B., Whiting, J., & Roller, P.P. (1985). Formaldehyde fixation. J Histochem Cytochem. 33(8): 845-853.

Gloor, P. (1997). The temporal lobe and limbic system. Oxford University Press, USA.

Grene, M.G. (1978). Spinoza: a collection of critical essays.

Harrison, P.T.C. (1984). An ethanol-acetic acid-formol saline fixative for routine use with special application to the fixation of non-perfused rat lung. Laboratory Animals. 18(4): 325-331.

Hameroff, S. & Penrose, R. (2014). Consciousness in the universe: A review of the 'Orch OR'theory. Phys Life Rev. 11(1), 39-78.

Hasenstaub, A., Shu, Y., Haider, B., Kraushaar, U., Duque, A., & McCormick, D.A. (2005). Inhibitory postsynaptic potentials carry synchronized frequency information in active cortical networks. Neuron. 47(3): 423-435.

Hopwood, D. (1972). Theoretical and practical aspects of glutaraldehyde fixation. Histochem J. 4(4): 267-303.

Huerta, P.T. & Lisman, J.E. (1995). Bidirectional synaptic plasticity induced by a single burst during cholinergic theta oscillation in CA1 in vitro. Neuron. 15(5): 1053-1063.

Hummel, E., Dettmar, R.J., & Wielebinski, R. (1986). Neutral hydrogen and radio continuum observations of NGC 55. Astron Astrophys. 166: 97-106.

Jensen, J.V. (1988). Return to the Wilberforce–Huxley Debate. The British Journal for the History of Science. 21(02): 161-179.

Kiernan, J.A. (2000). Formaldehyde, formalin, paraformaldehyde and glutaraldehyde: what they are and what they do. Microscopy Today. 1(5): 8-12.

Kobayashi, M., Takeda, M., Sato, T., Yamazaki, Y., Kaneko, K., Ito, K. et al. (1999). In vivo imaging of spontaneous ultraweak photon emission from a rat's brain correlated with cerebral energy metabolism and oxidative stress. Neuro Res. 34(2): 103-113.

Mach, E. (1919). The Science of Mechanics; a Critical and Historical Account of Its Development, by Dr. Ernst Mach. Tr. from the German by Thomas J. McCormack. With 250 Cuts and Illustrations. Chicago, The Open court publishing Company.

Merker, B. (2013). Cortical gamma oscillations: the functional key is activation, not cognition. Neuroscience & Biobehavioral Reviews. 37(3): 401-417.

Newcomer, J.W., Farber, N.B., Jevtovic-Todorovic, V., Selke, G., Melson, A.K., Hershey, T. et al. (1999). Ketamine-induced NMDA receptor hypofunction as a model of memory impairment and psychosis. Neuropsychopharmacology. 20(2): 106-118.

Oka, H., Shimono, K., Ogawa, R., Sugihara, H., & Taketani, M. (1999). A new planar multielectrode array for extracellular recording: application to hippocampal acute slice. Journal of neuroscience methods. 93(1): 61-67.

Pazos, A., Gonzalez, A.M., Waeber, C., & Palacios, J.M. (1991). Multiple Serotonin Receptors in the Human Brain. In Receptors in the human nervous system. Mendelsohn, F. A., & Paxinos, G. (Eds.). Academic Press, Inc. 74-95.

Persinger, M.A. (1979). Brain mast cell numbers in the albino rat: sources of variability. Behav Neur Bio. 25(3): 380-386.

Persinger, M.A. (2014). Infrasound, human health, and adaptation: an integrative overview of recondite hazards in a complex environment. Natural Hazards. 70(1): 501-525.

Persinger, M.A., Dotta, B.T., & Saroka, K.S. (2013). Bright light transmits through the brain: Measurement of photon emissions and frequency-dependent modulation of spectral electroencephalographic power. World Journal of Neuroscience. 3(1): 10-16.

Persinger, M.A. & Koren, S.A. (2007). A theory of neurophysics and quantum neuroscience: implications for brain function and the limits of consciousness. Int J of Neur. 117(2): 157-175.

Persinger M.A. & Saroka K.S. (2015). Human quantitative electroencephalographic and Schumann Resonance exhibit real time coherence of spectral densities: implications for interactive information processing. J Sig Inf Pro. 6: 153-164.

Persinger, M.A., Saroka, K.S., Koren, S.A., & St-Pierre, L.S. (2010). The electromagnetic induction of mystical and altered states within the laboratory. J Con Exp Res. 1(7): 808-830.

Persinger, M.A. & St-Pierre, L.S. (2015). The physical bases to consciousness: Implications of convergent quantifications. J. Sys. Integrat. Neurosci. 1: 55-64.

Quilichini, P, Sirota, A, & Buzsáki, G. (2010). Intrinsic circuit organization and theta–gamma oscillation dynamics in the entorhinal cortex of the rat. J of Neuro. 30(33): 11128-11142.

Rivier, F. & Clarke, S. (1997). Cytochrome oxidase, acetylcholinesterase, and NADPH-diaphorase staining in human supratemporal and insular cortex: evidence for multiple auditory areas. Neuroimage. 6(4): 288-304.

Rouleau, N & Persinger, MA. (2016). Differential responsiveness of the right parahippocampal region to electrical stimulation in fixed human brains: Implications for historical surgical stimulation studies?. Epi & Behav. 60:181-186.

Saroka, K.S., Caswell, J.M., Lapointe, A., & Persinger, M.A. (2014). Greater electroencephalographic coherence between left and right temporal lobe structures during increased geomagnetic activity. Neuro Let. 560: 126-130.

Saroka, K.S., Vares, D.E., & Persinger, M.A. (2016). Similar Spectral Power Densities Within the Schumann Resonance and a Large Population of Quantitative Electroencephalographic Profiles: Supportive Evidence for Koenig and Pobachenko. PloS one. 11(1): 1-22.

Scoville, W.B., & Milner, B. (1957). Loss of recent memory after bilateral hippocampal lesions. J Neuro Neurosurg Psych. 20(1): 11-21.

Serafetinides, E.A. (1965). The significance of the temporal lobes and of hemispheric dominance in the production of the LSD-25 symptomatology in man: a study of epileptic patients before and after temporal lobectomy. Neuropsychologia. 3(1): 69-79.

Sirota, A., Montgomery, S., Fujisawa, S., Isomura, Y., Zugaro, M., & Buzsáki, G. (2008). Entrainment of neocortical neurons and gamma oscillations by the hippocampal theta rhythm. Neuron. 60(4): 683-697.

Tagliazucchi, E., Roseman, L., Kaelen, M., Orban, C., Muthukumaraswamy, S.D., Murphy, K. et al. (2016). Increased global functional connectivity correlates with LSD-Induced ego dissolution. Cur Bio. 26(8): 1043-1050.

Tang, R. & Dai, J. (2014). Biophoton signal transmission and processing in the brain. J Photochem Photobio B: Bio. 39: 71-75.

Tegmark, M. (2000). Importance of quantum decoherence in brain processes. Phys Rev E. Apr 61(4): 4194-4206.

Wijdicks, E.F. (2002). Brain death worldwide Accepted fact but no global consensus in diagnostic criteria. Neurology. 58(1): 20-25.

Wijdicks, E.F. (2010). The case against confirmatory tests for determining brain death in adults. Neurology. 75(1): 77-83.

Zola-Morgan, S., Squire, L.R., & Amaral, D.G. (1986). Human amnesia and the medial temporal region: enduring memory impairment following a bilateral lesion limited to field CA1 of the hippocampus. J Neuro. 6(10): 2950-2967.

Chapter Transition: In Search of a Mechanism

The previous chapter highlighted the potential contribution of conventional ligand-receptor processes to periodic microvolt fluctuations within fixed, post-mortem tissues. We suspected that although receptors might be mediating some of the effects observed, the most likely explanation was that a tissue-level interaction involving gradients of charged particles potentially related to pH might be mediating the response. The following chapter explores this hypothesis. A series of experiments were conducted in order to quantify several key phenomena. First, we queried historical rat brain data in order to observe trends in expressed power as a function of region and when the tissue was originally fixed with respect to the present day. Next, we sought to determine the time-course of microvolt fluctuations throughout the fixation process and how it might be related to intrinsic pH changes associated with the immersion medium. Then we explored the role of pH and several physiological ions by immersing tissue specimens within artificial cerebral spinal fluid and allowing for both long-term and short-term perfusion. Together, the results indicate that pH and expressed power within the tissue are systematically related. These are both intrinsically related to time – a feature which we hypothesize is due to chemical reactions which are specified within the chapter. The results also indicate that certain physiological ions elicited responses preferentially over others by systematically isolating components of the artificial cerebral spinal fluid medium. Our data point to charged molecules and fixation phenomena interacting with the tissue as the primary sources of variance associated with many of our previous results.

Chapter 8:

Right Cerebral Hemispheric Sensitivity to pH and Physiological Ions in Fixed Post-Mortem Wistar Rat Brains

(Original Research)

Published in Cognitive Neurodynamics, Vol. 11

Nicolas Rouleau, Nirosha J. Murugan,

& Michael A. Persinger

DOI: 10.1007/s11571-017-9443-3

Abstract

Post-mortem human neural tissues fixed in ethanol and aldehyde-based solutions express modulated frequency-dependent microvolt potentials when probed by chemical and electrical stimuli. These observations run contrary to the assumption that basic tissue functions are irreversibly impaired upon fixation, in the absence of nutrients and sufficient concentrations of physiological ions. The aim of the current study was to investigate the relative effects of pH and specific charged particles relevant to normal cell physiology upon electric potentials associated with fixed post-mortem rat brain tissue. We identified a positive relationship between the time the brains had been immersed in ethanol-formalin-acetic acid and high-frequency microvolt potentials within the dorsal right hemisphere of the rat cerebrum. Measuring the pH of the fixative solution surrounding the brains indicated that as time increased, a logarithmic trend toward alkalinity could be observed. Further experiments revealed that high-frequency microvolt potentials were related to pH changes within the right hemisphere only. The right ventral cerebrum displayed a unique response to potassium chloride in ways uncounted for by pH alone. The results suggest that the fixed post-mortem right cerebrum of the rat is particularly sensitive to pH and physiological ions which explains a subset of previous findings with respect to stimulus-response patterns in human coronal brain sections. A concluding hypothesis is presented which suggests that brain tissue expresses material properties independent of metabolic activity though perhaps relevant to living brain function.

Introduction

Various methods have been developed which allow researchers to extract live tissues from organisms so as to observe their functions within controlled settings. Organotypic slice cultures represent one such *in vitro* method by which cellular and molecular investigations can be undertaken to further understand the mechanisms underlying the function of neural tissue (Noraberg et al., 2005). As experiments are typically performed shortly after the animal is sacrificed (Opitz-Araya and Barria, 2011), the method can be considered near *in vivo*, where proportions of cells continue to live by means of nutrient supplementation (Humpel, 2015). Without sufficient nutrients or the presence of physiological ions which are integral to the maintenance of membrane potential differences, the explant withers until normal function is lost entirely upon death. Assuming optimal conditions, cell survival in slice preparations is temporary where the typical culture period can last from hours to a few months (Egert et al., 1998; Humpel, 2015; Ostergaard et al., 1990).

If the specimens are treated with ethanol or an aldehyde-based fixative solutions, the structure of the tissue explant can remain intact for years – presumably at the cost of function. It is assumed that cell and tissue functions are irreversibly impaired upon fixation – stripped of their capacity to process electrochemical signals. Therefore applied stimuli would not be expected to elicit physiologically relevant responses post-fixation. If, however, some residual response capacity could be detected within fixed neural tissue by means of chemical and electric probes, the assumption of lost function would be subject to re-examination. Such observations would, in all likelihood, violate the basic principles governing normal cell physiology. Alternatively, the detection of stimulus-

response patterns in post-mortem tissue would represent a novel observation, separate and distinct from those observed in living organisms and their tissues. Rather than a violation of established principles, the phenomenon could represent a general property of brain tissue in the absence of metabolic function.

Several experiments have recently demonstrated that chemically fixed post-mortem human and rat brains exhibit regional, frequency-dependent electric potential differences which vary systematically in response to applied stimuli. Coronal sections of human brain tissue were selectively responsive to electrical (Rouleau and Persinger, 2016a) and chemical (Rouleau, Murugan, Tessaro, Costa, and Persinger, 2016) stimuli with evidence of dose-dependence and habituation. Most notably, opposing deviations of high-frequency spectral power were noted for applications of glutamate and ketamine – ligands which act upon the NMDA receptor as an agonist and antagonist respectively (Rouleau, Murugan, Tessaro, Costa, and Persinger, 2016). Stimulus-response patterns were observed in addition to baseline low-frequency spectral power cerebral hemispheric asymmetries (Rouleau, Lehman, and Persinger, 2016). In combination with the observation that proportions of theta spectral power (4 Hz – 7.5 Hz) differentiated between rat brains which were, several years earlier, experimentally induced to seize by a single system injection of lithium-pilocarpine and controls (Rouleau, Reive, and Persinger, 2016), it was clear that a mechanism underlying post-mortem brain tissue responses should be pursued. Whereas the physical-chemical environment imposed upon the tissue by the fixative solution should have, in principle, inhibited any capacity for the tissue to respond to applied stimuli, the evidence ran contrary to this assumption.

Rather, brains fixed in ethanol-formalin-acetic acid reliably demonstrated non-random, living-like signal processing capacities.

Our current approach was to investigate the fixation process with respect to changes of electric potential differences within the neural tissues in addition to the relative contribution of pH and physiological ions to regional spectral power differences across the neural axis. In search of a mechanism, we systematically investigated how pH changes over time were related to spectral power derived from microvolt fluctuations within the tissues. Further, we re-hydrated fixed tissues to determine whether or not morphologically preserved brains could be induced to express changes in electric potential differences within select regions when exposed to physiological ions typical of the neural environment.

Methods

Brain Specimens

Forty-eight (n=48) brains were extracted from Wistar (albino) rats and placed within solutions of ethanol-formalin-acetic acid (72% ethanol, C_2H_6O; 18% distilled water, dH_2O; 5% acetic acid, $C_2H_4O_2$; 5% formaldehyde, CH_2O, pH = 2.9) post-excision. Of the forty-eight, thirty-six (n=36) were examined previously by Rouleau, Reive, and Persinger (2016), where it was determined that lithium-pilocarpine seized rats (n=13) expressed reduced brain mass and proportional decreases of 4 Hz – 7.5 Hz spectral power as inferred by microvolt fluctuations obtained within the tissue relative to non-seized rats (n=23). Though sexually dimorphic brain masses were noted, male-female differences could not be identified when examining microvolt fluctuations within the tissue, indicating

that simple differences of mass or diffuse, sexually dimorphic nuclei were not driving the observed effects. Rather, regional pathologies were identified as the proximal cause of theta differences (Rouleau, Reive, and Persinger, 2016). Eleven (n=11) additional brains were utilized which were originally collected during neurobiology laboratory demonstrations associated with the Behavioural Neuroscience Program at Laurentian University between 1996 and 2008. A final brain (n=1) was harvested as a longitudinal case in order to experimentally validate observations which indicated temporal effects associated with the fixation process. Brains were stored in a darkened environment and remained undisturbed, some for over 20 years in solution.

Artificial Cerebrospinal Fluid

Tissues were subjected to a re-hydration protocol with supplemented physiological ions. The brains were immersed within different formulations of artificial cerebrospinal fluid (CSF) which are outlined in Table 1. The standard formula (134 Mm NaCl, 26 mM $NaHCO_3$, 10 mM D-Glucose, 2.5 mM KCl, 2 mM $CaCl_2$, 1.3 mM $MgCl_2$, 1.25 mM K_2HPO_4), which will be referred to as CSF 1, was experimentally manipulated by excluding compounds from the mixture in order to investigate the relative contribution of each component to any effects observed during tissue re-hydration. Alternative formulae which deviated from the standard CSF 1 solution were labelled CSF 2 – CSF 6 for brevity (Table 6). All solutions were gassed with 5% CO_2, 95% O_2 for 20 minutes before they were stored at 4 °C.

Table 6. Artificial Cerebrospinal Fluid (CSF) Condition Formulae

Cerebrospinal Fluid (CSF) Condition	Formula	
	Included	Excluded
CSF 1	134 Mm NaCl, 26 mM $NaHCO_3$, 10 mM D-Glucose, 2.5 mM KCl, 2 mM $CaCl_2$, 1.3 mM $MgCl_2$, 1.25 mM K_2HPO_4	
CSF 2	26 mM $NaHCO_3$, 10 mM D-Glucose, 2.5 mM KCl, 2 mM $CaCl_2$, 1.3 mM $MgCl_2$, 1.25 mM K_2HPO_4	134 Mm NaCl
CSF 3	134 Mm NaCl, 26 mM $NaHCO_3$, 10 mM D-Glucose, 2.5 mM KCl, 1.3 mM $MgCl_2$, 1.25 mM K_2HPO_4	2 mM $CaCl_2$
CSF 4	134 Mm NaCl, 26 mM $NaHCO_3$, 10 mM D-Glucose, 2.5, 2 mM $CaCl_2$, 1.3 mM $MgCl_2$, 1.25 mM K_2HPO_4	2.5 mM KCl
CSF 5	134 Mm NaCl, 10 mM D-Glucose, 2.5 mM KCl, 2 mM $CaCl_2$, 1.3 mM $MgCl_2$, 1.25 mM K_2HPO_4	26 mM $NaHCO_3$
CSF 6	10 mM D-Glucose, 1.3 mM $MgCl_2$, 1.25 mM K_2HPO_4	134 Mm NaCl, 26 mM $NaHCO_3$, 2.5 mM KCl, 2 mM $CaCl_2$,

Electric Potential Measurements

The brains were probed by needle electrodes inserted strategically into regions along the neural axis as was first attempted by Rouleau, Reive, and Persinger (2016). Recently, similar methods were applied to human brain sections (Rouleau & Persinger, 2016a; Rouleau, Murugan, Tessaro, Costa, and Persinger, 2016). Four needle electrodes were inserted into the spinal cord and caudal medulla, spatially in parallel (Figure 48B and 48C). These sensors constituted the electrical reference point for electric potential (μV) measurements. A fifth electrode, which served as the primary probe from which electric potentials were obtained, was inserted 6.6 mm into the dorsal or ventral

components of the left and right cerebral hemispheres. When inserted dorsally, the probe was positioned at equidistance between the rostral and caudal poles of the cerebrum as well as between the interhemispheric fissure and the lateral convexity of the hemisphere. When inserted ventrally, the probe was positioned at the caudal pole, inferior to the rhinal fissure, and just anterior to the cerebellum. The four resulting quadrants of measurement (i.e. left dorsal, left ventral, right dorsal, and right ventral) were observed for all brains over the course of the study.

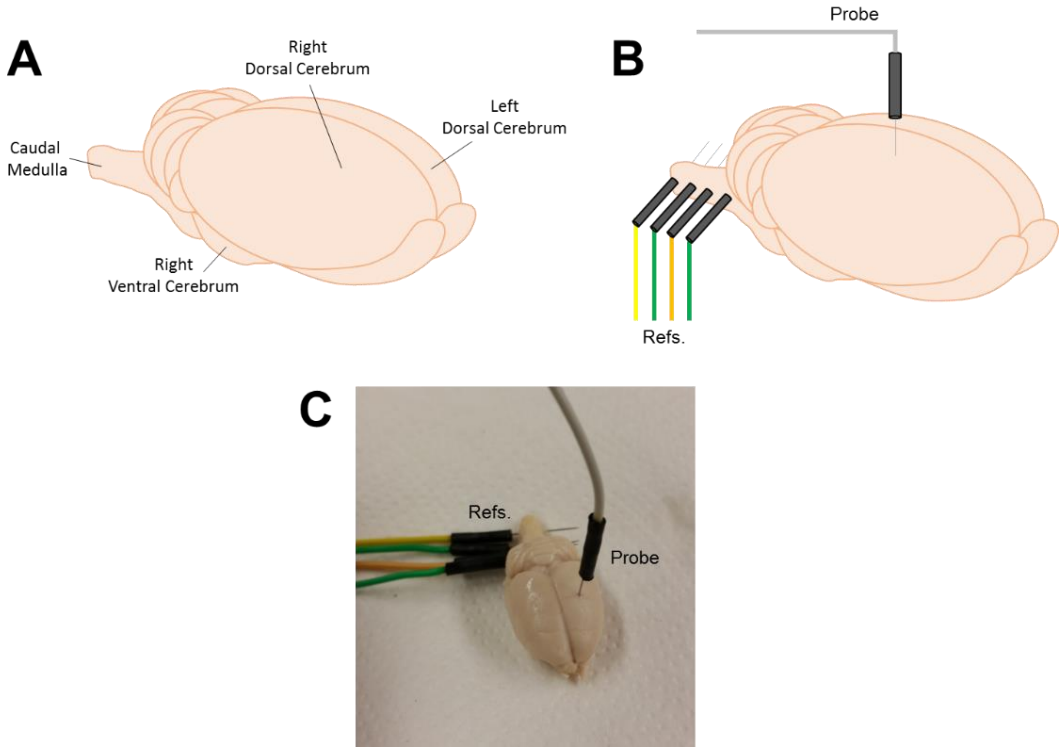

Figure 48. Rat brains (A) were probed (B and C) by needle electrodes inserted into the left and right dorsal and ventral cerebrum referenced to the caudal medulla and spinal cord.

Data (microvolt potentials) were collected using a Mitsar 201 quantitative electroencephalography (QEEG) amplifier which streamed live data to a laptop computer

(HP Envy) running WinEEG version 2.93.59 (07.2013) software with a Windows 8 operating system. The sampling rate of the device was 250Hz. A low-cut filter of 1.6 Hz and a high-cut filter of 50 Hz were applied while recording. An additional notch filter was toggled to eliminate frequency contributions between 50 Hz and 70 Hz as well as between 110 Hz and 130 Hz. The gain of the device was set to 150 µV. Raw microvolt potentials were converted to spectral power densities ($\mu V^2 \cdot Hz^{-1}$) within classical EEG bandwidths: delta (1.5 Hz – 4 Hz), theta (4 Hz − 7.5 Hz), alpha (7.5 Hz − 14 Hz), beta1 (14 Hz − 20 Hz), beta2 (20 Hz − 30 Hz), and gamma (30 Hz − 40 Hz).

pH Measurement

It was necessary to measure the pH of the fixative solution as well as other solutions which served as experimental manipulations of the tissues. A glass pH probe was inserted into volumes of solution while coupled to a DrDAQ board streaming live data to a ThinkPad laptop computer running Pico Technology (UK) software. The recording rate of the device was set to 1Hz with an intrinsic refresh rate of 50 ms. The device was calibrated using standard buffered solutions between 4.0 and 10.0 pH before use.

Data Analysis

Electrodynamic data were extracted within the WinEEG interface as spectral power densities within the aforementioned frequency bands. Averaged spectral power measures (e.g., alpha to gamma, beta 1 to gamma) were computed in order to observe generalized high-frequency modulations which were readily manipulated over the course of the experiments. Once extracted, data were imported to SPSS v20 and analyzed. Analyses are specified where results are presented though generally consisted of simple

measures of differences in addition to both parametric and non-parametric correlational analyses.

Results

Brains Fixed in EFA

Examining thirty-six (n=36) brains which could be identified as seized or non-seized animals based upon microvolt potentials and brain mass (Rouleau, Reive, and Persinger, 2016), a weak positive relationship was identified between an average of high-frequency (14 Hz – 40 Hz) spectral power densities and the number of days that the tissue had been immersed in EFA or, implicitly, time post-mortem, $r = .23$, $p<.005$, $rho = .20$, $p<.05$ (Figure 49). Isolating spectral power within the right dorsal quadrant from other probed regions increased the strength of the relationship, $r=.365$, $p<.05$, $rho=.40$, $p<.05$. This result suggested that cerebral quadrants were independently sensitive to unique factors. When comparing cerebral dorsal measurements for non-seized (n=23) and seized rats (n=13), no significant difference could be discerned ($z<1.96$, $p<.05$), though in both cases the strength of the association further increased ($r= 0.50 – 0.70$).

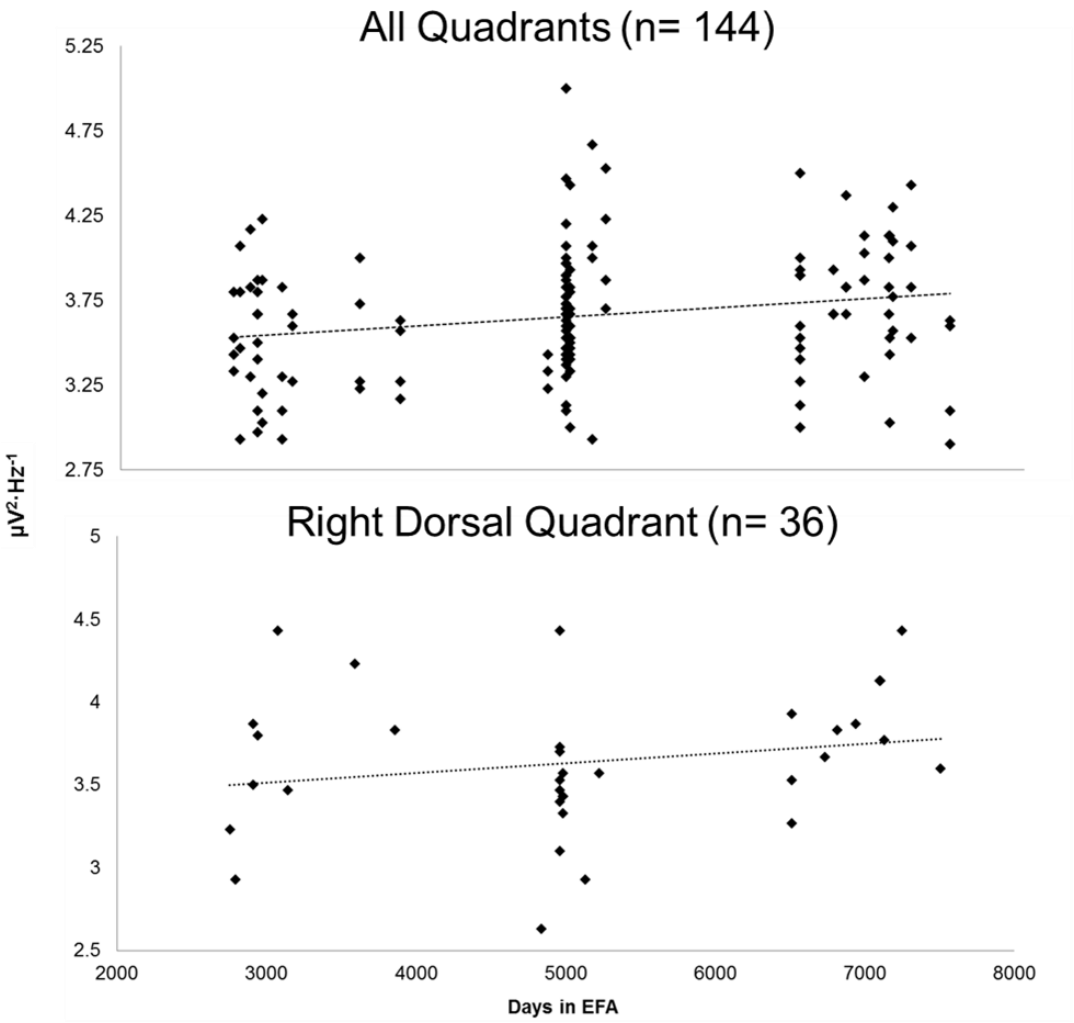

Figure 49. Averaged high-frequency (14 Hz – 40Hz) spectral power densities for all quadrants (top) and for right dorsal quadrant (bottom).

We then measured the pH of the fixative solution (EFA) within randomly selected containers holding rat brains from our collection extracted between 1996 and 2016. Brains were always immersed within EFA after the animal was sacrificed. Therefore all brains received the same post-mortem “treatment” of fixation with EFA. The data, presented in Figure 50, suggest that there was a logarithmic relationship between the pH of the fixative solution surrounding the rat brains and time. Over a relatively short period of time (12

days), the EFA (pH 2.9) became slightly more alkaline (pH 3.2). An inflection in the curve was noted around 3 years, which was followed by a weak linear relationship. At 7467 days post-mortem (20.5 years), the solution surrounding the tissue was associated with a pH of ~4.3. In other words, EFA surrounding brain tissue was associated with a relatively sharp trend toward neutral pH over the course of the 2 first months post-fixation followed by a relatively gradual trend subsequently which persisted over several years.

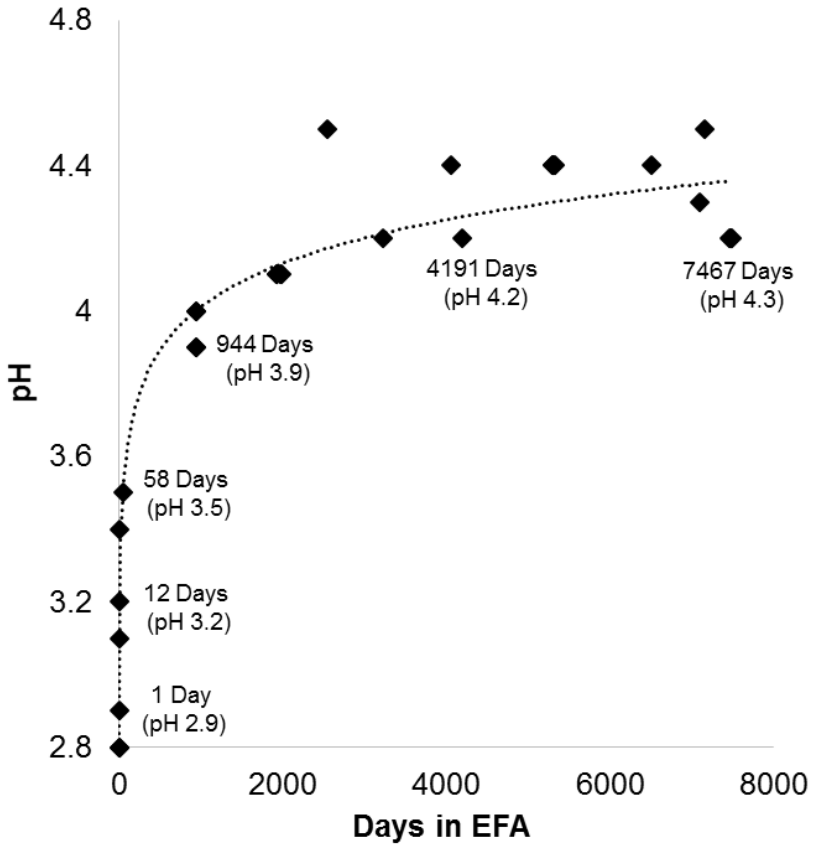

Figure 50. pH of EFA within containers surrounding rat brains as a function of time (days) that the brains were immersed in fixative solution and stored.

Our observations that pH and microvolt potentials were both related to time – though likely physical-chemical processes operating over time – suggested that

longitudinal observations of the same brain would reveal that, in fact, these factors could be observed to systematically change in concert with one another. To this end, we extracted the brain of an aged (1315 days old) male Wistar rat (n=1) on October 6th, 2016. The brain weighed (wet) 2.58 grams and was anatomically unremarkable at a gross structural level. It was subjected to immediate measurement (Fresh) of electric potential differences between cerebral hemispheric loci and the spinal cord, after which it was immersed within a 100 mL solution of EFA and stored at room temperature. Subsequent measurements were obtained at 30 minutes, 24 hours, 48 hours, 72 hours, and several other times 1-9 weeks post-fixation (Figure 51). The net result of the serial measurement protocol was a longitudinal case study of electric potential differences over the fixation period of the rat brain which could be compared to the greater (n=47) sample of electric potential measurements (Figure 49) and the pH phenomenon observed in Figure 50. Figure 51 demonstrates that high-frequency (14 Hz – 40 Hz) spectral power increased over the course of the 9 week period with a cumulative positive shift of 0.6 pH units. The average (smoothed, dashed line) trend over time expressed an amplitude peak between 3 and 6 weeks post-fixation.

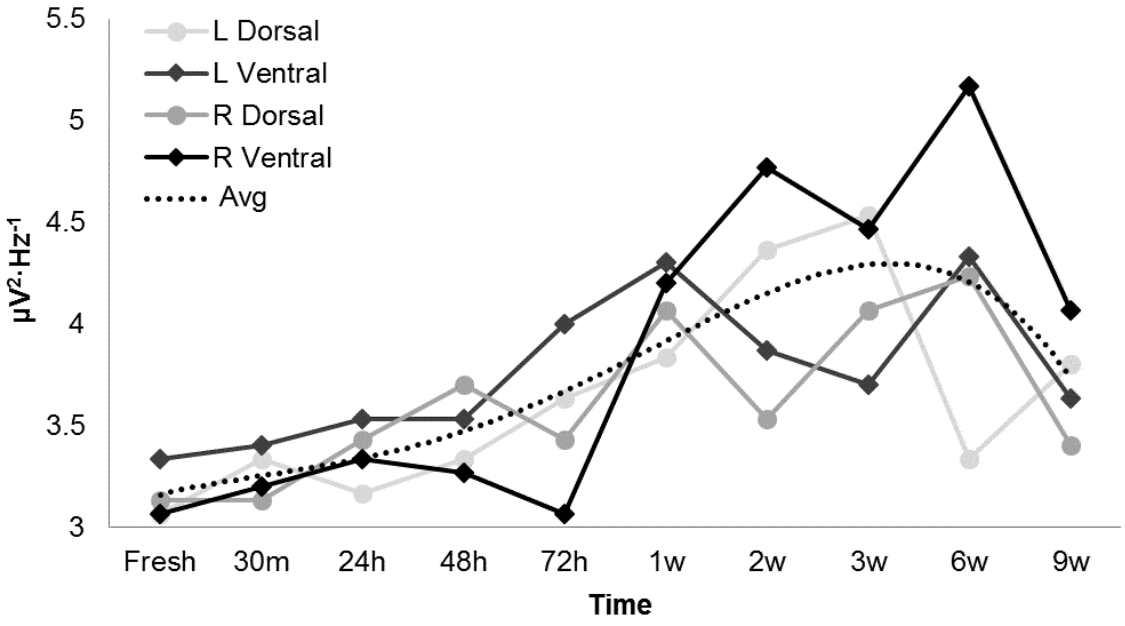

Figure 51. High-frequency (14Hz – 40Hz) spectral power densities within each cerebral quadrant for serial measurements of a rat brain undergoing fixation in EFA solution. A smoothed average is represented by the dashed line.

Re-hydrating Fixed Brains

Fixation is generally treated as a unidirectional phenomenon. That is, once the tissue is perfused by the fixative, the physiological mechanisms which were once present within the biological substrata are assumed to be irreversibly impaired. To evaluate this assumption, we re-hydrated rat brains using different formulations of artificial CSF (Table 6). Our original measurements indicated that global (1.5 Hz – 40 Hz) right hemispheric spectral power could be experimentally altered by consecutively (24 hour cycles) immersing the brains in EFA and CSF over a 5 day period (Figure 52A). Combined trials indicated that immersion within CSF 1 produced significantly different high-frequency (7.5 Hz – 30 Hz) spectral power excluding gamma frequencies (30 Hz – 40 Hz) over time,

$F(4,14)=4.56$, $p<.05$, $\eta^2=.65$ (Figure 52B). The major source of variance or most notable effect was a significant increase of 7.5 Hz – 30 Hz power within the right dorsal quadrant when the brains were re-introduced to the relatively acidic fixative solution (EFA) after 24 hours of CSF 1 immersion, $t(4)= 4.07$, $p<.05$, $r^2=.81$. The difference between power during the 24 hour CSF 1 immersion and baseline measures involving fixative solution (pre-EFA) was equivalent, $r^2=.80$. The most notable observation was that high-frequency spectral power returned to baseline levels as is observed when comparing the means of pre-EFA and post-EFA ($p>.05$). Based upon these observations, we conducted a series of counterbalanced between-subject experiments in order to investigate the potential relative contribution of components of CSF 1 to the re-hydration effect.

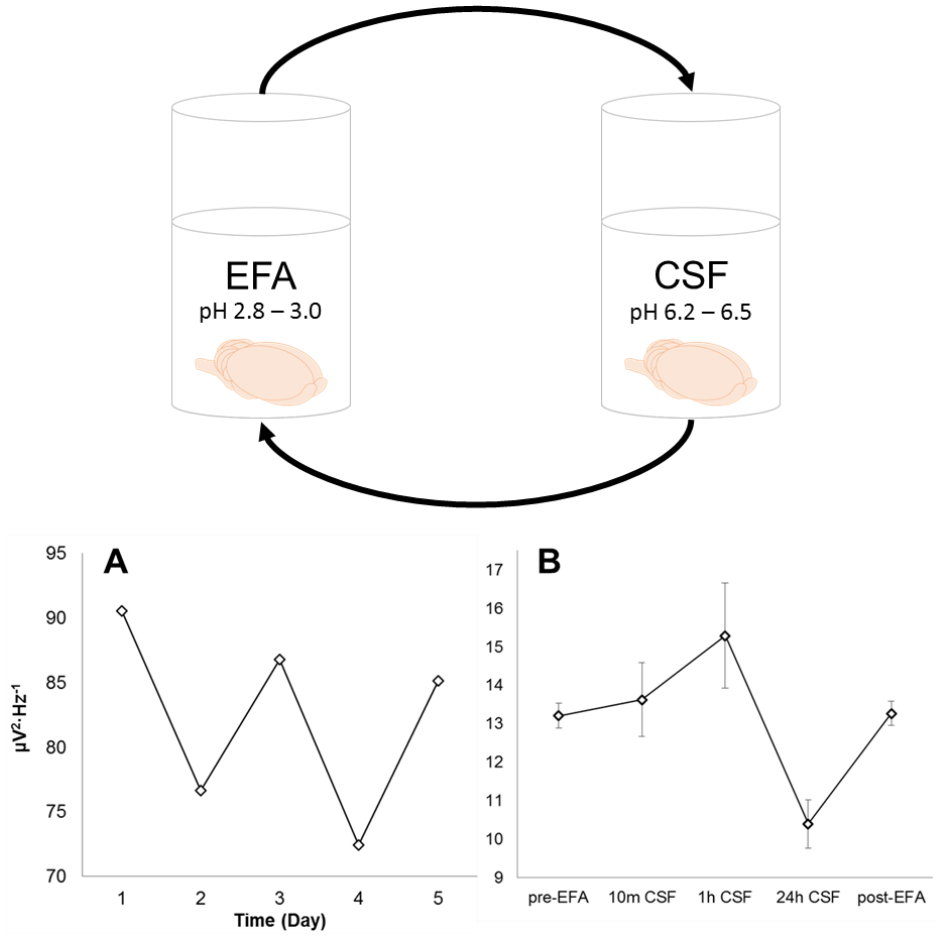

Figure 52. Global right hemispheric power of a single rat brain varied systematically when immersed for 24h within alternating EFA and CSF solutions over 5 consecutive days (A). Averaged high-frequency (7.5 Hz – 30 Hz) spectral power excluding gamma (30Hz – 40Hz) within the right dorsal quadrant of rat brains (n=3) measured serially over time indicates that power returns to baseline conditions once re-immersed in the fixative solution (B).

An analysis of variance (ANOVA) identified high-frequency spectral power differences between CSF formulations and control conditions (EFA, dH_2O) after 1 hour immersions within the right hemisphere only, $F(8,71)=2.10$, $p<.05$, $\eta^2=.21$ (Figure 53). Low-frequency power was unaffected ($p>.05$). The left hemisphere did not respond differentially to alternative formulations of CSF and control conditions ($p>.05$) as seen in Figure 54. It was subsequently identified that dH_2O was driving the right hemispheric effect, however, further investigation revealed that there was a significant positive relationship (Figure 53) between pH and beta 2 (20 Hz – 30 Hz) spectral power within the ventral ($r= .36$, $p<.005$, $rho = .39$, $p=.001$) right hemisphere which was not observed within the dorsal component of the same hemisphere ($r= .10$, $p>.05$, $rho= .12$, $p>.05$). Examining differences between expressed 7.5 Hz – 40 Hz power within the ventral and dorsal components of the right hemisphere, only CSF 1 (standard CSF, $r^2=.53$) and CSF 3 ($CaCl_2$ is removed, $r^2=.61$) produced reliable disparities ($p<.05$). The effects associated with CSF 2 (NaCl is removed) were ambiguous, $t(6)=2.31$, $p=.06$, demanding further investigation. These results suggested that $CaCl_2$ was not driving the dorsal-ventral differences produced by CSF 1 which were unobserved in the absence of physiological ions (EFA and dH_2O). However, we conducted further tests to experimentally

demonstrate the contribution of the physiological ions. Rather than removing components from the CSF 1 standard formula, we simply added $CaCl_2$, KCl, or NaCl (or a combination of these) to dH_2O and immersed the tissue for 1 hour before assessing microvolt potentials.

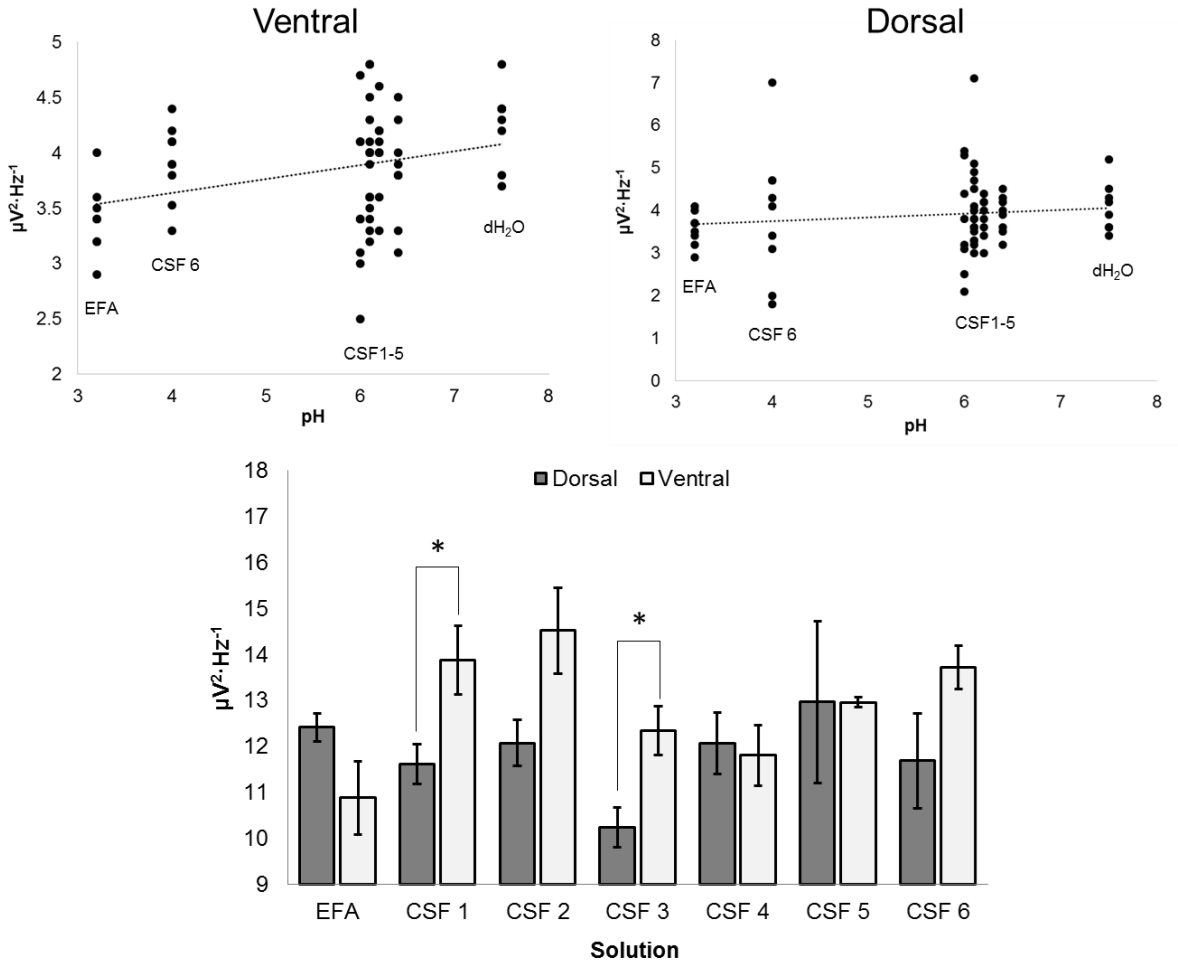

Figure 53. The relationship between right hemispheric ventral and dorsal beta 2 (20 Hz – 30Hz) spectral power and pH of the solution within which the tissue was immersed. Averaged wide-band high-frequency (7Hz – 40Hz) spectral power densities for dorsal and ventral measurements within the right hemisphere demonstrated significant differences

within the CSF 1 (no compound excluded) and CSF 3 ($CaCl_2$ excluded) conditions. Significant differences are indicated ($p<.05$).

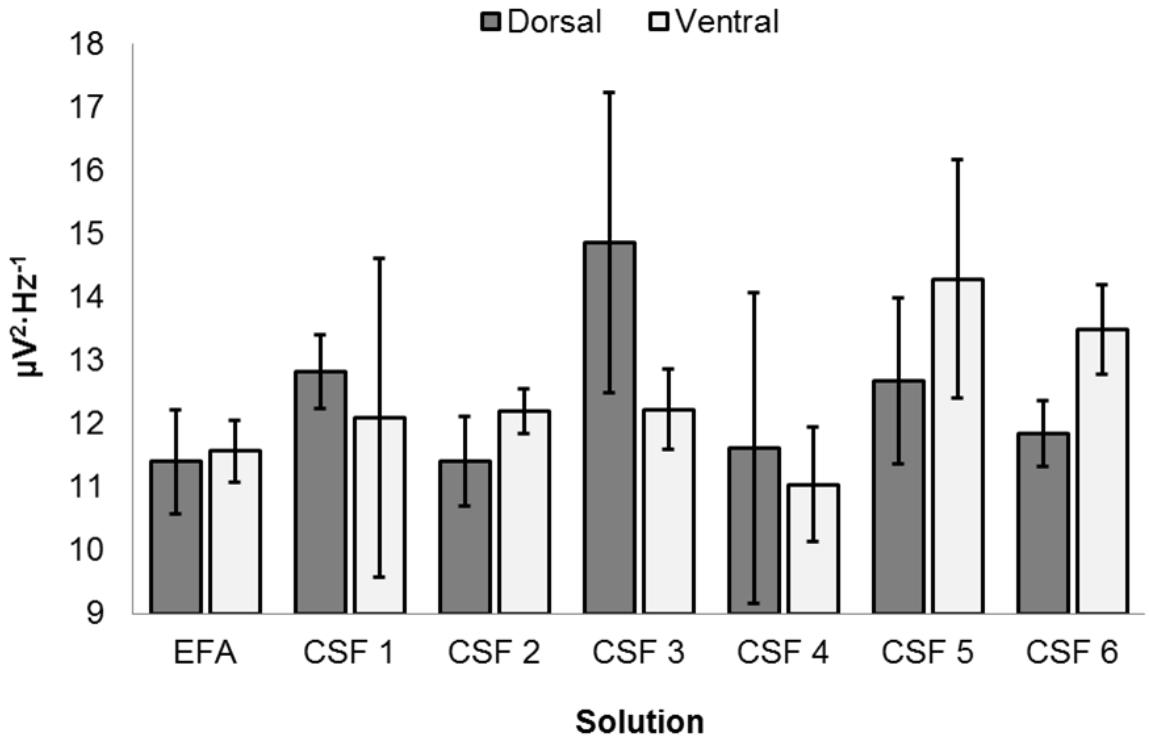

Figure 54. Averaged wide-band high-frequency (7.5 Hz – 40Hz) spectral power densities for dorsal and ventral measurements within the left hemisphere demonstrating no significant differences between any of the conditions ($p>.05$).

An ANOVA revealed that significant differences of beta 2 (20 Hz – 30 Hz) spectral power densities within the right hemisphere differed as a function of the solution within which the brains were immersed, $F(5, 75)= 4.86$, $p<.001$, $\eta^2=.26$ (Figure 55). Homogeneous subsets identified three groups which differed significantly: EFA, dH_2O, and all other conditions. However, when examining 7.5 Hz – 40 Hz spectral power differences between ventral and dorsal components of the left and right hemispheres, only right hemispheric effects could be discerned, $t(4)= 3.10$, $p<.05$, $r^2=.71$ (Figure 55A).

The major source of variance, which explained the results presented in Figure 53 and 55A, was a significant difference between dorsal and ventral components of the right hemisphere in brains exposed to KCl, $t(4)=3.62$, $p<.05$, $r^2=.77$. Whereas the removal of KCl (CSF 4) from the standard cerebrospinal fluid formula (CSF 1) abolished the effects in Figure 53, the addition of KCl to water produced dorso-ventral disparities within the right hemisphere. This confirmed our original suspicion that KCl was driving the CSF 1 effect.

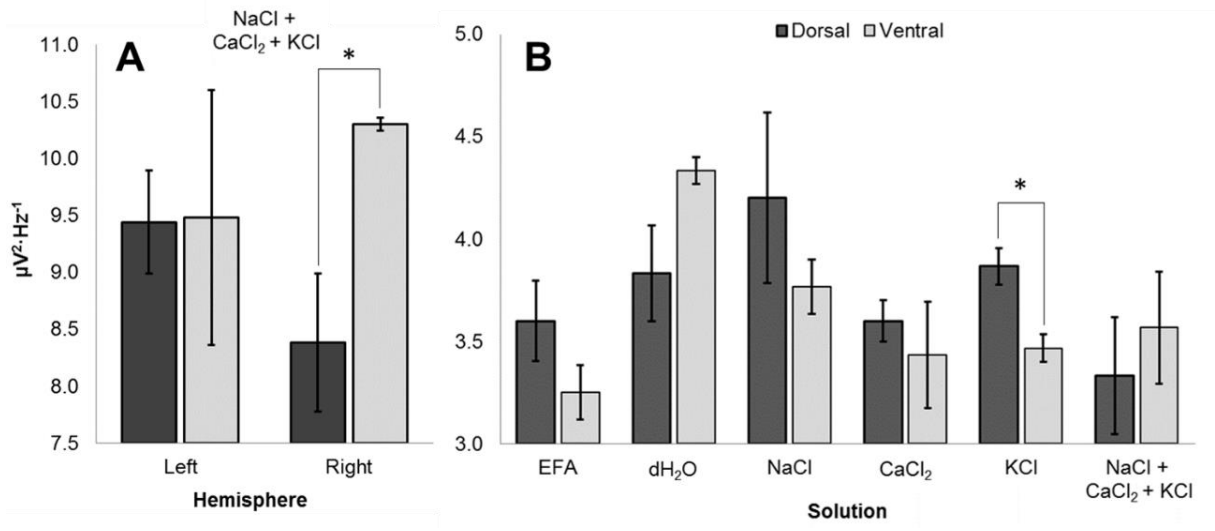

Figure 55. Averaged wide-band high-frequency (7.5 Hz – 40Hz) spectral power densities within the dorsal and ventral components of the left and right cerebral hemispheres when exposed to a combination of NaCl, $CaCl_2$, and KCl (A). Beta 2 (20Hz – 30 Hz) spectral power increases within the dorsal component of the right hemisphere relative to the ventral component when exposed to KCl. Significant differences are indicated ($p<.05$).

Discussion

The data indicate that the right cerebral hemispheres of Wistar rats are sensitive to pH changes within the fixative solution (the medium) as well as the presence of KCl in ways unaccounted for by pH. The findings reported in Figure 48 demonstrate the relationship between the time that the brains had been immersed in ethanol-formalin-acetic acid (EFA) and the high-frequency (14 Hz – 40 Hz) spectral power derived from microvolt potentials measured within the four quadrants of the cerebrum. The data suggested that this relationship was accentuated within the right dorsal cerebrum. Suspecting the medium was perhaps changing over time and influencing microvolt potentials within the tissue, we measured the pH of the fixative material surrounding the brains while noting the total time that the vat containing both the tissue and fixative solution had remained in storage. A logarithmic relationship was apparent, where trends toward neutral pH were sharp within the first ~60 days, followed by a relatively gradual increase over time (Figure 50). A total pH shift of ~1.5 units over 20.5 years was noted.

Having identified a process involving pH trends toward alkalinity with proportional increases of high-frequency microvolt potentials within the right cerebral hemisphere, we endeavored to observe the early phases of full brain fixation by serial measurement of a longitudinal case (n=1). Figure 51, which summarizes the 9 week data collection period, demonstrates that high-frequency (14 Hz – 40 Hz) spectral power derived from individual quadrants become increasingly disparate over time – suggesting non-isotropic distribution of the fixative material, or stated otherwise, unequal perfusion (or the direct molecular consequences of perfusion). The right ventral cerebral hemisphere displayed consistently elevated high-frequency spectral power relative to other quadrants over the fixation period. Also of note was the averaged (dashed lines) trend which suggested an

amplitude peak between 3 and 6 weeks post-fixation. This temporal period is significant as it represents the approximate time required for the solidification of methylene cross-bridges in aldehyde-based fixation (Kiernan, 2000; Bjorksten, 1951). We would therefore expect to see a relative reduction in the rate of change of spectral power after the first month of fixation. If methylene bridges ($-CH_2-$) continued to form at a reduced rate during the month following initial fixation, one might expect to observe the gradual liberation of hydroxyl ions into the medium which would manifest as increased alkalinity of the solution surrounding the tissue over long periods of time.

The process of hydroxyl liberation begins with formaldehyde dissolved in water which produces methylene hydrate:

$$H_2C{=}O + H_2O \rightarrow HO{-}CH_2{-}OH$$

Within an environment rich in amino acids, such as a brain, methylene cross-links ($-CH_2-$) would form between reactive atoms in proteins that are very close together, liberating free hydroxyl ions (OH^-) into the medium surrounding the tissue proper. The net result would be increased fixation of brain matter paired with an increase of pH within the medium due to the liberation of OH^-. If free protons were also sequestered by the brain or masked by protein cross-linking, pH increases would be amplified.

The next logical step was to experimentally manipulate the medium within which the tissues were immersed by varying pH, and the presence or absence of physiological ions. Re-hydrating the tissue in artificial CSF produced changes within 1 hour of immersion with the most pronounced effects emerging after 24 hours. If the brains were re-immersed in EFA after re-hydration, microvolt potentials returned to baseline

conditions (Figure 52B). It was apparent that re-hydration effects could only be observed for high-frequency spectral power within the right cerebral hemisphere. We observed that the right ventral quadrant was particularly sensitive to our experimental manipulations of pH (Figure 53) in ways unobserved within the dorsal component of the same hemisphere. The spectral power relationship centered upon the narrow 20 Hz – 30 Hz band. Brain immersion within CSF 1, the standard formula containing all essential components, as well as CSF 3, which involved the removal of $CaCl_2$, was associated with high-frequency dorsal-ventral disparity of spectral power within the right hemisphere only. The likely sources of variance were NaCl and KCl as their removal from solution abolished or partially abolished dorso-ventral power disparities. In order to experimentally demonstrate the relative effects of $CaCl_2$, KCl, and NaCl, each compound was added to water and served as solutions within which rat brains were placed for 1 hour before testing. This approach represented the inverse of what was presented in Figure 53 wherein compounds were systematically removed from solution. The results indicated that only solutions containing KCl reliably reproduced the high-frequency dorso-ventral spectral power disparities observed initially with CSF 1.

Together, our findings indicate that post-mortem rat brain measurements of electric potential differences are influenced by pH of the medium as well as by the presence of certain ion-producing compounds. In combination with results reported by Rouleau, Murugan, Tessaro, Costa, and Persinger (2016), these experiments further approximate mechanisms underlying post-mortem tissue responsiveness. Though receptor-mediated membrane events paired to ionic flow remain unlikely, further work should aim to investigate residual molecular capacities at the level of the cellular membrane in order to

establish a mechanism which explains post-mortem brain responses as have been reported here and elsewhere. However, some explanatory heavy lifting is currently required of molecular mechanisms to address why the right cerebral hemisphere as a gross structural aggregate is particularly sensitive to charged molecules, neurotransmitters (Rouleau, Murugan, Tessaro, Costa, and Persinger, 2016), and applications of direct current (Rouleau & Persinger, 2016a). Likewise, it is still unclear how particular frequencies emerge as reliable responses to particular stimuli. Future studies should aim to shift frequency responses contingent upon controlled applications of molecular agents.

Asymmetric hemispheric distributions of pH- or charge-sensitive molecules embedded within the tissues could explain why neuroanatomical loci express degrees of microvolt fluctuation independence as well as the capacity to display dose-dependent "responses" in the presence of neurotransmitters. Further studies should target likely candidates using immunohistological and other methods. Alternatively, fixed post-mortem tissue can be thought of as an intricate scaffold of microstructures with intrinsic resonant capacities. Perhaps the presence of charged particles within or across residual circuits of preserved brain material structures otherwise noisy electrical signals within the tissues into more coherent oscillations which are measured as reliable spectral power modulations. The former hypothesis assumes conventional mechanisms while the latter considers the possibility that subsections of preserved, post-mortem brain tissue can be observed and treated as a material with physical properties independent of biology though intimately related to physics and chemistry. If the electrical properties of brain material independent of life (e.g., metabolism, cell function, etc.) do impinge upon normal

neurophysiological functions, a thorough study of post-mortem brain tissue and its material properties is now warranted.

References

Bjorksten, J. (1951). Cross linkages in protein chemistry. Advances in Protein Chemistry, 6, 343-381.

Egert, U., Schlosshauer, B., Fennrich, S., Nisch, W., Fejtl, M., Knott, T., ... & Hämmerle, H. (1998). A novel organotypic long-term culture of the rat hippocampus on substrate-integrated multielectrode arrays. Brain Research Protocols, 2(4), 229-242.

Humpel, C. (2015). Organotypic brain slice cultures: A review. Neuroscience, 305, 86-98.

Kiernan, J. A. (2000). Formaldehyde, formalin, paraformaldehyde and glutaraldehyde: what they are and what they do. Microscopy Today, 1(5).

Noraberg, J., Poulsen, F. R., Blaabjerg, M., Kristensen, B. W., Bonde, C., Montero, M., ... & Zimmer, J. (2005). Organotypic hippocampal slice cultures for studies of brain damage, neuroprotection and neurorepair. Current Drug Targets-CNS & Neurological Disorders, 4(4), 435-452.

Opitz-Araya, X., & Barria, A. (2011). Organotypic hippocampal slice cultures. JoVE Journal of Visualized Experiments, (48), e2462-e2462.

Rouleau, N., Lehman, B., & Persinger, M.A. (2016). Focal Attenuation of Specif Electroencephalographic Power Over the Right Parahippocampal Region During

Transcerebral Copper Screening in Living Subjects and Hemispheric Asymmetric Voltages in Fixed Coronal Sections. *Brain Research.* 1644, 267-277.

Rouleau, N. & Persinger, M.A. (2016a). Differential Responsiveness of the Right Parahippocampal Region to Electrical Stimulation in Fixed Human Brains: Implications for Historical Surgical Stimulation Studies?. *Epilepsy & Behaviour.* 60, 181-186.

Rouleau, N. & Persinger, M.A. (2016b) Post-Mortem Neural Tissues Filter Electromagnetic Fields. In Review with Brain Stimulation.

Rouleau, N., Reive, B.S., & Persinger, M.A. (2016). Functional Neuroimaging of Post-Mortem Tissue: Lithium-Pilocarpine Seized Rats Express Reduced Brain Mass and Proportional Reductions of Left Ventral Cerebral Theta Spectral Power. Heliyon. 2(10), 1-10.

Chapter Transition: Explaining the Data

Previous chapters have presented data which collectively indicate that electrical anisotropies, response patterns, and repeated exposure phenomena are generated by fixed, post-mortem brain tissues. The following chapter serves to synthesize the previous chapters wherein a working hypothesis is formed. Several keys points are outlined in the following chapter though most centrally, the results are interpreted to indicate that preserved neural tissues transform inputs selectively as a function of subregions of the brain, the waveform or frequency of the signal, the intensity or amount of the applied stimulus, and in consideration of previous inputs as well as the medium. We have interpreted these observations to represent genuine functions insofar as input-output relationships of materials constitute genuine functions (e.g., resistors, capacitors, transistors, etc.). These features are observed in spite of what has been historically labelled “death” – a brain state defined by its functional absence. It is, in the following chapter, implied therefore that death is either a state of minimal function or that the label is inaccurate. The working hypothesis states that fixed, post-mortem neural tissues constitute a type of filtration medium or material which, if stimulated, transforms signals. The degree to which signal transformation implies a phenomenology is questioned – experience can be quite separate and unrelated to signal transformation as a general phenomenon. Instead, the results should be treated as a foundation for further studies which attempt to understand the computational properties of neural material with suggestions regarding the experimental design of tasks which might disconfirm suspicions of complex response capacity.

Chapter 9:

A Passive Organ: Deciphering Responsive Post-Mortem Brains

(Original Research)

In Review with Medical Hypotheses

Abstract

The brain is a highly metabolic, actively responsive organ. However, recent measurements have indicated that frequency-dependent microvolt potentials obtained within fixed, post-mortem brain tissue respond to applied electrochemical stimuli with dose-dependence and potential habituation. These results in combination with several other experiments indicated that fixed post-mortem, ametabolic brains express functionally non-random microvolt potential fluctuations. Here, I propose a hypothesis which considers the brain as a passive, receptive substrate superimposed upon an active, metabolic infrastructure. Calculations are presented which were considered under the assumption that the brain operates as a material. Estimates of current are provided based upon empirical measurements of voltage and resistance. Cerebral cortical resonance frequencies inherent to gray matter derived from permeability and permittivity are discussed as relevant to the observed 4 Hz – 14 Hz signal frequency which fluctuates in response to applied stimuli in the post-mortem brain. The perspective outlined here considers the brain's material structure as a determinant of function which persists beyond metabolically driven physiological processes. Experimental limitations are discussed in relation to proposed functional paradigms to test the passive properties of brain material.

Introduction

In its living state, the human brain operates by actively maintaining electrochemical gradients across synaptic interfaces (Davis & Goodman, 1998). Plastic networks, continually re-molded by consolidated sensory experiences, perform computations which govern cognition and behaviour. Upon death, the wetware responsible for performing these tasks breaks down. Cellular membranes, which maintain electric potential differences (Hodgkin & Huxley, 1952) and within which receptive protein complexes governing cell-to-cell communication are embedded (Winckler, Forscher, & Mellman, 1999), degrade without replacement. Without the presence of boundary conditions separating charged molecules, cells of the human brain lose their capacity to process signals or perform computational tasks. The structure of the brain, at both macro and micro levels, must be maintained if normal functions are to be preserved.

The observation that structure dictates function is central to the physical sciences and represents as simple of a principle as can be articulated in the study of the relationship between anatomy and physiology. That is, it has been observed that functions are derived from structures. Just as a motor vehicle should only be propelled forward by an engine or roll by dint of the circular structure of its wheels, so too should a neuron fire an action potential by dint of its channel density at the axon hillock. There is no biological function which exists without an inseparably associated structure. This principle can and has been tested in the biological sciences by ablating or destroying organic structures. To no surprise, sufficient structural damage incurred by any organ results in functional loss where the relationship between structure and function track or correlate such that increments of structural loss are met with proportional increments of

functional loss. The brain, though complex in its structure and resulting functions, does not represent an exception to this rule.

The structure of the brain is elegant and multiform. At the macroscopic level, its gyri and sulci provide a partially conserved, superficial landscape upon which a cortical architecture transitions morphologically from peak to valley. Stratified, the cortex is composed of cell bodies as well as dendrites and axons, organized into predictable layers, spatially oriented in parallel and along common polar axes. Several structures, such as the caudate nucleus and the hippocampus, retroflex – represented throughout the brain as C-shaped structures. Within the hippocampus, interlocking tissue subsections of the dentate gyrus and CA fields interface. Tract systems form insulated bridges between islands of cells separated by great expanses of tissue. These structures are seemingly inseparable from some of the most complex biological functions ever observed: creativity, intelligence, and consciousness among others. If brain structure were to be preserved immediately upon its removal from the cranial cavity before major decomposition has set in, would degrees of retained structural integrity be associated with scaled degrees of functional integrity?

Preserving the brain

Certain feats of engineering have allowed researchers to preserve the structure of the brain beyond death. Among them, the modern techniques of cryogenic preservation (Harding, 2004) and vitrification (Cobo & Diaz, 2011) have received considerable attention. Historically, however, the most common preservation technique has been chemical fixation. Using aldehyde- (Bodian, 1970; Fox, Johnson, Whiting, & Roller, 1985;

Karlsson & Schultz, 1965) or ethanol- (Perlmutter et al., 2004) based fixative solutions either separate or in combination (Harrison, 1984) allows one to preserve brain structure for decades or even centuries. The mechanisms by which aldehyde-based fixatives preserve structural integrity, protein cross-linking, has been described in detail (Jamur & Oliver, 2010; Kiernan, 2000). In brief, methylene bridges interlock adjacent proteins, bringing cells into a state of structural stasis. The initial 18-24 hour perfusion time for a 1 cc block of tissue is followed by a 30 day period during which tissue fixation stabilizes (Bjorksten, 1951; Kiernan, 2000). Additionally, amino groups are effectively masked, the tissue becomes increasingly acidic, and the net negative charge of the specimen increases (Puchtler & Meloan, 1985). Sophisticated histological studies have demonstrated that, once the tissue is perfused, fixative solutions maintain key cellular features which are consistent with the living brain (Eng & Bigbee, 1978; Jennes, Stumpf, & Kalivas, 1982; Kimura, McGeer, Peng, & McGeer, 1980). Mason & O'Leary (1991) verified that formaldehyde fixation, though capable of interfering with tertiary protein structure, locks proteins into their secondary structure which are largely determined by amino acid sequence. Immunohistology, which is entirely reliant upon the structural integrity of proteins sufficient to bind monocolonal antibodies (Farr & Nakane, 1981), could not be performed upon sectioned, fixed brain tissue if not for the reliable maintenance of cerebral protein structure and localization within cells.

Whereas long-term preservation of post-mortem brain structure has been achieved to variable degrees, it has been generally assumed that the preserved tissues are not functionally active. Unlike tissue preparations, which are common to neurophysiological investigations, the constituent cells of the fixed human brain no longer

display the typical biological signatures of living matter. That is to say, although the microstructure of the brain can be preserved long after death of the individual, functions including rudimentary neural computations are not considered possible for a number of reasons. First, the pH and active enzyme concentrations which normally define the biological environment are shifted to a considerable degree once immersed within most fixative solutions (Puchtler & Meloan, 1985). This disruptive shift is thought to impact electrochemical signalling by interfering with the maintenance of charge disparity across plasma membranes. Second, although the presence of membrane-bound proteins can be readily visualized by the methods associated with immunohistology (Farr & Nakane, 1981), their confirmations and associated dynamic components are subject to degrees of chemical and mechanical impedance due to protein cross-linking among other molecular hurdles. Douglas & Rogers (1998) demonstrated that extensive DNA damage is observed when fixing with 3.7% formaldehyde. Therefore conventional genetic function is likely lost entirely upon formaldehyde fixation as the structures required to produce downstream effects such as the active production of protein are lost. Third, in the absence of normal physiological activity including the availability of energy sources provided by vascular interfaces, the mechanisms which underlie molecular signalling are thought to be no longer operationally valid. That is to say, chemical reactions become increasingly energetically unfavourable – a non-starter for a system which processes information by fluctuation of membrane polarity. In general, chemically fixed human brains are not molecularly equipped at the cellular level to function by means of normal physiological mechanisms. The ubiquitous assumption that preserved brains are functionally inert is based upon the assumption that brains function by dint of active cellular processes and

that fixative-perfused cells are not functional. If, however, brain tissues were to elicit stimulus-response patterns after decades of fixation, the assumption of cellular dependence would require a re-examination.

The post-mortem response

The aforementioned assumptions underlying the necessary and sufficient conditions of brain function have been challenged by recent works which demonstrate basic signal processing capacities of neural tissue preserved in ethanol-formalin-acetic acid. Post-mortem brains, preserved by chemical fixation, express frequency-specific microvolt-scale fluctuations in response to various stimuli. For example, human brains fixed for over 20 years in ethanol-formalin-acetic acid responded with dose-dependence and potential habituation to nicotine, 5-HTP, L-glutamate, and ketamine (Rouleau, Murugan, Tessaro, Costa, & Persinger, 2016). The authors reported directionally opposed effects for glutamate and ketamine, suggestive of agonistic and antagonistic activations of the NMDA receptor. The results, which demonstrated that fixed brains effectively responded to applications of neurotransmitters and their precursors, were suggestive of receptor-mediated microvolt fluctuations despite the improbability of said mechanism within the EFA-rich brain microenvironment.

Cortical areas of coronal slices of fixed human brain tissue have expressed hemispheric asymmetries of electric potential differences when stimulated by patterns of applied current which simulate neural spike trains (Rouleau & Persinger, 2016). The effects were frequency-dependent and amplified within the right parahippocampal region, expressed as increased theta power – a frequency band characteristic of this region in

the living brain (Cornwell, Johnson, Holroyd, Carver & Grillon, 2008; O'Keefe & Burgess, 1999). The coronal slices filtered signals differently as a function of the area being stimulated. Further, the frequency-discrimination capacities of the tonotopically organized, medial component of the primary auditory cortex (Da Costa, van der Zwaag, Marques, Frackowiak, Clarke, & Saenz, 2011) as well as the functional differentiation of primary and secondary visual cortices were demonstrated in the post-mortem brain as indicated by experimental paradigms involving direct applications of current to the tissue (Rouleau, Murugan, Tessaro, Costa, & Persinger, 2016; Rouleau, Costa, & Persinger, 2016). Stated otherwise, the primary receptive cortical regions of fixed human brains filter signals in ways which were predicted while operating under the assumption that living-like responses could be retained post-mortem.

It is evident that when stimulated, post-mortem human brains express non-random patterns of microvolt potentials within a narrow frequency band – typically theta (4 Hz – 7.5 Hz) or alpha (7.5 Hz – 14 Hz). However, when measured without stimulation voltage gradients can be observed across the rostro-caudal and medial-lateral axes (Rouleau, Lehman, & Persinger, 2016). That is, fixed brain specimens express electrically polar properties. The degree to which the polar properties of full-brain voltage gradients are functionally relevant is somewhat unclear, though it was recently shown that microstructural pathologies associated with epilepsy could be identified in fixed, post-mortem Wistar rat brains (Rouleau, Reive, & Persinger, 2016). Reduced brain mass and proportional theta power decreases were observed in rats injected with lithium-pilocarpine to induce status epilepticus relative to controls. In consideration of the work performed by Peredery et al. (2000), perfuse tissue damage within the CA1 region of the hippocampus

and entorhinal cortices likely produced the effects. These studies demonstrate that deep structural information about the tissue can be elucidated without dissection or advanced imaging tools. Rather, tissue subsections differentially expressed voltage fluctuations at rest while employing a common electrical reference point. Whether or not basic or complex computations can be performed by the tissues remains to be tested empirically.

Whereas chemically fixed human brains are responsive when experimentally probed by electro-chemical stimuli, the means by which responses are generated are likely not driven by typical neural interfacing characteristic of the living brain. Alternatively, it is possible that the brain's cellular infrastructure – the synaptic networks and gross neuroanatomical organizations preserved in three-dimensional space – can be accessed to some degree by impinging, extrinsic forces. Rather than a physiological response, characterized by molecular pathways and tightly regulated electrodynamic processes, the observed post-mortem brain phenomena could be interpreted as consequences of signals propagating through materials which operate as a complex filters – incorporating, excluding, amplifying, attenuating, or otherwise modifying inputs by dint of brain structure alone. If the microanatomical pathways of the brain, preserved by chemical fixatives such as EFA are in this sense functionally relevant, experimental challenges which aim to elicit complex response patterns involving signal processing should reveal said functional relevance. In order to reconcile the classical understanding of central nervous system function and the aforementioned experimental results which have been observed within the post-mortem brain, a re-evaluation of the central paradigm itself is in order. A new perspective is now warranted which simultaneously maintains the classic understanding of active brain function which has been reliably verified over a century of detailed

electrophysiology, while accommodating recent discoveries concerning minimally preserved functions of post-mortem human brain tissue.

A materials science approach to neuroscience would involve evaluations of the mechanical, chemical, electrical, thermal, optical, and magnetic properties of the constituent tissues. The convergent properties of different preserved or otherwise non-degrading brain tissues could reveal the engineering potential of brain material itself. If it were determined that certain preserved brain tissues express physical properties in the absence of life-sustaining biological function which are of any functional consequence, the fixed post-mortem brain could be considered a non-trivial, functional object. Further, the intricate spatial distribution of cortical laminae as well as the interwoven tract systems and complex orientation of cell bodies within the brain could perhaps set up the conditions for a passive, receptive system superimposed upon a highly-metabolic substrate. An extensive body of literature has attempted to determine why the brain in particular is sensitive to electromagnetic fields (Bell, Marino, & Chesson, 1994; Kramarenko & Tan, 2003; Reiser, Dimpfel, & Schober, 1995). Adey (1981) discussed various mechanisms which might underlie tissue interactions with electromagnetic fields. Perhaps by blocking, absorbing, enhancing, attenuating, bending, or shifting electromagnetic waves (as is routinely performed by certain synthetic materials), specific brain tissues themselves – as opposed to the constituent cells which give rise to the brain material – imbue the organ with functionally consequential magnetoceptive capacities. Only a materials science approach, particularly in the absence of life-sustaining biological functions, can an intimate and nascent study of brain material be achieved. By fixing post-mortem tissue and essentially stripping away sources of variability associated with the living human

brain, the importance of the constituent materials as independently operating bodies can become clear, revealing new applications and implications.

Further experimental work involving post-mortem brains should consider the theoretical implications of the brain as a partially passive, functional object. Here, I have provided a few calculations which are performed while operating under the assumption that brain-scale dimensions of electrical resistance, voltage, permeability, and permittivity explain a subset of brain properties independent and separate from the metabolic brain. The approach serves as a means to explain the observed post-mortem stimulus-response phenomena without the assumption that the functions of tissues are entirely contingent upon the active, metabolic activity of constituent cells. I also propose a simple experimental paradigm which could test the computational capacities of post-mortem brain material. As the proposed re-evaluation is to some extent challenging the typical neuroscientific paradigm, the experimental methods can seem unintuitive if the underlying assumptions stated above are not held if only for the sake of testing.

Subthreshold residual current

Our empirical measurements using needle electrodes have revealed that the average electric potential difference between gray matter and attached cerebral arteries is approximately 10 μV, with interhemispheric differences of approximately 1 to 2 μV (Rouleau, Lehman & Persinger, 2016). Digital multimeter measurements of resistance within gray matter present within coronal slices of fixed, post-mortem human brain tissue were obtained, revealing values of 100-210 kΩ. With these known physical parameters, residual current can be calculated. Current in amps is predicted by the formula

$$I = V \cdot R^{-1} \qquad (2),$$

where I is current in amperes, V is voltage in volts, and R is resistance in ohms. When the aforementioned values are applied, the average predicted residual current would approximate 500 pA for post-mortem, fixed gray matter tissue – the cortical substrate containing densely packed cell bodies. This value is sensible given the average current associated with a living cell is $1 \cdot 10^{-9}$ A or 1000 pA as calculated by Persinger (2012) who assumed 10^3 channels per cell (Ackerman & Clapham, 1997) with 1 pA per channel (Kirichok, Krapivinsky, & Clapham, 2004; Zurborg, Yurgionas, Jira, Caspani, & Heppenstall, 2007), which is less than one order of magnitude increased relative to the predicted post-mortem equivalent at the tissue level presented here. These extremely weak currents, though derived by calculation from voltage and resistance, are within reasonable range and could represent a residual, sub-living-threshold expressed by the organic tissue aggregate within an environment of ambient electromagnetic noise. It is unlikely that residual pico-currents are being generated by the cells themselves. Individual membrane potentials are highly dependent upon the cell's capacity to regulate intra- and extra-cellular concentrations of specific physiological ions such as K^+, Cl^-, and Ca^{2+}. Rather, the material of the brain – once preserved after death – maintains electrical properties such as gradations of resistant material which approximate its former state, contributing to some of the experimental results we have published elsewhere. That is, in the absence of active bioelectricity, the electric potential difference between gray matter and an attached, non-neural reference (vasculature) flutters just below the threshold normally observed in living tissue instead of an absence of potential difference.

That voltage potentials, which are systematically related to current, change in response to chemical and electrical stimuli could point to the source of the stimulus-response effects observed experimentally. Without the assumption of the material-like properties of the brain, residual pico-currents expressed within the tissue can easily be dismissed as trivial. However, it is possible that sub-threshold oscillations within neural tissues contribute to stochastic resonance phenomena as has been predicted and demonstrated by many authors (Gluckman, Netoff, Neel, Ditto, Spano, & Schiff, 1996; Hänggi, 2002; Hidaka, Ichiro, Nozaki, & Yamamoto, 2000). In this case, the source of the noise would be picoAmp currents within the tissues induced by ambient electromagnetic energy from the environment interacting with the local electrical resistance (and other properties) of brain subsections.

Cerebral resonant frequency

When the magnetic field of an inductor collapses, electric current can be generated sufficient to charge a capacitor within the same circuit. The magnetic field of the inductor, in turn, can be re-activated by the discharging capacitor. This relationship between inductors and capacitors within a circuit is defined by a resonance frequency (s^{-1} or Hz) which defines the periodicity of the exchange. The resonance frequency of a circuit can be estimated

$$f = \frac{1}{(2 \cdot \pi \cdot (LC)^{\frac{-1}{2}})} \qquad (3),$$

where f is frequency in cycles per second (Hz), L is permeability or Henrys per meter, and C is permittivity or Farads per meter. Resonant circuits tune and filter signals, reducing noise and cancelling sources of distortion. Tsang and colleagues (2004) originally

calculated that cortical gray matter exhibits a resonant frequency of ~7Hz, assuming permeability was 10^{-2} $H \cdot m^{-1}$ and permittivity was $2 \cdot 10^{-1}$ $F \cdot m^{-1}$. Responses observed within the context of experiments involving the post-mortem brains preserved in ethanol-formalin-acetic acid were expressed in the form of increased or decreased spectral densities ($\mu V^2 \cdot Hz^{-1}$) and were consistently within the theta-alpha bands (4Hz – 14Hz) with few high-frequency (~40 Hz) exceptions.

If some subset of expressed electroencephalographic power in the living human can be attributed to intrinsic resonant features of gray matter, the post-mortem brain would be expected to express these features in the absence of normal metabolic and bioelectric function. In other words, the cytoarchitecture and aggregate tissues would be sufficient to display intrinsic, frequency-dependent microvolt fluctuations assuming the presence of electric current. The precise resonant frequency of brain material, determined by its electromagnetic properties, could be modulated by various chemical and spatial changes sufficient to alter either permeability or permittivity. For instance, holding permittivity constant, decreases of permeability of less than an order of magnitude ($6 \cdot 10^{-3}$ $H \cdot m^{-1}$) could increase the resonance frequency to the mid-alpha range or ~11Hz. The same approximate frequency is achieved by holding permeability constant and increasing permittivity by less than an order of magnitude ($4 \cdot 10^{-1}$ $F \cdot m^{-1}$). If the theta-alpha power fluctuations observed within the post-mortem brain are reflective of changes to cerebral resonant frequency, the source of the shift could be due to any number of stimuli influencing inductance or capacitance over space. That the frequency (4 HZ – 14 Hz) range most often reported associated with post-mortem brain stimulus-response patterns is predicted by the intrinsic resonance frequency of brain material could be illustrative of

how the assumption of metabolic activity is not entirely necessary when explaining some properties of brain function.

Experimental limitations and suggestions

An experimental evaluation of the proposed hypothesis would require designs which must accommodate some intrinsic limitations of the fixed human brain tissue. First, the brain as an independent organ does not move. Most stimulus-response tasks used in psychological studies rely upon motor activation. Whereas the human brain devotes considerable spaces to both the planning (e.g. frontal lateral convexities including Brodmann areas 6 and 8) and execution (e.g. pre-central gyrus or Brodmann area 4) of motor responses (Hoshi & Tanji, 2004), the brain as an independent organ is immobile and restricted once the cranial nerves and descending pyramidal fibers are severed, separated from their efferent targets. This same problem has been considered within the clinical context of patients which express varying degrees of awareness and cognitive capacities in the absence of motor function – most notably, in the case of Locked-In-Syndrome (Kübler, Furdea, Halder Hammer, Nijboer, & Kotchoubey, 2009). Recent advances using functional neuroimaging and feedback software have allowed researchers and clinicians to communicate with individuals which are limited by severe motor impairments (Birbaumer & Murguialday, 2010). In the case of the fixed human brain, any test of practical function must necessarily circumvent the problem of immobility. Consequently, quantitative measures of physical changes within the tissue are ideal including electrodynamic recordings. Alternatively, an apparatus could be constructed which transforms measurements obtained from the brain into useful analog activations

which, once amplified appropriately, could move a needle or power a light-emitting-diode (LED).

Another intrinsic limitation is that some form of energy must be applied to and transduced by the brain in order to evaluate stimulus-response patterns involved in task performance. Though the brain might, in principle, retain functional capacities beyond death the identification of practical implications requires stimuli so as to control for random events. The problem of receptivity is due to an absence of sensory transducing organs (i.e. cochlea, retina, mechanoreceptors, etc.). Whereas applications of light to the eyes or mechanical vibrations to the skin would normally result in transduced potentials which would be relayed up-stream to primary receptive as well as secondary and tertiary association cortices, the absence of a human body limits the receptivity of the brain itself. Therefore, only applications of energy which reliably induce responses when applied directly to the brain should be employed. The passive physical reception of applied stimuli must, however, not be confused with computation or stimulus processing. For example, simple increases in voltage potential differences between two points of the brain upon connecting a battery to the tissue must not be confused with a genuine response. A distinction might be made between unfiltered signal passage where both the input-output signals are identical in terms of information content and genuine signal transformations which involve an intermediate step during which the signal is processed computationally.

The phenomenology of a deceased human brain is both empirically and philosophically challenging. Similar to Nagel's (1974) central question regarding qualia, one might ask "What is it like to be a deceased human brain?". There is no evidence to suggest it experiences anything, though these questions cannot be dismissed out-of-hand

in consideration of the reliable stimulus-response patterns which have been observed. However, it is sensible to assume that any experiences attributable to the deceased brain would share roughly analogous experiences in its living counterpart. This intuition is based upon the central assumption that all experiences emerge from the brain and that cortical cytoarchitectures, conserved across members of the same species, are associated with qualitatively different though related experiences. For example, the primary visual cortex (BA17) is functionally associated with visual reception (Tusa, Palmer, & Rosenquist, 1978). The structure of the occipital pole, the koniocortex and line of Gennari as well as other features which surround the calcarine fissure, are thought to give rise to conscious visual experience. That is to say, the specific structure is paired to a specific function. Insofar as the fixed human brain retains these same structures, the capacity for visual experience – as opposed to auditory or somatosensory experiences – is plausible if structure dictates function. Therefore the experimental design can, in practice, incorporate subjective or phenomenal elements such as emotional valence if the area probed is known to produce the desired response once stimulated. For example, stimulation of the right amygdala results in a specific set of experiences, cognitive patterns, and behaviours in the living brain (Morris, Ohman, & Dolan, 1999). There is no reason to suggest that the multiform pathways associated with the interdigitated sub-nuclei which collectively form the right amygdala and which necessitate said responses, once perfused by fixative solution, are lost. To the contrary, tract systems can be visualized *ex vivo* using diffusion tensor imaging (D'Acreuil, Westmoreland, & de Crespigny, 2007).The only point of contention would be concerning the functional consequences of said connections.

A genuine sign of progress in this area would involve the development of an experimental paradigm to test the post-mortem brain's capacity to complete a task rather than respond reflexively to applied stimuli. It is entirely possible that reflexive, stimulus-response patterns represent the system's inherent functional limit. A valid, task-based paradigm represents a clear method by which said limit could be established. A shaping technique, which rewards successive approximations to the desired response, is ideally suited in this regard. If the frequency of expressed oscillatory patterns or transients of electric potential differences displayed by the brain could be increased by shaping, more complex paradigms could then be attempted. A feedback apparatus could be constructed wherein "desirable" outcomes could be rewarded by delivering current to known, intrinsic reward centers including the nucleus accumbens. An empirical evaluation within the fixed human brain could be undertaken by up- or down-training expressed spectral densities or weak amplitude-modulation by electrically stimulating the nucleus accumbens.

A minor technical hurdle which must be overcome consists of establishing the reward or punishment status of applied stimuli. Operationally, rewards are simply applied stimuli which increase the rate or amplitude of the responses to which they are paired. In this regard, applied stimuli which reliably up- or down-train frequency-dependent electric potential differences can be considered rewards or reinforcements (though these can be distinguished) in all practical senses. Therefore there should be no contention about whether or not a stimulus is a reward with regard to the post-mortem brain if in fact its application increases the rate or amplitude of a response to which it is paired. An experimental demonstration of fixed, post-mortem brain "preference" as indicated by response biases contingent upon a selective history of rewards would be fundamentally

disruptive to conventional neural science. Alternatively, failure to establish conditioned preference would set a clear limit upon the tissues capacity to maintain complex functions in the absence of physiological processes.

Conclusions and discussion

If the null hypothesis were rejected, the implications would be numerous. Post-mortem human brain computation would expand the reach of cognitive neuroscience to beyond cardiovascular death. Certain questions previously unthinkable or otherwise dismissed would immediately become relevant. For instance, the prospect of retrieving information from a deceased individual by selective probing would become a possibility. So too would there be the potential for investigations regarding the substrate-independence of consciousness or intelligence for which evidence is in short supply. A healthy skepticism of these concepts can only be maintained once the hypotheses are tested directly.

The predictive power of the classic model of neural function is not under threat. Brains, though complex, can be generally understood and manipulated by the perspectives and techniques offered by neurobiologists operating under the assumptions of channel-mediated electro-chemical signal propagation. Cells really do function as described classically, contributing to tissue functions which are heavily reliant upon metabolic activity. However, post-mortem neural tissue which has been chemically fixed for over 20 years should not be stimulus-responsive under the current assumptions. The perspective offered here considers the brain as both a biological organ as well as a convoluted volume of matter with intrinsic material properties quasi-independent of

biological processes. Synaptic networks provide the structural architecture of tissues which produce aggregate functions persistent beyond metabolic function. It is my contention that this perspective accommodates both the traditional view of the brain while offering explanatory power to emerging observations.

References

Ackerman, M. J., & Clapham, D. E. (1997). Ion channels—basic science and clinical disease. New England Journal of Medicine, 336(22), 1575-1586.

Adey, W. R. (1981). Tissue interactions with nonionizing electromagnetic fields. Physiological reviews, 61(2), 435-514.

Bell, G. B., Marino, A. A., & Chesson, A. L. (1994). Frequency-specific responses in the human brain caused by electromagnetic fields. Journal of the neurological sciences, 123(1), 26-32.

Bjorksten, J. (1951). Cross linkages in protein chemistry. Advances in Protein Chemistry, 6, 343-381.

Bodian, D. (1970). An electron microscopic characterization of classes of synaptic vesicles by means of controlled aldehyde fixation. The Journal of cell biology, 44(1), 115-124.

Bugbee, N. M., & Goldman-Rakic, P. S. (1983). Columnar organization of corticocortical projections in squirrel and rhesus monkeys: similarity of column width in species differing in cortical volume. Journal of comparative Neurology, 220(3), 355-364.

Cobo, A., & Diaz, C. (2011). Clinical application of oocyte vitrification: a systematic review and meta-analysis of randomized controlled trials. Fertility and sterility, 96(2), 277-285.

Cornwell, B. R., Johnson, L. L., Holroyd, T., Carver, F. W., & Grillon, C. (2008). Human hippocampal and parahippocampal theta during goal-directed spatial navigation predicts performance on a virtual Morris water maze. The Journal of Neuroscience, 28(23), 5983-5990.

Da Costa, S., van der Zwaag, W., Marques, J. P., Frackowiak, R. S., Clarke, S., & Saenz, M. (2011). Human primary auditory cortex follows the shape of Heschl's gyrus. The Journal of Neuroscience, 31(40), 14067-14075.

D'Arceuil, H. E., Westmoreland, S., & de Crespigny, A. J. (2007). An approach to high resolution diffusion tensor imaging in fixed primate brain. Neuroimage, 35(2), 553-565.

Davis, G. W., & Goodman, C. S. (1998). Synapse-specific control of synaptic efficacy at the terminals of a single neuron. Nature, 392(6671), 82-86.

Douglas, M. P., & Rogers, S. O. (1998). DNA damage caused by common cytological fixatives. Mutation Research/Fundamental and Molecular Mechanisms of Mutagenesis, 401(1), 77-88.

Eng, L. F., & Bigbee, J. W. (1978). Immunohistochemistry of nervous system-specific antigens. In Advances in neurochemistry (pp. 43-98). Springer US.

Farr, A. G., & Nakane, P. K. (1981). Immunohistochemistry with enzyme labeled antibodies: a brief review. Journal of immunological methods, 47(2), 129-144.

Fox, C. H., Johnson, F. B., Whiting, J., & Roller, P. P. (1985). Formaldehyde fixation. J histochem Cytochem, 33(8), 845-853.

Ginoux, J. M., & Letellier, C. (2012). Van der Pol and the history of relaxation oscillations: toward the emergence of a concept. Chaos: An Interdisciplinary Journal of Nonlinear Science, 22(2), 023120.

Gluckman, B. J., Netoff, T. I., Neel, E. J., Ditto, W. L., Spano, M. L., & Schiff, S. J. (1996). Stochastic resonance in a neuronal network from mammalian brain. Physical Review Letters, 77(19), 4098.

Hänggi, P. (2002). Stochastic resonance in biology how noise can enhance detection of weak signals and help improve biological information processing. ChemPhysChem, 3(3), 285-290.

Harding, K. (2004). Genetic integrity of cryopreserved plant cells: a review. CryoLetters, 25(1), 3-22.

Harrison, P. T. C. (1984). An ethanol-acetic acid-formol saline fixative for routine use with special application to the fixation of non-perfused rat lung. Laboratory animals, 18(4), 325-331.

Hidaka, I., Nozaki, D., & Yamamoto, Y. (2000). Functional stochastic resonance in the human brain: noise induced sensitization of baroreflex system. Physical review letters, 85(17), 3740.

Hodgkin, A. L., & Huxley, A. F. (1952). A quantitative description of membrane current and its application to conduction and excitation in nerve. The Journal of physiology, 117(4), 500.

Hoshi, E., & Tanji, J. (2004). Differential roles of neuronal activity in the supplementary and presupplementary motor areas: from information retrieval to motor planning and execution. Journal of Neurophysiology, 92(6), 3482-3499.

Jamur, M. C., & Oliver, C. (2010). Cell fixatives for immunostaining. Immunocytochemical methods and protocols, 55-61.

Jennes, L., Stumpf, W. E., & Kalivas, P. W. (1982). Neurotensin: topographical distribution in rat brain by immunohistochemistry. Journal of Comparative Neurology, 210(3), 211-224.

Karlsson, U., & Schultz, R. L. (1965). Fixation of the central nervous system for electron microscopy by aldehyde perfusion: I. Preservation with aldehyde perfusates versus direct perfusion with osmium tetroxide with special reference to membranes and the extracellular space. Journal of ultrastructure research, 12(1), 160-186.

Kiernan, J. A. (2000). Formaldehyde, formalin, paraformaldehyde and glutaraldehyde: what they are and what they do. Microscopy today, 1(5).

Kimura, H., McGeer, P. L., Peng, F., & McGeer, E. G. (1980). Choline acetyltransferase-containing neurons in rodent brain demonstrated by immunohistochemistry. Science, 208(4447), 1057-1059.

Kramarenko, A. V., & Tan, U. (2003). Effects of high-frequency electromagnetic fields on human EEG: a brain mapping study. International Journal of Neuroscience, 113(7), 1007-1019.

Mason, J. T., & O'leary, T. J. (1991). Effects of formaldehyde fixation on protein secondary structure: a calorimetric and infrared spectroscopic investigation. Journal of Histochemistry & Cytochemistry, 39(2), 225-229.

Morris, J. S., Öhman, A., & Dolan, R. J. (1999). A subcortical pathway to the right amygdala mediating “unseen” fear. Proceedings of the National Academy of Sciences, 96(4), 1680-1685.

Nagel, T. (1974). What is it like to be a bat?. The philosophical review, 83(4), 435-450.

O’Keefe, J., & Burgess, N. (1999). Theta activity, virtual navigation and the human hippocampus. Trends in cognitive sciences, 3(11), 403-406.

Peredery, O., Persinger, M. A., Parker, G., & Mastrosov, L. (2000). Temporal changes in neuronal dropout following inductions of lithium/pilocarpine seizures in the rat. Brain research, 881(1), 9-17.

Perlmutter, M. A., Best, C. J., Gillespie, J. W., Gathright, Y., González, S., Velasco, A., ... & Chuaqui, R. F. (2004). Comparison of snap freezing versus ethanol fixation for gene expression profiling of tissue specimens. The Journal of Molecular Diagnostics, 6(4), 371-377.

Persinger, M. A. (2012). Brain electromagnetic activity and lightning: potentially congruent scale-invariant quantitative properties. Frontiers in integrative neuroscience, 6.

Puchtler, H., & Meloan, S. N. (1985). On the chemistry of formaldehyde fixation and its effects on immunohistochemical reactions. Histochemistry, 82(3), 201-204.

Reiser, H., Dimpfel, W., & Schober, F. (1995). The influence of electromagnetic fields on human brain activity. European journal of medical research, 1(1), 27-32.

Rouleau, N., Costa, J. N., & Persinger, M. A. (2017). Evaluating the Signal Processing Capacities of Post-Mortem Cerebral Cortical Tissue by Artificial Phototransduction of Dynamic Visual Stimuli. 7, 1-13.

Rouleau, N., Murugan, N. J., Tessaro, L. W., Costa, J. N., & Persinger, M.A. (2016). When Is the Brain Dead? Living-Like Electrophysiological Responses and Photon Emissions from Applications of Neurotransmitters in Fixed Post-Mortem Human Brains. PloS one, 11(12), e0167231.

Rouleau, N., Lehman, B., & Persinger, M. A. (2016). Focal attenuation of specific electroencephalographic power over the right parahippocampal region during transcerebral copper screening in living subjects and hemispheric asymmetric voltages in fixed brain tissue. Brain research, 1644, 267-277.

Rouleau, N., & Persinger, M. A. (2016a). Differential responsiveness of the right parahippocampal region to electrical stimulation in fixed human brains: Implications for historical surgical stimulation studies?. Epilepsy & Behavior, 60, 181-186.

Rouleau, N., Reive, B. S., & Persinger, M. A. (2016). Functional neuroimaging of post-mortem tissue: lithium-pilocarpine seized rats express reduced brain mass and

proportional reductions of left ventral cerebral theta spectral power. Heliyon, 2(10), e00181.

Tsang, E. W., Koren, S. A., & Persinger, M. A. (2004). Power increases within the gamma range over the frontal and occipital regions during acute exposures to cerebrally counterclockwise rotating magnetic fields with specific derivatives of change. International Journal of Neuroscience, 114(9), 1183-1193.

Tusa, R. J., Palmer, L. A., & Rosenquist, A. C. (1978). The retinotopic organization of area 17 (striate cortex) in the cat. Journal of Comparative Neurology, 177(2), 213-235.

Zurborg, S., Yurgionas, B., Jira, J. A., Caspani, O., & Heppenstall, P. A. (2007). Direct activation of the ion channel TRPA1 by Ca2+. Nature neuroscience, 10(3), 277-279.

Chapter 10

Summary, Conclusions, Thoughts, and Future Directions

Summary of Findings

This dissertation presents the argument that post-mortem neural tissues are responsive systems which operate as if filters, amplifying and deconstructing signals. The data indicate that structures and functions of the post-mortem brain are intimately related and produce unintuitive, living-like characteristics which require further examination. The fixed, post-mortem brain expresses electrically non-random periodicities which vary over space and time. These change as a function of structure, respond to electrochemical probes, and are significantly perturbed by the medium within which the brain is immersed. There are observable functions of brain structure which persist beyond death. What remains is to determine how these functions are potentiated and the degree to which they are related to experience or not. Is the post-mortem brain merely a conductive albeit structurally interesting medium through which current passes and is frequency- or amplitude-modulated? Is there a phenomenology which can be accessed beneath the surface? The data are in short supply in these areas of inquiry, though what is reported demarcates a fork in the road of possibilities. To the left of the fork, we find confirmatory evidence indicating brain death represents a bold line past which meaningful signal processing and the capacity to experience are not found. To the right of the fork: A long and winding road which runs opposite to the former and which makes no promises in the form of signs placed at equal intervals along its trajectory.

Conclusion

At the beginning of this dissertation, a central question was asked which can be reformulated in the following way: Is brain function lost upon death? The answer, it would seem, is dependent upon what is meant by function. If the capacity for a medium to receive a signal, transform it, and re-emit it is sufficiently dynamic to be labelled “function”, the answer to the former question can’t possibly be in the affirmative. What I think we’ve demonstrated, perhaps unsurprising to some readers, is that the structure-function relationship of the brain is not strictly contingent upon metabolic activity. One further implication is that brain activity is reliant upon exogenous factors which, if unavailable or removed, might be imputed by other exogenous factors, satisfying thresholds for activation.

One should hesitate to call the relationship between metabolic and brain activity “endogenous” as the living brain is always reliant upon nutrients, oxygen, and inputs of information via the senses. None of these factors originate within the tissue and are therefore always subject to factors of external supply and internal demand. Nutrients and oxygen provide living brain matter with molecular building blocks and energy sufficient to construct, maintain, and operate intracellular machinery. In combination, these *vital forces* allow the brain to temporarily avoid entropy over a period of decades. If brain structure, which is dependent upon nutrients and oxygen, determines brain function, then brain function is reliant to some degree upon said external factors. From this perspective, functions of the living brain are dependent upon quantized vital factors of external origin delivered to cells which maintain structure. Again, this is likely unsurprising or maybe even trivial to some readers though I would suggest that pointing out the brain’s reliance upon

sources of energy external to its self is an important step in recognizing the insufficiency of the “productive” model of brain function which postulates that brain activity is wholly a consequence of the parts of the brain. That is, the reader should notice that brain cells and the tissues within which they are embedded are never functioning without recruitment of external energy sources, even *in vivo*.

Nutrients and oxygen are not required to maintain structural stasis in fixed tissues. Instead, cellular matrices are structurally preserved by freezing, cross-linking, and other methods of binding. Nutrients and oxygen, once vital, become irrelevant when usurped by fixative. At no point, however, is brain material independent of external factors – even fixed, post-mortem tissues are reliant upon the fixing compound or method without which structure would be lost. The answer to the question of whether or not function persists in any practical or meaningful capacity in the fixed, post-mortem brain is dependent upon the relevance of information processing and its broader implications with regard to thought, behaviour, and consciousness.

Upon death, the brain is stripped of its capacity to impinge upon the musculature. Further, neurons become increasingly incoherent, dysfunctional, and dissolute. Preserving brain structure prevents this latter eventuality, fixing cells within their spatial coordinates relative to all other cells. Our data indicate that fixed, post-mortem neural tissues are capable of many unexpected features under the current paradigm. Characteristic “response” patterns indicating habituation to concentration-dependent chemical probes, for example, represent a full frontal assault upon the underlying assumption of non-function after the brain is isolated from its life-sustaining systems. Data, however, are always subject to interpretation. I concede that it is entirely possible

that we are now operating under a misapprehension. However, I fail to see how someone might contend that the data are trivial or not worthy of further pursuit given their fundamental disagreement with historical assumptions and control-verified regional effects. There is currently no serious study of brain function beyond the immediate period after death. However, responses in non-living systems have been reported throughout the history of science (Bose, 1902) – a largely unacknowledged field of inquiry which has often been centered upon the measurement of electricity.

Philosophical Considerations

Where does a thought go when you stop thinking? Patterns of electrical activity which define our moment-to-moment experience seem to come and go reliably. If I were to ask you, the reader, to pay close attention to the strain on your lower back or the sensation of your feet, you'll experience what it's like to momentarily change the electrical state of your brain in such a way that your experience changes too. Even this sentence is only relevant to the discussion insofar as you, the reader, can hold the previous sentences in your working memory for context. In life, the electrical state of the brain is transient where any particular thought can be temporarily silenced for durations of time both short and long, replaced instead by other thoughts – a continuous stream. Each thought, paired to its electrical pattern within the brain, only exists insofar as it is being continuously re-generated within the same neural pathways. When that electrical activity stops or is re-directed, the thought ceases to exist. A host-parasite metaphor could be relevant here. Whereas host-like brain structures are required as an antecedent condition for thought, the thought itself, defined by its electrical state, is parasitic in that it depends upon and is functionally inseparable from the host structures. Without structure, the

thought cannot exist. However, structure alone is likely insufficient to generate thought – electrical patterns must be represented within said structures. Whether these electrical patterns are generated by membrane potentials at the level of cells or directed through the tissue by external sources of current – passively filtered through common pathways – their structural dependences remain inexorable.

Death, as it were, represents a more permanent relegation to the moments in between thoughts – and yet we don't think of the brain as oscillating between life and death with every changing thought. Having lost its capacity to readily change its electrical states, the post-mortem brain likely remains thoughtless or confined to a single state. However, if the brain is preserved in fixative solution, are the retained neural structures sufficient to, whether assisted by external sources of energy or not, generate patterns of activity sufficient to constitute meaningful brain signals? It would seem that an answer to such a question would require a direct measurement of experience – a reality which has historically burdened psychologists, biologists, and neuroscientists (Chalmers, 1995). Together, the present series of studies constitute a foundation on which to base a study of brain function after death. Whereas the question of post-mortem brain function should continue to evoke a strong sense of having not understood what I means for an organ or organism to be dead, I would suggest that a re-evaluation of the underlying assumptions is due in any case.

The definition of "nothing" has been endlessly debated by physicists and philosophers only to have generated what are essentially two definitions in opposition. The first, favored by some physicists, posits that "nothing" is made up of a bubbling quantum field (Krauss, 2012). Philosophers continue to insist that quantum fields and

virtual particles are, indeed, “something” (Gallagher, 2012). Instead, they (the philosophers and other physicists) suggest “nothing” is simply the absence of “all things” – a state which has yet to be observed and which the laws of thermodynamics prevents (i.e., zero entropy is impossible). I would hope that discussions surrounding “death” do not become bogged down in similarly unhelpful quarrels about definitions. A practical approach can be employed here. It is either the case that what we now refer to as “death” is just another position on a continuum of possible experiential states associated with brains or that it represents some cut-off point. This dissertation, in keeping with the former, makes the argument that functions are inseparable from structures, and that if structures are preserved indefinitely, their function (or potential function requiring energy input) must also continue to be preserved. It is therefore the case that if brain structure determines brain function – everything from walking and talking to the greatest sense of pleasure or pain – preserving structure must entail preserving function insofar as structure is genuinely preserved and to the degree that its morphological and topological integrity is not sufficiently disturbed.

Prince Rupert’s Drop and Why Structure Matters

The findings presented in this dissertation suggest that the post-mortem brain is functional. The function in question appears to involve the filtration of external applications of energy which are dependent upon the neuroanatomical region being probed. This operation produces signal outputs as strings of fluctuating electric potentials whose spectral frequencies contain information including signatures which indicate repeated exposures or historical traces. Chemical fixation of neural tissue which results in preserved micro- and macrostructure has allowed us to study these “functions” of brains

beyond death. These experiments strongly support the notion that “structure dictates function” by demonstrating the preserved structure necessitates degrees of preserved function as inferred by stimulus-response patterns. Metaphors can be useful when attempting to illustrate the significance of a concept which might seem otherwise trivial. Here, I will discuss the Prince Rupert’s Drop in relation to the presented works.

Dripping molten glass into cold water generates a toughened material with very high, internal, residual stress called a Prince Rupert’s drop characterized by a quasi-spherical bulb fused to an elongated tail segment (Brodsley, Frank & Steeds, 1986). While the exterior of the glass bulb quickly cools upon entering the water, the interior remains molten for some time. When the core eventually cools, it contracts inwards, producing a state of high compressive stress on the surface with high tensile stress in the core. These stresses are imprinted upon the structure and remain long after the original cause of the stressor is removed – a type of stress-based memory. The structural anisotropy which results produces some interesting material consequences. First, the glass is very difficult to break at its bulb where significant applications of energy by hammer or projectile are futile. However, even the slightest fracture of the tail segment by trivial applications of energy causes a high-velocity, propagating wave which results in an explosion at the bulb – a rapid release of potential energy stored within the internal structure as residual stress (Johnson & Chandrasekar, 1992).

Just as Prince Rupert’s Drops store potential energy by dint of uneven cooling gradients across the glass, the fixed brain might store electric potential (or a capacity to elicit electric potentials) by uneven perfusion of the fixative solution and its effects upon the tissue over time. Once removed from the cranial cavity, the brain continues to express

residual function as steady state potentials. In fact, rodent brains are readily sectioned for *ex vivo* electrophysiological measurements in culture, supplemented by nutrient-rich media. However, when human brains are immersed within fixative, perfusion of the 1,300 cc volume can take weeks to months considering the perfusion rate of a 1 cc block of tissue is on the order of 24 hours with a subsequent period of “solidification” which can last several weeks. Fixative rushes into the intervening spaces between and within cells, pushing out water. Since water content is observed to differ as a function of spatial coordinates within the brain (Whittall et al., 1997), it stands to reason that replacement by fixative would follow similar gradients. Indeed, gross-structural asymmetries across hemispheres such as differential proportions of gray and white matter must also determine alternative perfusion features. These boundary conditions, analogous to stress gradients within Prince Rupert’s Drops, could imbue the post-mortem brain’s microstructure (i.e., cell bodies, dendrites, axons, etc.) with a residual function: a capacity to filter externally-applied energies including electrical signals, electromagnetic fields, or charged molecules whether alive or not.

Future Directions

At this time, there are several directions that the research might take. One of the most exciting prospects concerns passive functions of human brain tissue. That is, the capacity for brain tissue to selectively tune-in to applied electromagnetic fields or amplify patterned current must be further explored from a materials sciences perspective. The brain’s antenna-like properties could underlie some of the most fundamental and challenging functions with which neuroscientists are charged to explain. Consciousness, chief among them, has long been suspected by some to involve the transduction of

transmitted waves by an antenna-like brain (Nunez, 2010). Indeed, William James, one of the founders of modern psychology, described brain transmission “rays”. He described the brain, which “encased” consciousness, as a filter with properties of “permissiveness”, using a light-prism metaphor (Hawkins, 2007; James, 1992). Some variants of the theory would suggest that brains are just some of the forms of matter which might transduce the “psychic field” and be imbued with the capacity to experience (Van Cleve, 1990). Though it would seem that most brain-phenomena can be explained by standard neurobiological models, these fail to accommodate some of the most interesting and esoteric observations as well as experiences which have been reported for thousands of years including those which are culturally labelled as “divine” or of “other worldly” origins – often involving access to recondite information about individuals, distant places, or imminent events.

Practical applications of these findings might involve engineering bio-tissues into modern electronic systems. Just as ceramics can be used in resistors, perhaps brain tissue could be integrated into modern circuitry as band-pass filters where different cytoarchitectures would determine the properties of the circuit. Intrinsic resonance frequencies as well as the contribution of matrix-like dendritic arrays could have untold applications when integrated with modern technology such as advanced robotics – perhaps to introduce noise or fuzzy signals (Kosko & Mitaim, 2003). Alternatively, a complete understanding of brain death might yield some method of reversal. In earnest, the full implications of the reported data are unclear. What is required at this time is a serious study of brain material and its functional correlates within a framework that is not limited by metabolism. To understand death, it seems, we must clearly delineate life’s

borders on the map of all possible states while observing its potential imports and exports. The answer to our most primal question beckons. We stand eye-to-eye, separated by a chasm whose depth, determined by taboo, is of our own design. If we want to know what we claim to want to know, we will get out of our own way in pursuit of these truths.

It is predicted that this type of research, which is likely avoided for many dozens of reasons, will become increasingly unavoidable as we enter an era marked by artificial intelligences and brain-robot integration. Scientific breakthroughs in genetic engineering and computer sciences have brought us to a precipice – we must now fly lest we fall to the rocks. Faced with the looming prospect of human immortality and the always hanging Sword of Damocles – with the risks of general AI now rivaling nuclear war – it is incumbent upon us as a species to challenge the taboos which cast the longest shadows and to transcend our more undesirable primate impulses. A new enlightenment, marked by a genuine study of death, religious experiences, and all “untouchable” things should be pursued without prejudice. If something is untrue, make it known. If something is true, make that known too. What we must not forget, in pursuit of the unknown, is that no answer is final. Though some will rest on their accolades or dismiss challenges of scientific dogma as denialism, the battle of ideas marches forward unimpeded and without regard for the individual desires of scientists. Max Planck’s (1949) principle remains relevant today: “A new scientific truth does not triumph by convincing its opponents and making them see the light, but rather because its opponents eventually die, and a new generation grows up that is familiar with it.”.

References

Bose, J. C. (1902). Response in the Living and Non-living. Longmans, Green, and Company.

Brodsley, L., Frank, C., & Steeds, J. W. (1986). Prince Rupert's drops. Notes and Records of the Royal Society, 41(1), 1-26.

Chalmers, D. J. (1995). Facing up to the problem of consciousness. Journal of consciousness studies, 2(3), 200-219.

Gallagher, D. B. (2012). John F. Wippel, ed., The Ultimate Why Question: Why is There Anything at All Rather than Nothing Whatsoever?. Philosophy in Review XXXII, no.3.

Hawkins, S. L. (2007). William James, Gustav Fechner, and early psychophysics. Networking of Psychophysics, Psychology and Neurophysiology, 13.

James, W. (1992b). “On human immortality,” in William James: Writings 1878 – 1899 (Original 1898), ed. E. M. Gerald (New York: The Library of America), 1100–1127.

Johnson, W., & Chandrasekar, S. (1992). Rupert's glass drops: residual-stress measurements and calculations and hypotheses for explaining disintegrating fracture. Journal of materials processing technology, 31(3), 413-440.

Kosko, B., & Mitaim, S. (2003). Stochastic resonance in noisy threshold neurons. Neural networks, 16(5), 755-761.

Krauss, L. M. (2012). A universe from nothing: Why there is something rather than nothing. Simon and Schuster.

Nuñez, P. L. (2010). Brain, Mind, and the Structure of Reality. Oxford: Oxford University Press.

Planck M. (1949), Scientific Autobiography, F. Gaynor, (trans). Philosophical Library, New York.

Van Cleve, J. (1990). Mind--Dust or Magic? Panpsychism Versus Emergence. Philosophical perspectives, 4, 215-226.

Whittall, K. P., Mackay, A. L., Graeb, D. A., Nugent, R. A., Li, D. K., & Paty, D. W. (1997). In vivo measurement of T2 distributions and water contents in normal human brain. Magnetic Resonance in Medicine, 37(1), 34-43.